NASA-CR-159838
19800014245

NASA CR-159838

Development of Procedures for Calculating Stiffness and Damping of Elastomers in Engineering Applications

Part VI

by A. Rieger, G. Burgess, E. Zorzi

Mechanical Technology Incorporated

Prepared for

National Aeronautics and Space Administration

NASA Lewis Research Center
Contract NAS3-18546

1. Report No.	2. Government Accession No.	3. Recipient's Catalog No.
CR-159838		

4. Title and Subtitle	5. Report Date
Development of Procedures for Calculating Stiffness and Damping of Elastomers in Engineering Applications - Part VI	April 1980
	6. Performing Organization Code
7. Author(s)	8. Performing Organization Report No.
A. Rieger, G. Burgess, and E. Zorzi	80TR29
	10. Work Unit No.
9. Performing Organization Name and Address	
Mechanical Technology Incorporated 968 Albany-Shaker Road Latham, New York 12110	11. Contract or Grant No. NAS3-18546
	13. Type of Report and Period Covered
12. Sponsoring Agency Name and Address	Contractor Report
NASA-Lewis Research Center Washington, DC 20546	14. Sponsoring Agency Code

15. Supplementary Notes

Data Report

16. Abstract

An elastomer damper has been designed, tested, and compared with the performance of a hydraulic damper for a power transmission shaft. The six-button Viton-70 damper was designed so that the elastomer damper or the hydraulic damper could be activated without upsetting the imbalance condition of the assembly. This permitted a direct comparison of damper effectiveness. The results show that the elastomer damper consistently performed better than the hydraulic mount and permitted stable operation of the power transmission shaft to speeds higher than obtained with the squeeze film damper.

Tests have been performed on shear specimens of Viton-70, Buna-N, EPDM, and Neoprene to determine performance limitations imposed by strain, temperature, and frequency. Frequencies of between 110 Hz and 1100 Hz were surveyed with imposed strains between 0.0005 and 0.08 at temperatures of 32°C, 66°C, and 80°C. From this data a set of design curves have been generated in a unified format for each of the elastomer materials.

17. Key Words (Suggested by Author(s))		18. Distribution Statement
Viscoelasticity Elastomers Dynamic Properties Damping Vibrations	Critical Speeds Resonance Testing Gas Turbine Strain Effects	Unclassified - Unlimited N80-22733#

19. Security Classif. (of this report)	20. Security Classif. (of this page)	21. No. of Pages	22. Price*
Unclassified	Unclassified	159	

* For sale by the National Technical Information Service, Springfield, Virginia 22161

TABLE OF CONTENTS

LIST OF FIGURES

LIST OF FIGURES (Cont'd)

LIST OF FIGURES (Cont'd)

LIST OF FIGURES (Cont'd)

ABSTRACT

An elastomer damper has been designed, tested, and compared with the performance of a hydraulic damper for a power transmission shaft. The six-button Viton-70 damper was designed so that the elastomer damper or the hydraulic damper could be activated without upsetting the imbalance condition of the assembly. This permitted a direct comparison of damper effectiveness. The results show that the elastomer damper consistently performed better than the hydraulic mount and permitted stable operation of the power transmission shaft to speeds higher than obtained with the squeeze film damper.

Tests have been performed on shear specimens of Viton-70, Buna-N, EPDM, and Neoprene to determine performance limitations imposed by strain, temperature, and frequency. Frequencies of between 110 Hz and 1100 Hz were surveyed with imposed strains between 0.0005 and 0.08 at temperatures of 32°C, 66°C, and 80°C. From this data a set of design curves have been generated in a unified format for each of the elastomer materials.

I - SUMMARY

A program has been undertaken to: (1) determine the effectiveness of an elastomer damper and compare it to that of a hydraulic mount on a power transmission shaft and (2) determine the effects of frequency, strain, and temperature on the dynamic properties of Viton-70, Buna-N, EPDM, and Neoprene.

The Viton-70 elastomer damper has clearly showed its viability as an effective rotor damper on the power transmission shaft. The elastomer permitted higher operational speeds of the rotor and excellent control of synchronous and nonsychronous excitation through all phases of testing. The Viton-70 damper was superior to the hydraulic mount. The elastomer damping capabilities were predictable and offered no special problems in this rotor application.

EPDM, Viton-70, Buna-N, and Neoprene shear specimens were subjected to a schedule of frequency, temperature, and strain. The maximum loss coefficients obtained were for Viton-70 at 32°C. EPDM, unlike the other materials, showed a decrease in loss coefficient with increasing frequency. All materials showed a decrease in loss coefficient of between 0.1 and 0.2 at 500 Hz and 80°C. Viton-70 had the largest value of loss coefficients, approaching 1.0 at 1000 Hz and 32°C.

II - INTRODUCTION

A shaft operating above one or more of its critical speeds is subjected to any number of destabilizing mechanisms. Splines, material hysteresis, aerodynamic forces, and fluid bearings can and do produce rotor loads which encourage instabilities. With the trend towards higher power density gas turbines and more compact power transmission shafting with long unsupported shafts operating at higher speeds, significant expenditures of manpower and facilities are required to insure safe, reliable operation.

Balancing technology has matured to a point at which the control of synchronous vibrations is generally not an inhibiting factor in rotor design. However, the control of nonsynchronous excitations may require additional consideration, such as the use of a hydraulic mount or squeeze film damper to dissipate undesirable vibration and stabilize the rotor bearing assembly. It is not surprising then to find squeeze film dampers on a wide variety of high-speed rotating machinery. But a squeeze film damper is expensive in a number of ways. Close tolerance machining, oil supply, and associated plumbing are generally required.

It is desirable to find a convenient dry compact damper which offers a wide range of stiffness and damping characteristics and which can achieve the same control of rotor vibrations offered by the squeeze film. However, factors which have inhibited the growth and applications of elastomer dampers are the limited availability of design-oriented data on their dynamic performance, environmental stability, and consistency of predictable performance. For several years, a program has been pursued at Mechanical Technology Incorporated (MTI) whose intent is to quantify dynamic performance of elastomer dampers, to provide the capability to design for desired characteristics, to evaluate the effects of environment, to demonstrate the effectiveness of elastomers in vibration control, and to assess problems which may occur in applications to high-speed rotating machinery. References 1, 2, 3, and 4 document previous work under this MTI program.

Under this program a powerful test method for determining elastomer component properties has been developed, entitled "The Base Excitation

Resonant Mass Method." This test method employs a large electromagnetic shaker on which test specimens are mounted. The test specimens comprise a one-degree-of-freedom spring-mass-damper system in which a variable mass is excited at or near the resonant frequency of that mass mounted on an elastomeric spring. Transmissibility and phase angle across the elastomer spring are measured and, in the region of resonance, allow accurate determination of both stiffness and damping.

Under past test programs the effects of excitation frequency, specimen geometry, environmental temperature, dynamic strain, and material have been tested. Empirical approaches to predicting component properties have evolved and their effectiveness has been evaluated under both translatory and rotating excitation.

As will be shown, the influence of strain was pronounced on each of the materials tested: Viton-70, EPDM, Neoprene, and Buna-N. However, unlike previous data obtained for polybutadiene (ref. 1), strain did not necessarily provide a better unification of the data for all materials. In fact, for Buna-N consistency of data was more apparent when plotted versus frequency.

Viton and Neoprene exhibited an increase in loss coefficient with frequency and a decrease in loss coefficient with temperature, typical of materials operating in the rubbery region. Buna-N does not show a consistent decrease in loss coefficient with temperature and, in fact, for low frequencies (less than 300 Hz), the loss coefficient increased between 32°C and 66°C. EPDM shows a similar behavior with temperature and, in addition, a pronounced increase in loss coefficient with frequency for all temperatures, indicating a possible transition region behavior for this elastomer.

As a further part of this program, MTI has been actively engaged in evaluating the dynamic properties of elastomers as well as evaluating their potential for practical applications. To permit a comparison of an elastomeric damper with a squeeze film damper, a power transmission test facility with an existing squeeze film damper was fitted with an interchangeable elastomeric damper. The drive shaft tested was formed from a section of aluminum tubing, 7.62 cm (3 in.) in diameter, 3.66 m (12 ft) long with a wall thickness of 3.175 mm (0.125 in.).

Design requirements for the elastomeric damper included consideration of shaft diassembly and reassembly imbalance changes. The elastomers were required to replace the squeeze film damper, without the necessity of shaft/damper disassembly. An outer ring elastomer support was fabricated as a split ring and consequently could be removed without disturbing the shaft balance. This change was made to the damper using six Viton-70 buttons (3 equally circumferentially spaced on each end), 0.635 cm (0.25 in.) in diameter, 0.635 cm high and preloaded to 10% strain. The six buttons provided a stiffness of approximately 7×10^5 N/m (4000 lb/in.) with a loss factor of 0.75. This stiffness and damping selected was based upon a rotor dynamics optimization study performed for both the squeeze film and elastomeric damper.

As will be shown, the elastomeric damper was clearly superior to the squeeze film. Even when the shaft was carefully balanced just for squeeze film operation, the elastomer constantly permitted high-speed operation. Later balancing with the elastomer in place permitted safe operation to 13,000 rpm, 1000 rpm higher than achieved with the squeeze film. As the maximum speed of this rotor has been restricted in past operation due to subsynchronous excitation of the first mode (16 Hz), the elastomer clearly demonstrated its ability to control synchronous as well as nonsynchronous excitation and its viability as a damper for high-speed rotating machinery.

III - DESIGN OF ELASTOMER DAMPER FOR POWER TRANSMISSION SHAFT

Test Facility

The test facility used for this project was designed and constructed at MTI for demonstrating the use of supercritical shafting. A sketch of the test rig is presented in figure 1. A 224-kW (300 horsepower) electric motor is the prime mover for this facility. The motor drives a variable-speed magnetic coupling while output speed is continuously variable from 50 to 3600 rpm. A gearbox with a ratio of approximately 5.7:1 was used to produce a drive-shaft speed of up to 20,000 rpm. The test shaft was formed from a section of aluminum tubing 7.62 cm (3 in.) in diameter and 3.66 m (12 ft) long with a wall thickness of 3.175 mm (0.125 in.). Early testing without a damper did not permit rig operation above 1200 rpm due to an instability resulting from the subsynchronous excitation of the first critical speed at 16 Hz (ref. 5). The stability problems identified during this early stage of testing clearly established that some form of external damping, coupled with balancing, would be required to control shaft vibrations.

Several methods for applying external damping were investigated. An oil squeeze film type damper was initially selected, based upon its proven reliability and predictability in the level of damping achieved. Optimization studies performed for the squeeze film had shown (ref. 5) that a hydraulic mount 7.62 cm (3 in.) long, 10.16 cm (4 in.) in diameter and with a radial clearance of 0.635 mm (25 mils) would provide the "best" tradeoff in stability in the first and third mode (the second mode was overdamped).

Testing showed that the dynamic stability of the test rig was improved as a result of the squeeze film damper (figure 2). However, the addition of external damping alone could not provide complete control of all test shaft vibrations; the test shaft also had to be balanced to achieve safe operation throughout its speed range. Through the combined use of external squeeze film damping and balancing (ref. 5), the rig was safely operated to over 12,000 rpm while negotiating the first four flexural critical speeds of the test shaft. This was over 10 times the speed which could be negotiated without any external damping. The 16 Hz subsynchronous excitation of the first mode, however, still limited performance (see figure 3).

Rotor Support Optimization Studies

Previous rotor stability analysis performed for the design of the squeeze film damper showed that the second mode permits heavy participation of the damper (figures 4 and 5). This was confirmed by testing as the second mode was not observed, verifying the stability analysis which indicated a highly damped critical speed when operated with the squeeze film mount (ref. 5). For the squeeze film damper, the stability assessment motivated a selection of 7.5×10^5 N/m (4000 lb/in.) stiffness with a viscous damping of 8750 N-s/m (50 lb-sec/in.) to permit a reasonable tradeoff in the stability of the first and third criticals and higher modes.

The analysis performed for the power transmission shaft mounted on the squeeze film is applicable for the shaft mounted on the elastomer dampers. Certainly, if an elastomeric material could be found to provide relatively equivalent stiffness and damping to that of the squeeze film, then the optimization would be complete. However, for a given stiffness and material loss coefficient, the equivalent viscous damping diminishes as higher speeds are attained, assuming that the stiffness remains fairly constant over the range of testing. Therefore, an analytic model (figure 6) of the power transmission shaft was constructed and used to evaluate the first two critical speeds, the first two modes were selected because:

- The first critical has been the most sensitive and has been the cause of stability problems in limiting the maximum speed of the rotor.
- The second critical was found to be overdamped for operation with the squeeze film. If this mode was not highly damped on the elastomer, an additional balancing stage would be required.
- Higher modes have generally not been a problem for the shaft mounted on the squeeze film.

Figure 7 illustrates the effect on the log decrement of the first and second mode as stiffness and elastomeric loss coefficient are varied. As shown, for a stiffness range of between 4000-5000 lb/in. (typical of the squeeze film damper), the log decrement of the first mode is approximately

0.09 and the log decrement of the second mode is greater than 2.0, for a material loss coefficient of 0.75. This is compatible with the previous analysis of the squeeze film damper support on the power transmission shaft.

From previous testing of Viton-70 O-rings (ref. 6), value of loss coefficient of 0.75 was considered reasonable. Further design studies, performed in reference 1, indicate that a double row of three equally spaced, circumferentially located Viton-70 buttons of 0.635 cm (0.25 in.) in diameter and 0.635 cm (0.25 in.) high would produce an approximate stiffness of 7×10^5 N/m (4000 lb/in.).

Elastomer Damper Design

It is desirable, when comparing two damper configurations, namely, a squeeze film and an elastomeric damper, to be able to accommodate change by using a modular configuration which may be switched without requiring assembly and disassembly of the system components. This provides not only time savings, but also, and more important, permits minimum disturbance to the balanced configuration. The modular, quick interchangeable configuration was precisely the objective in this program. To accomplish this, a trade-off had to be made, namely in compactness. Therefore, the design selected for this work was not considered one which might be characteristic of a production rotor environment, but one which could provide a meaningful comparison between an existing hydraulic mount and elastomeric damper.

Figure 8 illustrates the squeeze film as well as the elastomer design of the damper for the power transmission shaft. The left side of the illustration presents the squeeze film configuration with an O-ring provided for added mobility of the mount assembly. The right side shows the modified, or added parts, (shaded) along with the bumper screws for overload protection, and the additional proximity probes to monitor elastomer excursions. These modifications were made to both ends of the squeeze film assembly. To mount the elastomer elements on the squeeze film assembly does not require disassembly of the damper/power transmission shaft. A split outer ring (figure 9) permitted the damper to be changed without shaft disassembly. The two-piece ring has provisions for up to six equally spaced elastomer elements

(three were used for this test). The slots guide the outer support platens for the elastomer buttons (figure 10). The preload screws were adjusted for a 10% preload on all buttons. Figures 11, 12, and 13 show the elastomer damper assembly mounted on the squeeze film housing. The elastomer buttons were attached to the upper platens with Reis plastic TWA-1077 adhesive.

Test Setup and Sequence

The rig was originally set up for checkout and initial operation with the hydraulic mount active. Initial operation of the rig provided difficulty as repeatability was not apparent. In fact, several "jumps" in unbalance response were prevalent throughout early testing. Disassembly of the power transmission shaft and inspection of the couplings showed extreme distortion of the disk elements comprising the Rexnord couplings. These were replaced, the power transmission shaft realigned, and testing resumed with the operation of the shaft satisfactory for this effort.

Figure 14 illustrates the location and designation of the proximity probes which were active throughout this testing. In addition, phase reference was provided through a Spectral Dynamics Fiber-Optics Tachometer. A Digital Equipment Corp. PDP 11/34 was used for automatic data acquisition and balancing. All data were recorded on a Sangamo Sabre VI recorder. The test sequence was as follows:

- Run rig with squeeze film to first critical as a baseline condition.
- Install elastomers and drain squeeze film (do not flush yet as oil coating provides protection for possible overload condition). Operate through third critical.
- Flush squeeze film (Toluene and Acetone). Operate with elastomer damper.
- Remove elastomers, fill hydraulic mount and compare results with above.
- Balance for squeeze film operation.

- Drain and flush squeeze film, install elastomers and compare results with above.
- Operate elastomer damper to maximum operating speed.

IV - TEST RESULTS - ELASTOMER DAMPER FOR POWER TRANSMISSION SHAFT

Figures 15 through 20 provide synchronous response traces (runout corrected) for selected proximity probes. This represents data obtained from the first balancing attempt using the elastomer damper. The shaft was balanced to 7600 rpm without any special problems. At this speed, the shaft was climbing the fourth bending mode and, at this point, it was decided to disassemble the elastomer and activate the hydraulic mount.

The maximum speed obtained with the squeeze film active (without rebalance) was 3500 rpm as shown in figures 21 through 26. The speed limitation was a result of the very large and rapidly increasing orbits for Probe #3, as shown in figure 26. A comparison of the response of Probe #3 for the elastomer and squeeze film damper is shown in figure 27. It is noteworthy that, although the shaft orbits were larger when the squeeze film was in operation which limited the operating speed of the rotor, the damper orbits were larger for the elastomer than for squeeze film operation (figures 16 and 22).

With the power transmission shaft still mounted on the squeeze film damper, additional balancing was performed to reduce the severity of the first and third mode. The elastomer was then installed, the squeeze film cavity drained and flushed, and the shaft operated to maximum speed. Figure 28 illustrates the results. The elastomer, although providing poorer response through the first critical than the hydraulic mount, did permit operation through the third mode to 7400 rpm.

In this final configuration, the elastomer-supported power-transmission shaft was balanced for operation to maximum obtainable speed. Although subsynchronous excitation of the first mode again limited the maximum speed of operation (figure 29), the elastomer damper permitted operation to 13,000 rpm (figure 30), which is 1000 rpm higher in speed than achieved at any time with the squeeze film damper operational.

Observation of operation of the elastomer damper performance did not show any of the observed severity of nonsynchronous effects previously

documented with the squeeze film (ref. 7). In fact, the rig performed in a consistent fashion with the one/rev dominating all speed conditions at maximum speed (figure 29). The previously observed cage excitation of lower modes as well as the two-per-rev excitation of higher modes was not evident with the elastomer damper, but was present, as previously documented in reference 7, with operation of the squeeze film.

V - CONCLUSIONS/RECOMMENDATIONS

ELASTOMER DAMPER FOR POWER TRANSMISSION SHAFT

- The elastomer damper permitted operation of the power transmission shaft to 13,000 rpm; 1000 rpm higher than obtained in previous balancing effort with the squeeze film damper.
- Nonsynchronous excitation of the first mode (16 Hz) limited the maximum speed obtained with elastomer damper active.
- The elastomer damper provided superior control over the nonsynchronous excitation previously observed with the squeeze film damper active.
- The low-cost and simple elastomer damper has proven to offer a viable damper alternative to a hydraulic mount for certain applications.
- Elastomers are generally restricted to temperature environments less than 400°F. Efforts to increase this limitation are recommended in order to permit elastomers to be used in applications, such as gas turbines, where temperatures may exceed this limitation.
- Future efforts are recommended to evaluate elastomer dampers in sustaining overload, rotor transient and the effects of oil and fuel contamination to permit a selection of elastomers which may sustain many environmental conditions.
- A compact low-cost elastomer configuration, suitable to high technology advanced rotor designs should be evaluated on engines such as for the cruise missile mission.

VI - TEST PROGRAM - ELASTOMER PERFORMANCE LIMITS

The investigation of effects of strain, ambient temperature, and frequency on elastomer component properties was performed using the Base Excitation Resonant Mass test method. This test method was developed under preceding phases of the program and the details are provided in references 2, 3, and 4. For completeness, a brief discussion of the method follows.

The Base Excitation Resonant Mass test method employs an electromagnetic shaker to apply base excitation to a one-degree-of-freedom spring-mass-damper system. The elastomer test elements form the spring and damper upon which a rigid mass is supported whose magnitude can be varied over a wide range. The response of the supported mass is a function of the input excitation and the dynamic characteristic of the spring mass damper system. Accelerometers are used to measure the shaker excitation and the response of the mass. A tracking filter, phase meter, and digital voltmeter are employed to determine the amplitude of the input excitation, the amplitude of the response component at the same frequency as the input excitation, and the phase angle between input excitation and response. Amplitude across the test specimen is a controlled, independent variable which is measured by a capacitance probe.

A computerized data acquisition system acquires amplitude and phase information for one input accelerometer and three output accelerometers mounted on the resonant mass and from the capacitance displacement probe. In addition, temperature values are acquired via a computer-controlled scanner from as many as twenty different thermocouples at various locations in the test specimen. Data is acquired over a range of frequencies for which resonant or near resonant behavior is observed. The criterion normally employed is that the phase angle should lie between 15° and 165°. A wide range of test frequencies is achieved by varying the supported mass and acquiring data satisfying this criterion for each mass tested.

Data reduction software determines the transmissibility between input excitation and response and, from this quantity and the phase angle, stiffness and damping of the elastomer test specimen are readily calculated.

Other quantities calculated include the amplitude across the elastomer and the energy dissipation per unit volume. The operator is provided with an immediate printout of stiffness, damping, strain, dissipation, and temperature values as each test point is completed. These quantities can be reviewed for consistency and the point rejected or accepted. Preserved data is stored on a disk and is available for subsequent summary printout at the end of each test series.

Figure 31 provides a schematic of the Base Excitation Resonant Mass test rig. Included in this figure are a number of items not referred to in the preceding summary description. The preload air spring is a pressurized air cylinder which can apply a downward force on the elastomer specimen and is used for all compression tests to ensure that the test elements never go into tension. The axial motion mass guide spokes are used when very large masses are supported on the elastomer to ensure that motion is purely vertical and that undesirable rocking motion does not occur. The mass support air spring is used to relieve the force applied by very large masses to the test specimen. In the present series of tests, mass values were limited to those which did not require the axial motion guide spokes or the mass support air spring. Figure 32 is a photograph of the electromagnetic shaker with part of the Base Excitation Resonant Mass test rig mounted upon it. The outer dark-colored metal casing is the outside of the preload air spring and its means of attachment to the table. Protruding from the top of the casing is a small added mass; through the side of the casing may be seen part of a test specimen and to the left of the shaker may be seen a heater which provides a source of hot air for controlling the ambient temperature of the elastomer test specimen. Figure 33 is a schematic of the data acquisition system for the elastomer tests. The data acquisition items previously discussed may now be seen in more detail. In addition to the items previously discussed, this schematic shows the various ways that the operator can monitor the testing process, i.e., via oscilloscopes, the temperature indicator readout, and the teletype terminal.

As shown in figure 34, the typical elastomer shear test specimen employed in the present series of tests consists of a central square metal block surrounded by four similar slotted blocks. The slotted blocks are

clamped to the shaker table and the central mass is attached to each slotted block via an elastomer sheet of approximately 3.15 mm (1/8 in.) thickness and 50.8 mm x 31.75 mm (2.0 in. x 1.25 in.) in sheared area for each interface. Thus the central block forms the resonant mass. This mass may be added to by passing a rod through the central hole and adding mass at the top of the rod. Three output accelerometers are shown mounted on the central block together with a fourth dummy accelerometer for inertial symmetry.

Test Plan

For each of the elastomer materials (Viton-70, Buna-N, Neoprene, EPDM) the test plan followed for this investigation of strain, frequency, and ambient temperature effects is defined by tables I, II, and III (pages 22 and 23). In table I are listed the test series executed for the shear specimen. As may be seen, a full combination of frequency and strain values was executed at each of the three ambient temperatures (32°C, 66°C, 80°C).

Table I defines the combinations of strain and frequency which were executed. Strain values between 0.0005 and 0.08 were tested while frequencies between 100 Hz and 1100 Hz were tested. Table III defines the actual vibration amplitudes for the shear specimens which were required to achieve the strain amplitudes of table II. Actual values of strain frequency combinations which were tested for each specimen are presented in figures 35 through 46.

Test Procedure

The following step-by-step process defines the procedure followed by the operator in executing the tests for elastomer performance limits:

1. A resonant mass is selected and installed.
2. Operator enters information describing the test conditions and resonant mass.
3. The elastomer test sample cavity is enclosed and the temperature control system given time to adjust ambient temperature to the desired value.

4. With low vibration levels applied to the base of the elastomer holding fixture, frequency scans are conducted until the approximate resonant frequency of the system is found. It may be noted here that for a base-excited, single-degree-of-freedom spring-damper-mass system, resonance occurs at an angle smaller than 90°. The deviation from 90° is essentially determined by the amount of damping in the system.

5. While the predetermined strain in the elastomer test sample is maintained by adjustment of the shaker power input level, the vibration frequency is adjusted to obtain the nearest specified test frequency. Provided none of the acceleration and displacement signals show signs of abnormalities (distortions or indications of nonaxial motion of the resonant mass), the operator instructs the computer to acquire data.

6. Computer acquires data in the form of amplitude and phase for each sensor and temperature for each thermocouple. The computer provides to the operator an immediate calculation of stiffness, damping, and power dissipation per unit volume of elastomer along with the raw data from the sensors and thermocouples.

7. Operator reviews these data and calculated results and indicates to the computer that either the data point is acceptable or not acceptable (normally it is acceptable).

8. If acceptable, the computer stores the data on a disk file; if not acceptable, the data point is discarded.

9. The vibration frequency is changed to the next nearest test frequency (with the phase angle between 15° and 165°).

10. Steps five through nine are repeated for each specified value of strain.

11. Tests, comprising Steps 1 through 10, are then repeated with each of the remaining masses in turn, each mass giving a dynamic system with a different resonant frequency, permitting data to be taken at other test frequencies.

12. The ambient temperature in the test sample cavity is adjusted to the next specified value.

13. Steps 1 through 12 are repeated until data at all desired temperatures are obtained.

In addition to testing for dynamic properties, Neoprene, Viton-70, Buna-N, and EPDM were tested to determine their thermal conductivity, coefficient of expansion, specific heat, and chemical content. Some of these properties are for use in analytical predictions while other properties are considered to be of value in design applications. The tests were performed by the Rubber and Plastics Research Association of Great Britain (RAPRA). Results are reported in tables IV through VIII.

TABLE I - TEST PLAN FOR ELASTOMER PERFORMANCE LIMITS

Shear Specimen Tests for Each Material

A. For a temperature of 32°C at each combination of frequency and strain defined by table II, measure elastomer stiffness and damping.

B. For a temperature of 66°C at each combination of frequency and strain defined by table II, measure elastomer stiffness and damping.

C. For a temperature of 80°C at each combination of frequency and strain defined by table II, measure elastomer stiffness and damping.

TABLE II - FREQUENCY AND STRAIN COMBINATIONS TO BE TESTED

	Frequency Number									
Strain	1	2	3	4	5	6	7	8	9	10
0.0005	S	S	S	S	S	S	S	S	S	S
0.001	S	S	S	S	S	S	S	S	S	S
0.002	S	S	S	S	S	S	S	S	S	S
0.004	S	S	S	S	S	S	S	S	S	S
0.005	S	S	S	S	S	S	S	S	S	S
0.008	S	S	S	S	S	S	S	S	S	S
0.01	S	S	S	S	S	S	S	S	S	S
0.02	S	S	S	S	S	S	S	S	S	S
0.05	S	S	S	S	S	S	S	S	S	S
0.08	S	S	S	S	S	S	S	S	S	S

S = Shear Specimen Test

TABLE III - VALUES OF STRAIN AND ACTUAL AMPLITUDES

Strain	Amplitude For Shear Specimen (microns/Mils P-P)
0.0005	1.59/0.0625
0.001	3.18/0.125
0.002	6.35/0.25
0.004	12.70/0.5
0.005	15.88/0.625
0.008	25.40/1.0
0.01	31.75/1.25
0.02	63.50/2.5
0.05	158.80/6.25
0.08	254.00/10.0

TABLE IV - COMPOSITION (PARTS BY WEIGHT)

EPDM	
NORDEL 1440	600.0
ZINC OXIDE	30.0
STEARIC ACID	6.0
HAF N330	540.0
SUNPAR 2280	240.0
VULCAFOR 2DBC	12.0
TMTD	3.0
MBT	6.0
SULPHUR	9.0
TOTAL	1446.0

BUNA-N	
PERBUNA N 3302	700.0
ZINC OXIDE	35.0
STEARIC ACID	14.0
N774 SRF BLACK	525.0
DOP	105.0
ANTIOXIDANT 4010NA	7.0
SULPHUR MC	10.5
MBTS	10.5
TMTM	3.5
TOTAL	1410.5

VITON	
VITON B 70	1700.0
SEVACARB MT	510.0
MAGLITE D(MGO)	51.0
STURGE VE	102.0
VITON CURATIVE 20	31.0
VITON CURATIVE 30	54.4
TOTAL	2448.4

NEOPRENE	
NEOPRENE WRT	800.0
MAGLITE D	32.0
FEF N550	520.0
DOS	80.0
CIRCOLITE RPO	40.0
FACTICE 820	64.0
PARAFFIN WAX	8.0
OCTAMINE	8.0
ZINC OXIDE	40:0
STEARIC ACID	8.0
ROBAL PM	6.0
TOTAL	1606.0

TABLE V - THERMAL CONDUCTIVITY (WATTS/METER KELVIN)

VITON TEMPERATURE (DEGREE C)	K
27.7	0.2924
48.4	0.2926
57.7	0.2928
67.4	0.2930
77.6	0.2948
94.4	0.2937
95.1	0.2887
100.7	0.2882
BUNA-N	
28.4	0.4105
37.2	0.4079
46.6	0.4067
57.3	0.4045
66.4	0.4044
78.5	0.3983
87.2	0.3947
98.6	0.3902
NEOPRENE	
32.4	0.4216
36.7	0.4226
50.8	0.4223
66.0	0.4222
101.5	0.4235
EPDM	
32.8	0.3985
45.3	0.3961
56.3	0.3969
65.8	0.3958
76.2	0.3957
85.0	0.3958
94.1	0.3930
103.1	0.3901

TABLE VI - SPECIFIC HEAT (JOULES/GRAM KELVIN)

TEMP. (DEGREE C)	VITON	BUNA-N	NEOPRENE	EPDM
45	1.17	1.45	1.30	1.61
50	1.19	1.49	1.34	1.63
55	1.20	1.50	1.36	1.66
60	1.21	1.53	1.36	1.72
65	1.22	1.54	1.41	1.75
70	1.23	1.57	1.43	1.70
75	1.23	1.60	1.45	1.72
80	1.24	1.63	1.47	1.72
85	1.25	1.66	1.49	1.74
90	1.25	1.69	1.51	1.77
95	1.25	1.71	1.54	1.81
100	1.26	1.70	1.59	1.83

TABLE VII - THERMAL COEFFICIENT OF LINEAR EXPANSION

(Per °C) x 10^5

VITON	15.9
BUNA-N	27.7
NEOPRENE	20.4
EPDM	21.3

TABLE VIII - HARDNESS (SHORE A)

VITON	78
BUNA-N	70
NEOPRENE	74
EPDM	75

VII - TEST RESULTS - ELASTOMER PERFORMANCE LIMITS

Table I presented a schedule of frequency and strain combinations to be tested for EPDM, Buna-N, Viton-70 and Neoprene. However, as previously noted, indications of nonaxial motion or inability to maintain a phase angle difference of between 15° and 165° for various weight combinations would be cause for data rejection. Figures 35 through 46 represent the actual test points which were used to create the material data base. As shown, frequencies as low as 100 Hz (figure 37) and as high as 1100 Hz (figure 43) were achieved at various stages of testing. Figures 35 through 37 provide the test conditions for EPDM, figures 38 through 40 for Buna-N, figures 41 through 43 for Viton-70, and figures 44 through 46 for Neoprene.

Six weights were used throughout this testing. Thus several combinations (including no weight addition) were available to obtain acceptable data. Table IX provides a listing of the weights used.

Data obtained from the minicomputer-based Data Acquisition System has been prepared for presentation in four distinct formats for each material and at each of the temperatures of interest (32°C, 66°C and 80°C). These are:

- Stiffness and damping (N/m) versus frequency (Hz)
- Loss coefficient versus frequency (Hz)
- Stiffness and damping (N/m) versus strain
- Loss coefficient versus strain

Therefore, for figures 47 through 94, a linear least squares curve fit has been obtained with frequency as the independent variable. With strain as the independent variable, a second order least squares fit has been used. Data from these curves have been used to generate figures 95 through 103 which presents temperature and frequency behavior of the loss coefficient for each material. As will be discussed in detail below, the data have also been used for additional nonlinear regression models to provide design curves in a unified format for extracting shear storage and loss moduli as a function of frequency, strain and temperature (figures 104 through 111).

TABLE IX - VALUES OF WEIGHT ADDITIONS

Kg	Lbs
0.974	2.14
1.686	3.71
2.054	4.52
3.025	6.66
7.050	15.5
12.276	27.0

EDPM Test Results

The test results for EPDM are plotted in figures 47 through 50 for 32°C, figures 51 through 54 for 66°C, and figures 55 through 58 for 80°C. The data can be said to suggest the following general trends:

- Stiffness increases with increasing frequency
- Stiffness decreases with increasing temperature
- Loss coefficient slightly decreases with increase in frequency
- Loss coefficient decreases between 32°C and 66°C, but increases between 66°C and 80°C.

To provide some clarity with respect to the sensitivity of loss coefficient with frequency and temperature, figure 98 was generated from the regression curves of figures 47 through 58. From figure 98, it is apparent that the loss coefficient at 32°C is more frequency sensitive than at either 66°C or 80°C. Further, below 400 Hz, the loss coefficient decreases between 32°C and 66°C, but increases for all frequencies from 66°C to 80°C. As these trends are based upon least square curve fits of data which have considerable scatter, one must be cautious in interpretation. This trend may indicate that EPDM is operating closer to the transition region than the rubbery region. Further substantiation of this is the fact that, for all the materials tested, EPDM has the highest value of stiffness reported. Figures 47 through 58 clearly indicate that a wide scatter of data is achieved when plotting data versus frequency and that the compactness and dependency upon strain is more consistent and pronounced.

Buna-N Test Results

Data obtained for the Buna-N specimen is presented in figures 59 through 62 for 32°C, figures 63 through 66 for 66°C, and figures 67 through 70 for 80°C. From this data, the following trends are suggested:

- Stiffness increases with increase in frequency
- Loss coefficient increases with increase in frequency

- Loss coefficient increases or decreases with temperature increase (depending upon frequency domain)
- Stiffness decreases with a temperature increase.

Unlike EPDM, the data for Buna-N suggests a compactness when plotted against frequency, figure 62 and a more pronounced scatter when plotted versus strain, figure 60. A plot of loss coefficient versus frequency for the three temperatures (32°C, 66°C and 80°C), figure 99 indicates an increase and then a decrease in loss coefficient with a corresponding increase in temperature for low frequencies (less than 250 Hz). For higher frequencies the loss coefficient steadily decreases with a temperature rise. Unlike EPDM (figure 98), the loss coefficient of Buna-N increases with an increase in frequency at a prescribed temperature (positive slope of curves on figure 99).

Viton-70 Test Results

Figures 71 through 81 presents the data for Viton-70 from this series of elastomer shear specimen tests. The 32°C data is presented in figures 71 through 74, the 66°C data in figures 75 through 78, and the 80°C data in figures 79 through 81. Viton-70 showed the highest values of loss coefficient for any of the materials tested with values close to 1.0 at 32°C, figure 72. The general data trends for Viton-70 are:

- Stiffness increasing with frequency
- Stiffness decreasing with temperature
- Loss coefficient increasing with frequency
- Loss coefficient decreasing with temperature.

Figure 100 provides a plot of temperature and frequency dependence of the Viton-70 test series. The trends provided by the shear specimen tests for Viton-70 were compared with previous tests performed at MTI on Viton-70 O-rings (ref. 6). Figure 102 shows this comparison. As seen, excellent comparison was achieved and all data appear to provide reasonable results.

The consistency of loss coefficient sensitivity with temperature and frequency strongly suggests that Viton-70 is operating in the rubbery region for elastomers. As temperature was increased, the general compactness of the data was apparent when plotted against frequency (figures 78 and 81), with the large scatter of data when plotted versus strain at lower temperatures (figures 73 and 74).

Neoprene Test Data

The test results for Neoprene are plotted in figures 83 through 86 for 32°C, figures 87 through 90 for 66°C, and figures 91 through 94 for 80°C. The data for Neoprene follows the same general trends as that reported above for Viton-70. The main exception is the magnitude of values. The maximum value of this loss coefficient for Neoprene is approximately 0.3, figure 85 for 32°C, 1100 Hz. As seen from figure 101, the temperature/frequency trends are consistent and again indicate the influence of rubbery behavior for this elastomer.

Material Comparison

The values of loss coefficient obtained from the least squares curve fit have been plotted for the three temperatures for each material. Figure 95 shows the frequency dependent behavior of the four materials at 32°C. Viton-70 has the largest values of loss coefficient for the entire frequency spectrum. The trend of increased loss coefficient with an increase in frequency is maintained by Viton, Neoprene and Buna. Only EPDM shows a reduction of loss coefficient with increase in frequency. EPDM maintains its negative slope for the 66°C data (figure 96) and the 80°C data (figure 97). It is interesting that at 80°C all materials tested show a loss coefficient of between 0.1 and 0.2 for the entire frequency envelope. This trend is shown again in figure 103 which provides an illustration of the sensitivity of the loss coefficient to temperature of all materials tested at 500 Hz.

Power Law Coefficients

The regression curves can be expressed analytically by a power law relationship in frequency. The coefficients have been calculated for the relationships and are provided in table X.

Unified Format Design Curves

By assuming that the first order log approximation is reasonable for frequency dependence and that the influence of strain is reasonably approximated by the second order regression, then further approximation can be achieved to assist in using this data in a design environment. The development of the equations used in this regression process are documented in Appendix A. The final form of the equations are:

$$\log_{10}\left(G'\frac{T_c}{T}\right) = a_7 + a_2\left(\log_{10}\alpha_T + \log_{10}\omega\right) + a_4\log_{10}\varepsilon + a_5\left(\log_{10}\varepsilon\right)^2;\ a_7 = \log_{10}a_6$$

$$\log_{10}\left(G''\frac{T_c}{T}\right) = b_7 + b_2\left(\log_{10}\alpha_T + \log_{10}\omega\right) + b_4\log_{10}\varepsilon + b_5\left(\log_{10}\varepsilon\right)^2;\ b_7 = \log_{10}b_6$$

where a_5 through a_7, b_5 through b_7 have been determined from a least squares evaluation of the elastomer data obtained from shear testing: further defining

G', and G" as the storage and loss shear moduli

$$\log_{10}\alpha_T = \frac{C_1\,(T-T_c)}{C_2 + (T-T_c)}$$

where C_1, C_2 are constants per table XI

T_c is the characteristic temperature (°K) per table XI

ω is the circular frequency (rad/sec)

T is the temperature (°K)

ε is the strain

TABLE X - POWER LAW COEFFICIENTS

	STIFFNESS COEFFICIENT		DAMPING COEFFICIENT		LOSS COEFFICIENT	
	A_1	B_1	A_2	B_2	A_3	B_3
EPDM-32°C	1.500×10^7	0.005724	2.586×10^6	0.03136	0.1724	-0.02588
EPDM-66°C	8.372×10^6	0.08814	1.346×10^6	0.0529	0.1601	-0.03524
EPDM-80°C	3.194×10^6	0.01985	9.204×10^6	0.09834	0.2882	-0.1002
BUNA-N-32°C	3.523×10^6	0.1435	4.980×10^4	0.5215	0.01413	0.3780
BUNA-N-66°C	1.543×10^6	0.1822	6.346×10^4	0.3736	0.04113	0.1914
BUNA-N-80°C	2.620×10^6	0.1157	1.057×10^5	0.2731	0.04033	0.1574
VITON-70-32°C	1.384×10^6	0.3359	4.203×10^4	0.7276	0.03037	0.3918
VITON-70-66°C	4.132×10^6	0.1200	5.729×10^4	0.4805	0.01386	0.3605
VITON-70-80°C	4.973×10^6	0.08202	1.753×10^5	0.2753	0.03525	0.1933
NEOPRENE-32°C	3.088×10^6	0.1673	2.455×10^5	0.3019	0.1258	0.013
NEOPRENE-66°C	1.630×10^6	0.2167	1.844×10^5	0.2526	0.1132	0.03588
NEOPRENE-80°C	3.979×10^6	0.1003	3.664×10^5	0.01415	0.0921	0.04116

WHERE: STIFFNESS: $k' = A_1\omega^{B1}$ N/m

DAMPING: $k'' = A_2\omega^{B2} = \eta k'$ N/m

LOSS COEFFICIENT: $\eta = A_3\omega^{B3}$

ω IS CIRCULAR FREQUENCY RAD/SEC

TABLE XI

Values for C_1, C_2 and Characteristic Temperature (T_c)

for the Test Materials

Elastomer Material	C_1	C_2	T_c (°K)**
Viton (CFM)	-8.86	101.6	306
Buna-N (NBR)	-8.86	101.6	293
Neoprene (CR)	-8.86	101.6	272
EPDM	-8.86	101.6	267

** Estimated from transition temperature (Tg + 50)

By applying the results of the regression analysis for the purposes of developing design curves, figures 104 through 111 result where:

- EPDM properties are shown in figures 104 and 105
- Buna-N properties are shown in figures 106 and 107
- Viton-70 properties are shown in figures 108 and 109
- Neoprene properties are shown in figures 110 and 111

The steps necessary to use the design curves are as follows:

1. Select a frequency of interest (ω, rad/sec)
2. Select a temperature of interest (T, °K)
3. Find values of C_1, C_2 and T_c from table XI
4. Calculate α_T
5. Find values of reduced moduli $(G' \frac{T_c}{T})$, $(G'' \frac{T_c}{T})$
6. Calculate G' and G"

Physical and Chemical Properties

Physical and chemical properties as reported by Rubber and Plastics Research, Association of Great Britain (RAPRA) are reported in Tables IV through VIII and contain composition, thermal conductivity, specific heat, thermal coefficient of expansion and hardness.

VIII - CONCLUSIONS/RECOMMENDATIONS - ELASTOMER PERFORMANCE LIMITS

The following observations have been made from the results of these tests:

- Viton-70 is extremely sensitive to frequency and temperature (loss coefficient rises with increasing frequency and falls with increasing temperature).
- Unlike the other materials, loss coefficient for Viton-70 falls at high strain (may be related to self-heating and temperature sensitivity).
- Unlike the other materials, loss coefficient for EPDM falls with increasing frequency.
- At low temperature, the loss coefficient for Viton-70 (0.7) is substantially higher and Buna-N (0.15) somewhat lower than for the other materials.
- At high temperature, the loss coefficients for all the materials are approximately equal (0.15) for an excitation of 500 Hz.
- Buna-N and EPDM are the least affected by temperature.
- Elastomers capable of withstanding temperatures in excess of 400°F should be evaluated for dynamic properties.
- Hot rig testing of elastomer dampers is recommended to permit evaluation of dampers in controlled thermal environments.
- Materials with loss coefficients in excess of the 0.15 value at 80°C should be evaluated to provide a more flexible data base for elastomer damper design.

APPENDIX A

APPENDIX A

Treating the distortion in the shear specimens as pure shear, the shear storage and loss moduli are directly proportional to the measured stiffness and damping values, respectively, and may be calculated from

$$G' = K'\frac{t}{A} \tag{A-1}$$

$$G'' = K''\frac{t}{A} \tag{A-2}$$

where

G' = shear storage modulus - N/m^2
G'' = shear loss modulus - N/m^2
K' = stiffness of shear specimen (real part) - N/m
K'' = damping of shear specimen (imaginary part of stiffness) - N/m
t = thickness of shear elements - m
A = total bonded area (one side only) of shear elements - m^2

Thus the shear moduli (like the stiffness and damping) are functions of frequency, temperature and dynamic strain.

Assuming that dynamic strain is the other important independent variable and that the effects of strain and reduced frequency can be separated, the reduced shear moduli are given by

$$G'_r = f'(\alpha_T\omega)\, g'(\varepsilon) \tag{A-3}$$

$$G''_r = f''(\alpha_T\omega)\, g''(\varepsilon) \tag{A-4}$$

where the f's and g's represent unknown functions, $\alpha_T\omega$ is the reduced frequency, and ε is the dynamic strain. The coefficient α_T is determined from

$$\log_{10}\alpha_T = \frac{C_1(T - T_c)}{C_2 + (T - T_c)} \tag{A-5}$$

where the constants C_1 and C_2 depend on the elastomer material composition.

Using the approximation that the logarithms of the shear moduli vary approximately linearly with the logarithm of the frequency and extending

this relationship to the reduced frequency, the logarithm of the functions f' and f" are linearly related to the logarithm of the reduced frequency. Thus, the functions themselves are of the form

$$f'(\alpha_T\omega) = a_1(\alpha_T\omega)^{a_2} \tag{A-6}$$

$$f''(\alpha_T\omega) = b_1(\alpha_T\omega)^{b_2} \tag{A-7}$$

where the a's and b's are constants which are determined empirically for any particular elastomer material.

The logarithms of the shear moduli have been shown to possess a quadratic relationship to the logarithm of the dynamic strain. Thus, the logarithm of the functions g' and g" take the form

$$\log_{10}g'(\varepsilon) = a_3 + a_4 \log_{10}\varepsilon + a_5(\log_{10}\varepsilon)^2 \tag{A-8}$$

$$\log_{10}g''(\varepsilon) = b_3 + b_4 \log_{10}\varepsilon + b_5(\log_{10}\varepsilon)^2 \tag{A-9}$$

to give

$$g'(\varepsilon) = a_3'\varepsilon^{a_4 + (a_5\log_{10}\varepsilon)} \tag{A-10}$$

$$g''(\varepsilon) = b_3'\varepsilon^{b_4 + (b_5\log_{10}\varepsilon)} \tag{A-11}$$

where a_3' and b_3' are the antilogarithms of a_3 and b_3, respectively, i.e.,

$$a_3' = 10^{a_3},\quad b_3' = 10^{b_3}$$

Equations (A-6), (A-7), (A-8) and (A-9) may be substituted into equation (A-3) and (A-4) to give the reduced shear moduli as

$$G_r' = a_6(\alpha_T\omega)^{a_2}\varepsilon^{a_4(a_5\log_{10}\varepsilon)};\quad a_6 = a_1 \cdot a_3' \tag{A-12}$$

$$G_r'' = b_6(\alpha_T\omega)^{b_2}\varepsilon^{b_4(b_5\log_{10}\varepsilon)};\quad b_6 = b_1 \cdot b_3' \tag{A-13}$$

The relations for the original shear moduli can be determined from the definition reduced frequency, $G'_r = G' \left(\frac{T_c}{T}\right)$; $G''_r = G'' \left(\frac{T_c}{T}\right)$; then:

$$G' = a_6\left(\frac{T}{T_c}\right) (\alpha_T\omega)^{a_2}\varepsilon^{a_4}\varepsilon^{(a_5\log_{10}\varepsilon)} \tag{A-14}$$

$$G'' = b_6\left(\frac{T}{T_c}\right)(\alpha_T\omega)^{b_2}\varepsilon^{b_4}\varepsilon^{(b_5\log_{10}\varepsilon)} \tag{A-15}$$

Equations (A-14) and (A-15) can be made linear with respect to the unknown coefficients by taking the logarithm of both sides of these equations to give

$$\log_{10}\left(G'\frac{T_c}{T}\right) = a_7 + a_2(\log_{10}\alpha_T + \log_{10}\omega) + a_4\log_{10}\varepsilon + a_5(\log_{10}\varepsilon)^2 \quad 1\ a_7 = \log_{10}a_6 \tag{A-16}$$

$$\log_{10}\left(G''\frac{T_c}{T}\right) = b_7 + b_2(\log_{10}\alpha_T + \log_{10}\omega) + b_4\log_{10}\varepsilon + b_5(\log_{10}\varepsilon)^2;\ b_7 = \log_{10}b_6 \tag{A-17}$$

From the experimental data which has been generated for a particular elastomer material, the unknown coefficients of equations (A-16) and (A-17) can be found using a standard statistical regression analysis. The results have been plotted in figures 105 through 111.

APPENDIX B

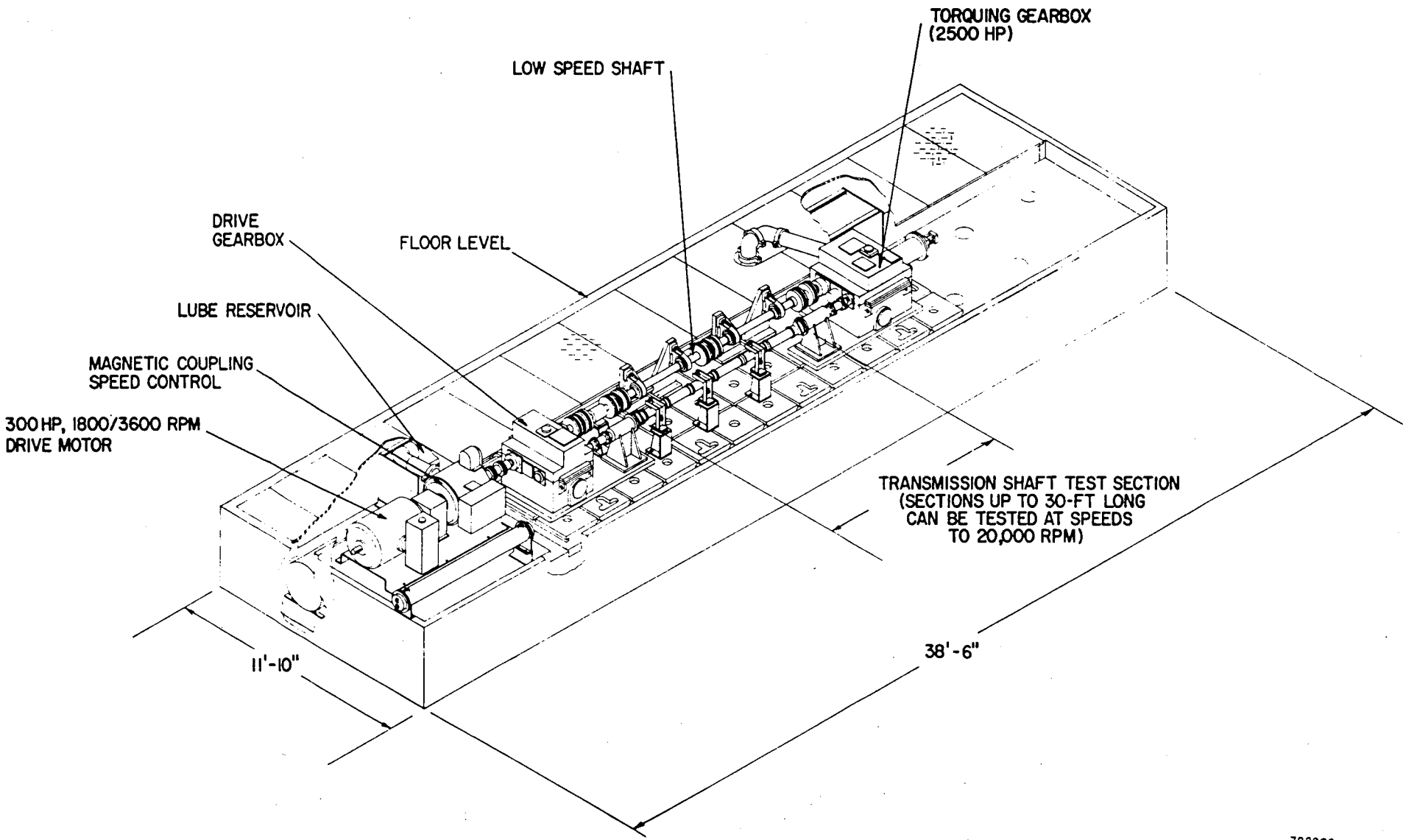

Figure 1 Drive Train Technology Test Rig Configuration for High-Speed Shaft Balancing

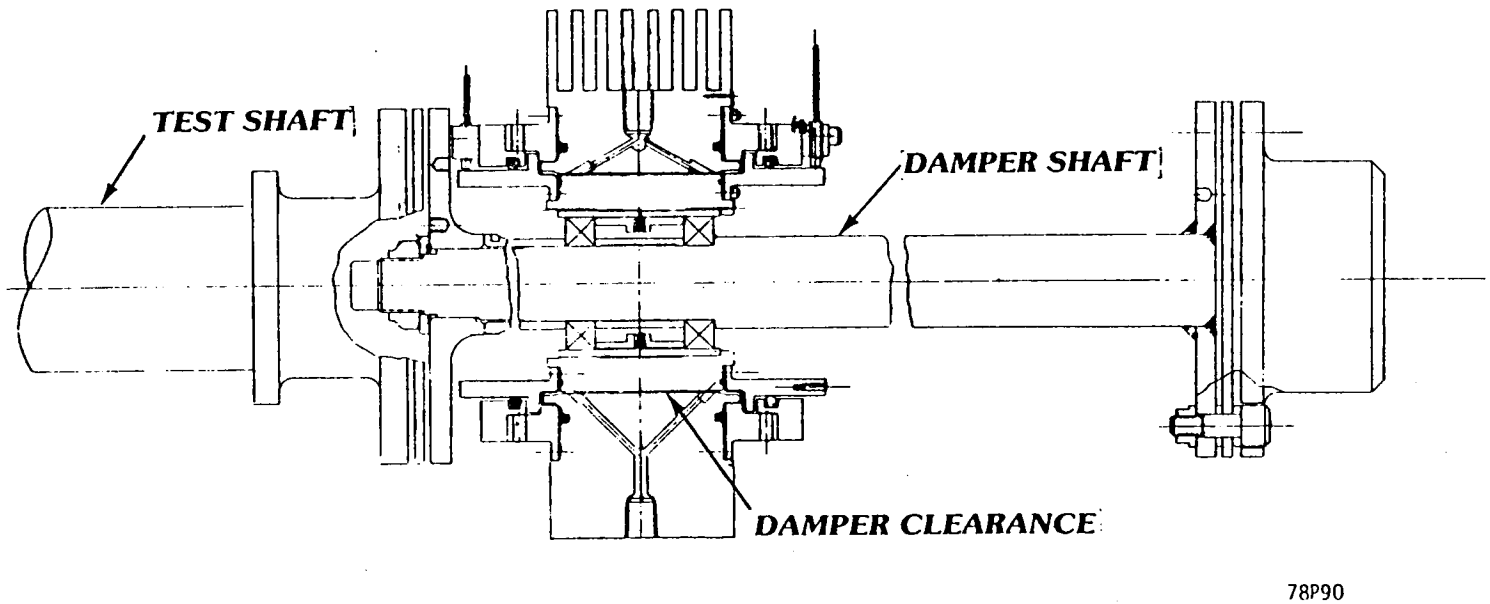

Figure 2 Sketch of Squeeze-Film Damper Designed to Suppress Vibrations in Supercritical Power Transmission Shaft

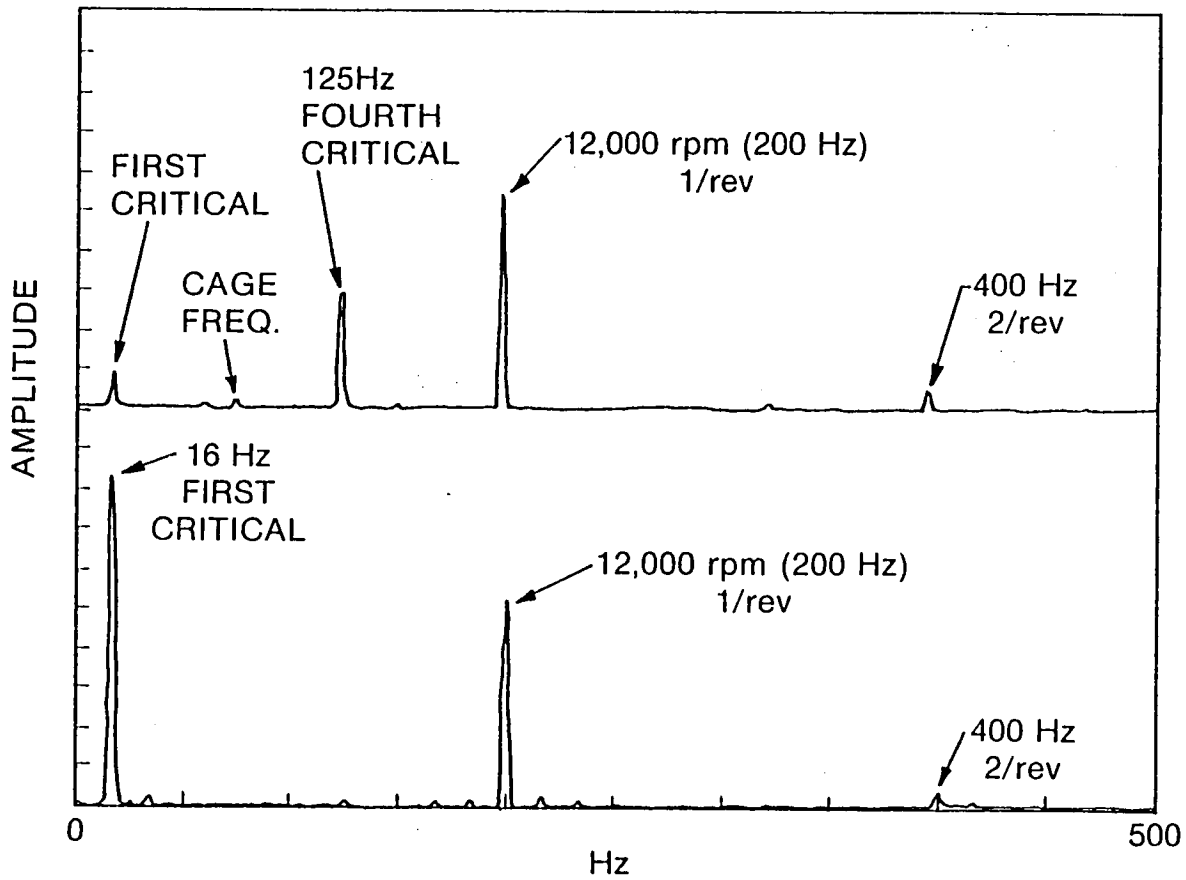

Figure 3 Frequency Spectrum Plots of Test Shaft Vibrations with a Squeeze-Film Damper Running Near 12,000 rpm

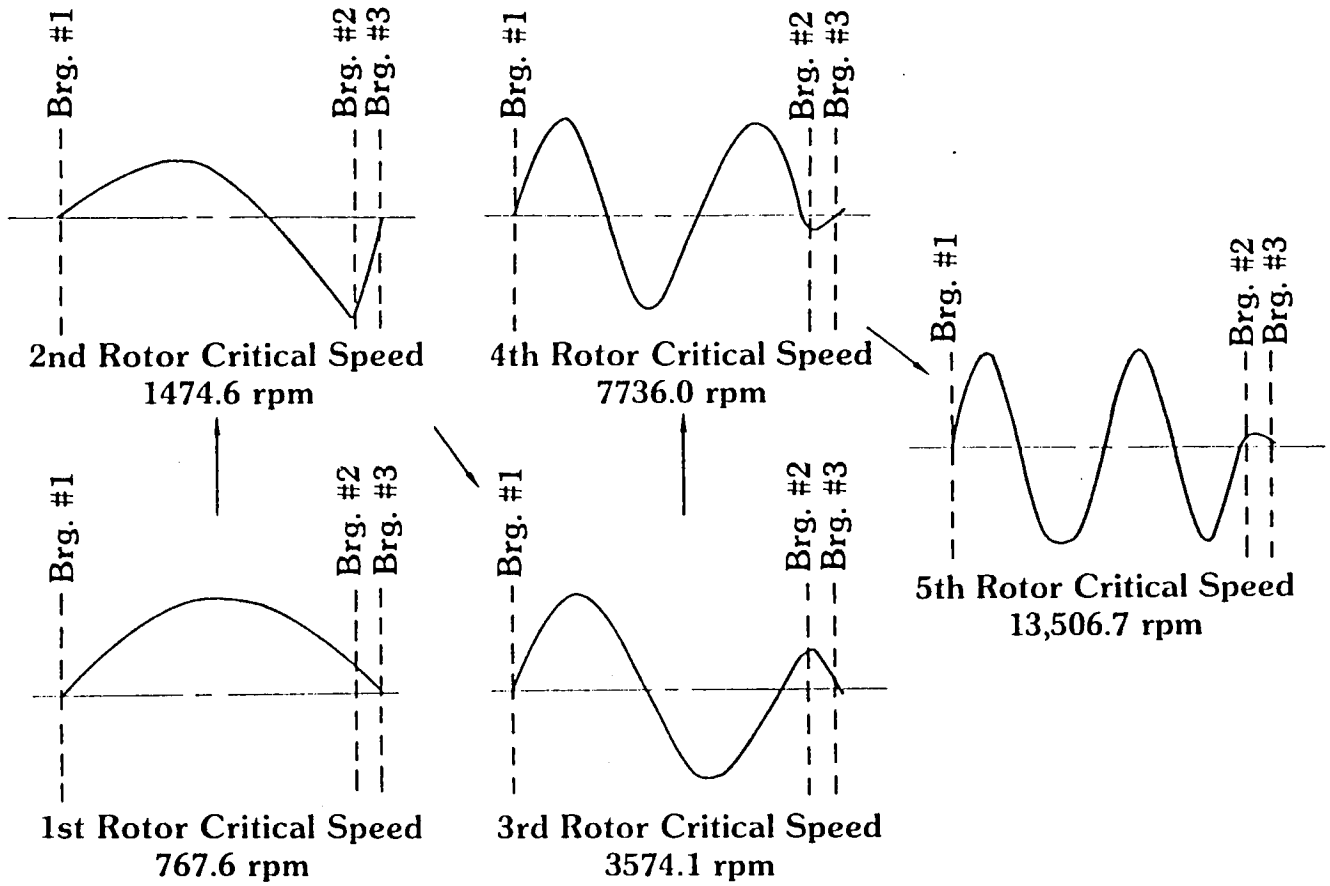

Figure 4 Mode Shapes of the First Five Critical Speeds, Original Shaft with Extension To Carry Squeeze-Film Dampers

801192

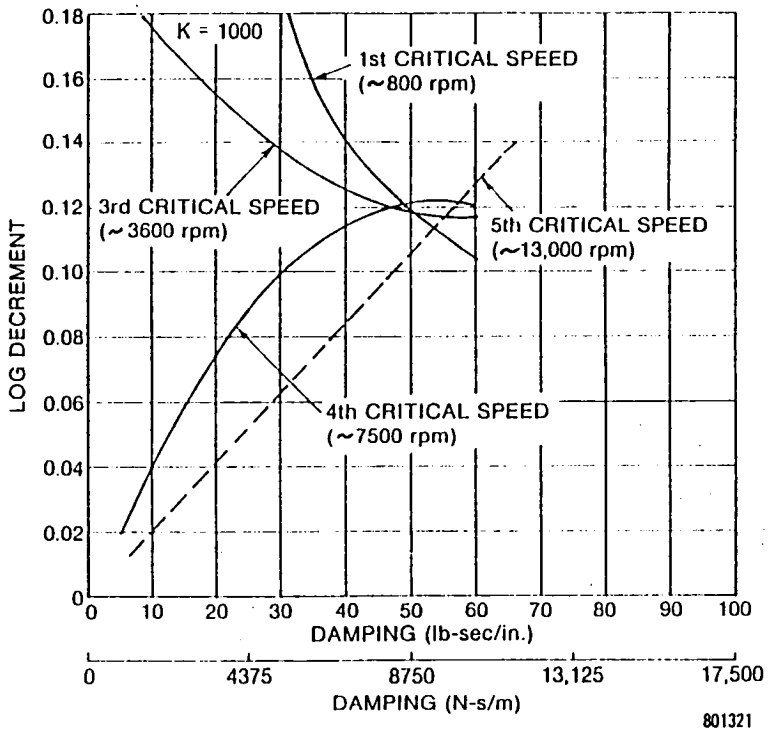

Figure 5a Log Decrement as a Function of Damping (Stiffness = 1.75 × 10^5 N/m [1,000 lb/in.])

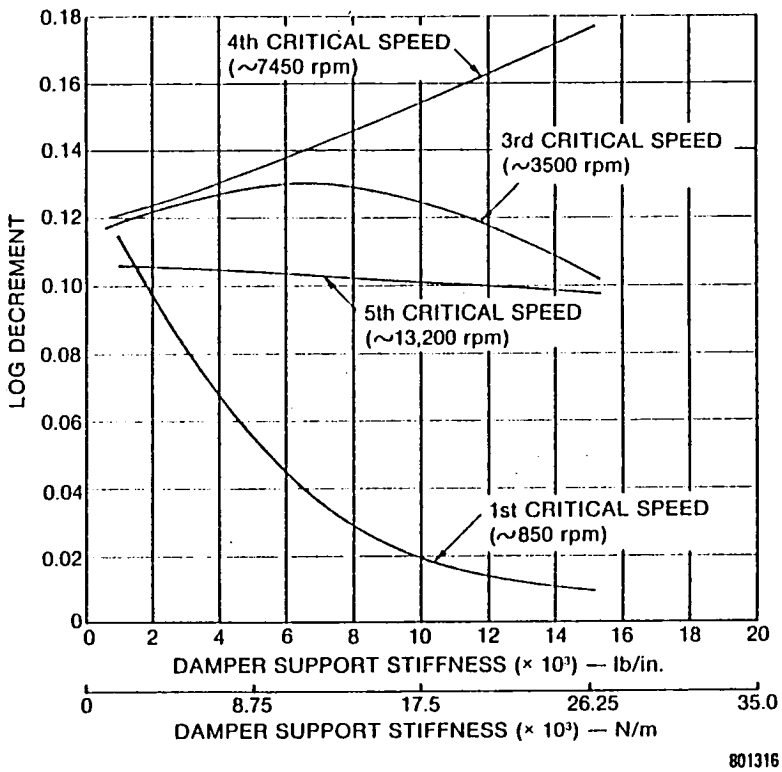

Figure 5b Log Decrement as a Function of Support Stiffness (Damping = 8,750 N-s/m [50 lb-sec/in.])

FLEX. SHAFT - SPLINE COUPLING ANALYSIS - TPROPOSAL NASA 11-6-78 F.G.

NO.STATIONS	NO.BEARINGS	MATERIALS	LOG.DECRMNT	NO.TABLES	NO.SPEEDS	ITERATIONS	ADJ.VECTOR	INPUT	N365C	NOMEG
32	3	3	0	0	1	15	0	1	3	0

52

IPRINT	IUNITS	MDIAG	NCOUP
0	0	0	22

CONV.EXTRAPOL.	CONV.ITERATION
.1000000E-04	.1000000E-04

ROTOR DATA

STATION	MASS,LBS	POLAR M.IN	TRNSV.M.IN	LENGTH	DIA(STIFF)	DIA(MASS)	INNER DIA.	YOUNGS MOD	(SHEAR)*G	DENSITY
1	0.	0.	0.	.2400E+02	.3000E+01	.3000E+01	.2750E+01	.1000E+08	.2989E+07	.1000E+00
2	0.	0.	0.	.5000E+00	.3000E+01	.3889E+01	.2750E+01	.1000E+08	.2989E+07	.1000E+00
3	0.	0.	0.	.1750E+02	.3000E+01	.3000E+01	.2750E+01	.1000E+08	.2989E+07	.1000E+00
4	0.	0.	0.	.5000E+00	.3000E+01	.3889E+01	.2750E+01	.1000E+08	.2989E+07	.1000E+00
5	0.	0.	0.	.1750E+02	.3000E+01	.3000E+01	.2750E+01	.1000E+08	.2989E+07	.1000E+00
6	0.	0.	0.	.5000E+00	.3000E+01	.3889E+01	.2750E+01	.1000E+08	.2989E+07	.1000E+00
7	0.	0.	0.	.1750E+02	.3000E+01	.3000E+01	.2750E+01	.1000E+08	.2989E+07	.1000E+00
8	0.	0.	0.	.5000E+00	.3000E+01	.3889E+01	.2750E+01	.1000E+08	.2989E+07	.1000E+00
9	0.	0.	0.	.1750E+02	.3000E+01	.3000E+01	.2750E+01	.1000E+08	.2989E+07	.1000E+00
10	0.	0.	0.	.5000E+00	.3000E+01	.3889E+01	.2750E+01	.1000E+08	.2989E+07	.1000E+00
11	0.	0.	0.	.1750E+02	.3000E+01	.3000E+01	.2750E+01	.1000E+08	.2989E+07	.1000E+00
12	0.	0.	0.	.5000E+00	.3000E+01	.3889E+01	.2750E+01	.1000E+08	.2989E+07	.1000E+00
13	0.	0.	0.	.1750E+02	.3000E+01	.3000E+01	.2750E+01	.1000E+08	.2989E+07	.1000E+00
14	0.	0.	0.	.5000E+00	.3000E+01	.3889E+01	.2750E+01	.1000E+08	.2989E+07	.1000E+00
15	0.	0.	0.	.1150E+02	.3000E+01	.3000E+01	.2750E+01	.1000E+08	.2989E+07	.1000E+00
16	0.	0.	0.	.3140E+01	.3000E+01	.3000E+01	.2750E+01	.1000E+08	.2989E+07	.1000E+00
17	0.	0.	0.	.5000E+00	.3000E+01	.4325E+01	.2750E+01	.1000E+08	.2989E+07	.1000E+00
18	0.	0.	0.	.1900E+00	.3000E+01	.3400E+01	.2750E+01	.1000E+08	.2989E+07	.1000E+00
19	0.	0.	0.	.1480E+01	.3000E+01	.3325E+01	.2750E+01	.1000E+08	.2989E+07	.1000E+00
20	0.	0.	0.	.1900E+00	.3000E+01	.3400E+01	.2750E+01	.1000E+08	.2989E+07	.1000E+00
21	0.	0.	0.	.6790E+00	.3000E+01	.6550E+01	.2750E+01	.1000E+08	.2989E+07	.1000E+00
22	0.	0.	0.	.1000E-02	.1000E+00	0.	0.	.3000E+08	.8680E+07	.2830E+00
23	.1933E+01	.9017E+01	.4550E+01	.5000E+00	.1378E+01	.1378E+01	0.	.3000E+08	.8650E+07	.2830E+00
24	.3300E+00	.5030E+00	.2500E+00	.5000E+00	.1378E+01	.1378E+01	0.	.3000E+08	.8650E+07	.2830E+00
25	0.	0.	0.	.2330E+01	.1620E+01	.1620E+01	0.	.3000E+08	.8650E+07	.2830E+00
26	.7480E+00	0.	0.	.1200E+01	.1378E+01	.1378E+01	0.	.3000E+08	.8650E+07	.2830E+00
27	0.	0.	0.	.4220E+01	.1700E+01	.1700E+01	0.	.3000E+08	.8650E+07	.2830E+00
28	0.	0.	0.	.4780E+01	.1700E+01	.1700E+01	0.	.3000E+08	.8650E+07	.2830E+00
29	.5840E+00	.7710E+00	.4340E+00	.1000E+01	.1250E+01	.1250E+01	0.	.3000E+08	.8650E+07	.2830E+00
30	.4070E+00	0.	0.	.5000E+00	.3000E+01	.3000E+01	.2460E+01	.1000E+08	.2989E+07	.1000E+00
31	0.	0.	0.	.1000E+01	.3210E+01	.3210E+01	.2680E+01	.1000E+08	.2989E+07	.1000E+00
32	0.	0.	0.	0.	0.	0.	0.	.1000E+08	.2989E+07	.1000E+00

ASYMMETRIC ROTOR ANALYSIS
ELASTIC ASYMMETRY AT THE FOLLOWING STATIONS

STA. NO.	NOMINAL DIAM. (D) - INCH	DISTANCE A/C FLATS (F)-INCH	MOMENTS OF INERTIA I-XI	I-ETA
60	0.	0.	.1000E+01	.1000E+01

ROTOR WEIGHT	TRANS.MOM.IN	POLAR MOM,IN	STATION 1-CG	ROTOR LENGTH
.3392243E+02	.8989189E+05	.6789199E+02	.1114959E+03	.1662100E+03

Figure 6 Rotor Model Data

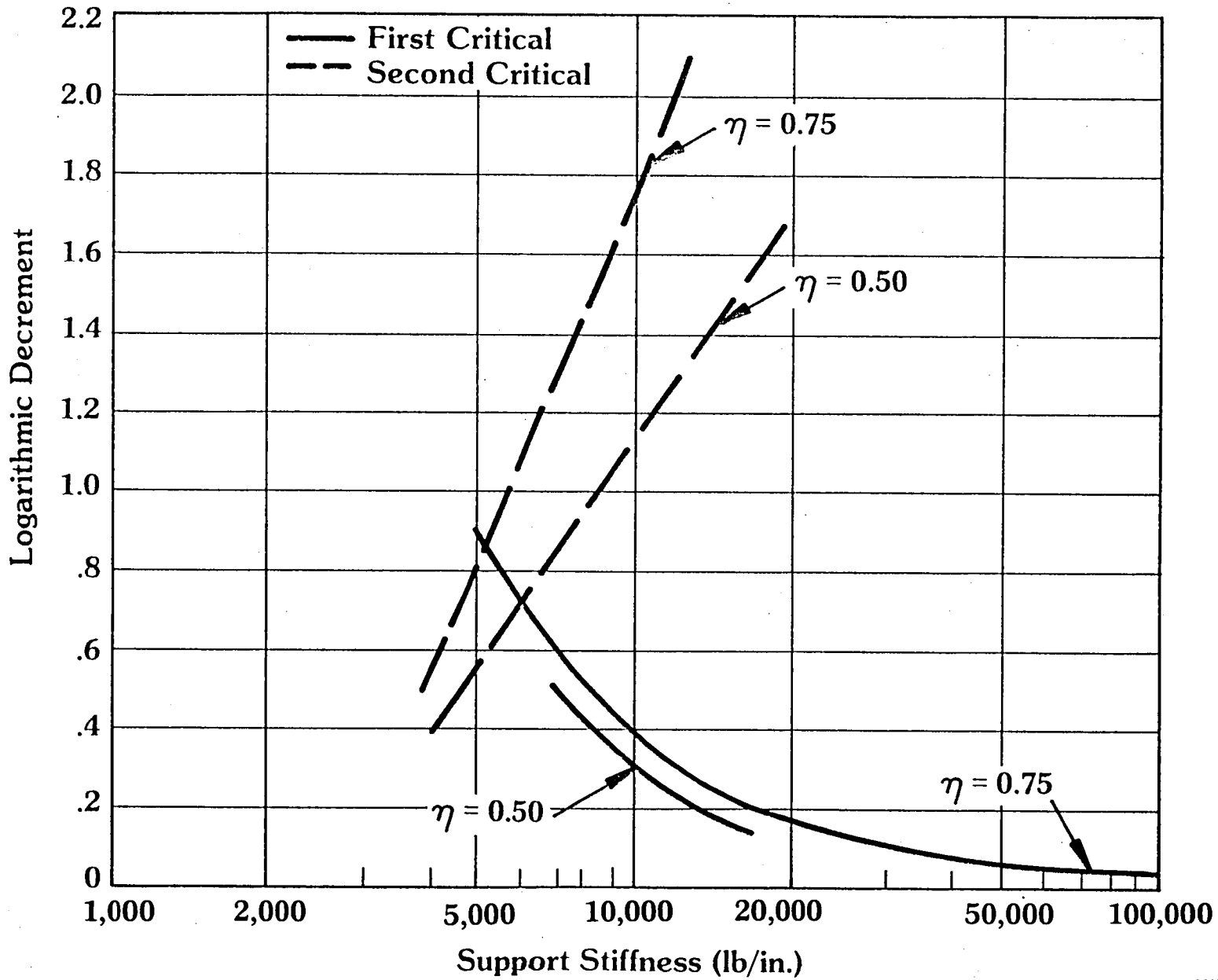

Figure 7 Log Decrement of First and Second Modes as a Function of Elastomeric Damper Properties

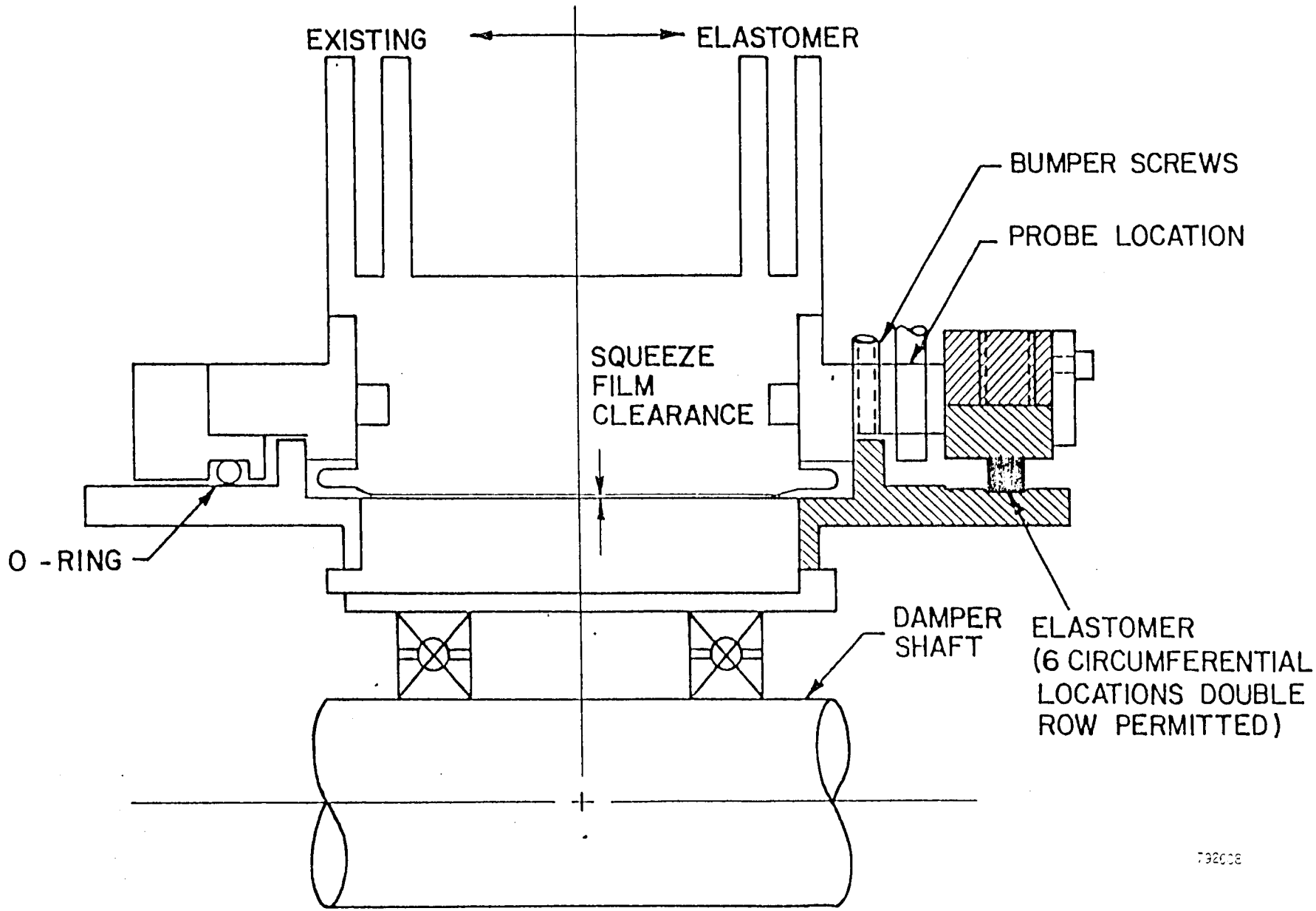

Figure 8 Elastomer Damper for Supercritical Shaft

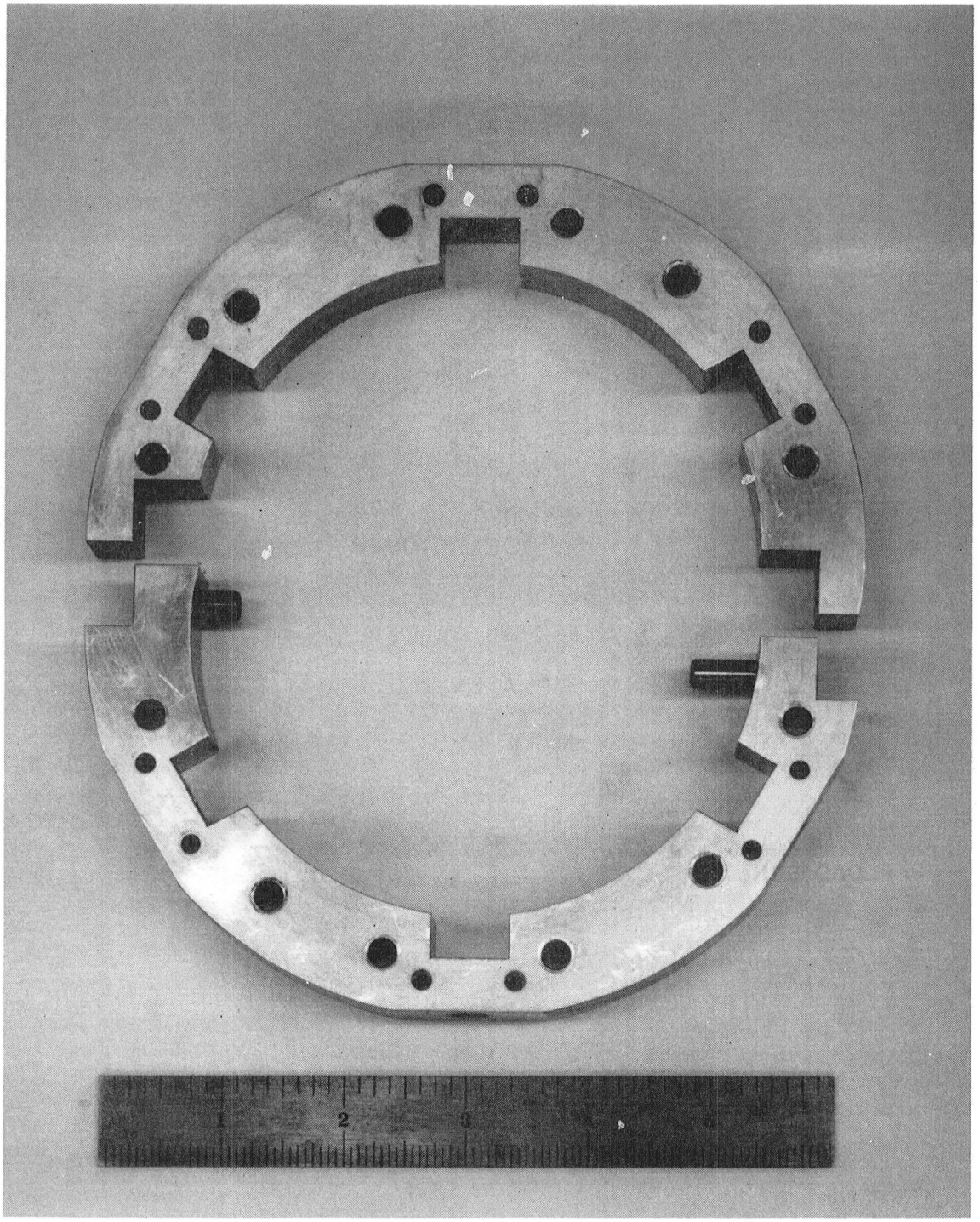

Figure 9 Split Ring Configuration Elastomer Damper

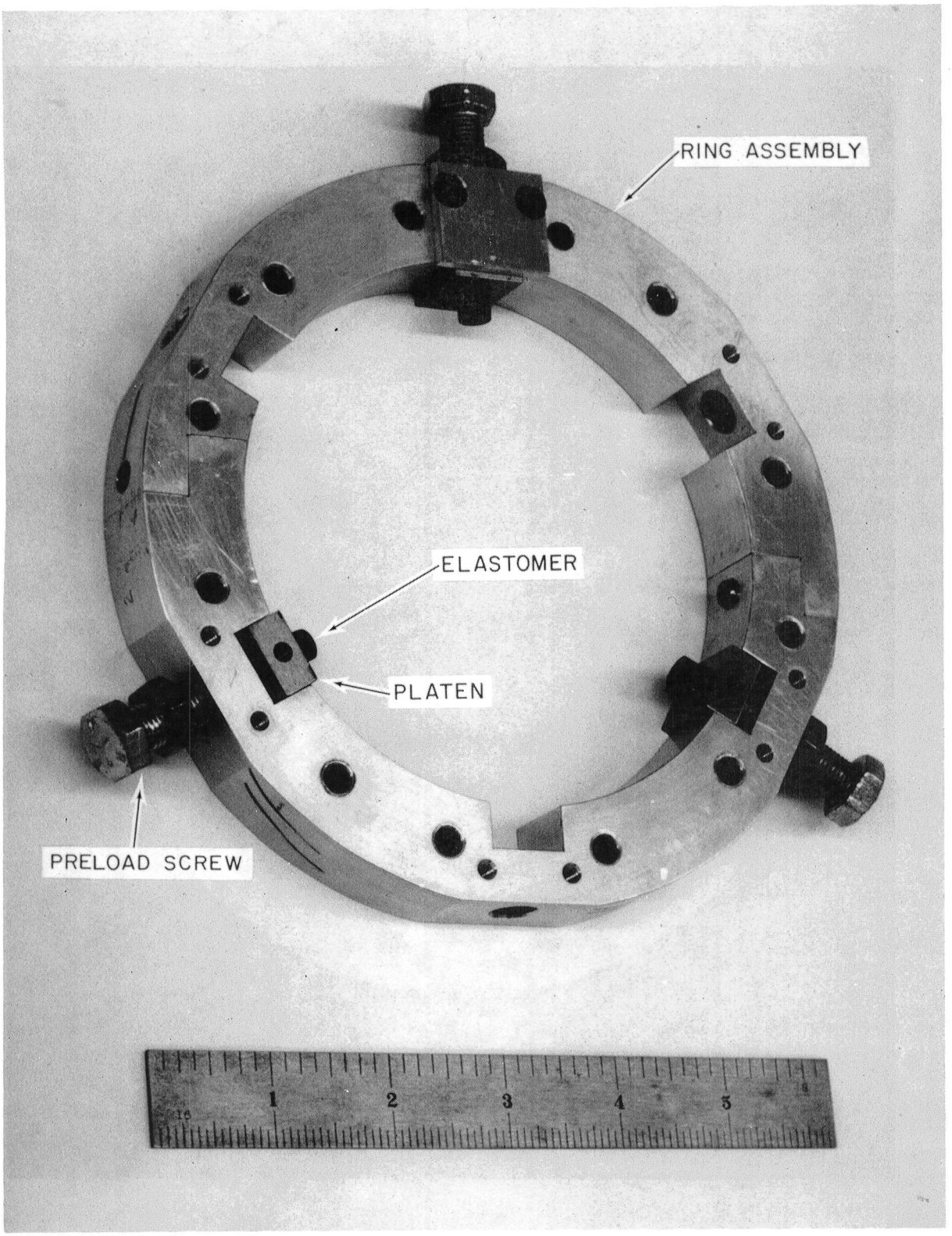

Figure 10 Elastomer Damper Assembly

MTI-18795

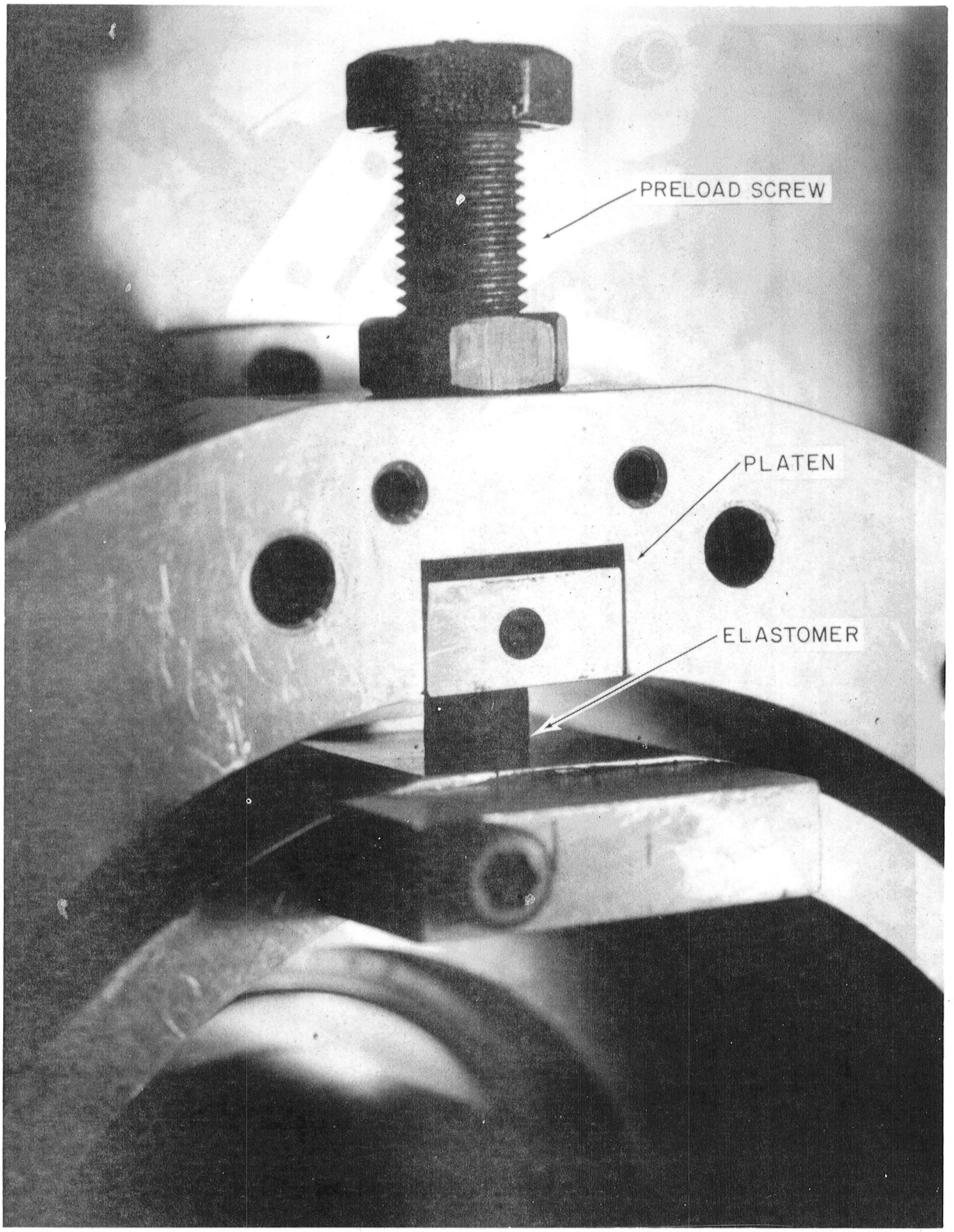

Figure 11 Elastomer Damper Installation

MTI-18794

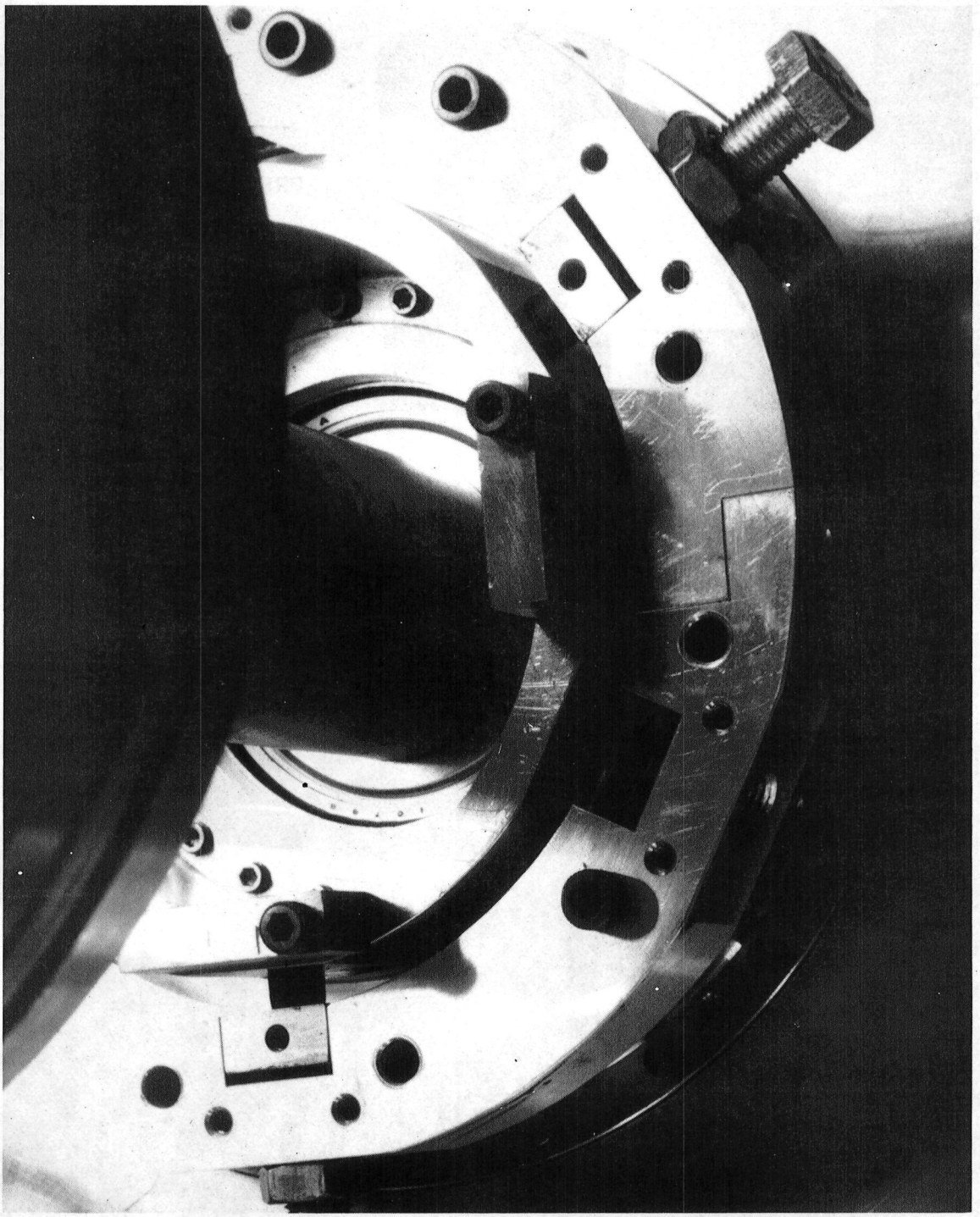

Figure 12 Alternate View of Elastomer Damper Installation

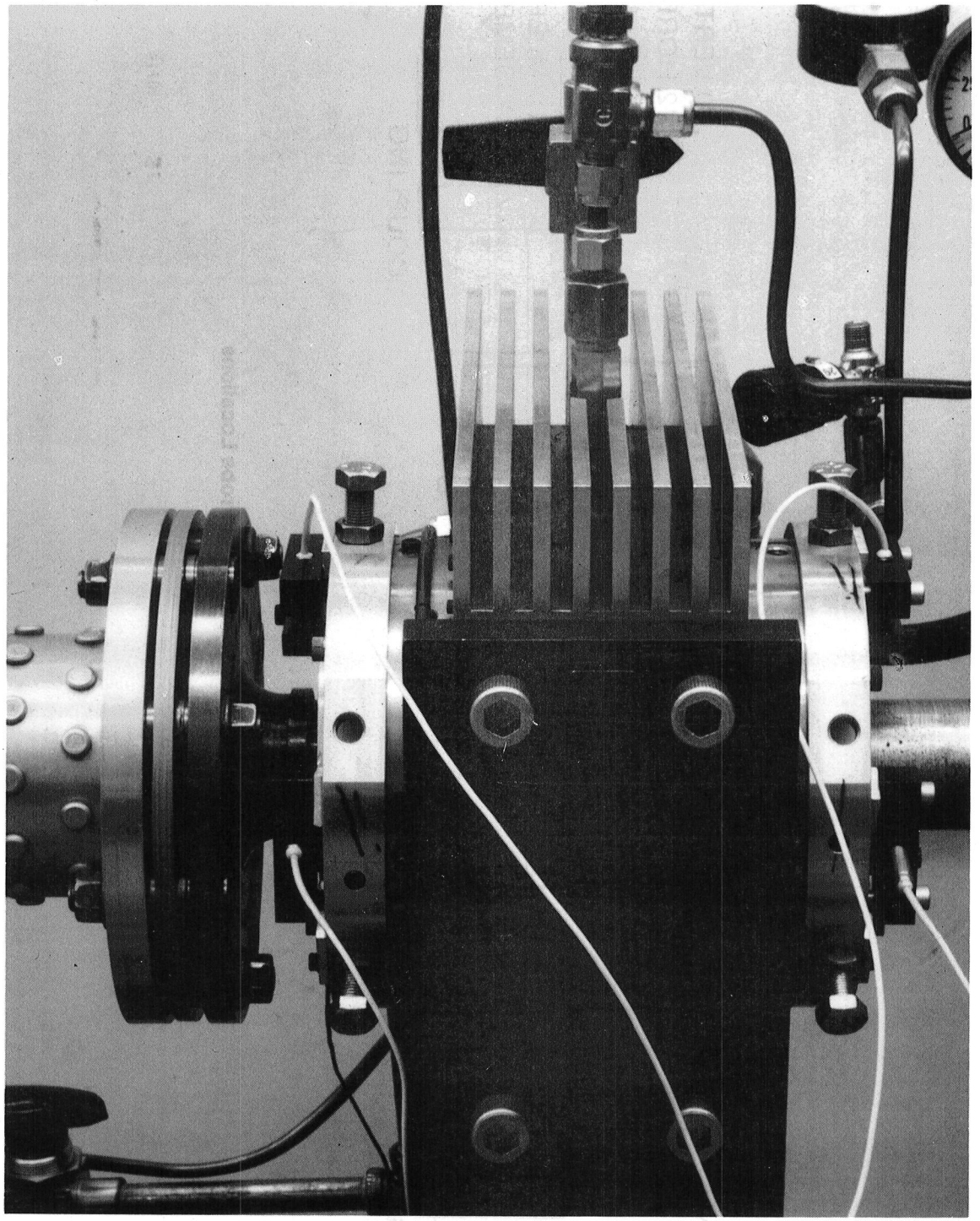

Figure 13 Elastomer Damper Modification of Squeeze-Film Assembly

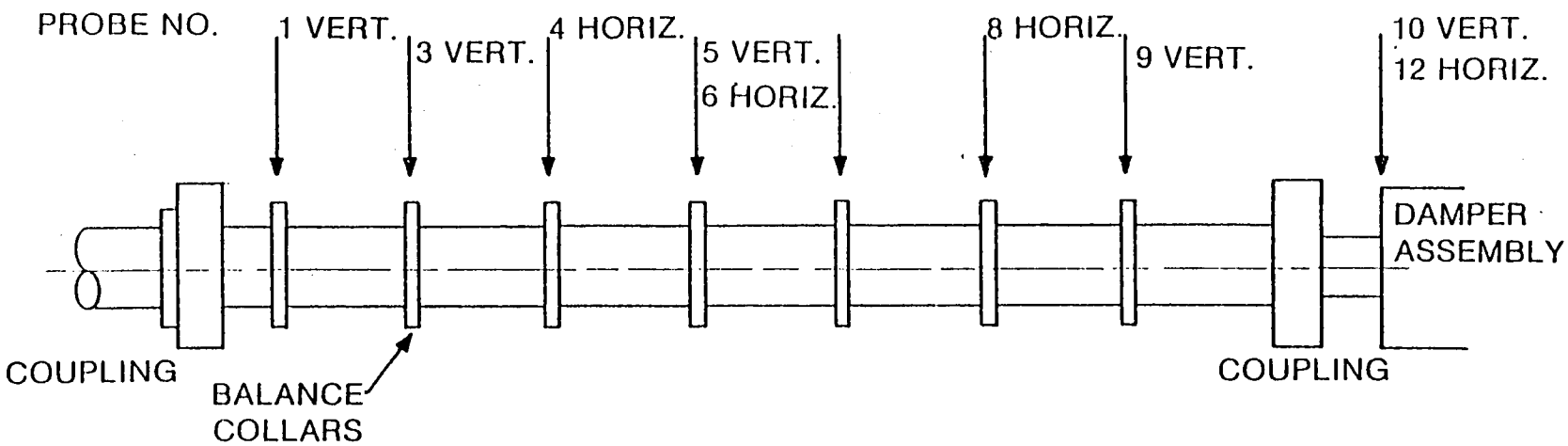

Figure 14 Schematic of Test Assembly and Probe Locations

80715

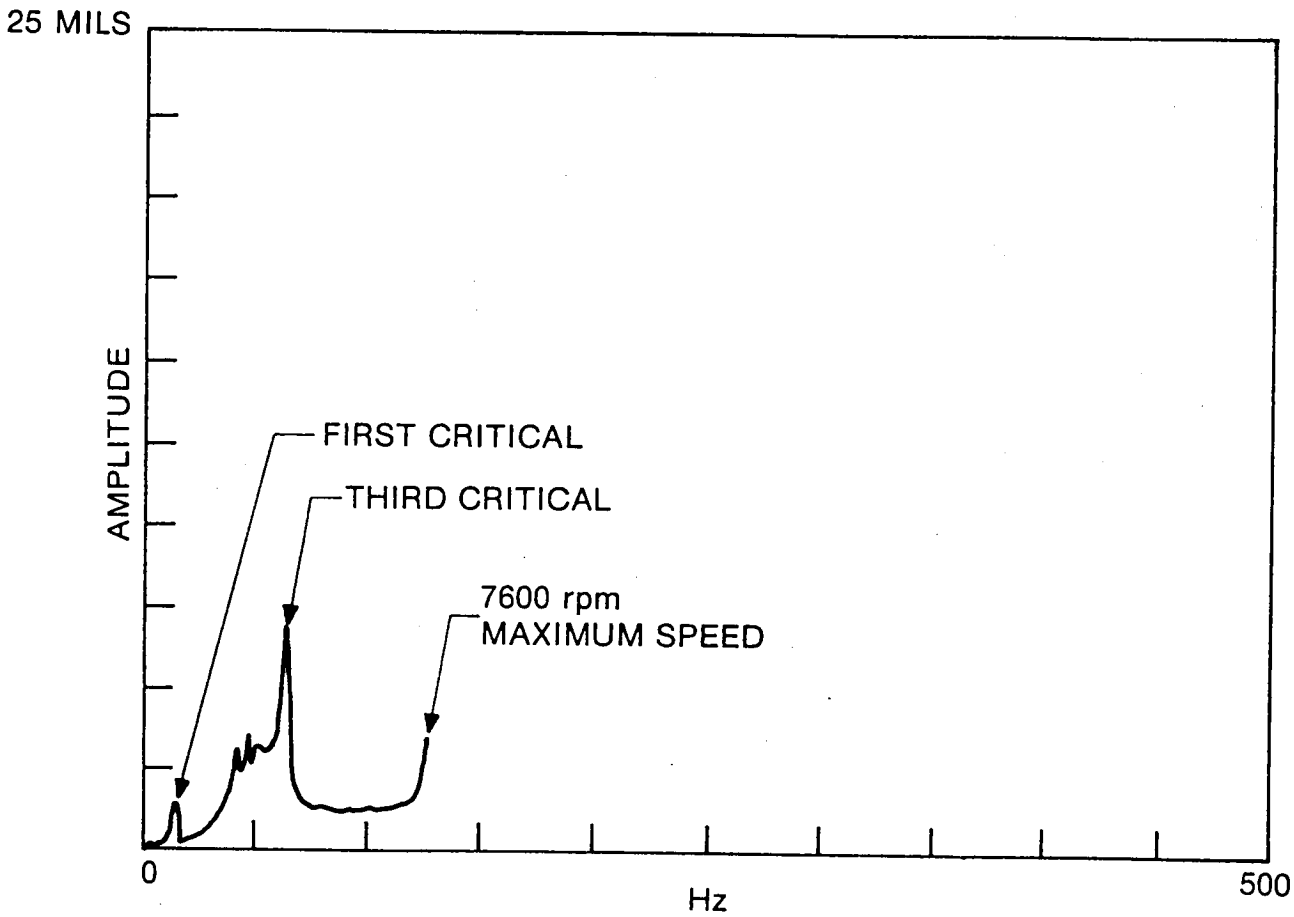

Figure 15 Damper Probe #12, Synchronous Response with Elastomer Damper

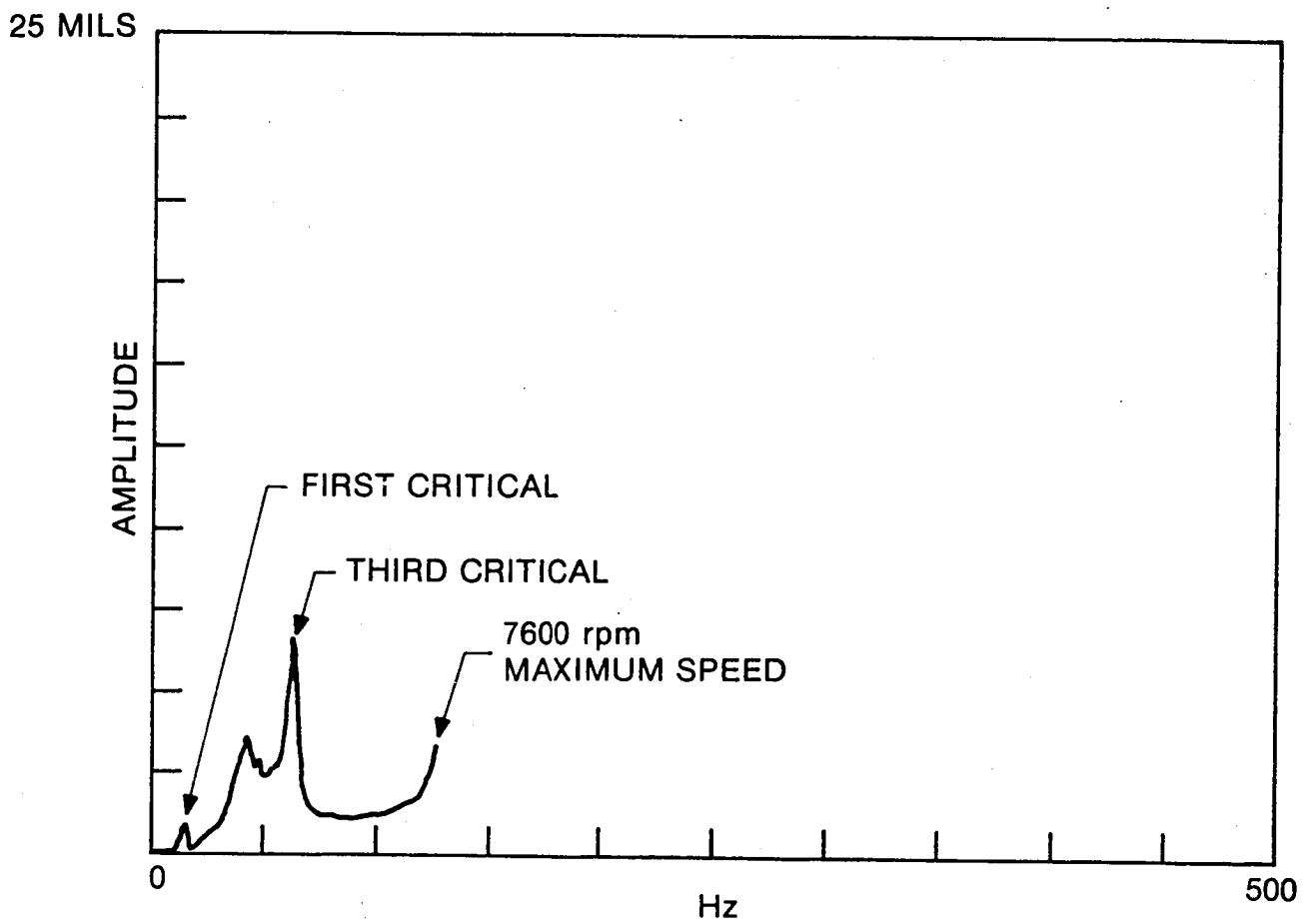

Figure 16 Damper Probe #10, Synchronous Response with Elastomer Damper

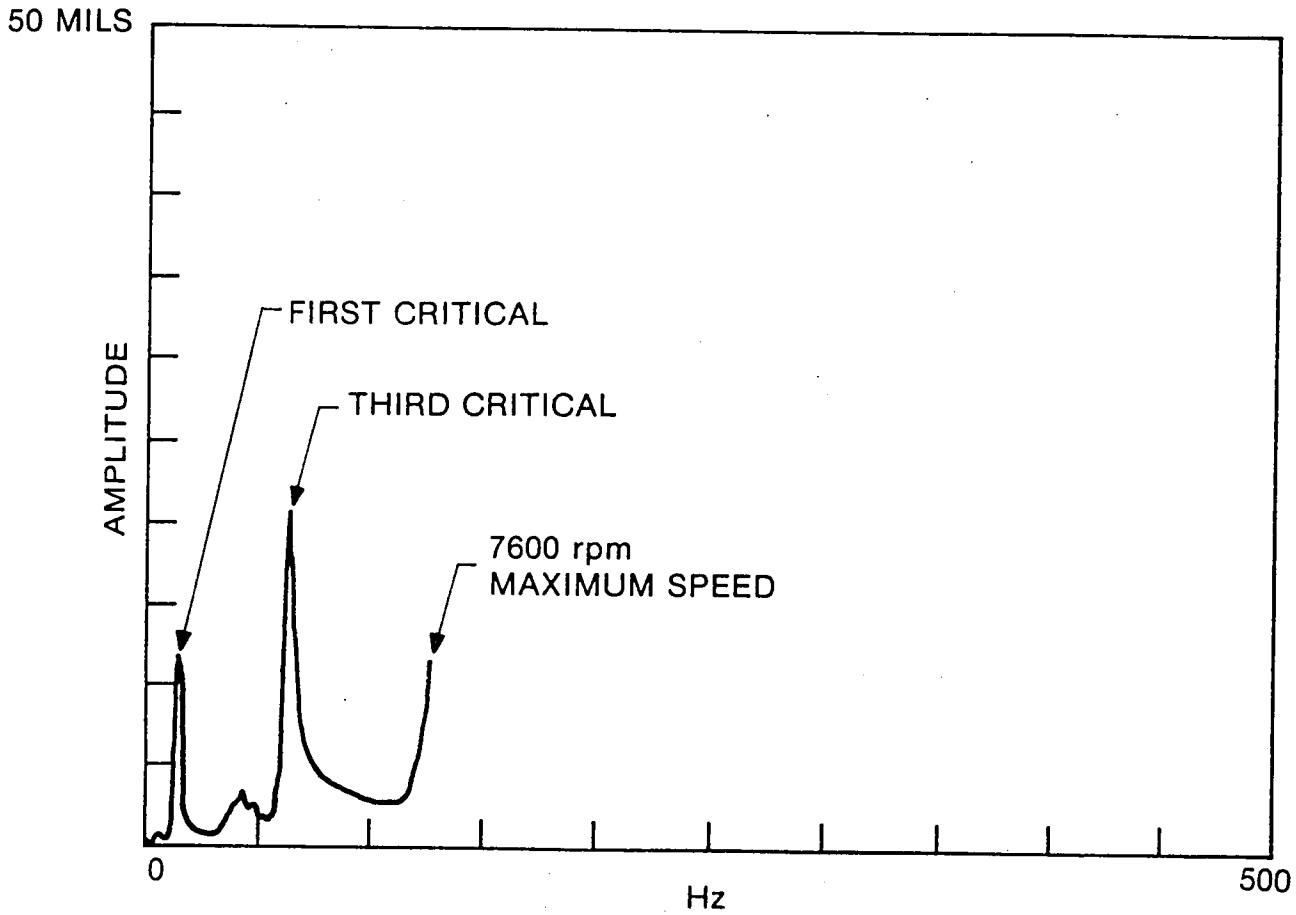

Figure 17 Shaft Probe #8, Synchronous Response with Elastomer Damper

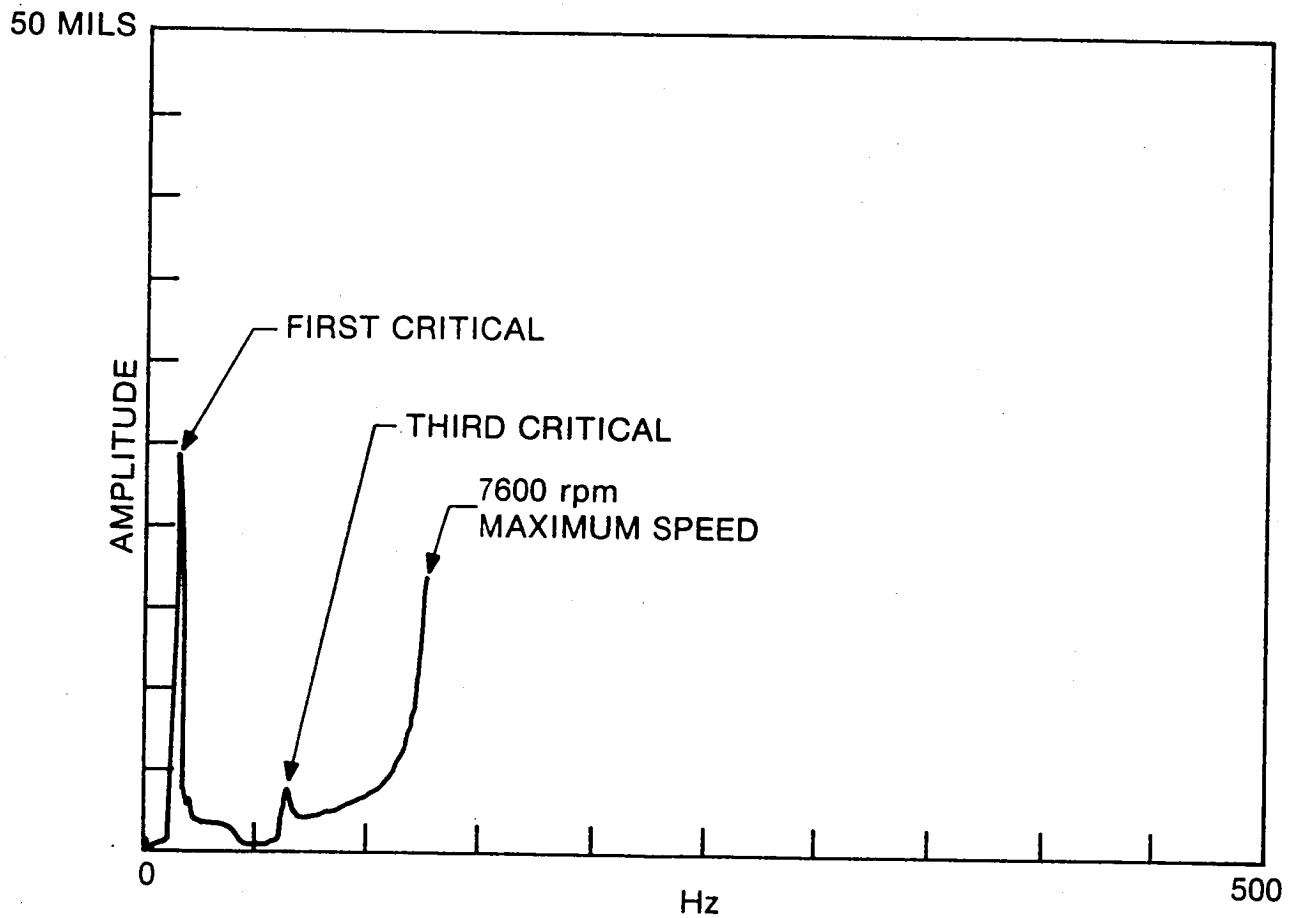

Figure 18 Shaft Probe #6, Synchronous Response with Elastomer Damper

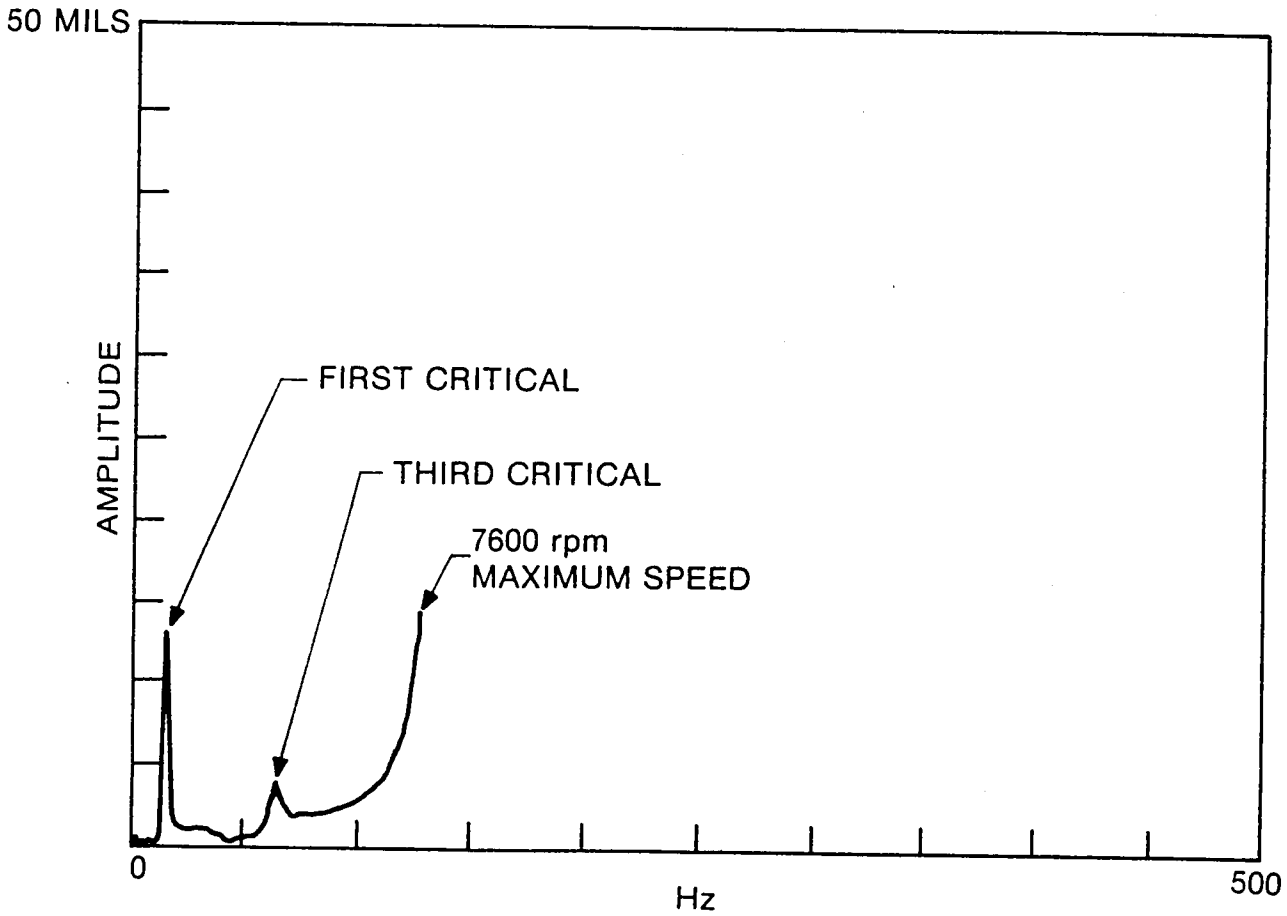

Figure 19 Shaft Probe #5, Synchronous Response with Elastomer Damper

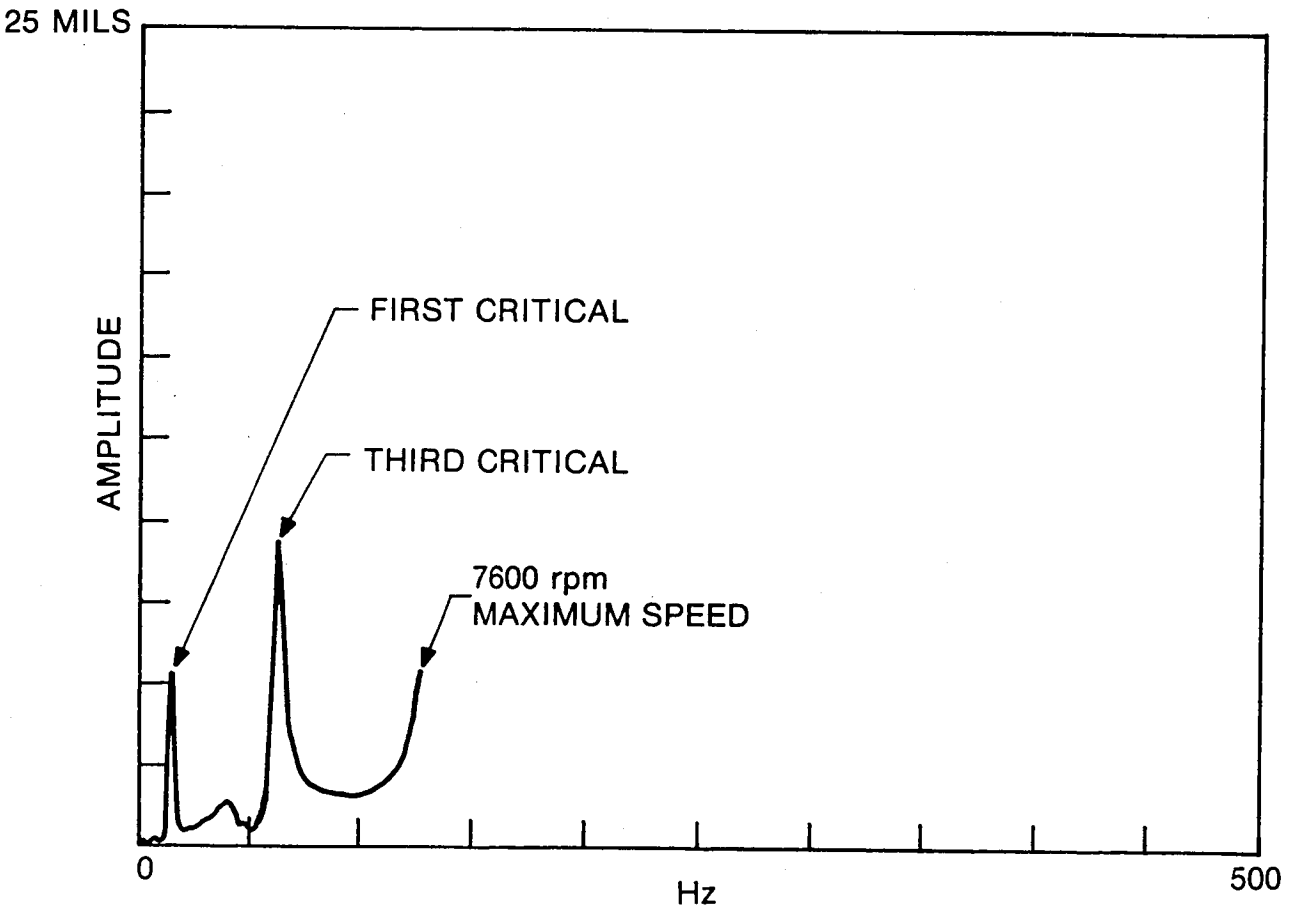

Figure 20 Shaft Probe #3, Synchronous Response with Elastomer Damper

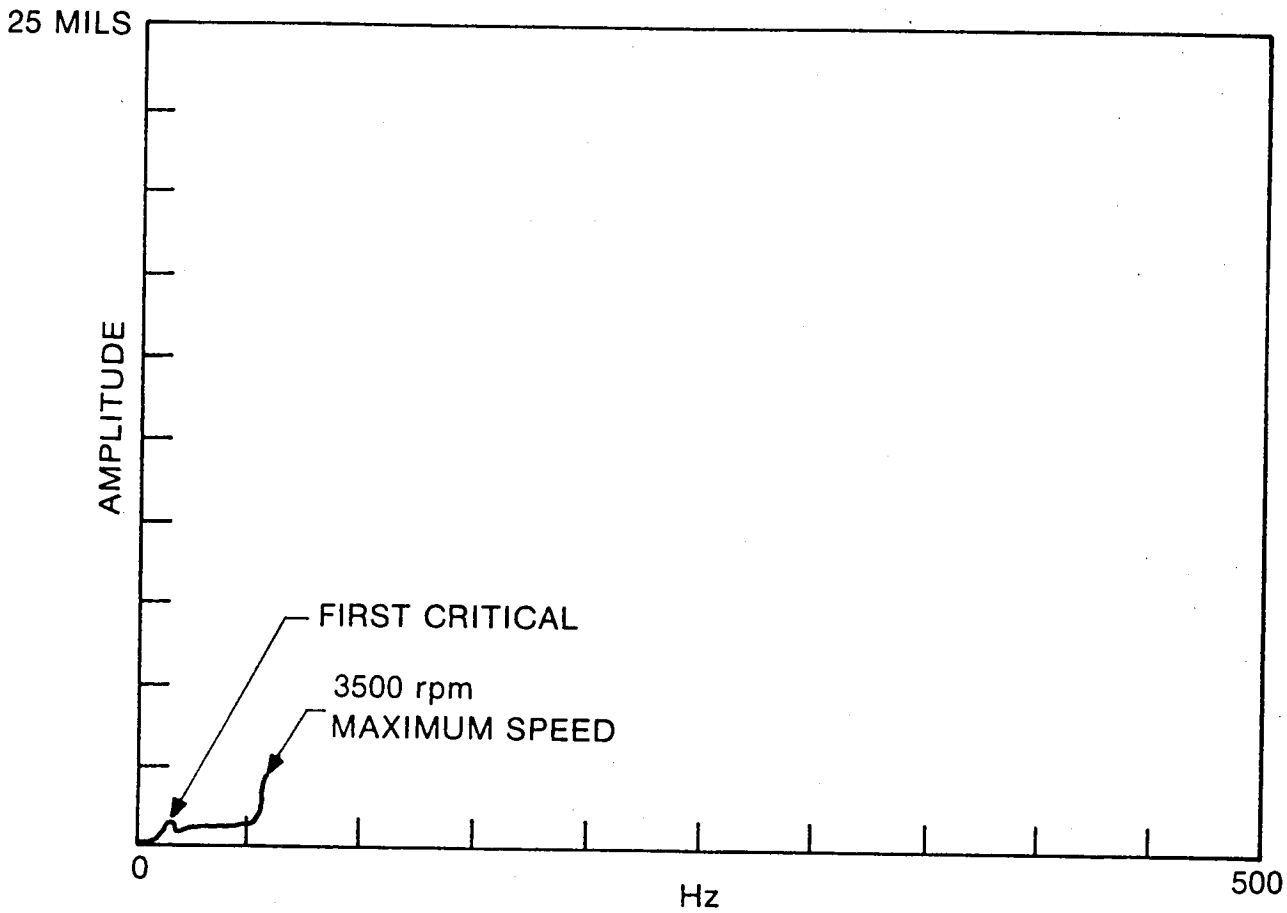

Figure 21 Damper Probe #12, Synchronous Response with Hydraulic Damper

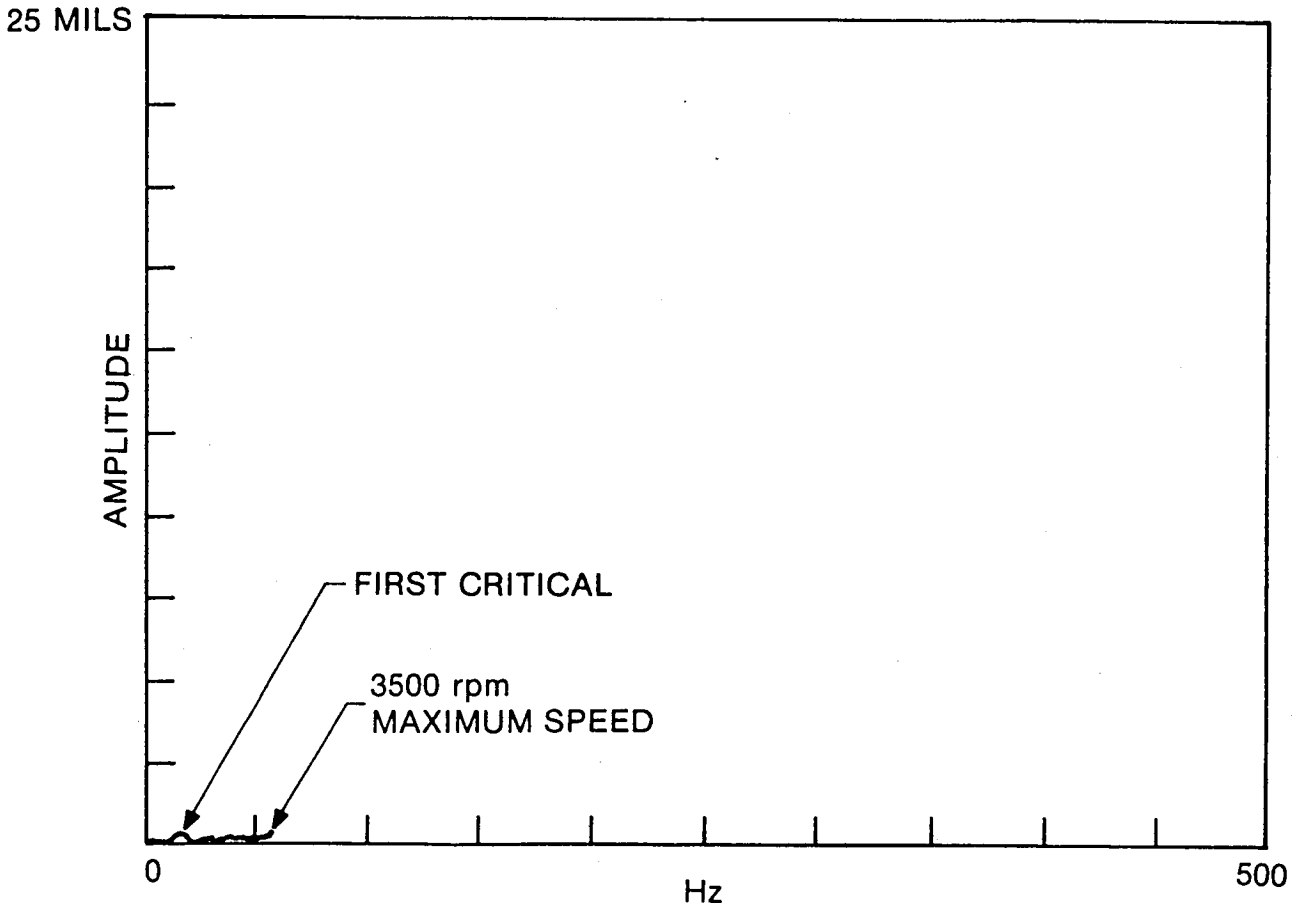

Figure 22 Damper Probe #10, Synchronous Response with Hydraulic Damper

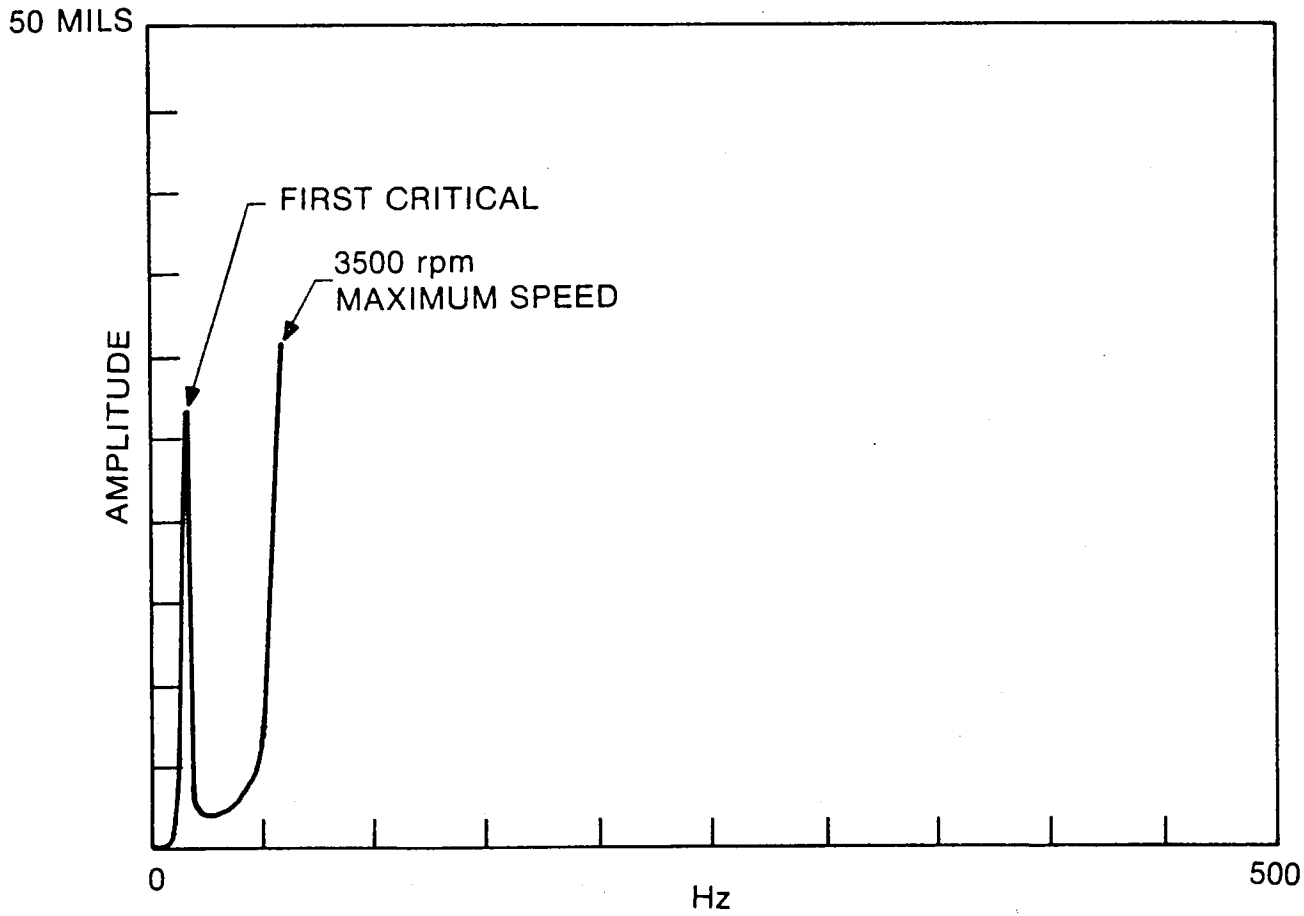

Figure 23 Shaft Probe #8, Synchronous Response with Hydraulic Mount

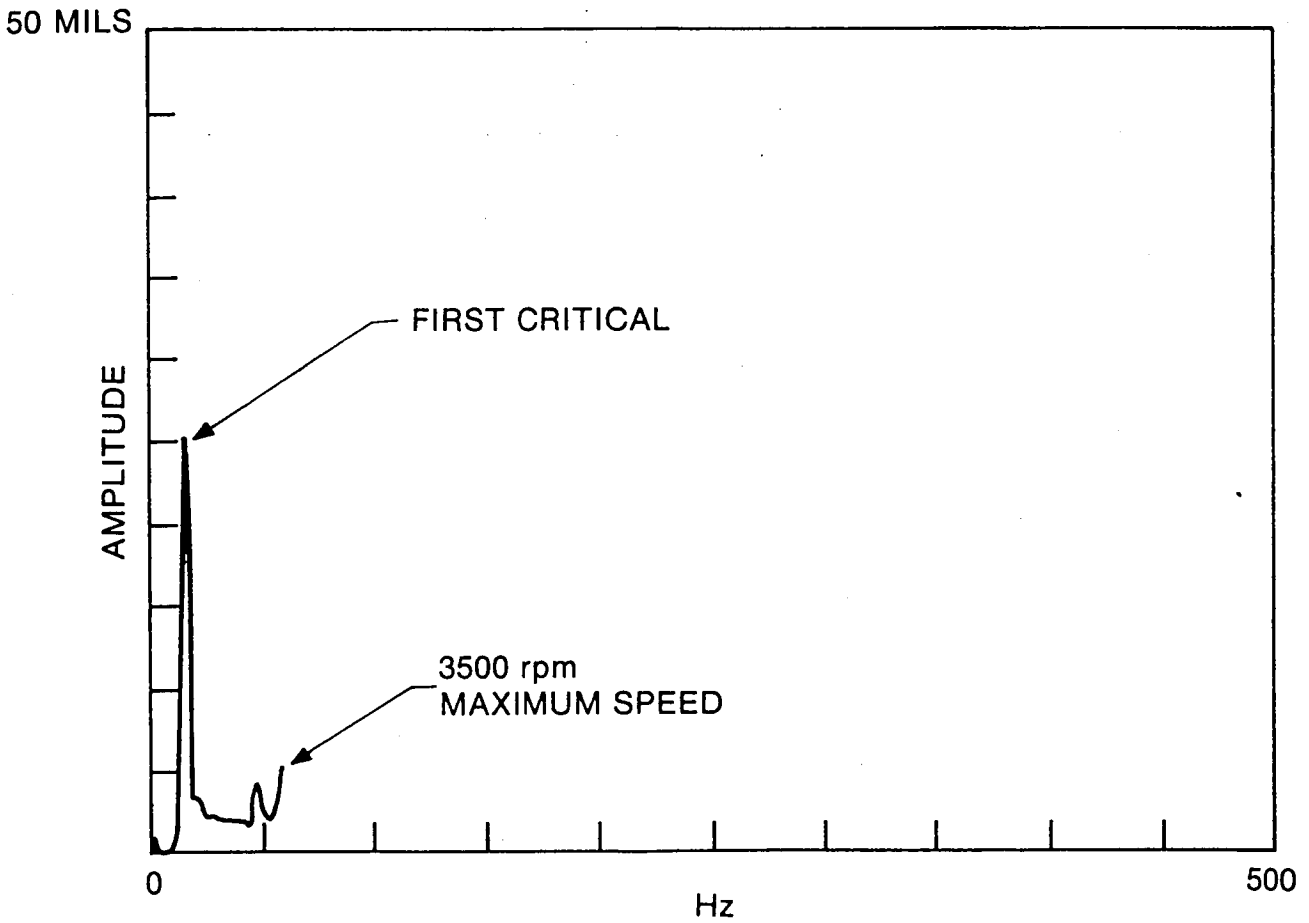

Figure 24 Shaft Probe #6, Synchronous Response with Hydraulic Mount

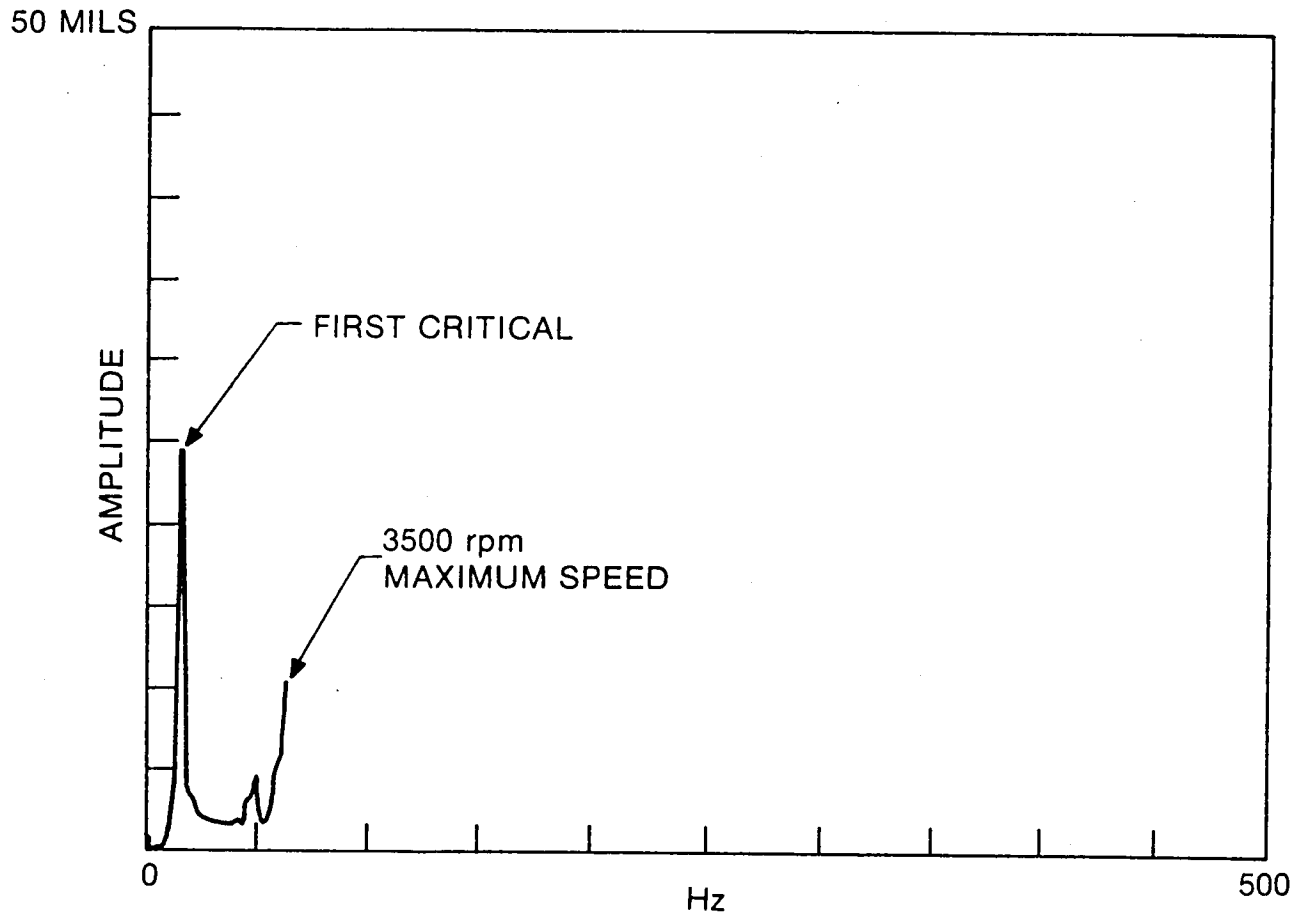

Figure 25 Shaft Probe #5, Synchronous Response with Hydraulic Mount

801143

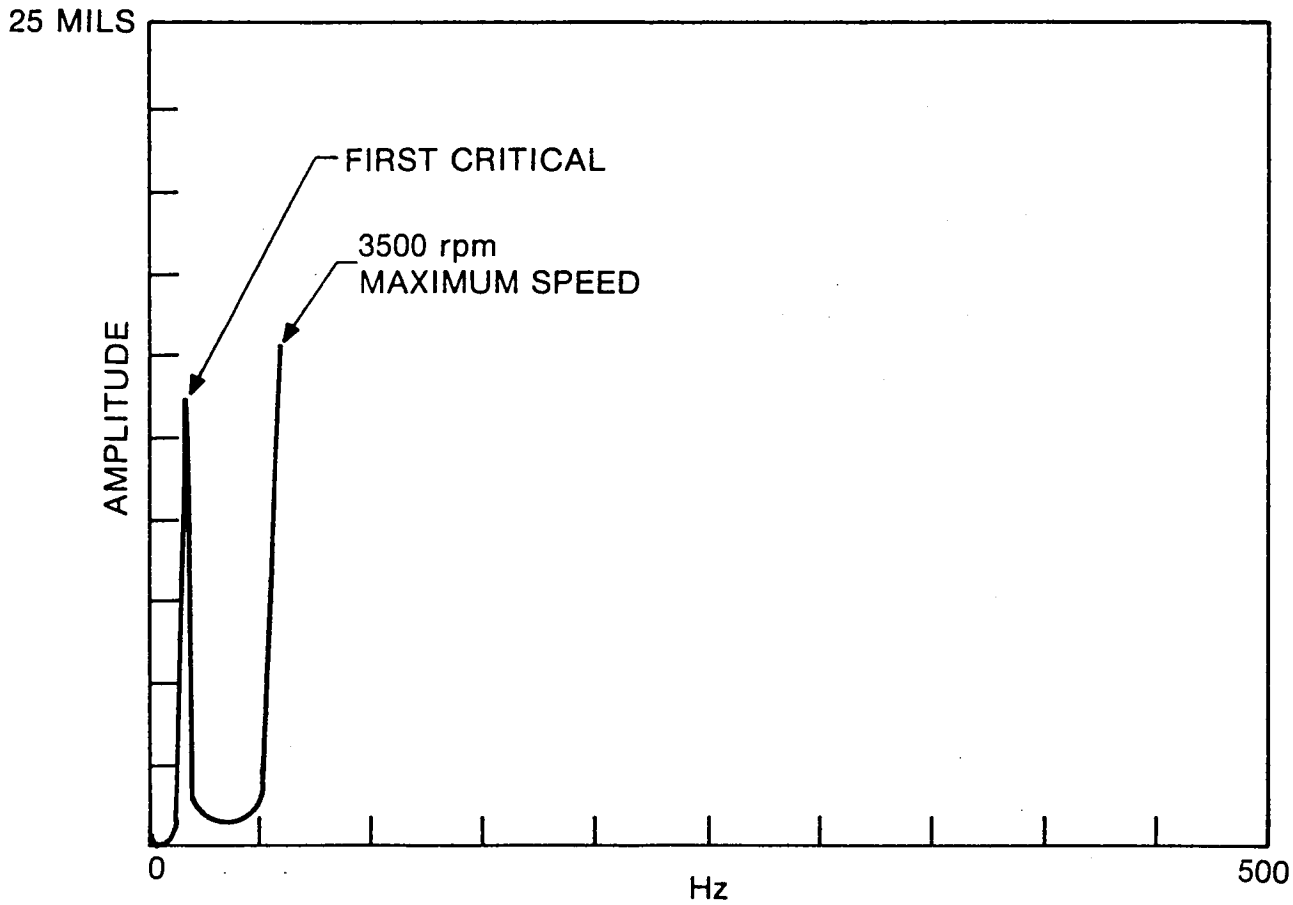

Figure 26 Shaft Probe #3, Synchronous Response with Hydraulic Mount

30725

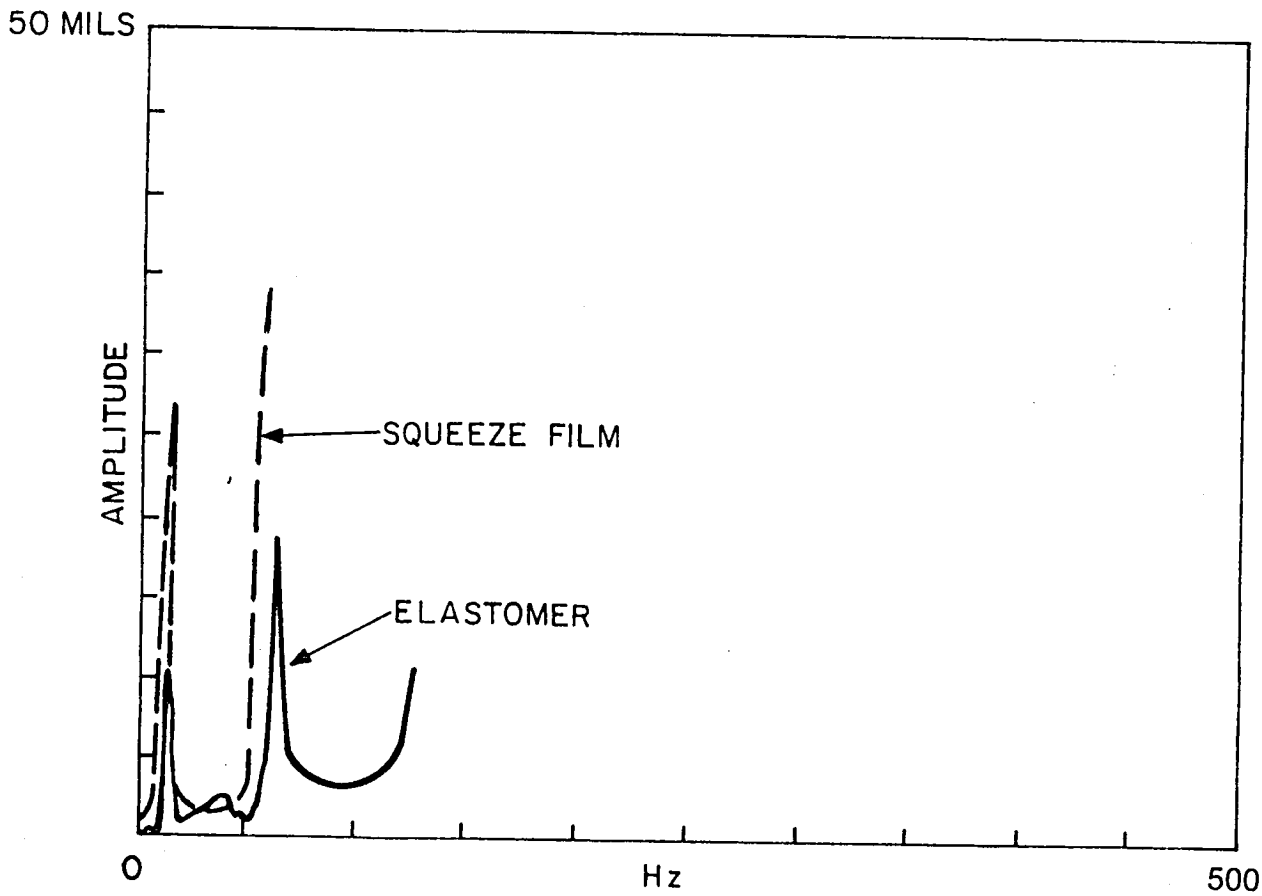

Figure 27 Synchronous Response Comparison, Probe #3

792378

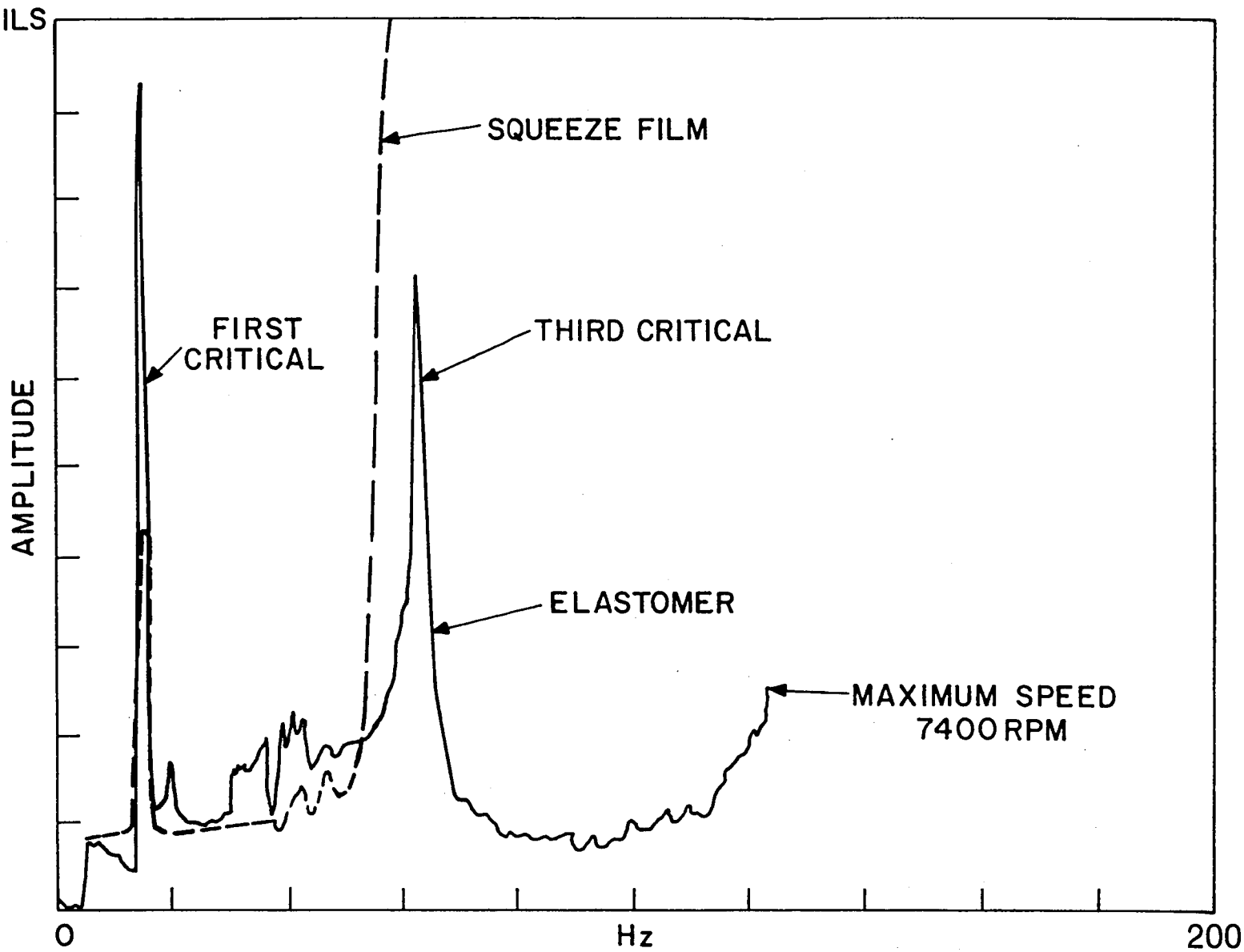

Figure 28 Synchronous Response Comparison, Probe #3

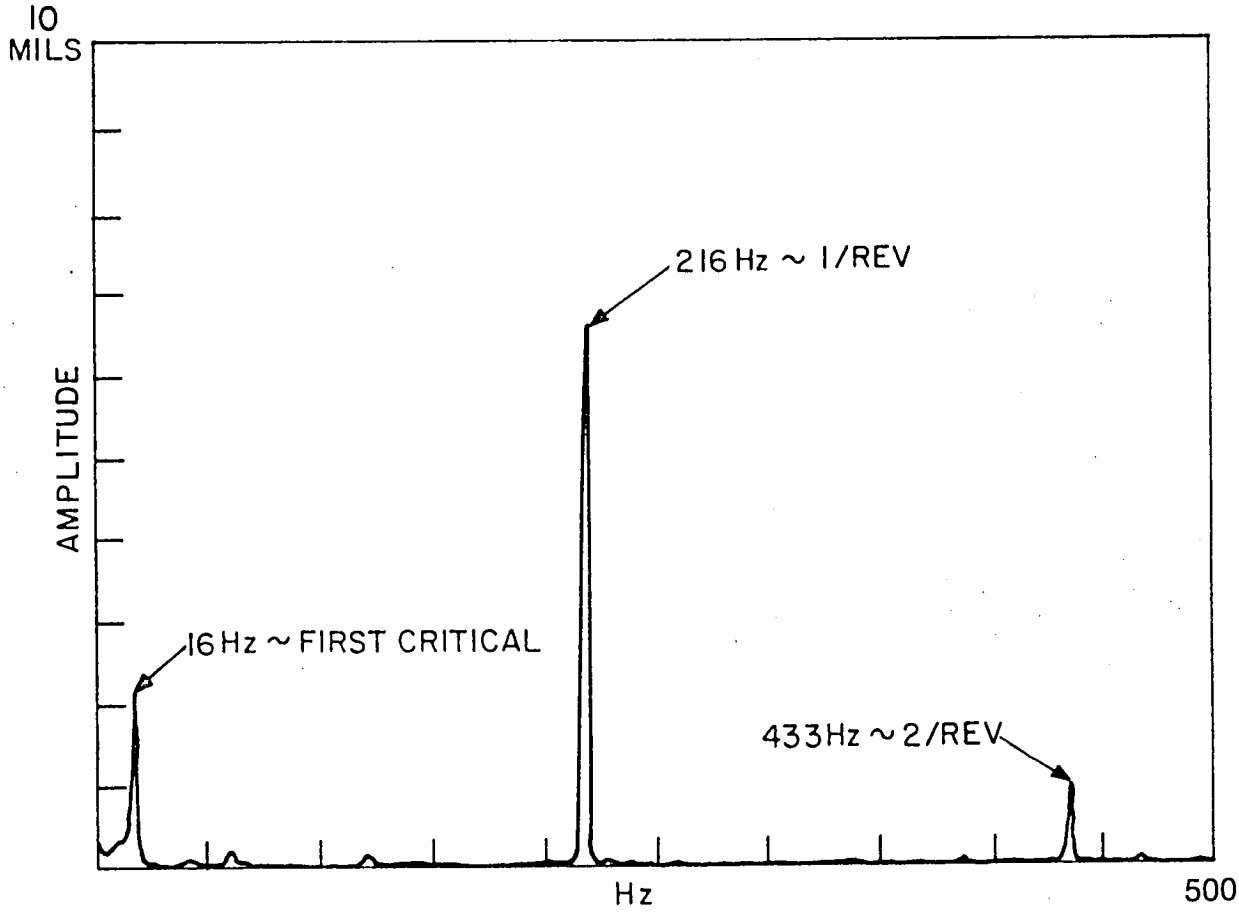

Figure 29 Frequency Spectrum Probe #5 at 13,000 rpm with Elastomer Damper Operational

792377

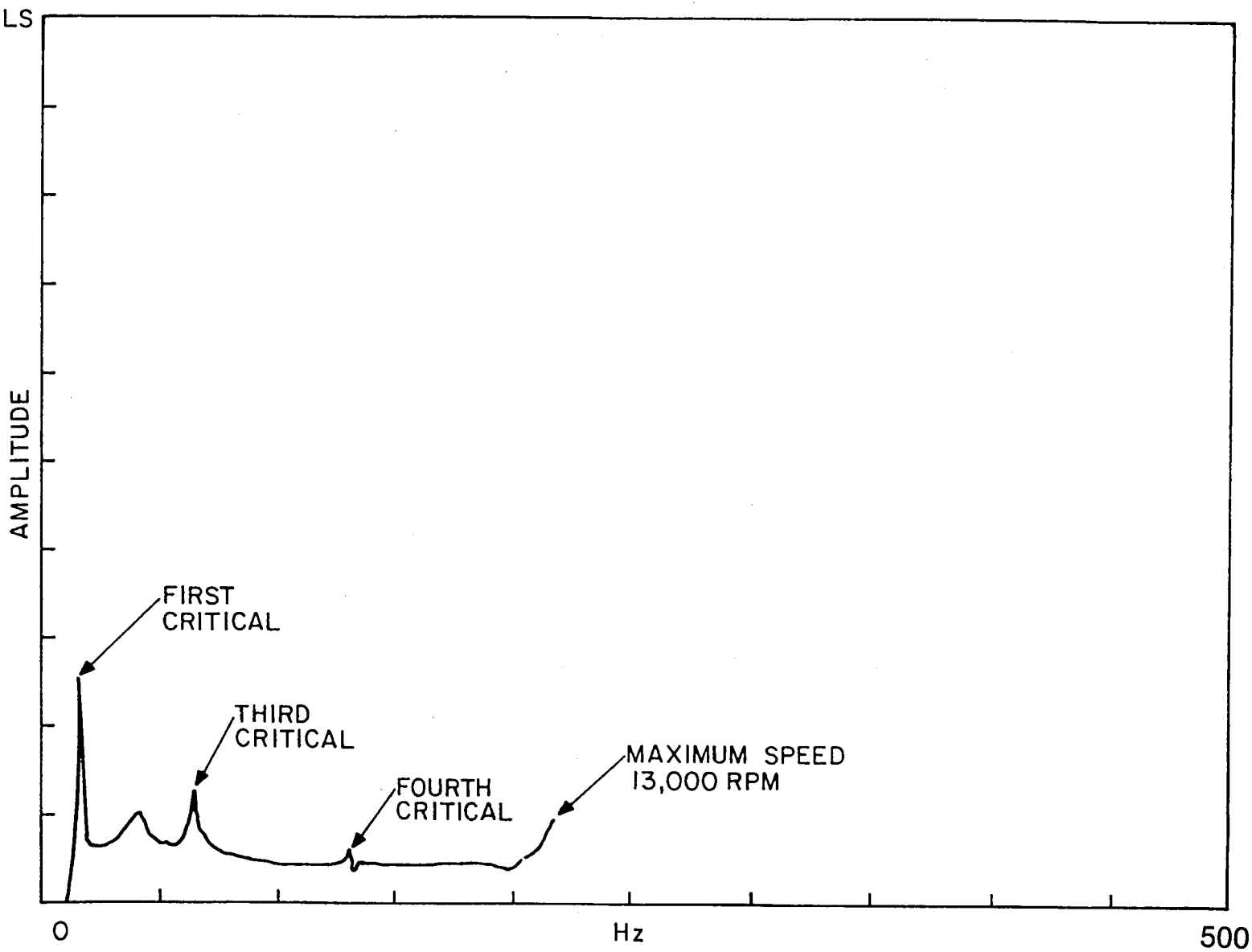

Figure 30 Synchronous Response Probe #3 on Elastomer Damper

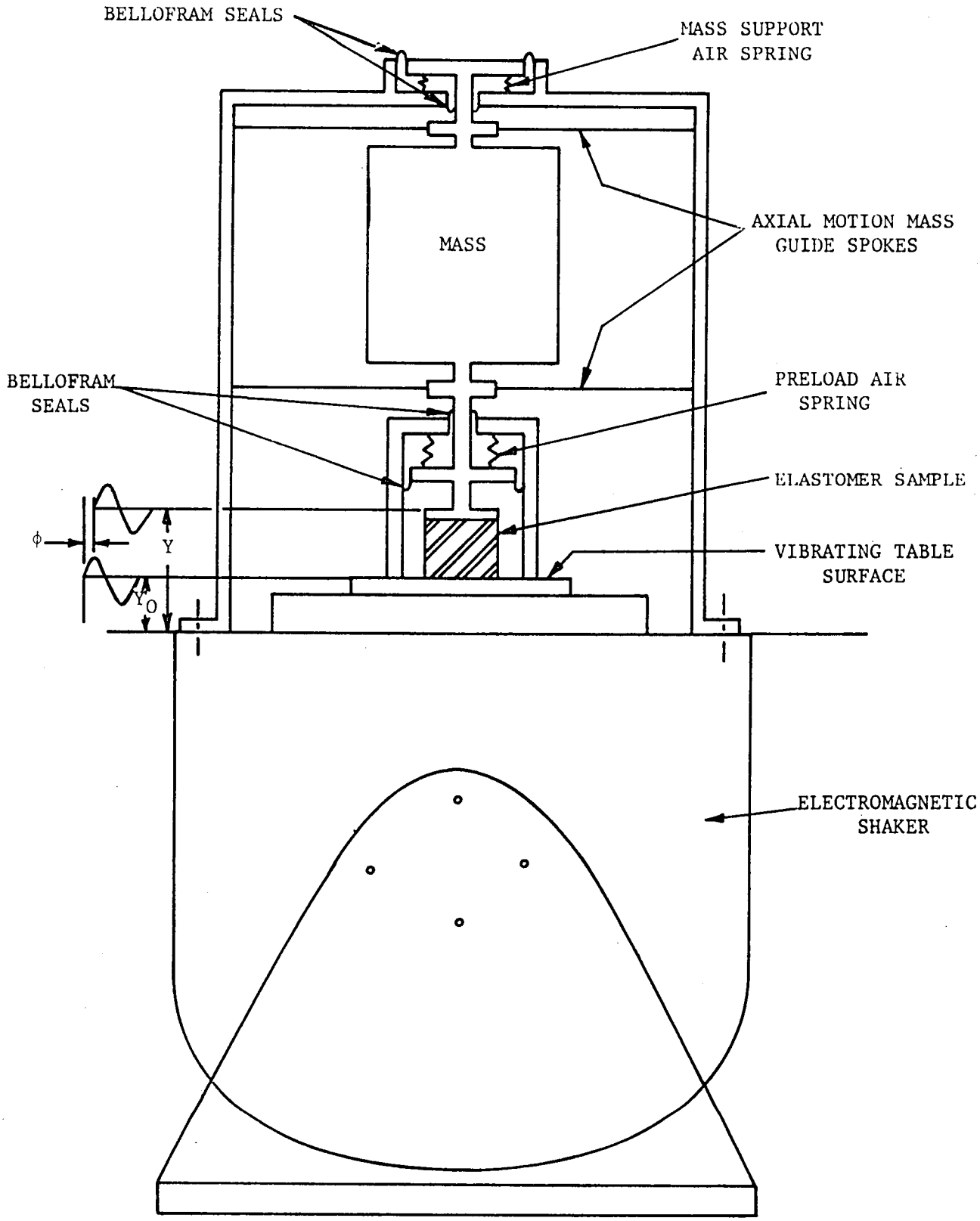

Figure 31 Schematic of Elastomer Test Rig Showing All Components

791161

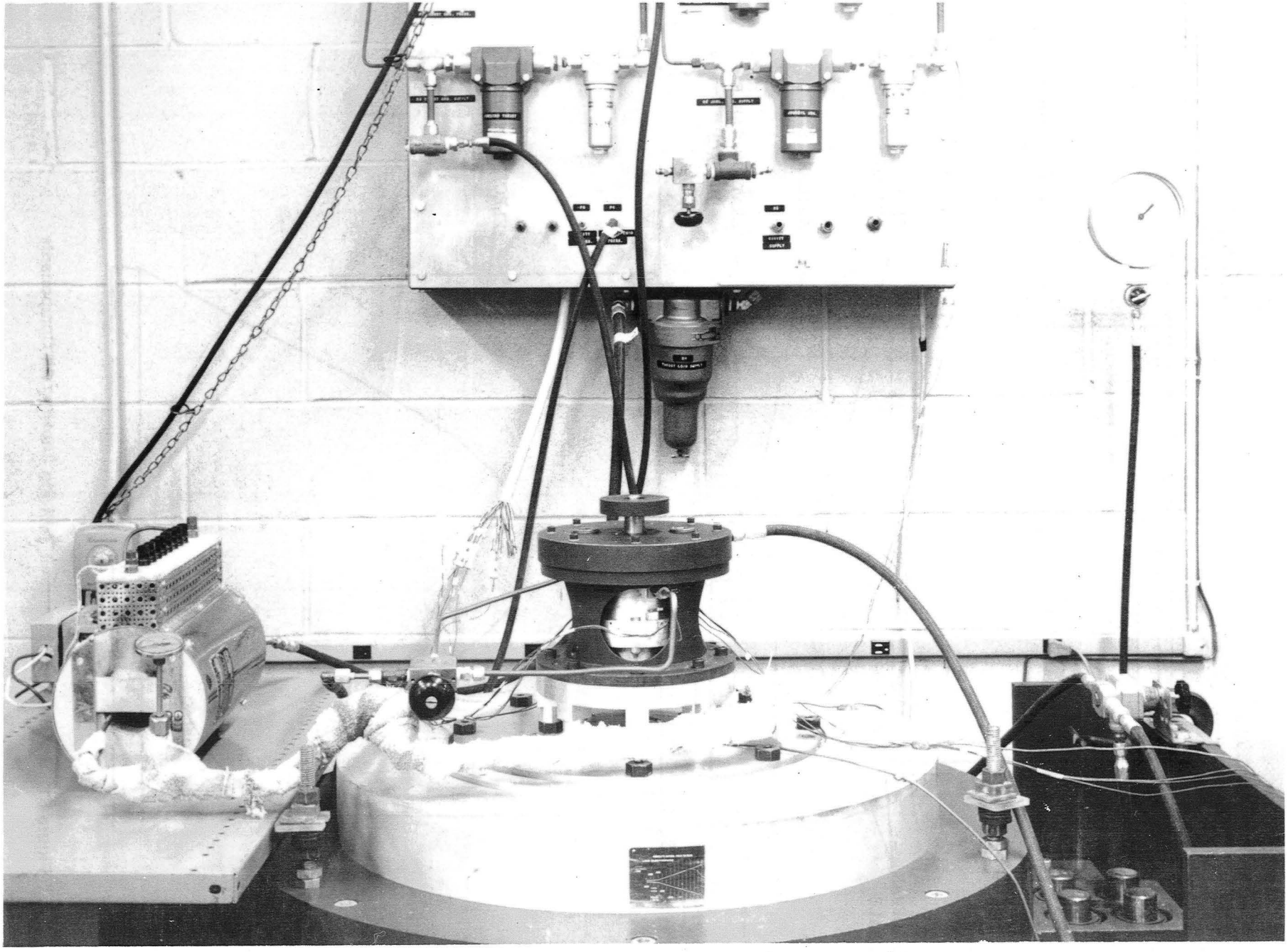

Figure 32 View of Shake-Table-Mounted Elastomer Test Rig with Preload Cylinder and Small Mass

MTI-16654

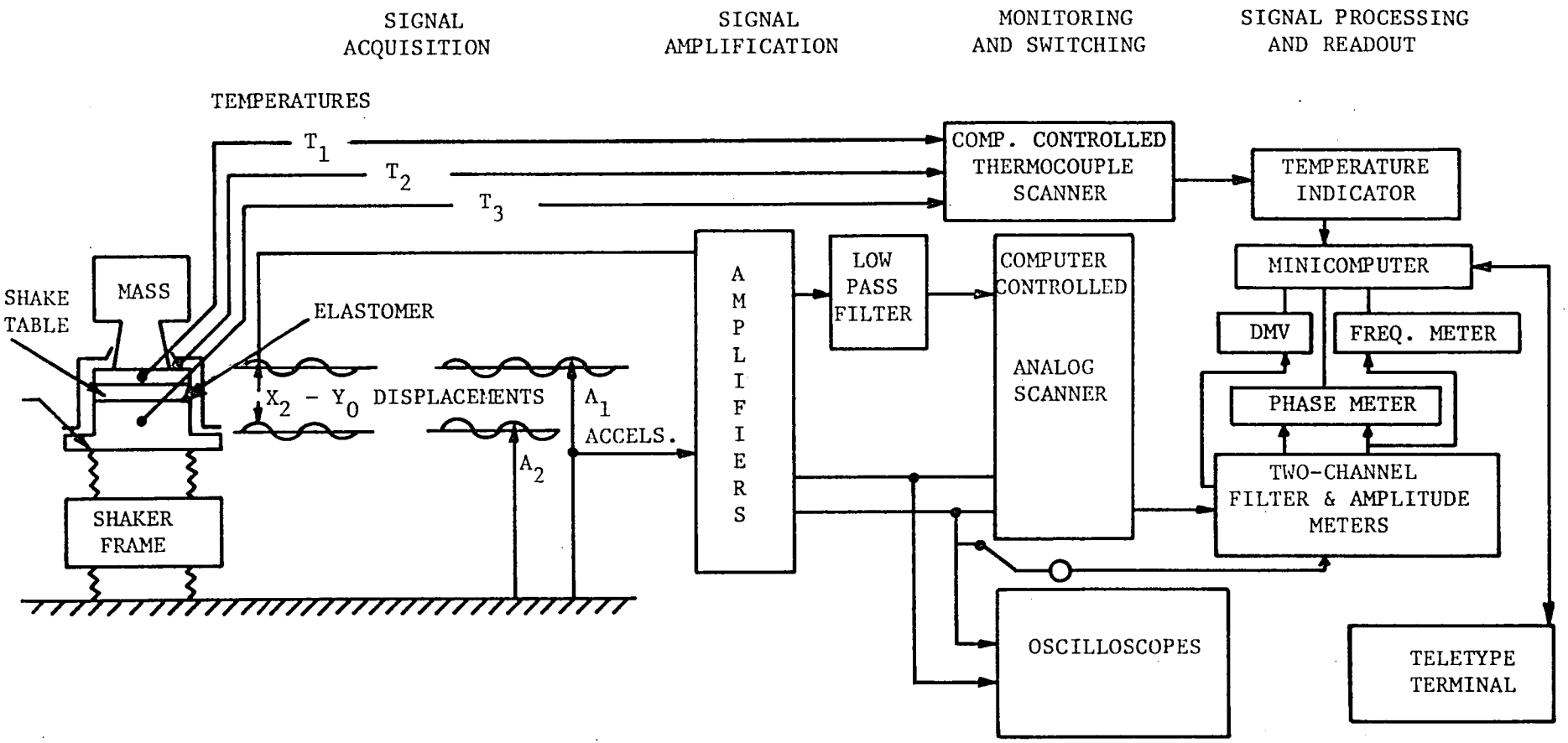

DATA ACQUISITION PROBES

T_1	-	TEMPERATURE OF METAL, ELASTOMER MASS
T_2	-	TEMPERATURE OF TEST ENCLOSURE AMBIENT
T_3	-	TEMPERATURE OF METAL, ELASTOMER-SHAKE TABLE
$Y - Y_0$	-	DISPLACEMENT MASS RELATIVE TO SHAKE TABLE
A_1	-	ACCELERATION OF MASS
A_2	-	ACCELERATION OF SHAKE TABLE

791162

Figure 33 Schematic of Data Acquisition for Measurement of Elastomer Dynamic Properties

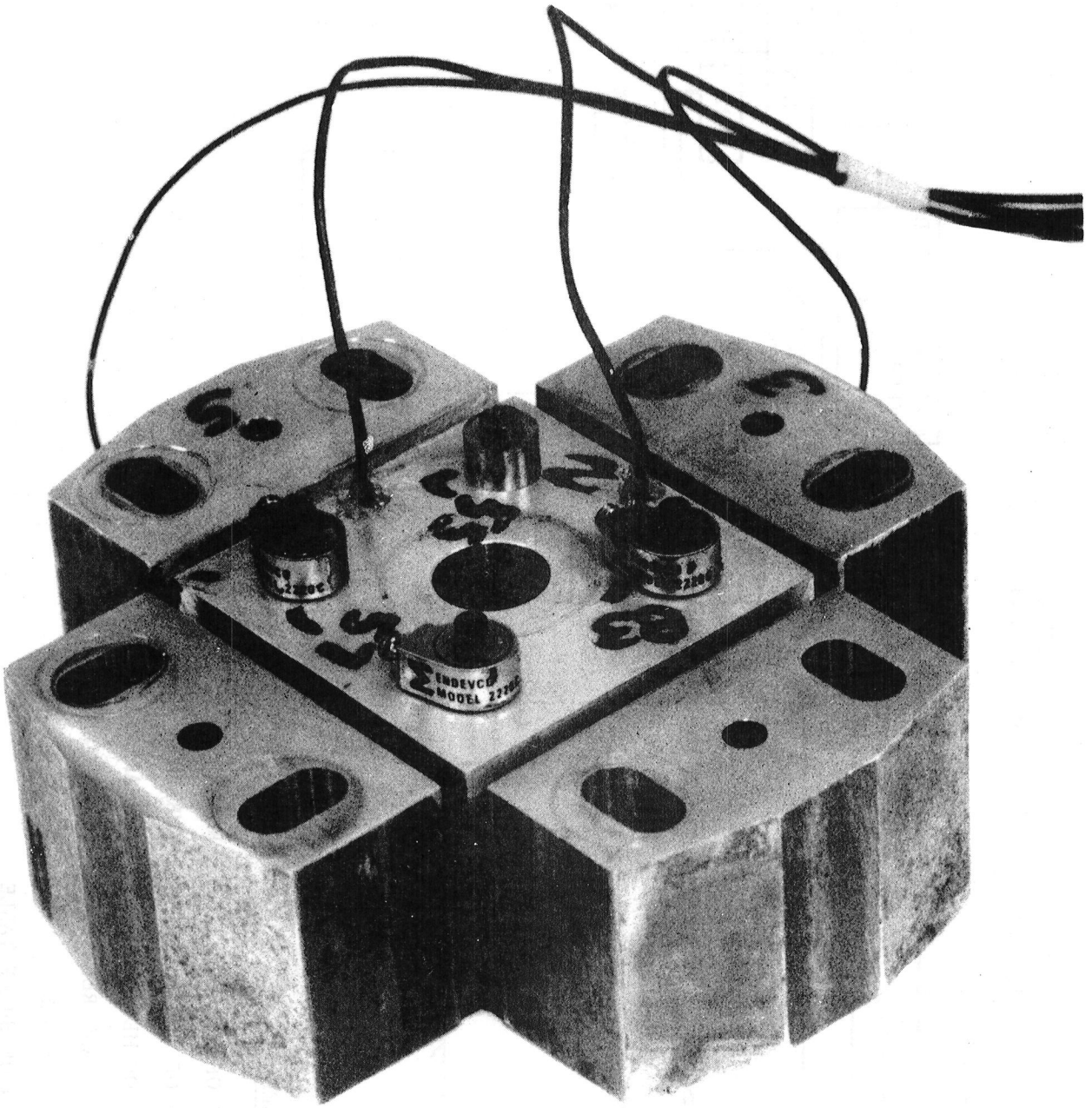

Figure 34 Test Assembly of Four Elastomer Shear Specimens

FREQUENCY (Hz)

STRAIN	150 1	200 2	300 3	400 4	450 5	500 6	600 7	800 8	900 9	1000 10
.0005										
.001										
.002										
.004										
.005										
.008										
.01										
.02										
.05										
.08										

Figure 35 Test Conditions for EPDM at 32°C

FREQUENCY (Hz)

STRAIN	150 1	200 2	320 3	400 4	500 5	620 6	700 7	800 8	900 9	1000 10
.0005										
.001										
.002										
.004										
.005										
.008										
.01										
.02										
.05										
.08										

Figure 36 Test Conditions for EPDM at 66°C

FREQUENCY (Hz)

STRAIN	100 1	150 2	200 3	300 4	320 5	400 6	500 7	620 8	700 9	800 10	900 11	1000 12
.0005												
.001												
.002												
.004												
.005												
.008												
.01												
.02												
.05												
.08												

Figure 37 Test Conditions for EPDM at 80°C

FREQUENCY (Hz)

STRAIN	140 1	200 2	280 3	450 4	550 5	650 6	750 7	850 8	950 9	1050 10
.0005										
.001										
.002										
.004										
.005										
.008										
.01										
.02										
.05										
.08										

Figure 38 Test Conditions for Buna-N at 32°C

FREQUENCY (Hz)

STRAIN	100 1	200 2	300 3	320 4	400 5	550 6	650 7	750 8	850 9	10
.0005										
.001										
.002										
.004										
.005										
.008										
.01										
.02										
.05										
.08										

Figure 39 Test Conditions for Buna-N at 66°C

FREQUENCY (Hz)

STRAIN	110 1	200 2	250 3	280 4	400 5	500 6	600 7	700 8	9	10
.0005										
.001										
.002										
.004										
.005										
.008										
.01										
.02										
.05										
.08										

Figure 40 Test Conditions for Buna-N at 80°C

FREQUENCY (Hz)

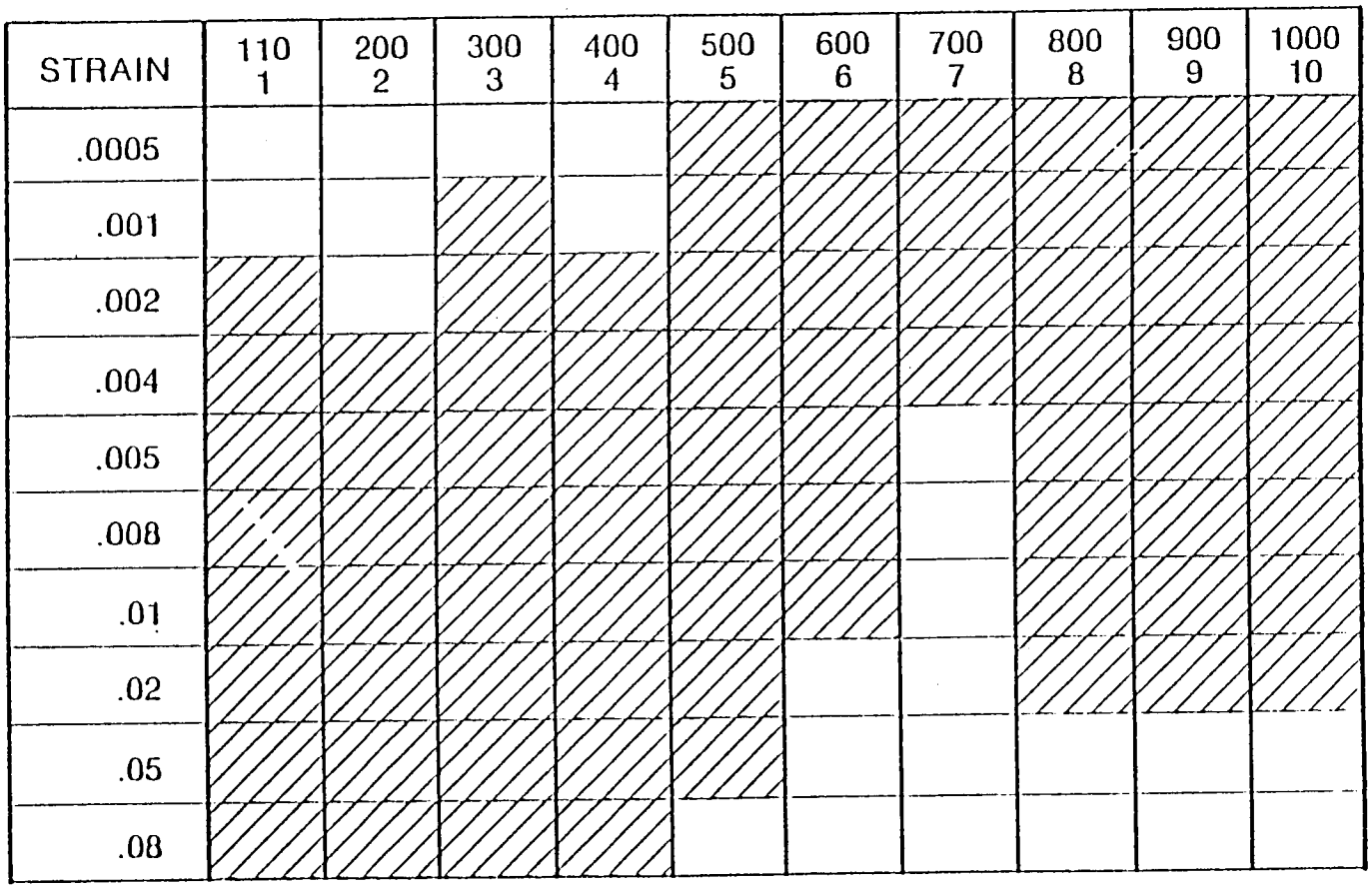

Figure 41 Test Conditions for Viton-70 at 32°C

FREQUENCY (Hz)

STRAIN	110 1	200 2	300 3	400 4	500 5	600 6	700 7	800 8	900 9	1000 10
.0005										
.001										
.002										
.004										
.005										
.008										
.01										
.02										
.05										
.08										

Figure 42 Test Conditions for Viton-70 at 66°C

FREQUENCY (Hz)

STRAIN	110 1	200 2	300 3	400 4	500 5	600 6	700 7	800 8	900 9	1000 10
.0005										
.001										
.002										
.004										
.005										
.008										
.01										
.02										
.05										
.08										

Figure 43 Test Conditions for Viton-70 at 80°C

FREQUENCY (Hz)

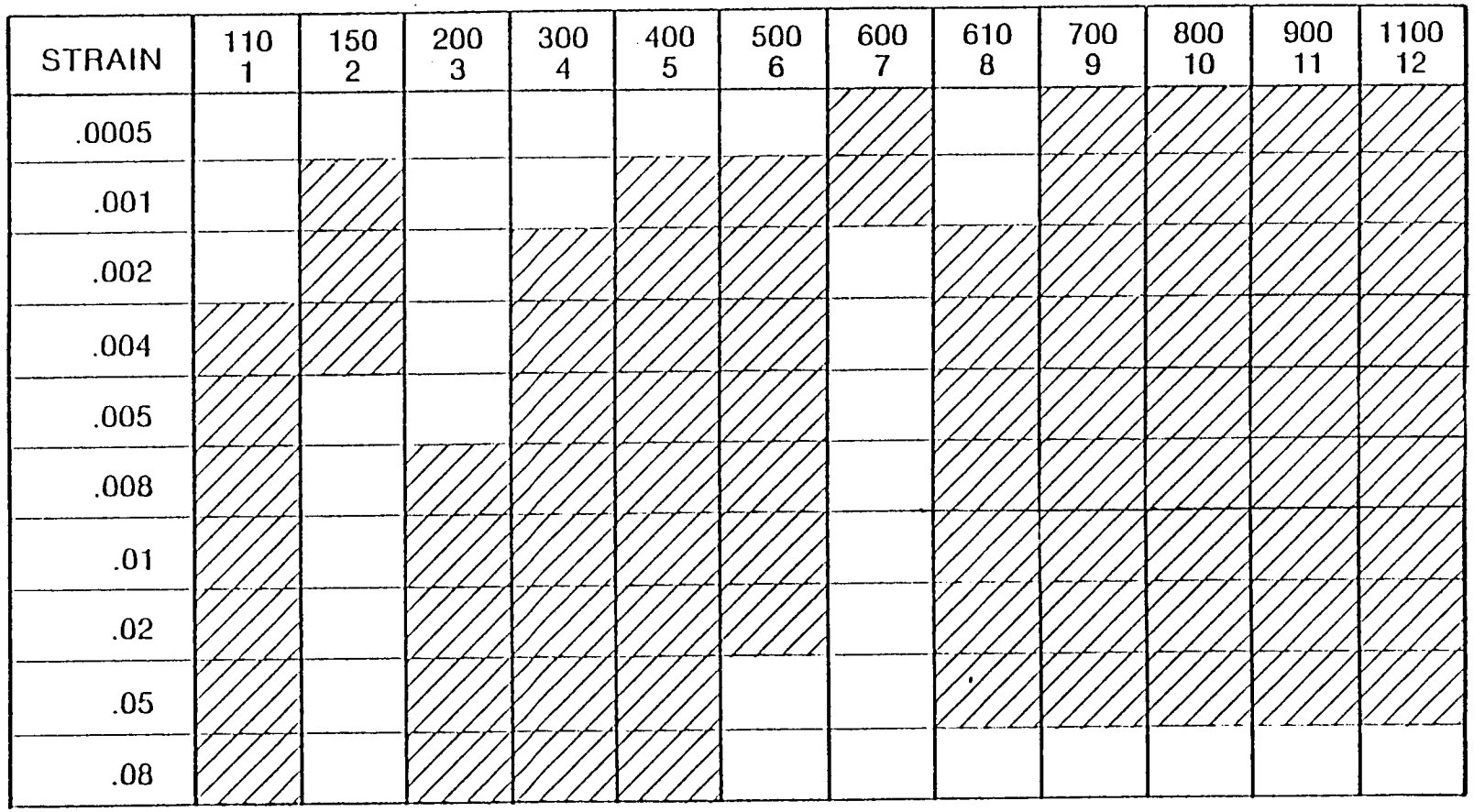

Figure 44 Test Conditions for Neoprene at 32°C

FREQUENCY (Hz)

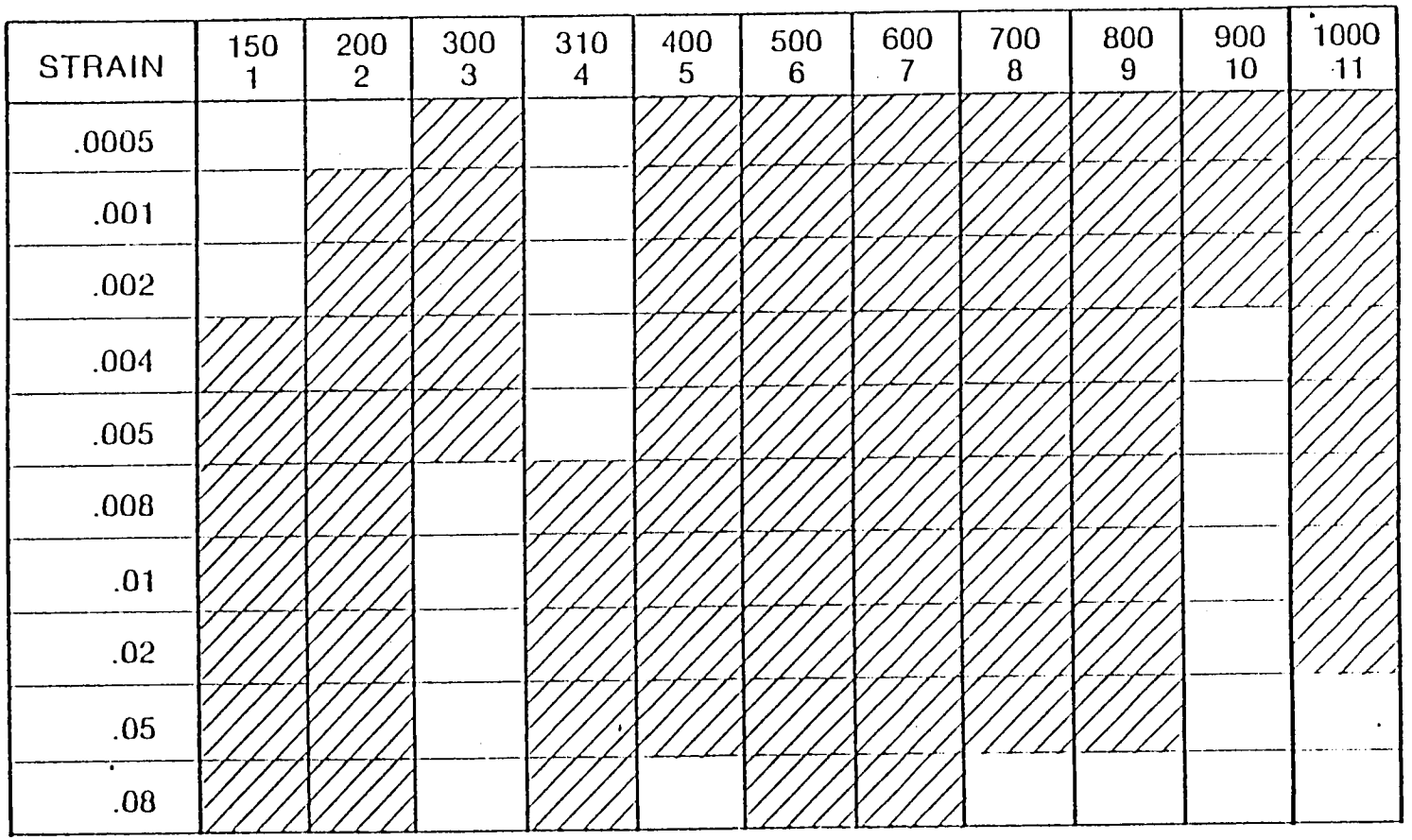

Figure 45 Test Conditions for Neoprene at 66°C

FREQUENCY (Hz)

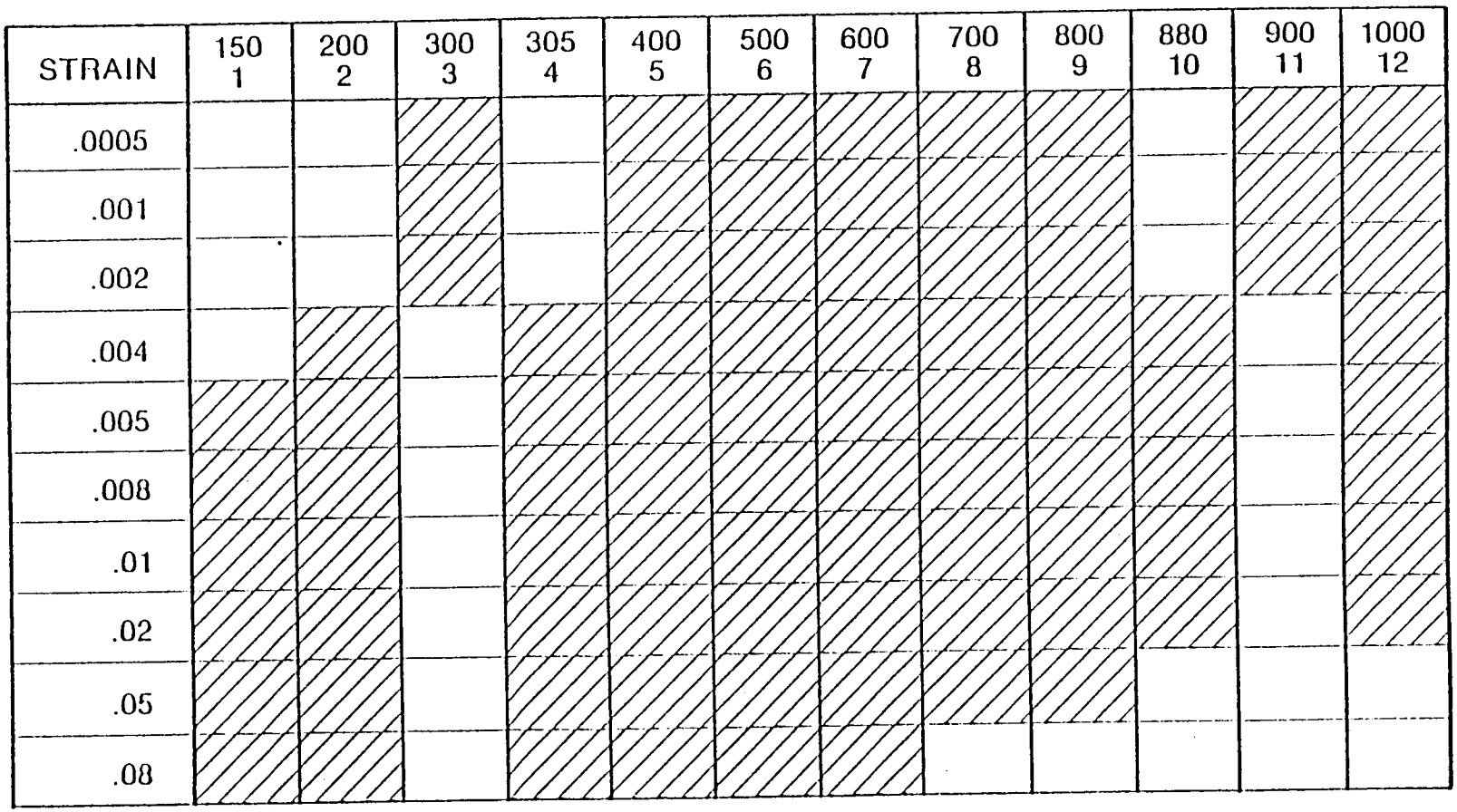

Figure 46 Test Conditions for Neoprene at 80°C

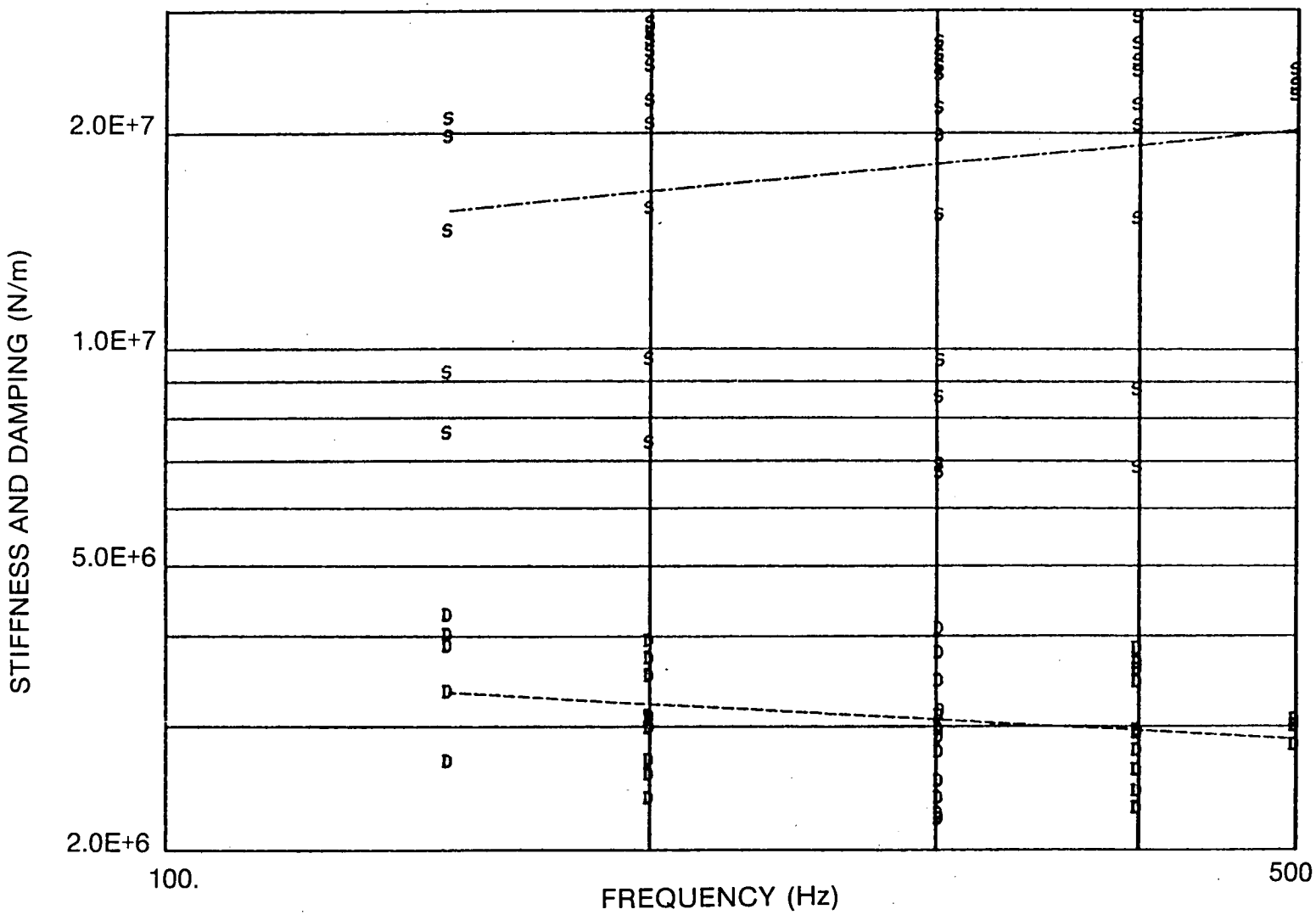

Figure 47 Shear Specimen Data EPDM at 32°C

80475

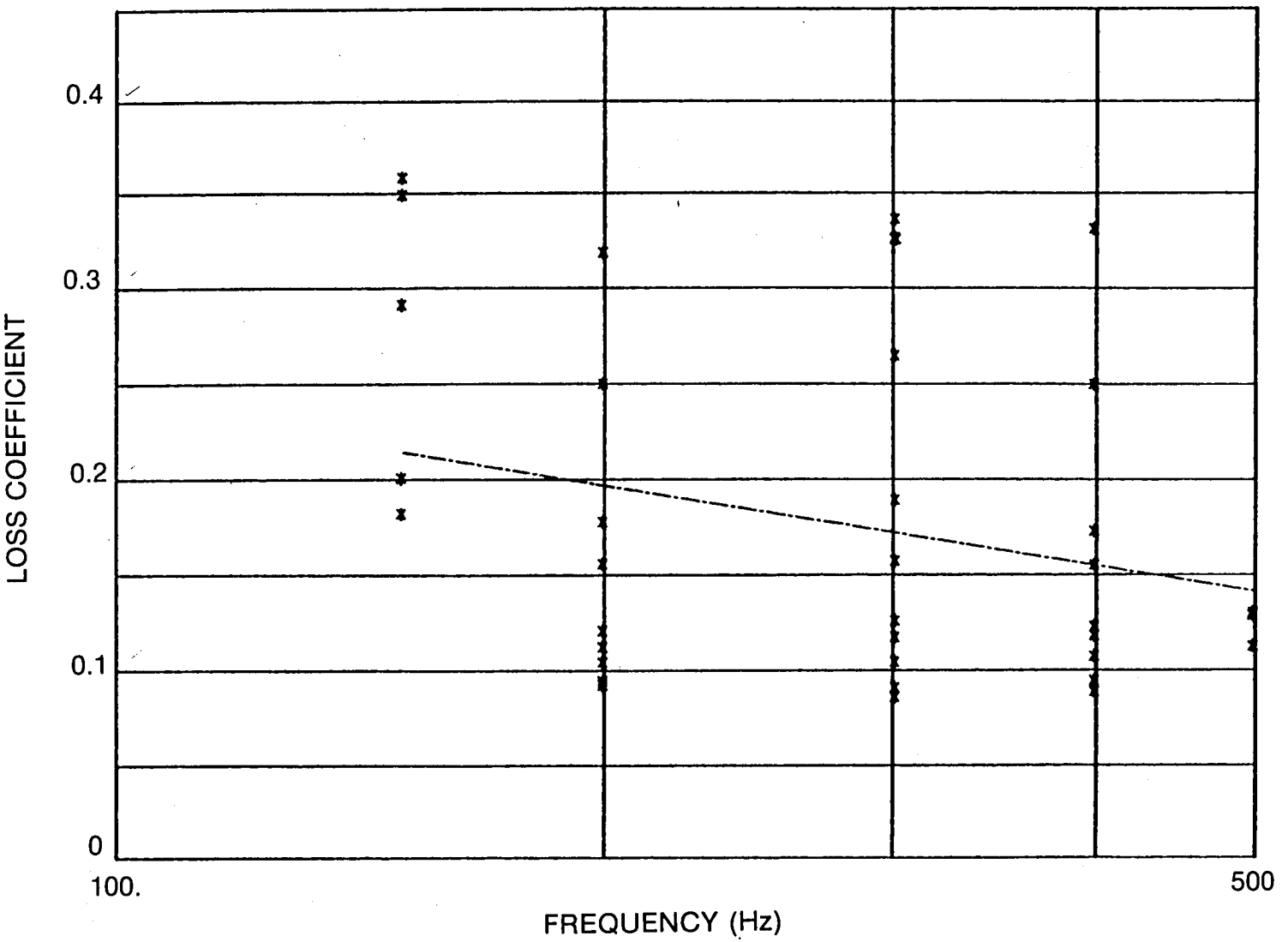

Figure 48 Shear Specimen Data EPDM at 32°C

80476

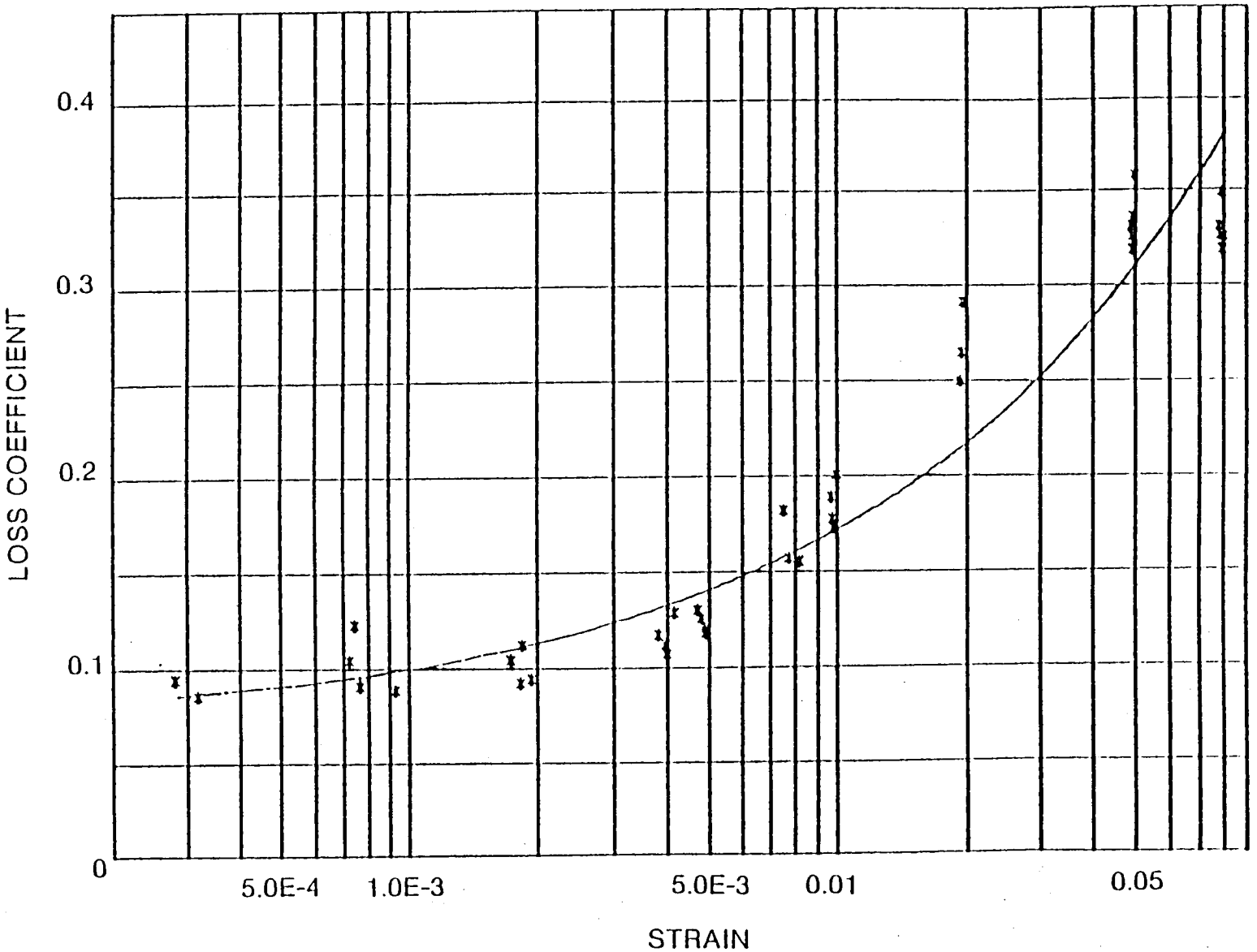

Figure 49 Shear Specimen Data EPDM at 32°C

30477

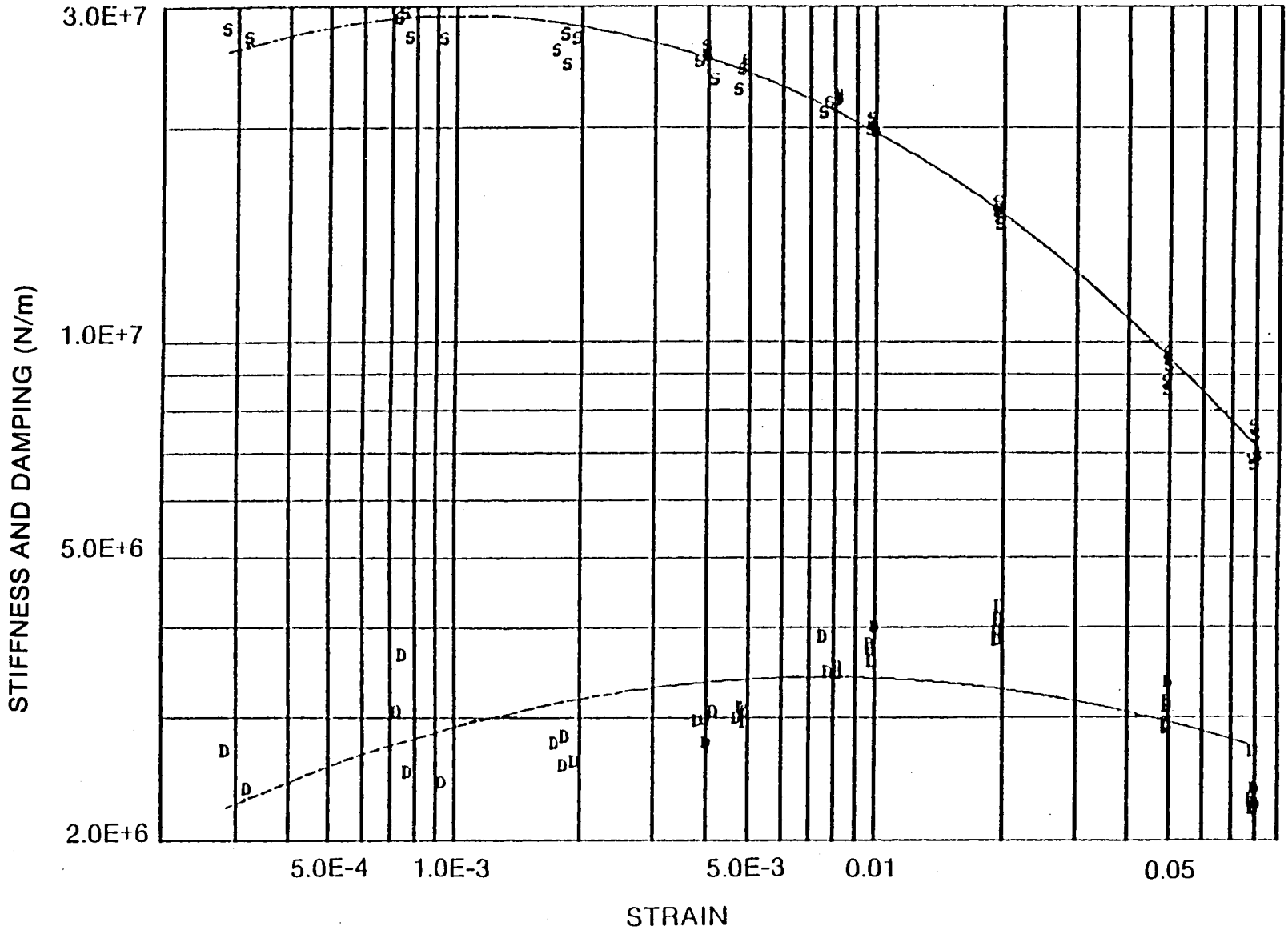

Figure 50 Shear Specimen Data EPDM at 32°C

80478

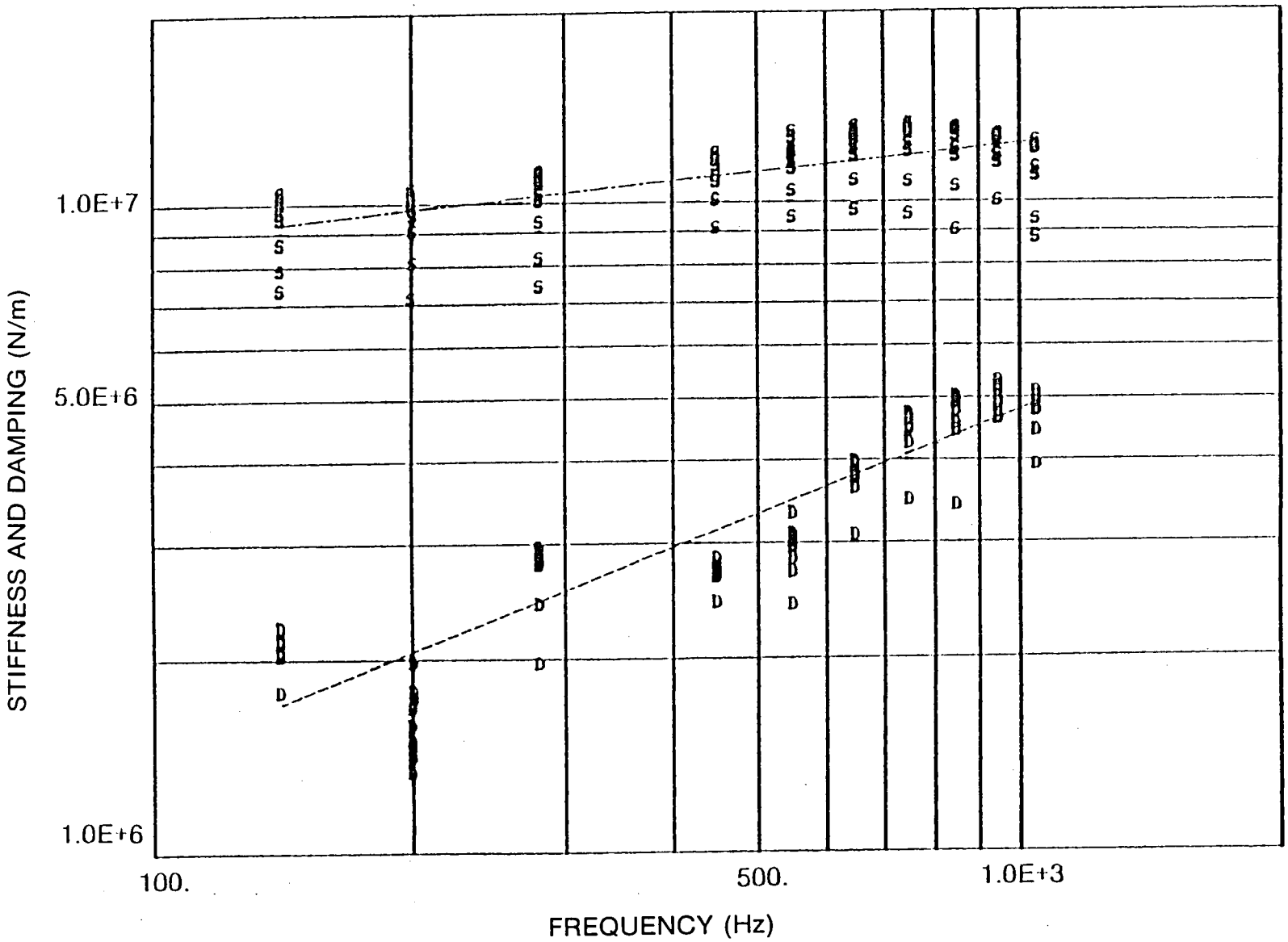

Figure 51 Shear Specimen Data EPDM at 66°C

80479

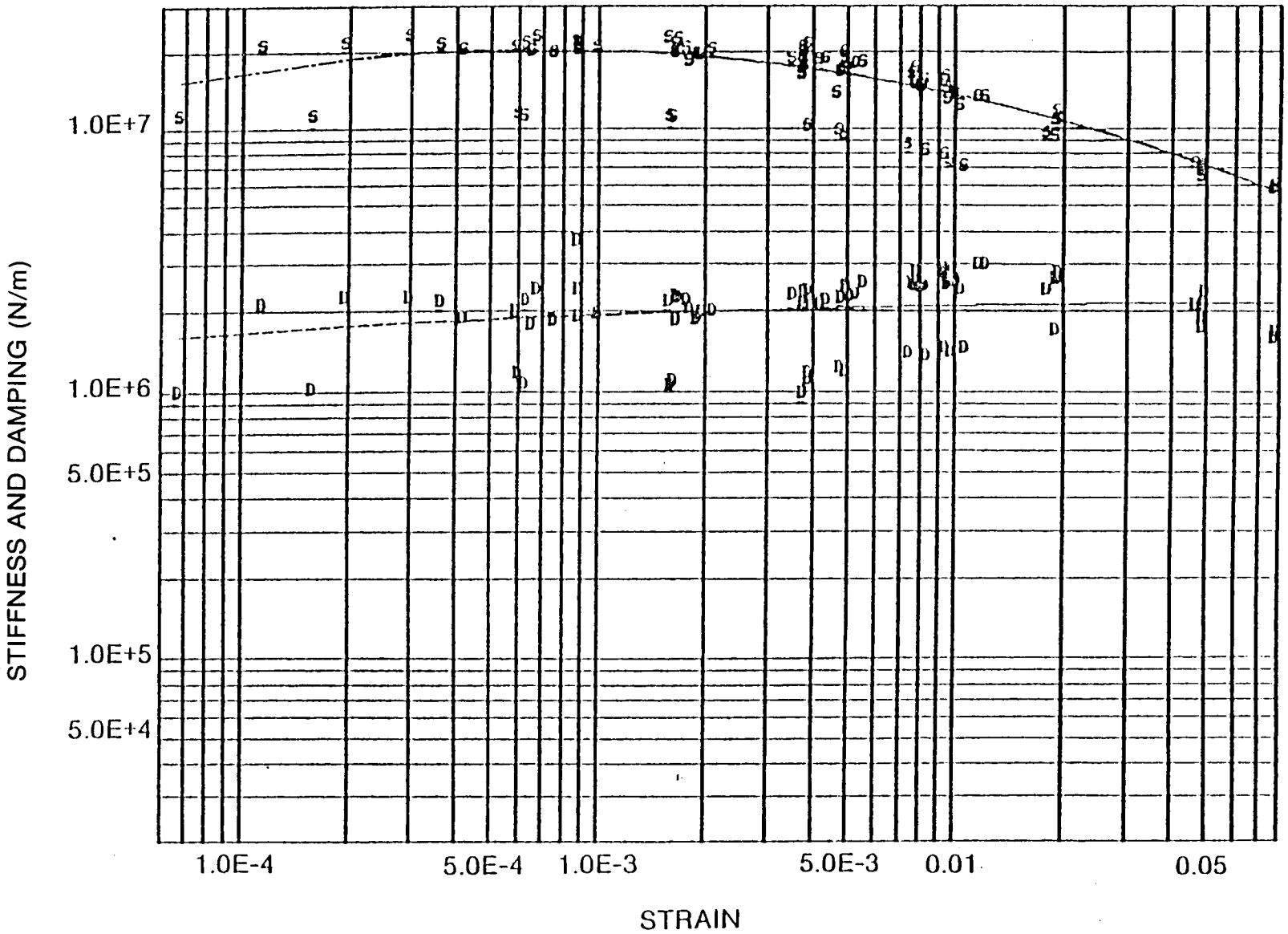

Figure 52 Shear Specimen Data EPDM at 66°C

80480

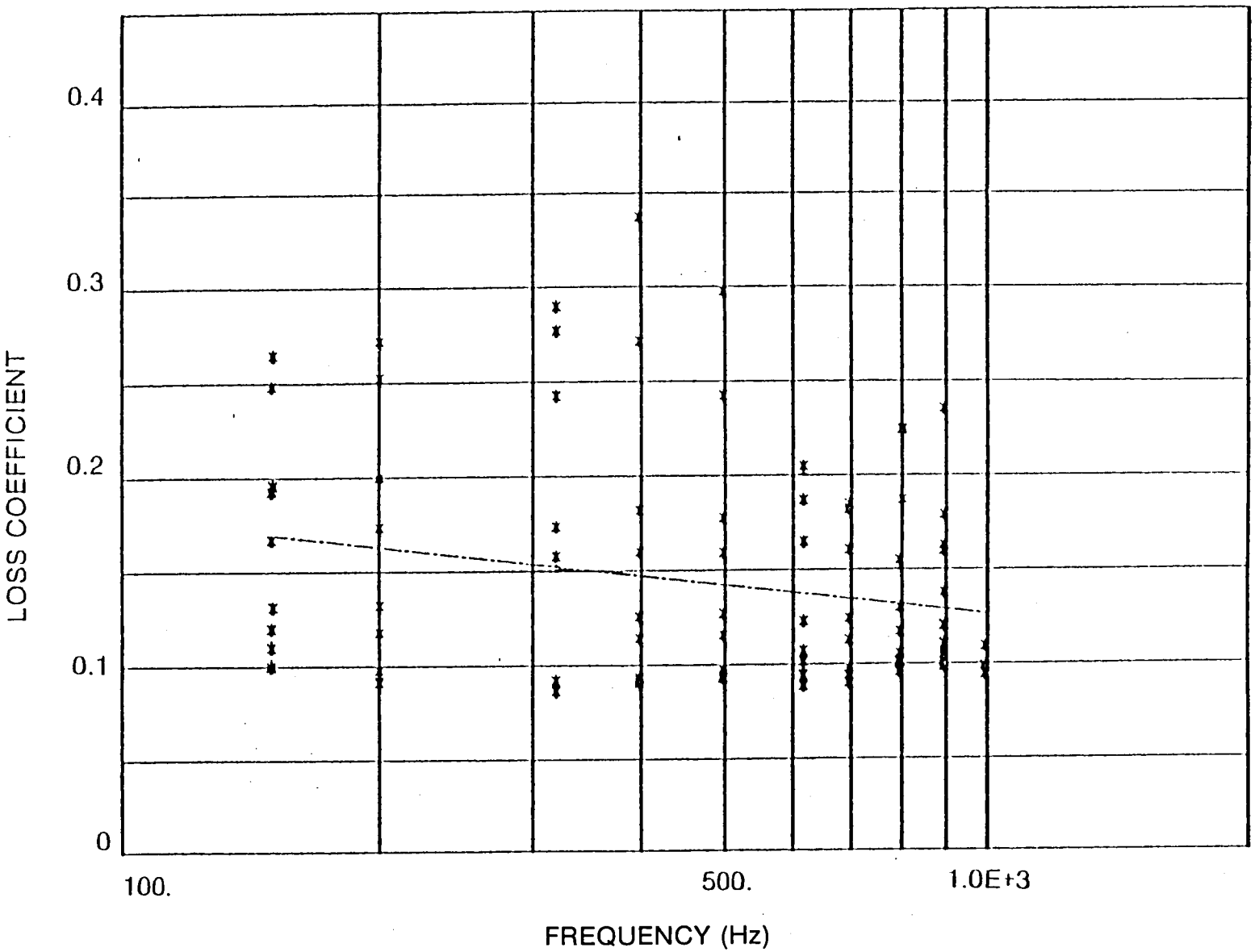

Figure 53 Shear Specimen Data EPDM at 66°C

80481

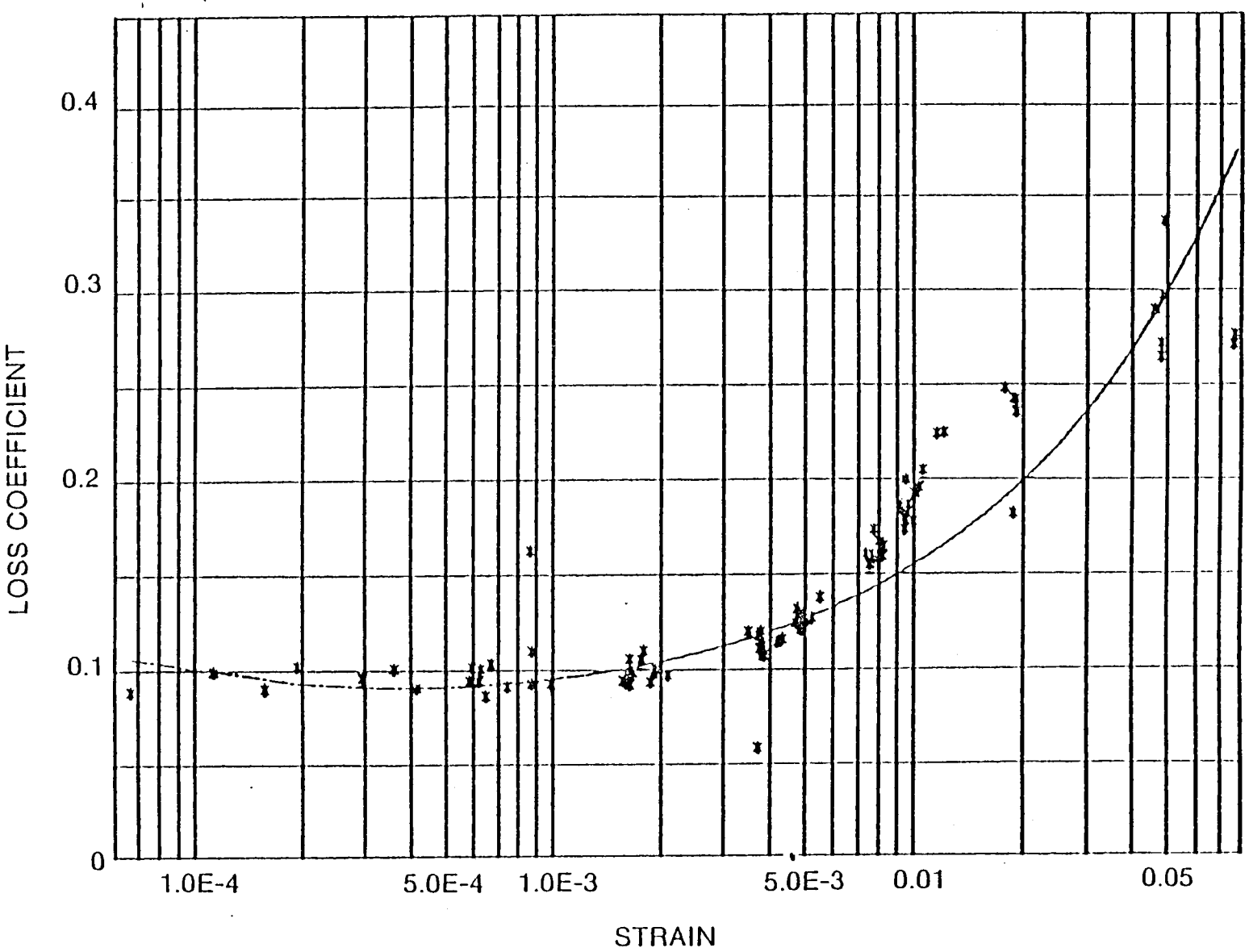

Figure 54 Shear Specimen Data EPDM at 66°C

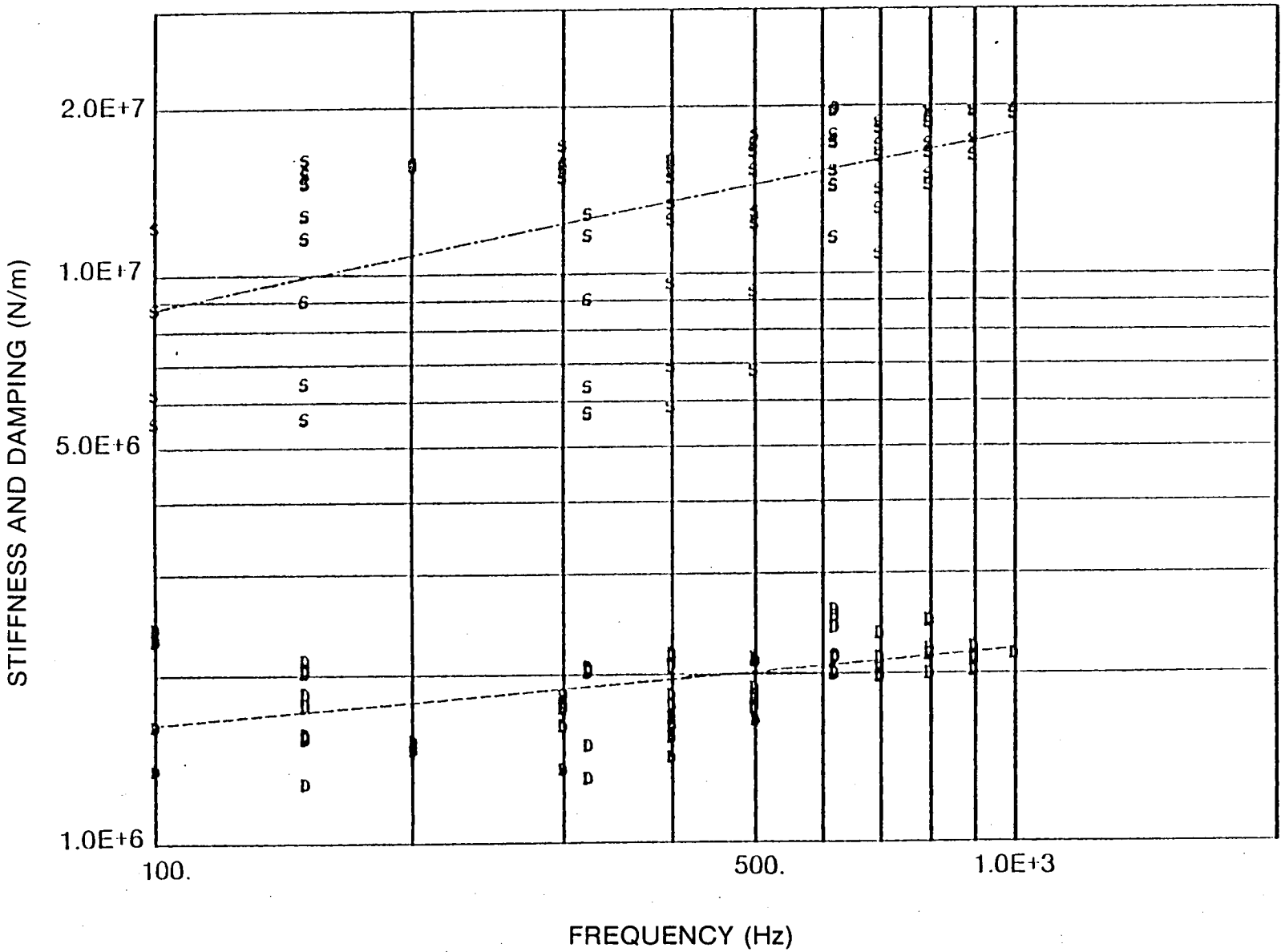

Figure 55 Shear Specimen Data EPDM at 80°C

80483

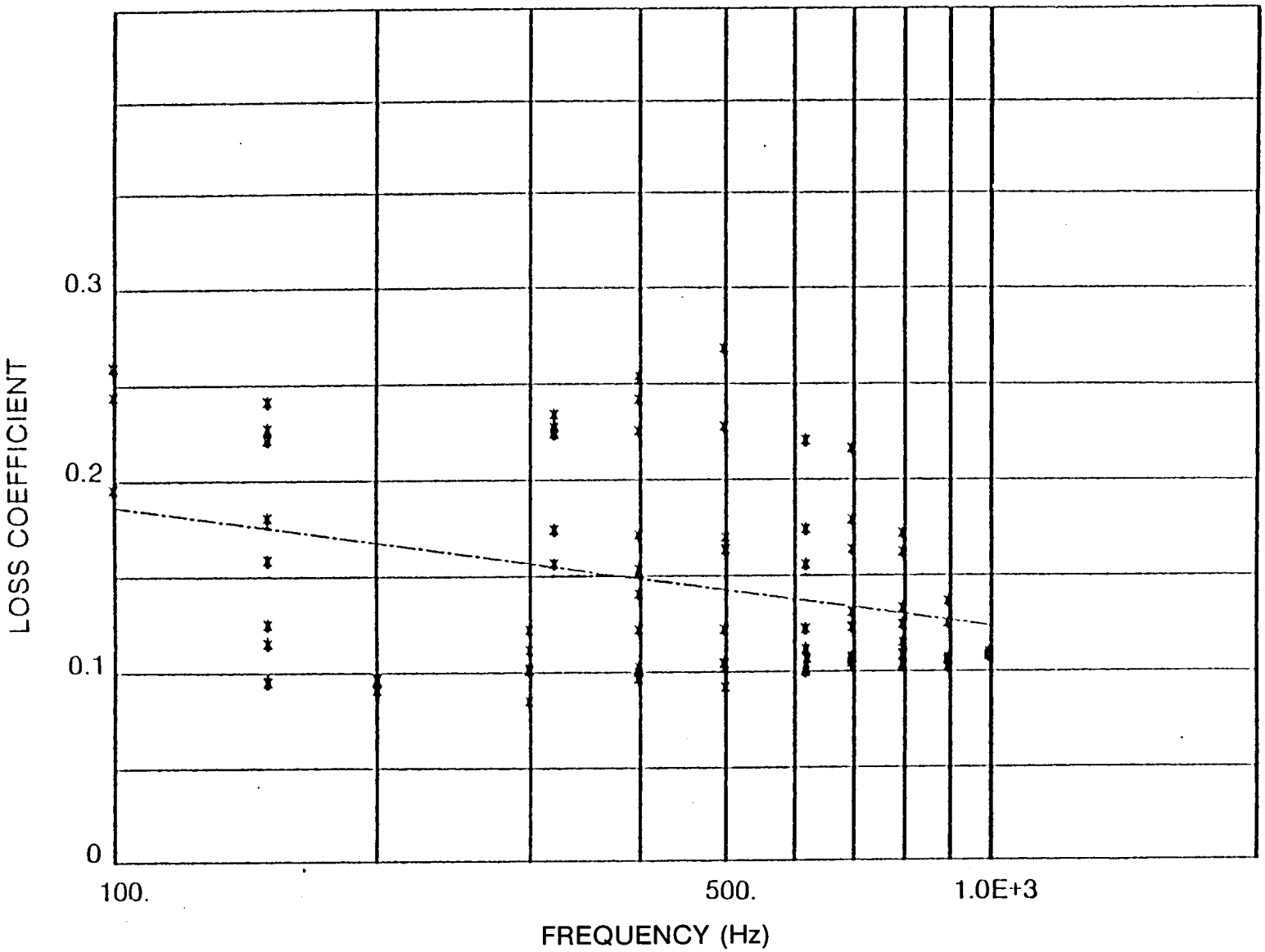

Figure 56 Shear Specimen Data EPDM at 80°C

30484

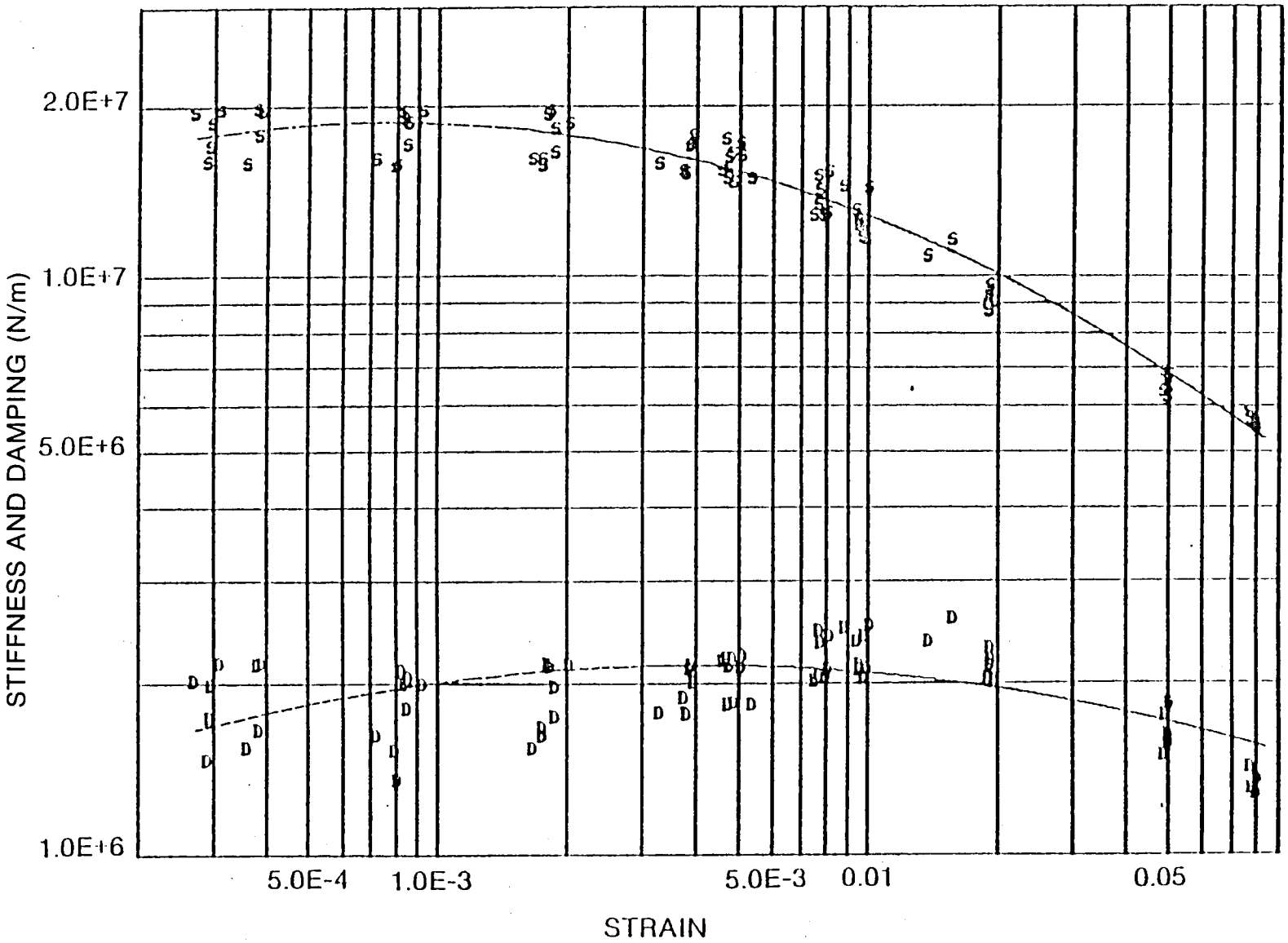

Figure 57 Shear Specimen Data EPDM at 80°C

80485

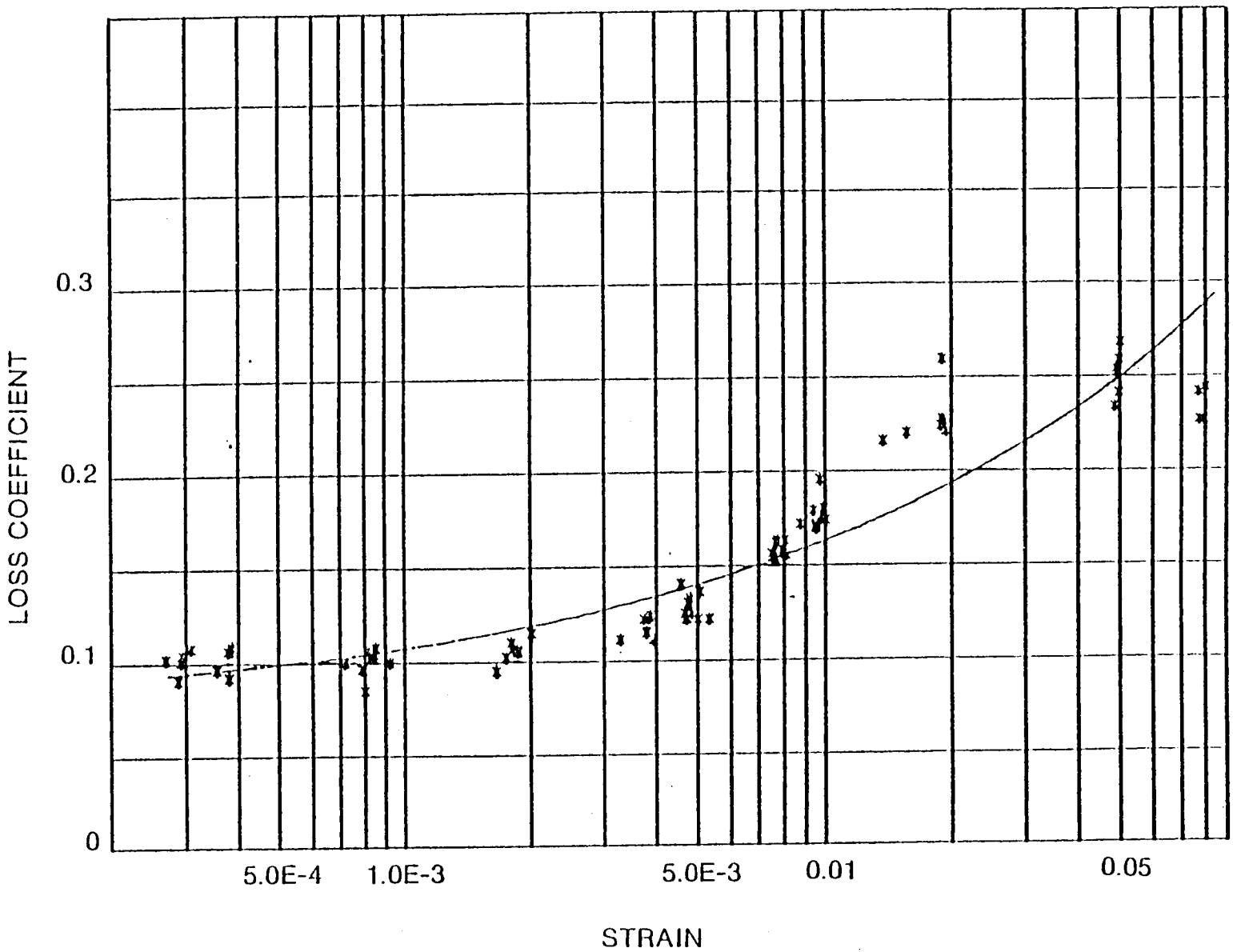

Figure 58 Shear Specimen Data EPDM at 80°C

80486

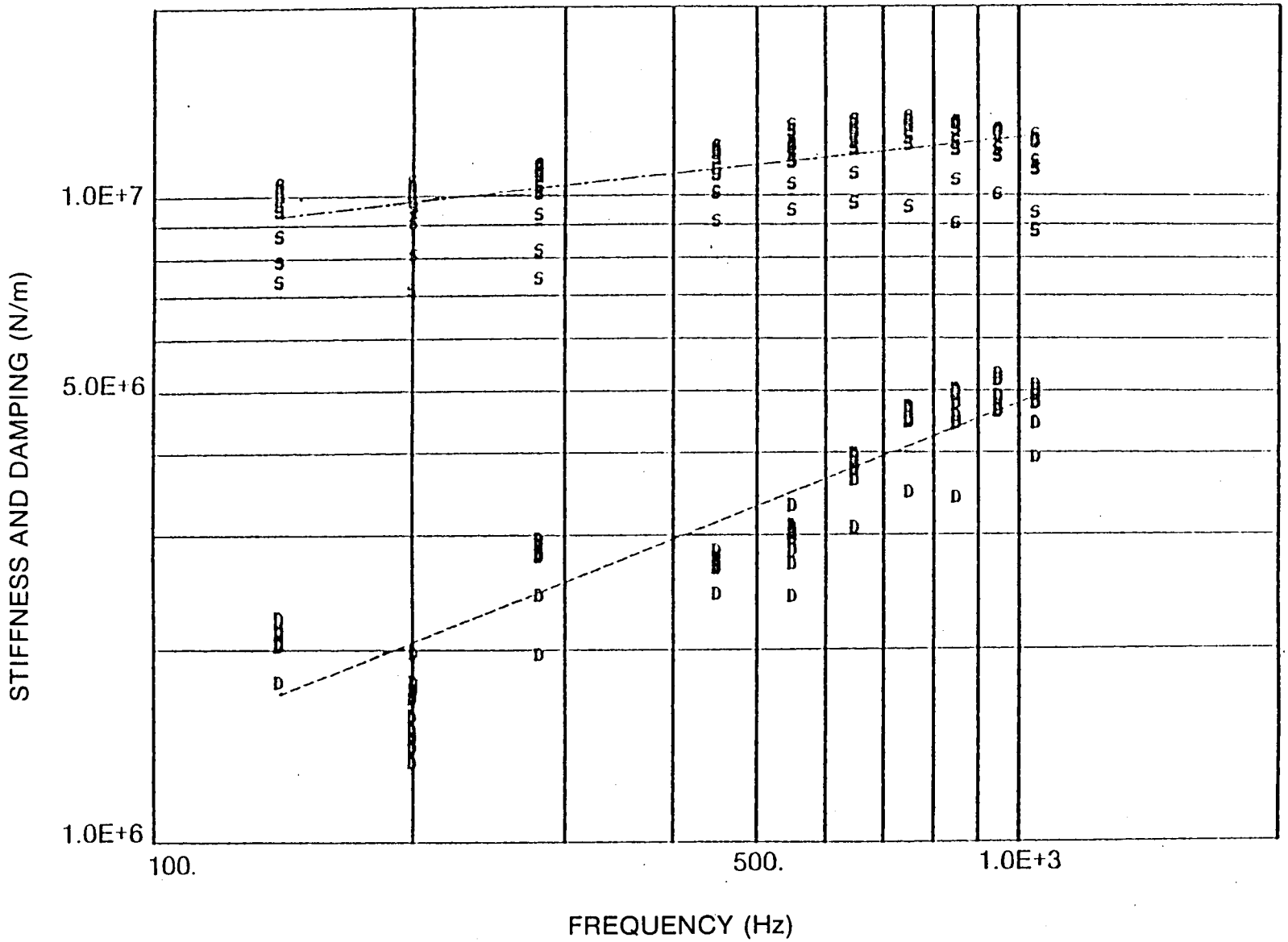

Figure 59 Shear Specimen Data Buna-N at 32°C

90487

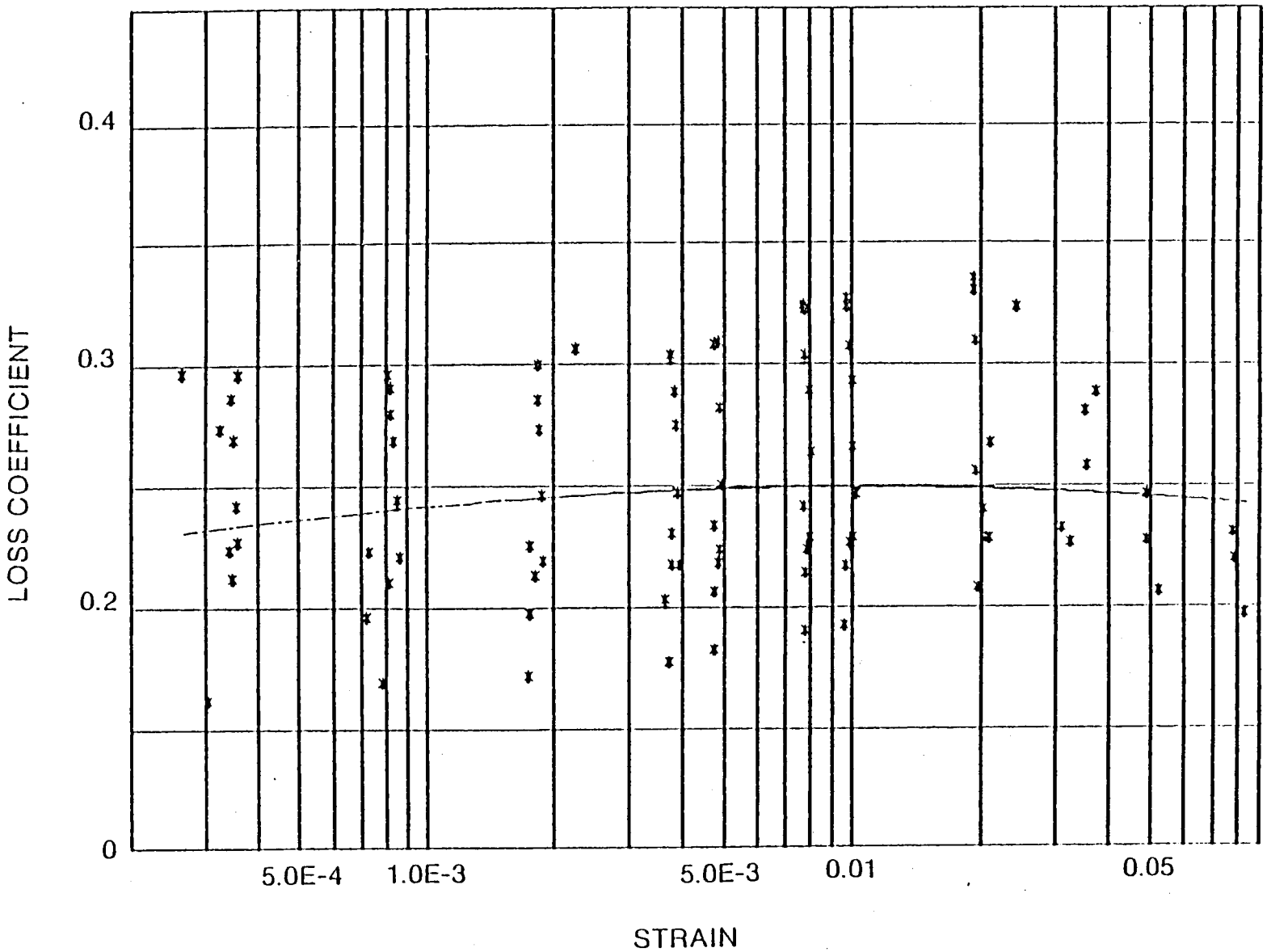

Figure 60 Shear Specimen Data Buna-N at 32°C

80468

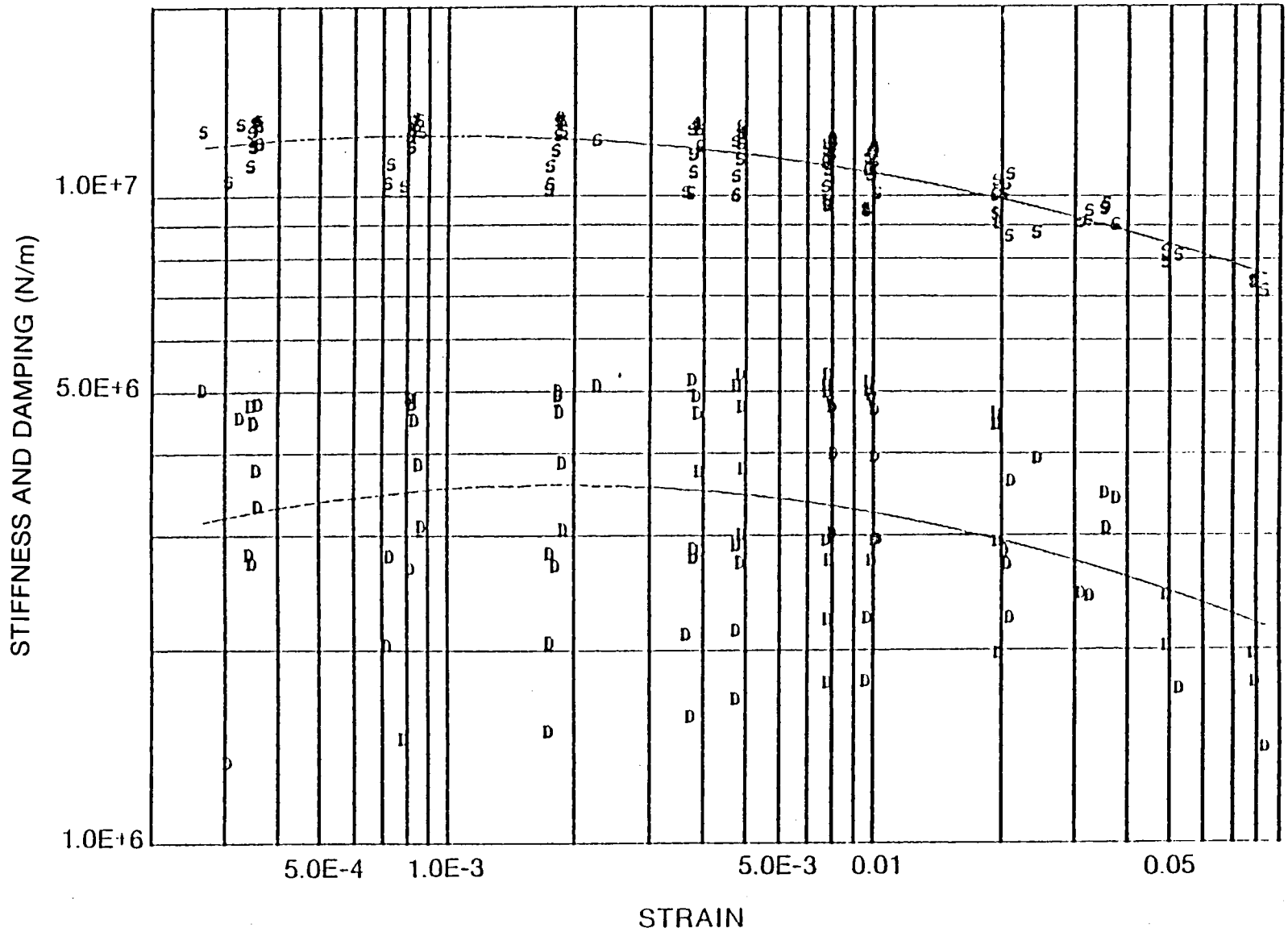

Figure 61 Shear Specimen Data Buna-N at 32°C

80489

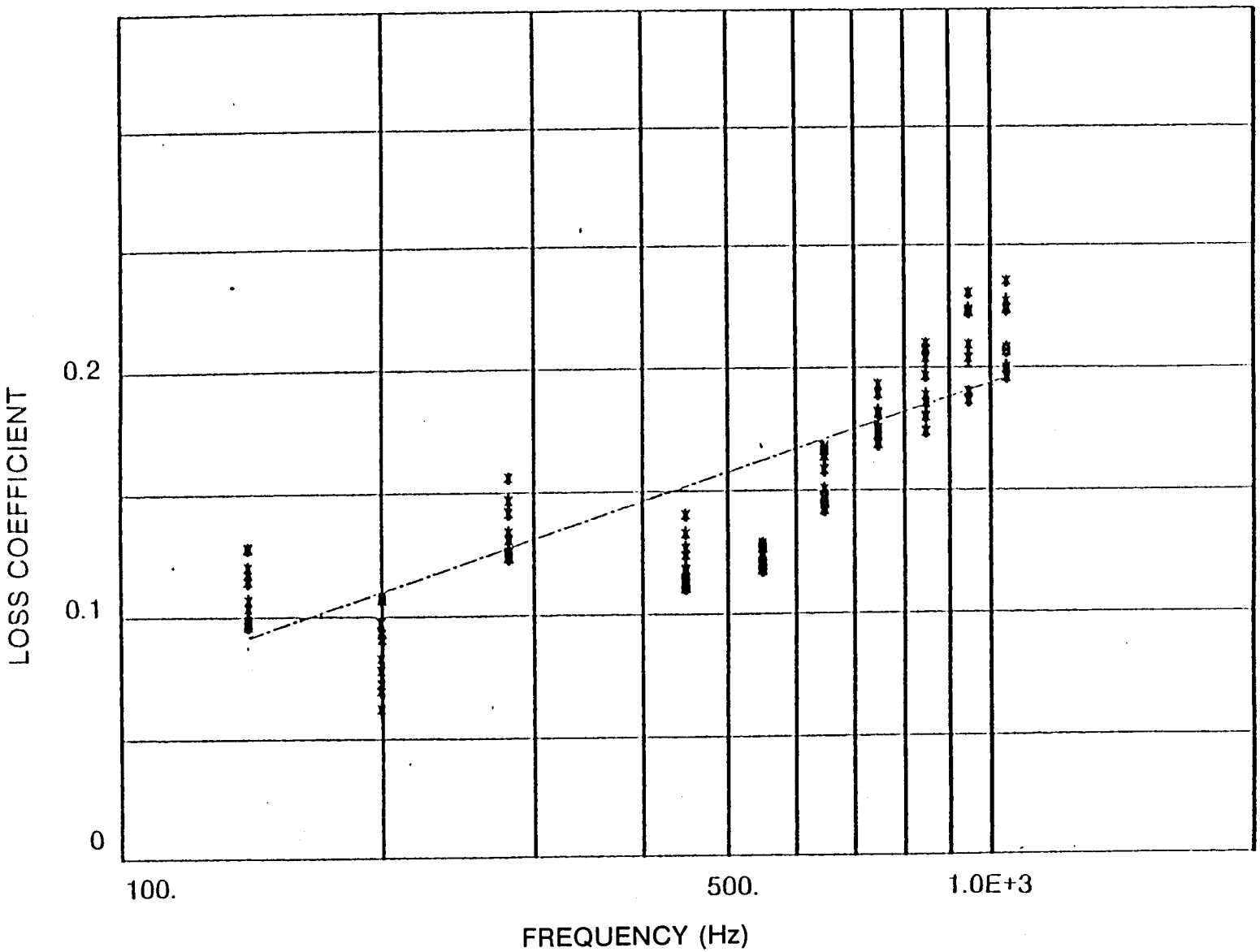

Figure 62 Shear Specimen Data Buna-N at 32°C

80490

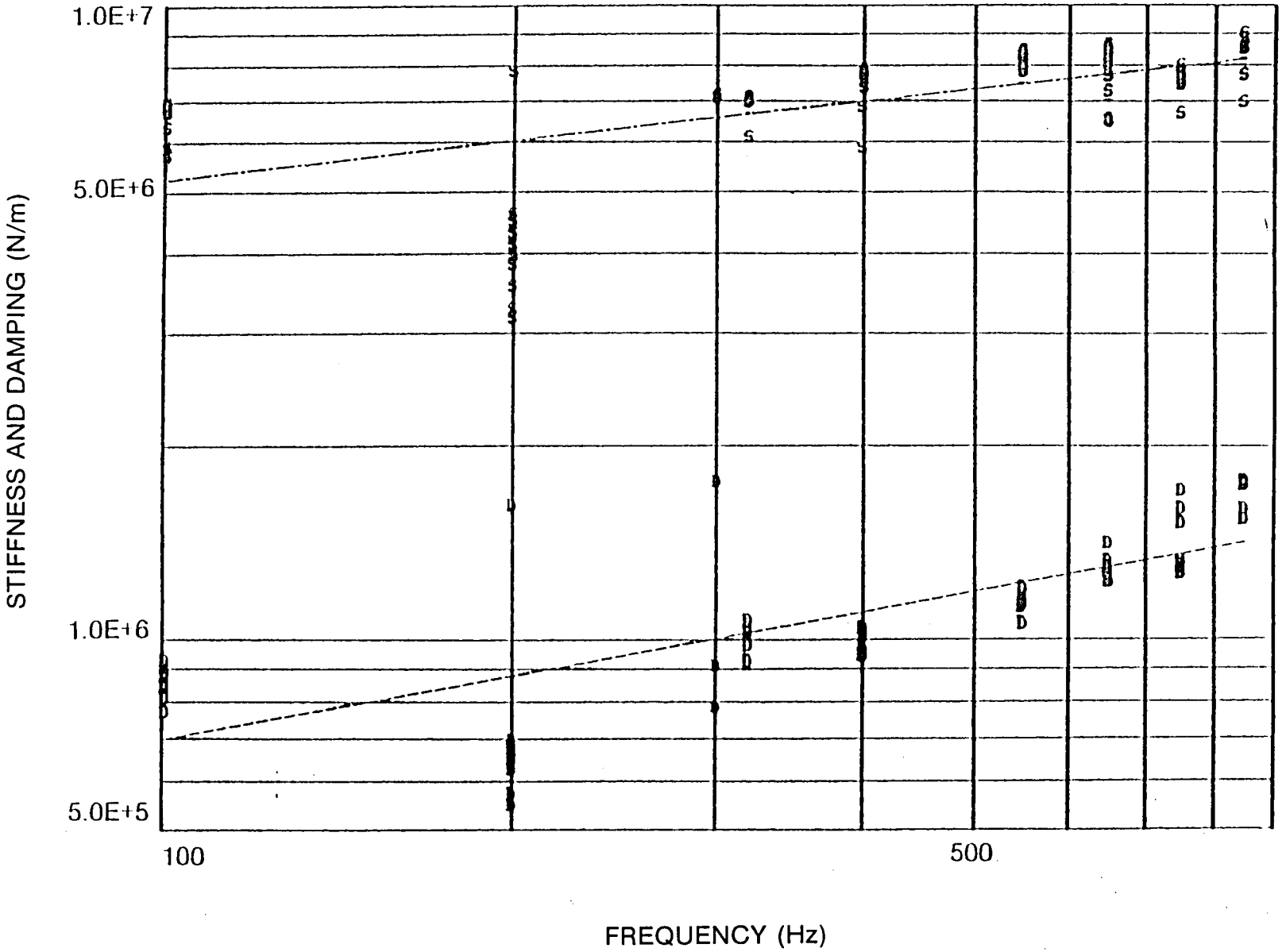

Figure 63 Shear Specimen Data Buna-N at 66°C

80491

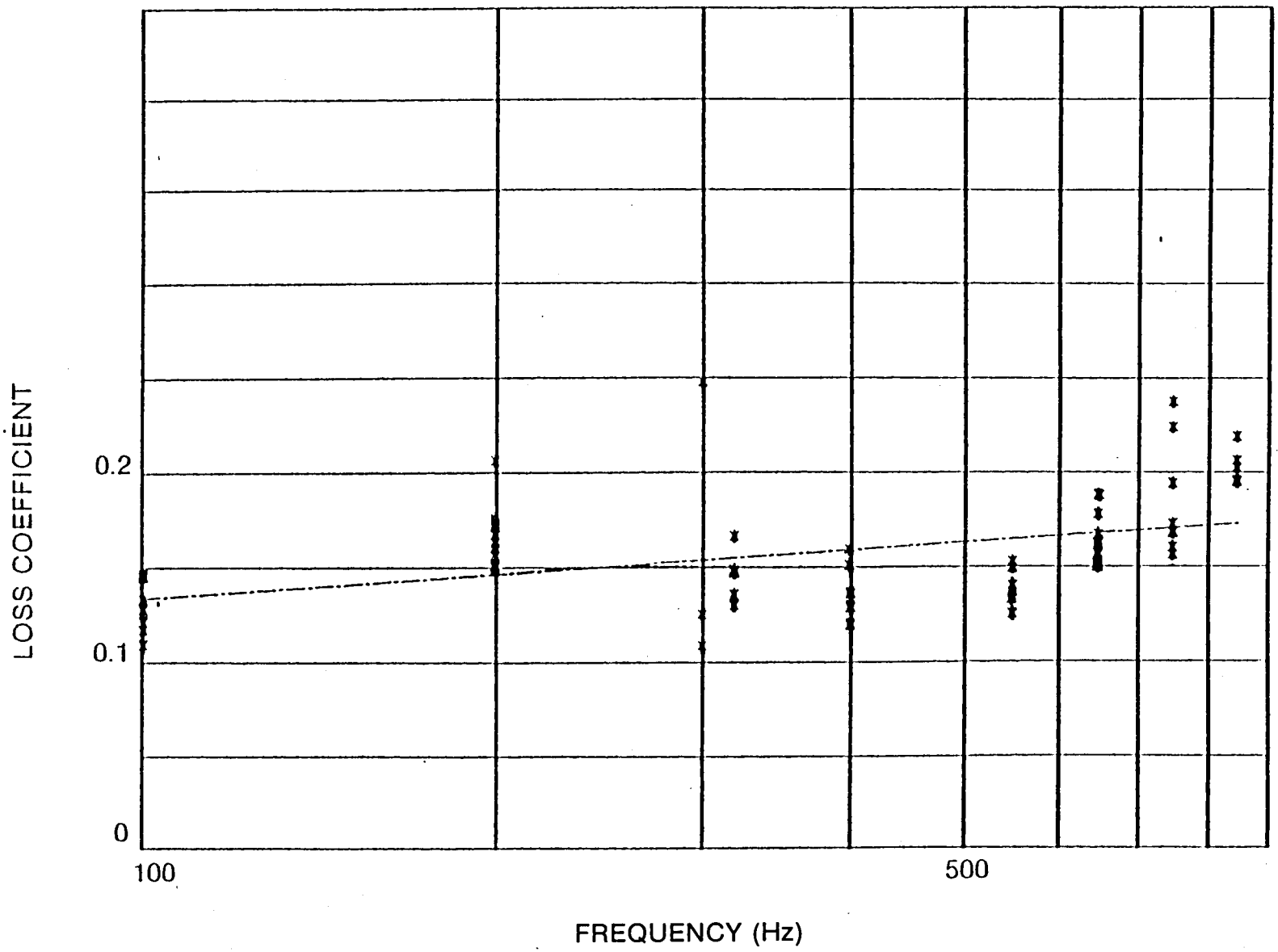

Figure 64 Shear Specimen Data Buna-N at 66°C

30492

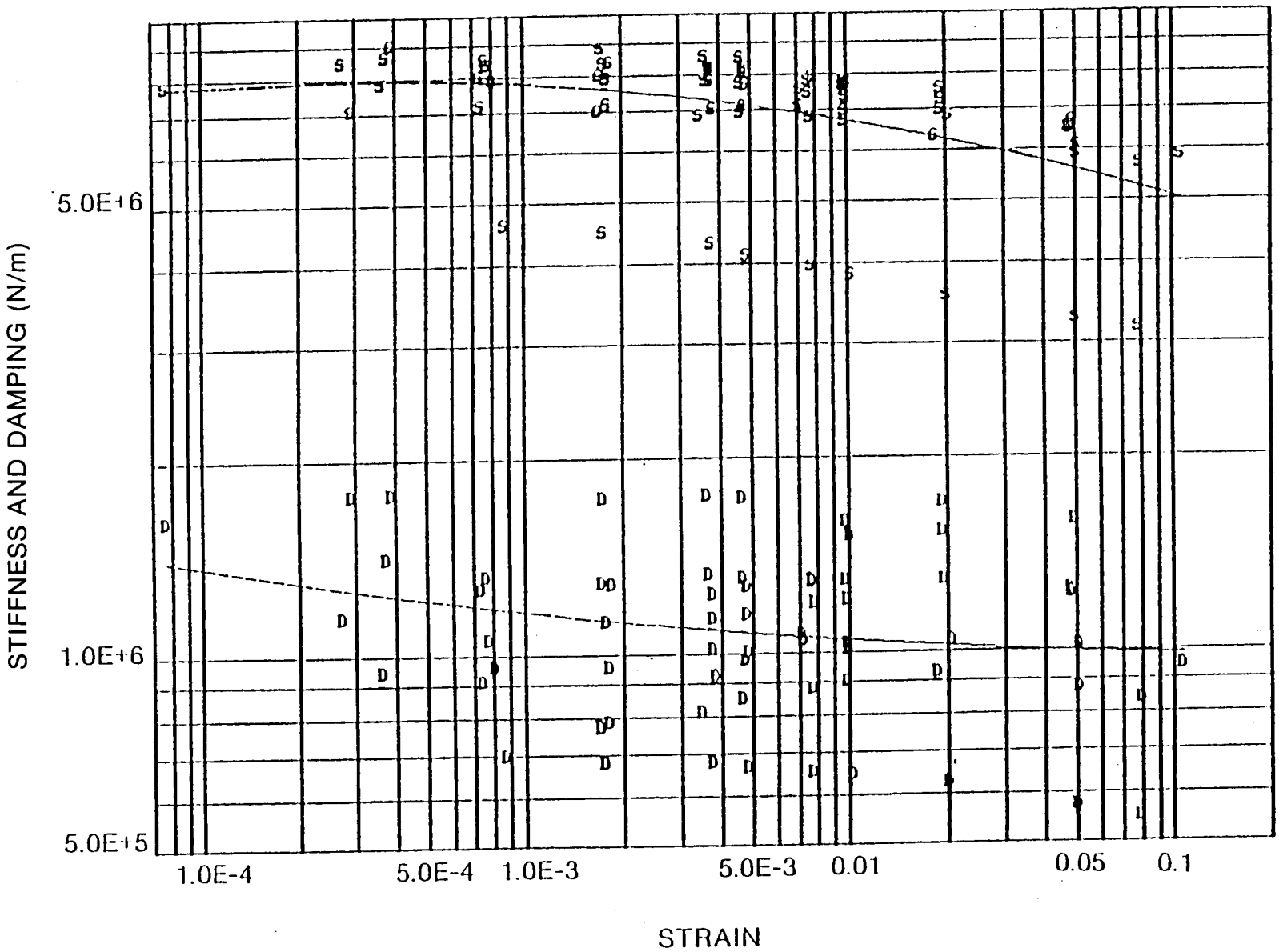

Figure 65 Shear Specimen Data Buna-N at 66°C

80493

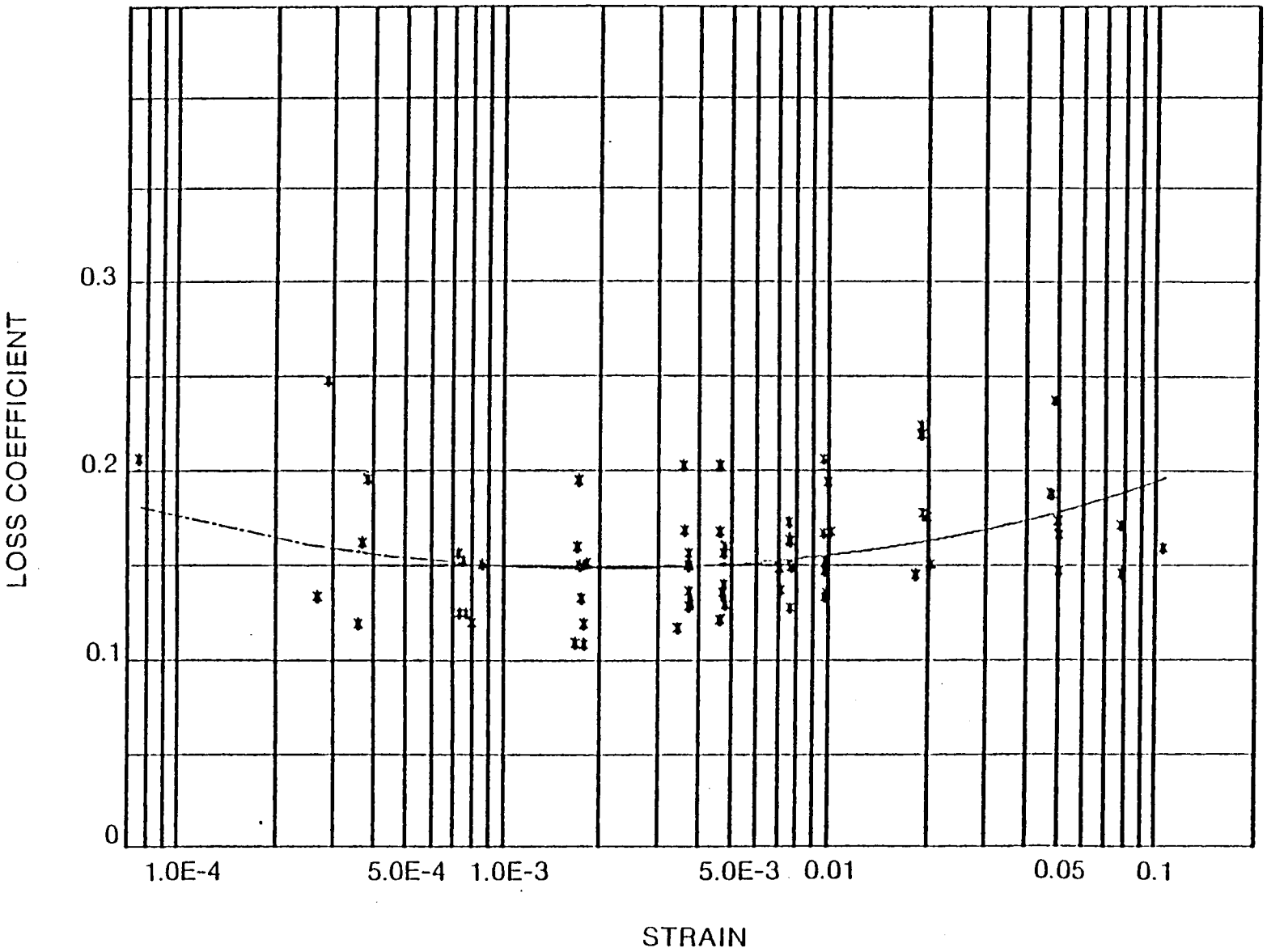

Figure 66 Shear Specimen Data Buna-N at 66°C

80494

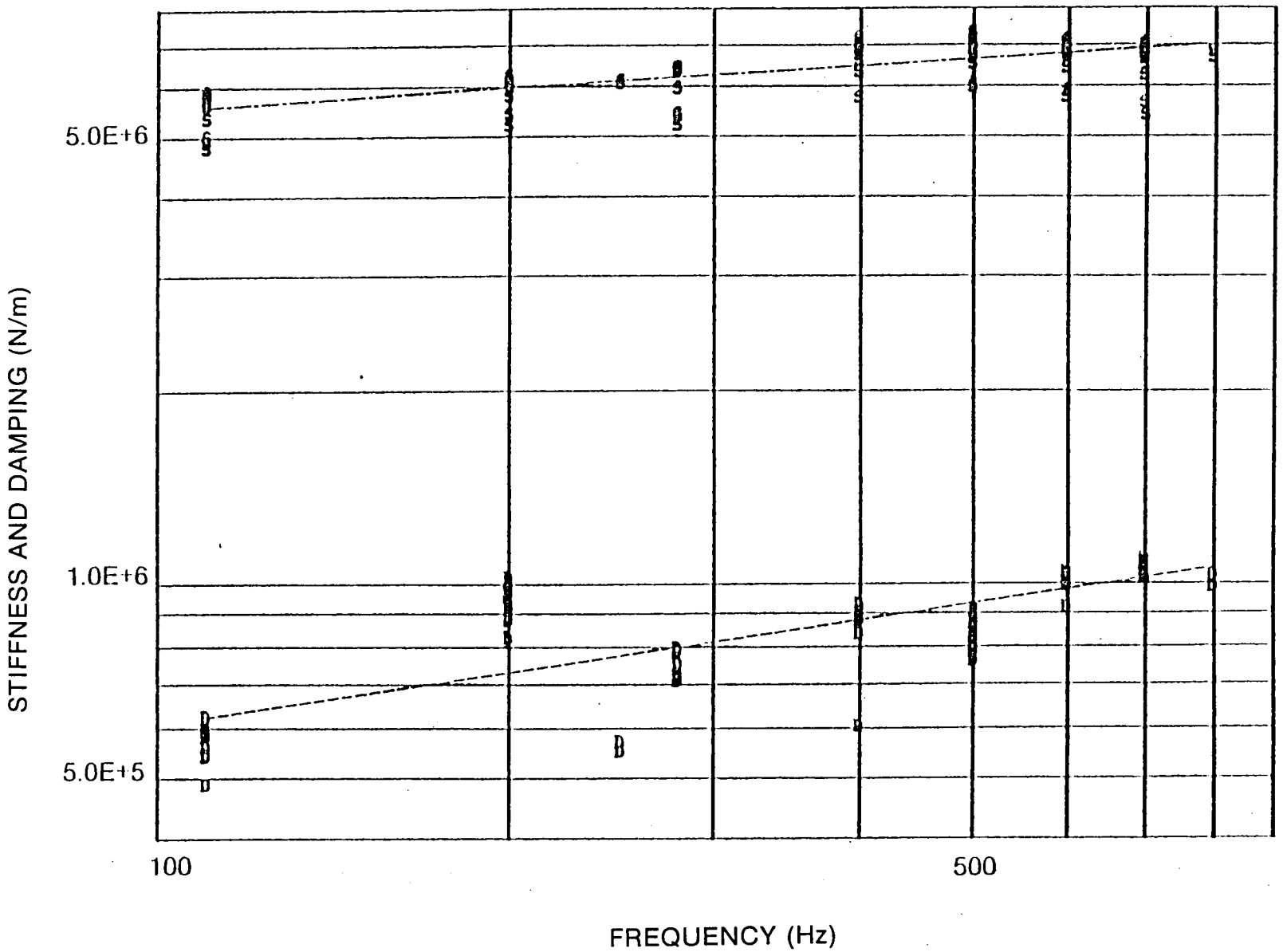

Figure 67 Shear Specimen Data Buna-N at 80°C

80495

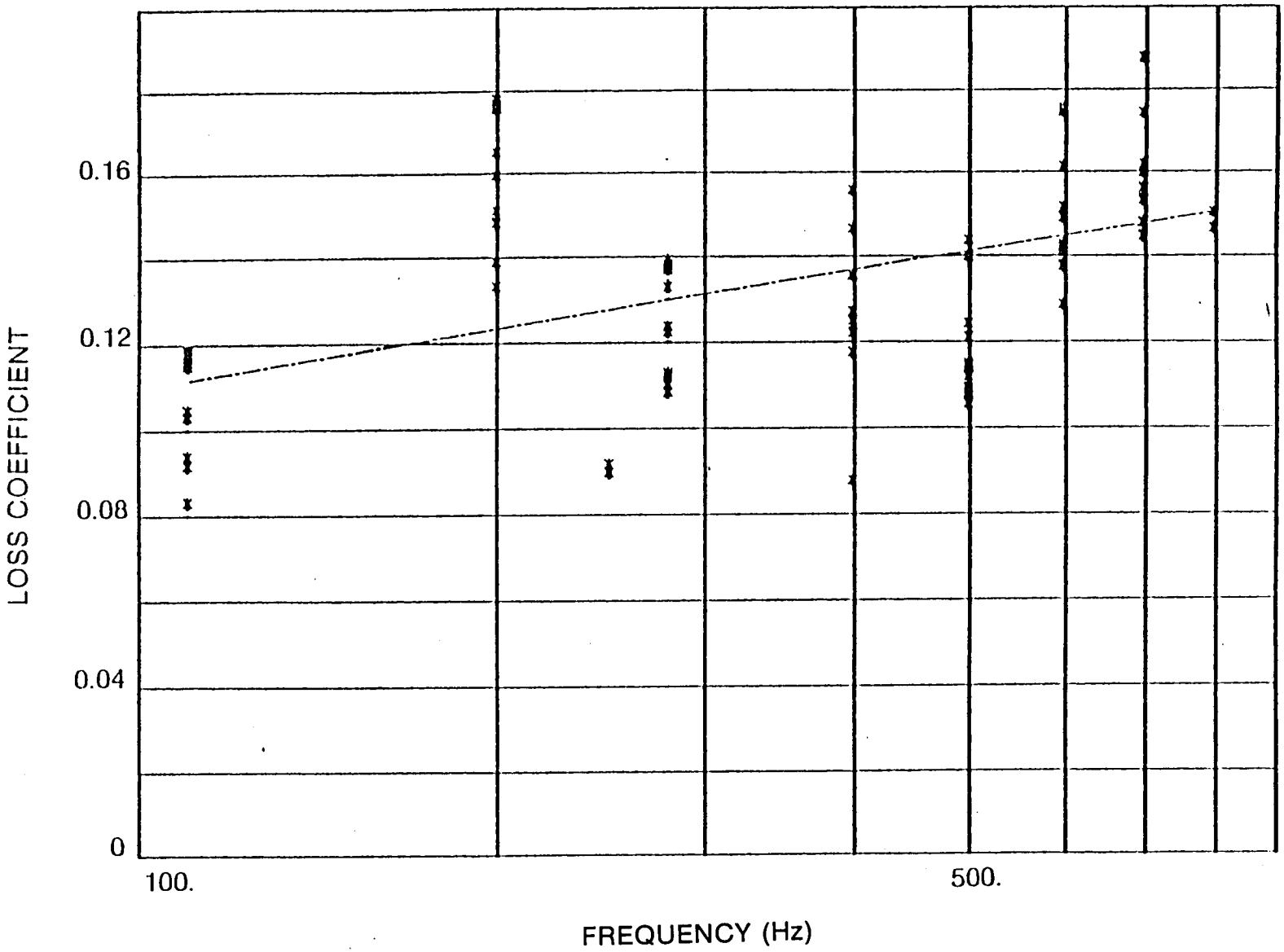

Figure 68 Shear Specimen Data Buna-N at 80°C

80496

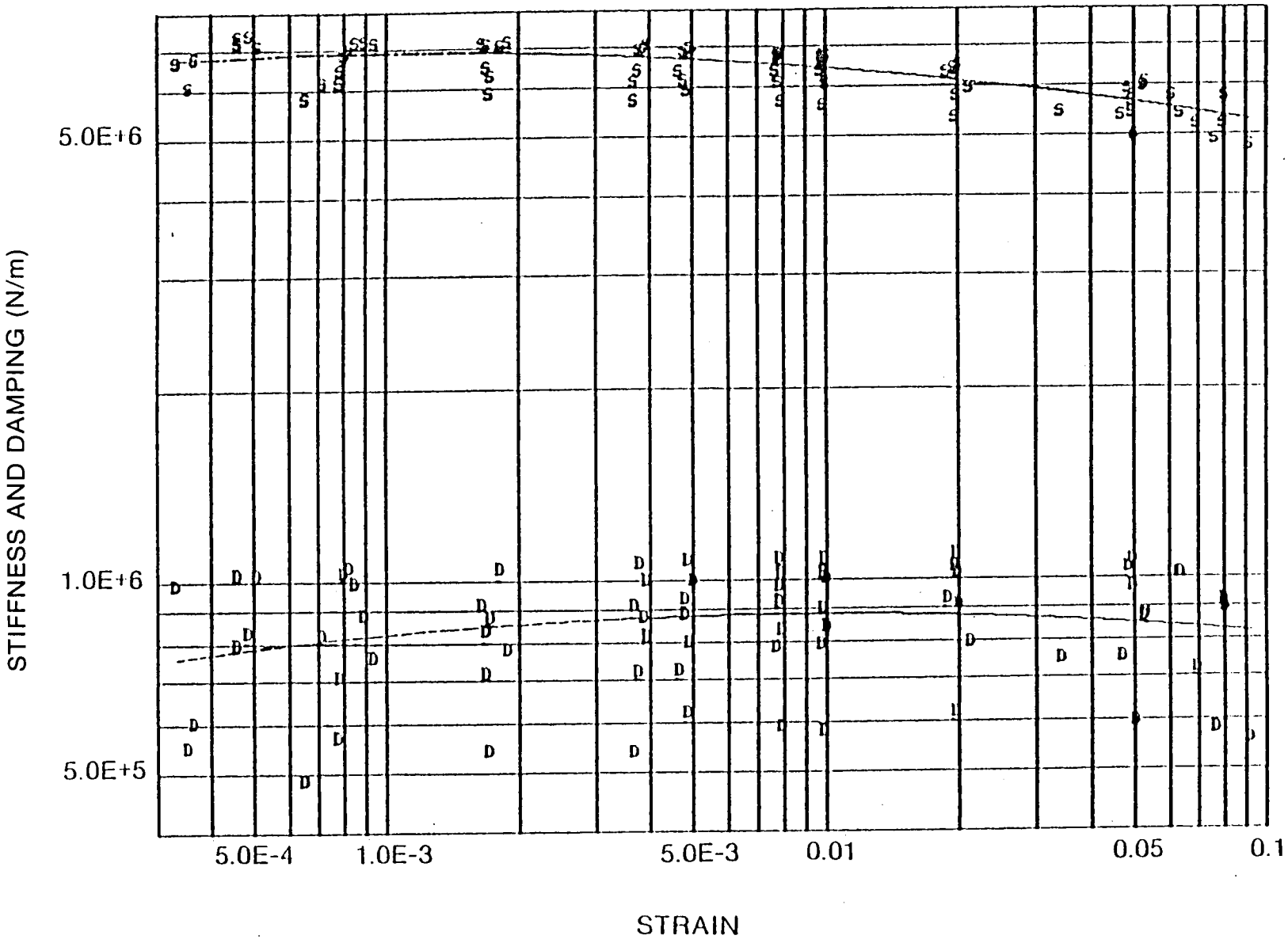

Figure 69 Shear Specimen Data Buna-N at 80°C

30497

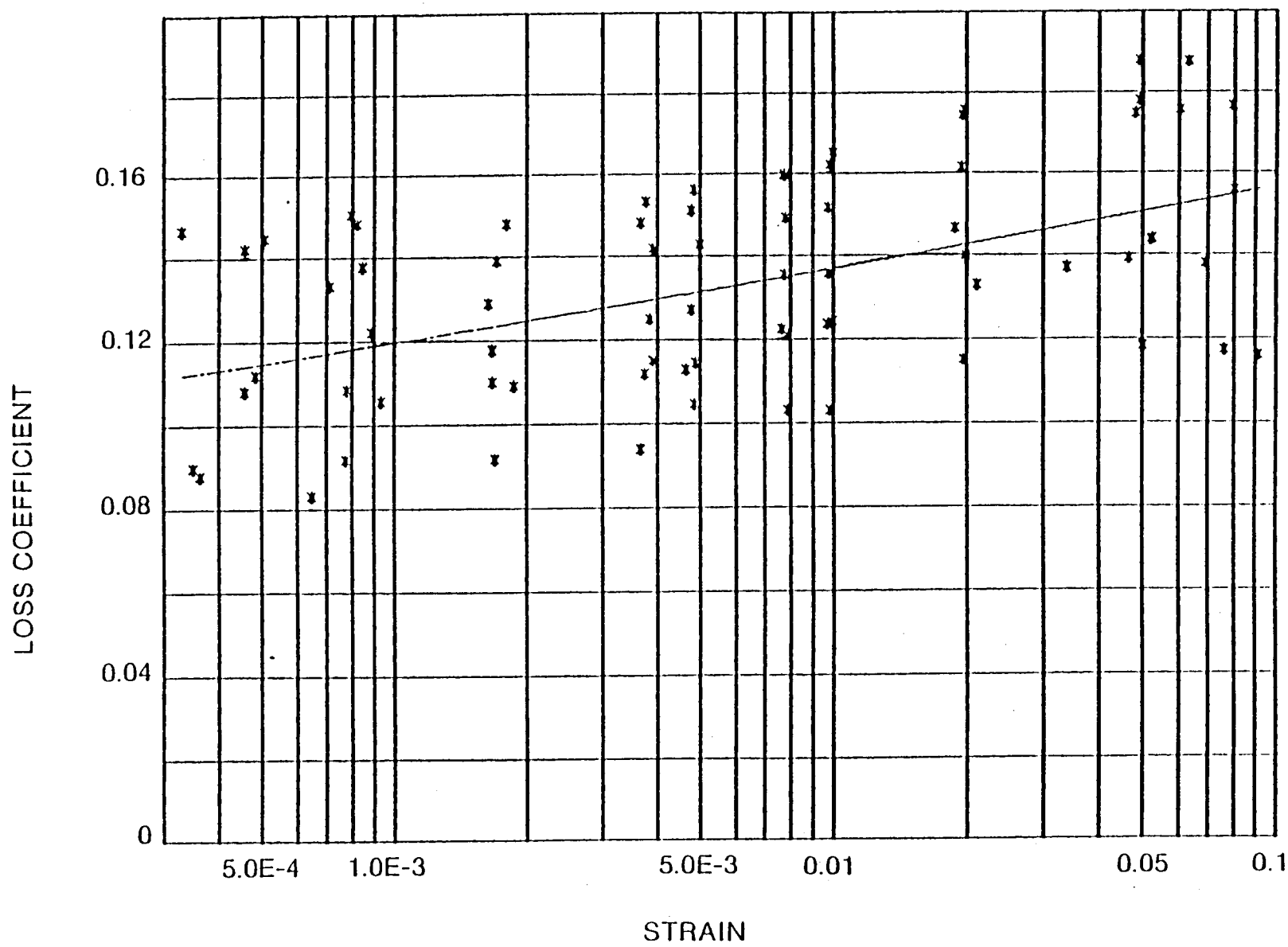

Figure 70 Shear Specimen Data Buna-N at 80°C

80498

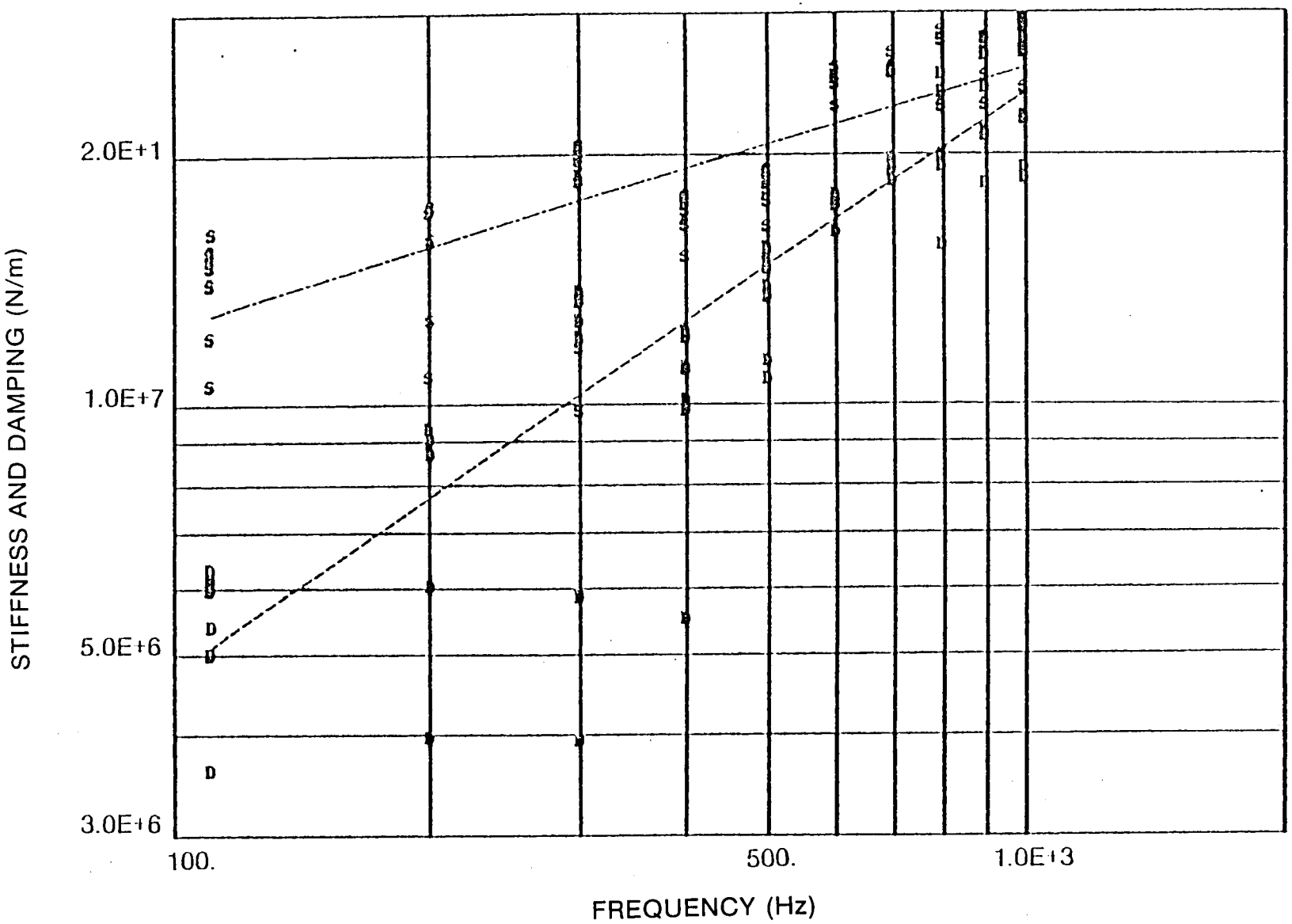

Figure 71 Shear Specimen Data Viton-70 at 32°C

80499

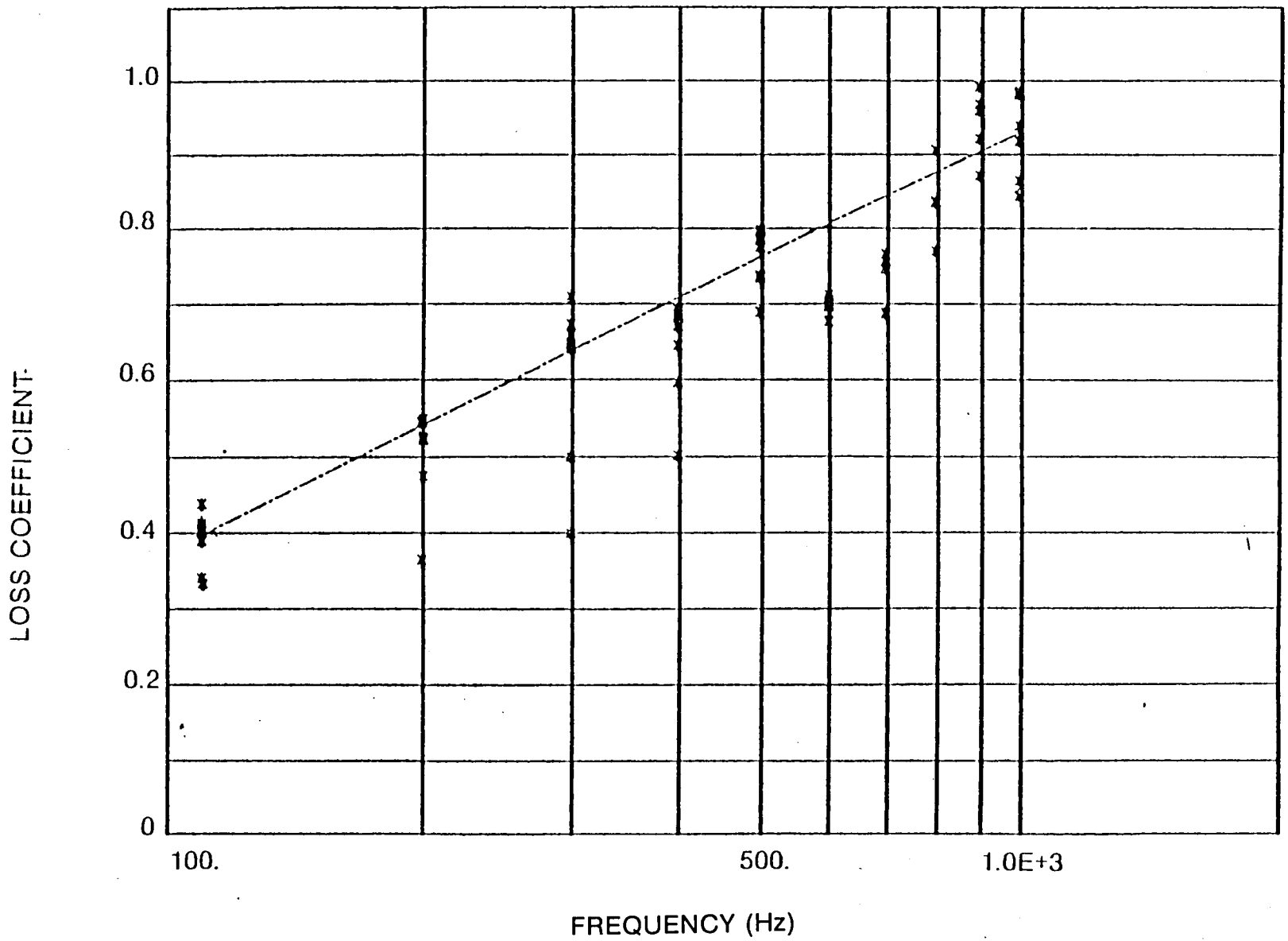

Figure 72 Shear Specimen Data Viton-70 at 32°C

80500

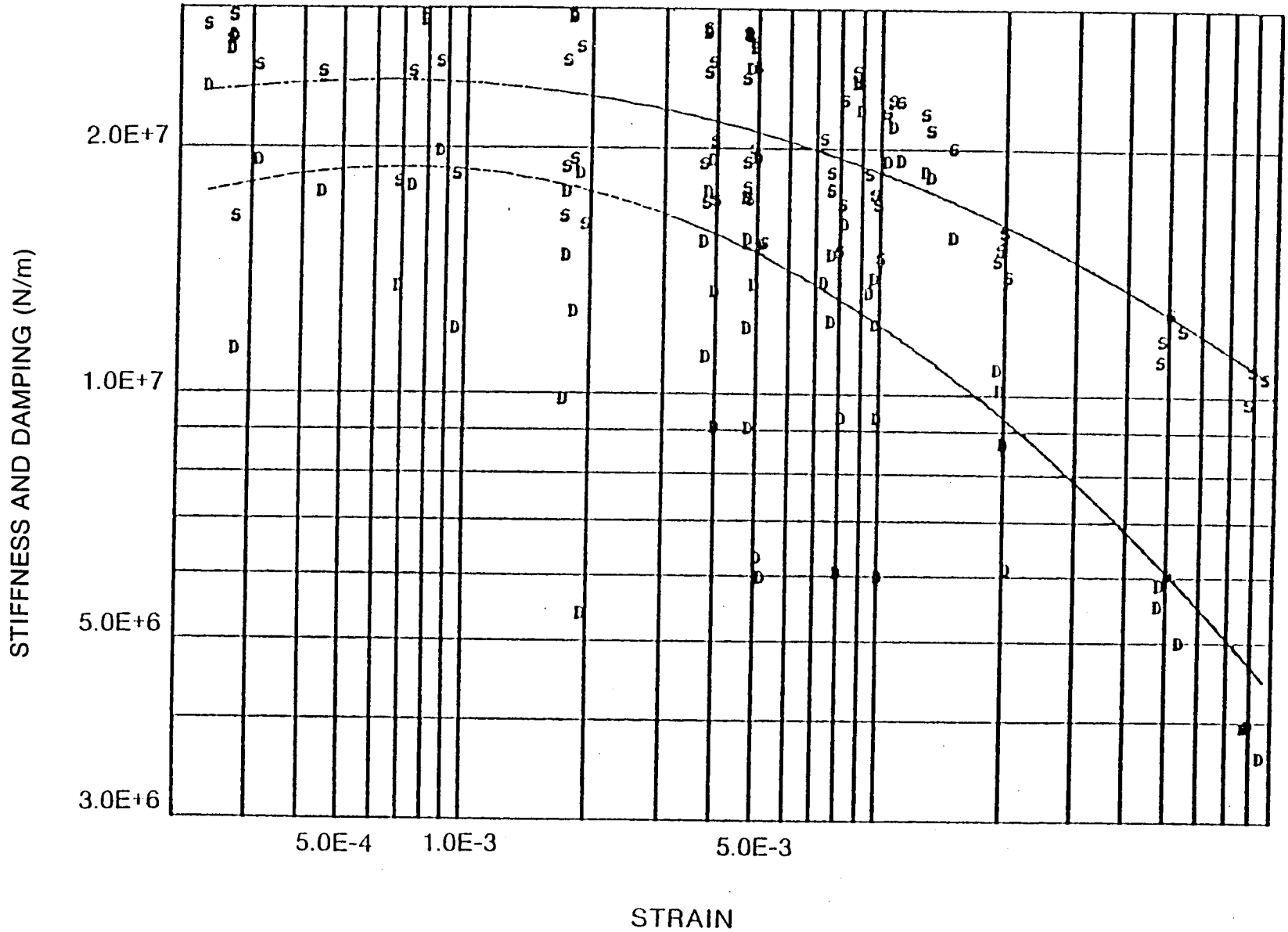

Figure 73 Shear Specimen Data Viton-70 at 32°C

80501

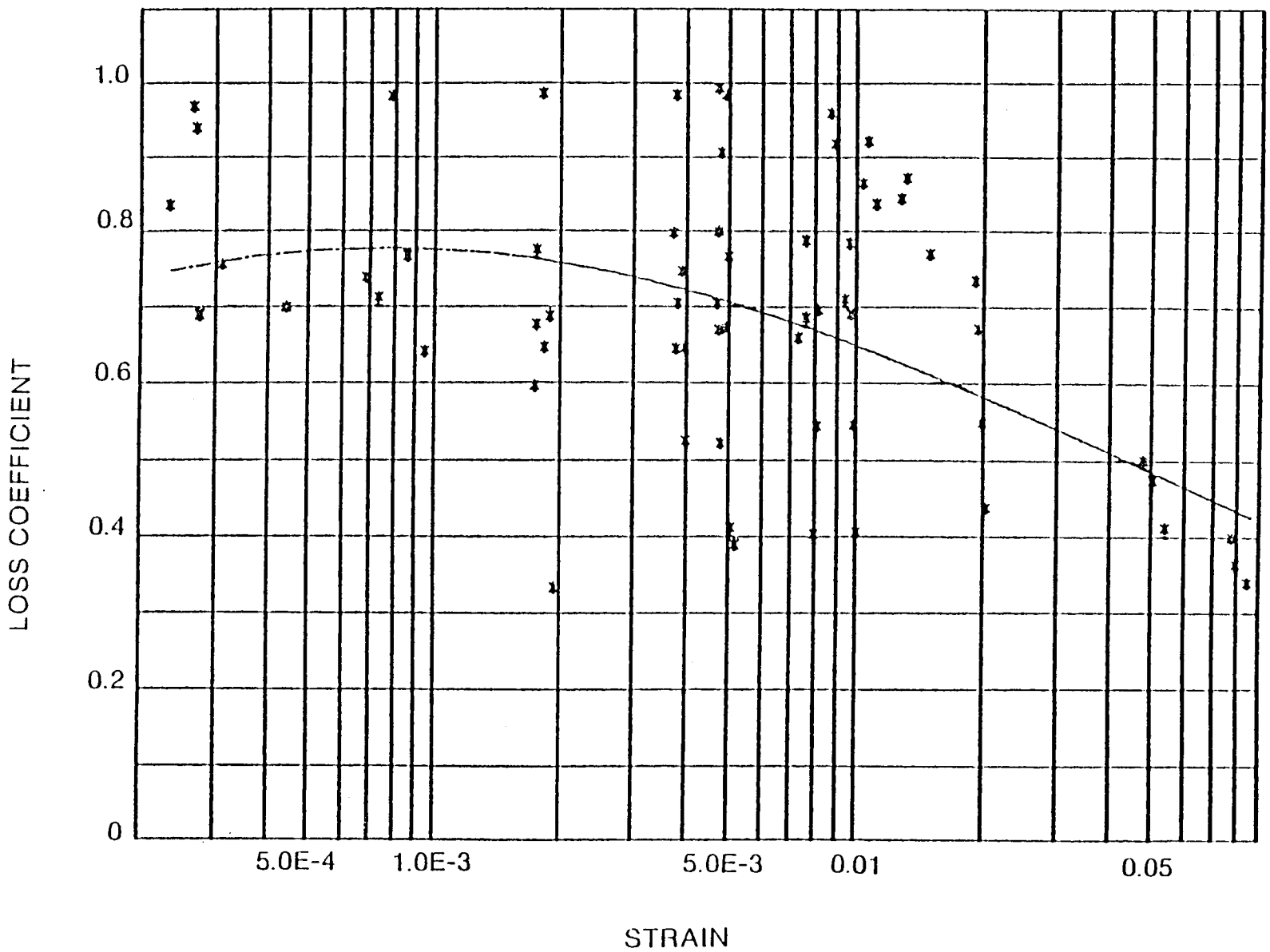

Figure 74 Shear Specimen Data Viton-70 at 32°C

30502

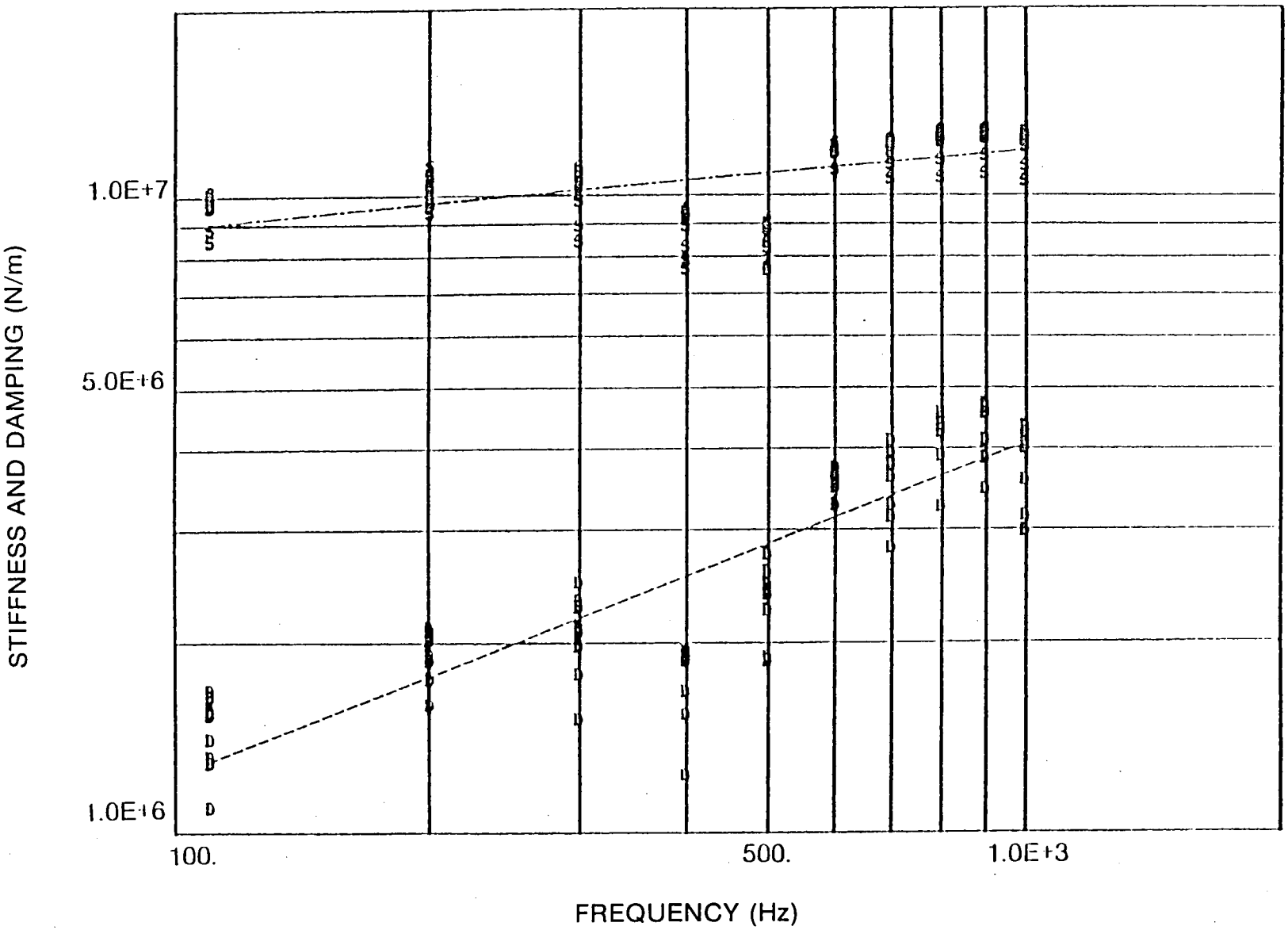

Figure 75 Shear Specimen Data Viton-70 at 66°C

80503

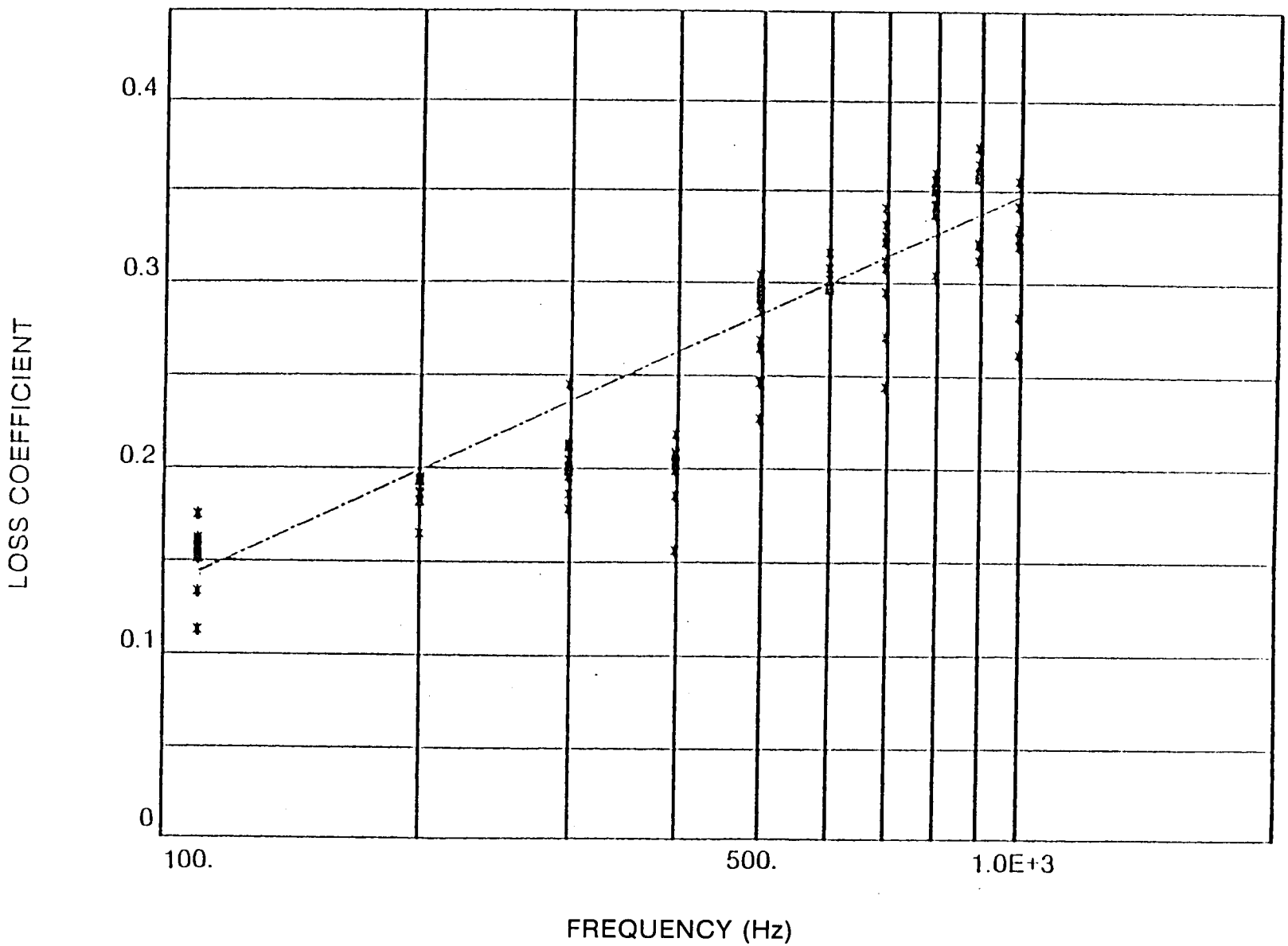

Figure 76 Shear Specimen Data Viton-70 at 66°C

90504

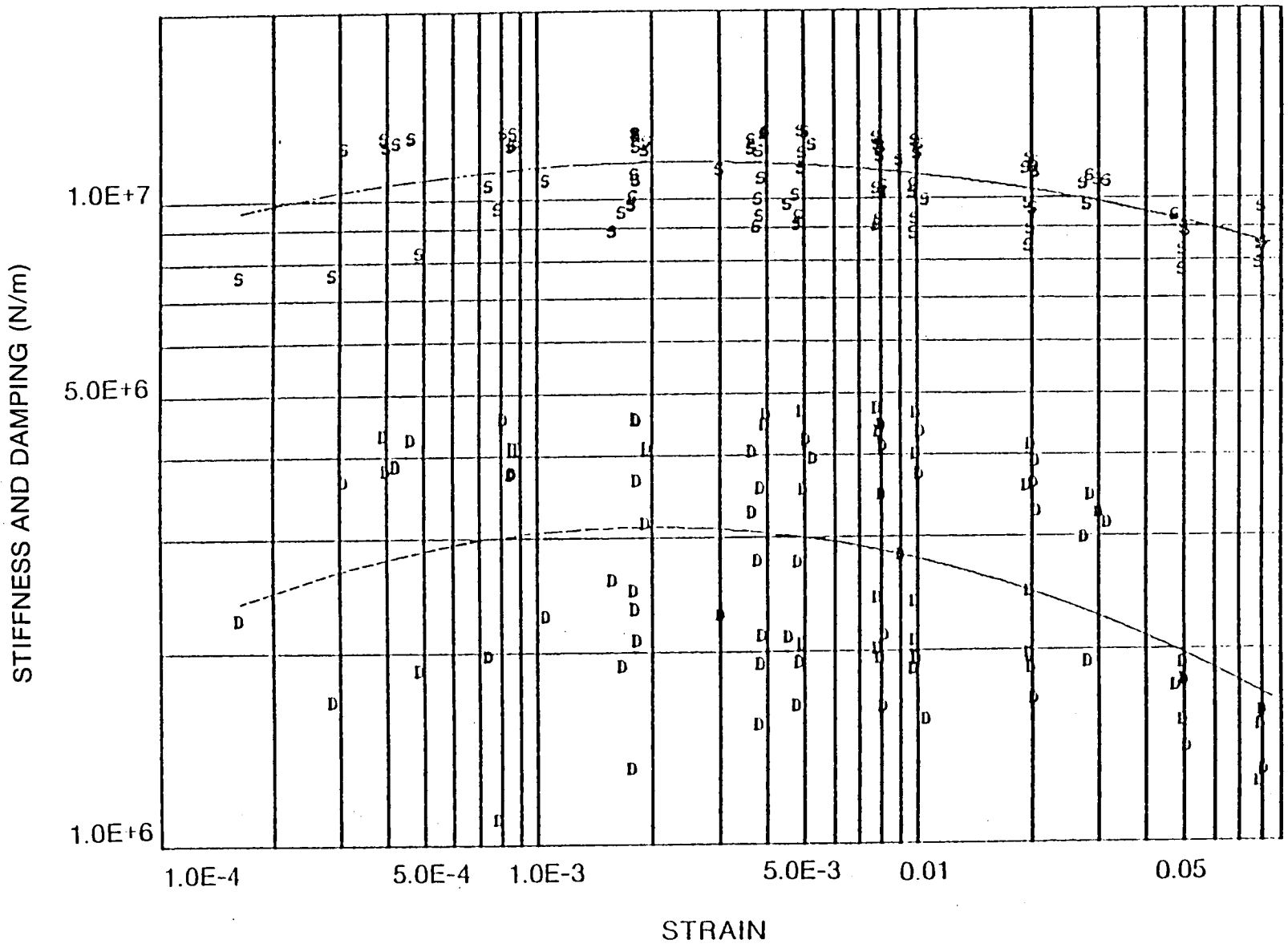

Figure 77 Shear Specimen Data Viton-70 at 66°C

80505

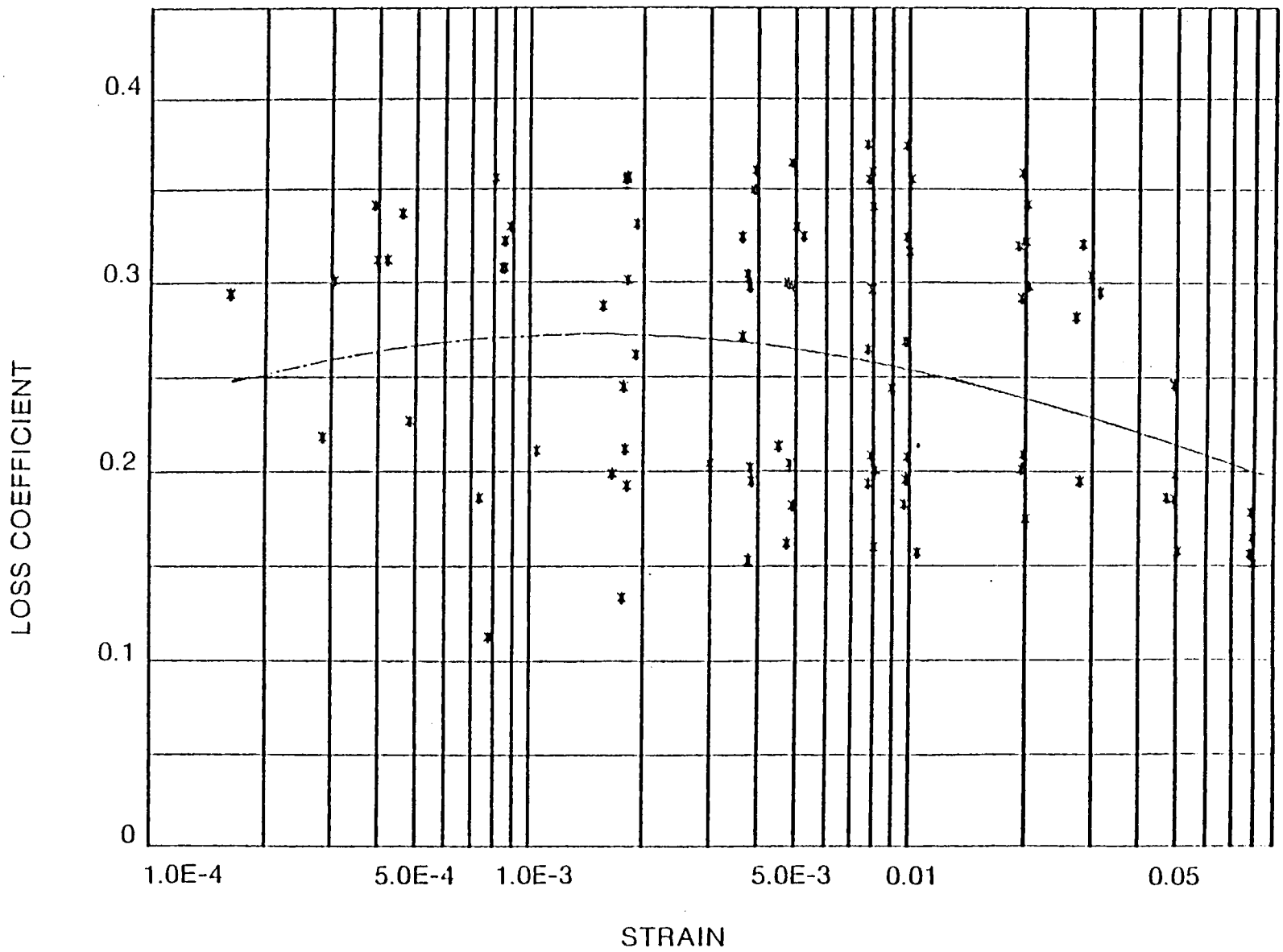

Figure 78 Shear Specimen Data Viton-70 at 66°C

80506

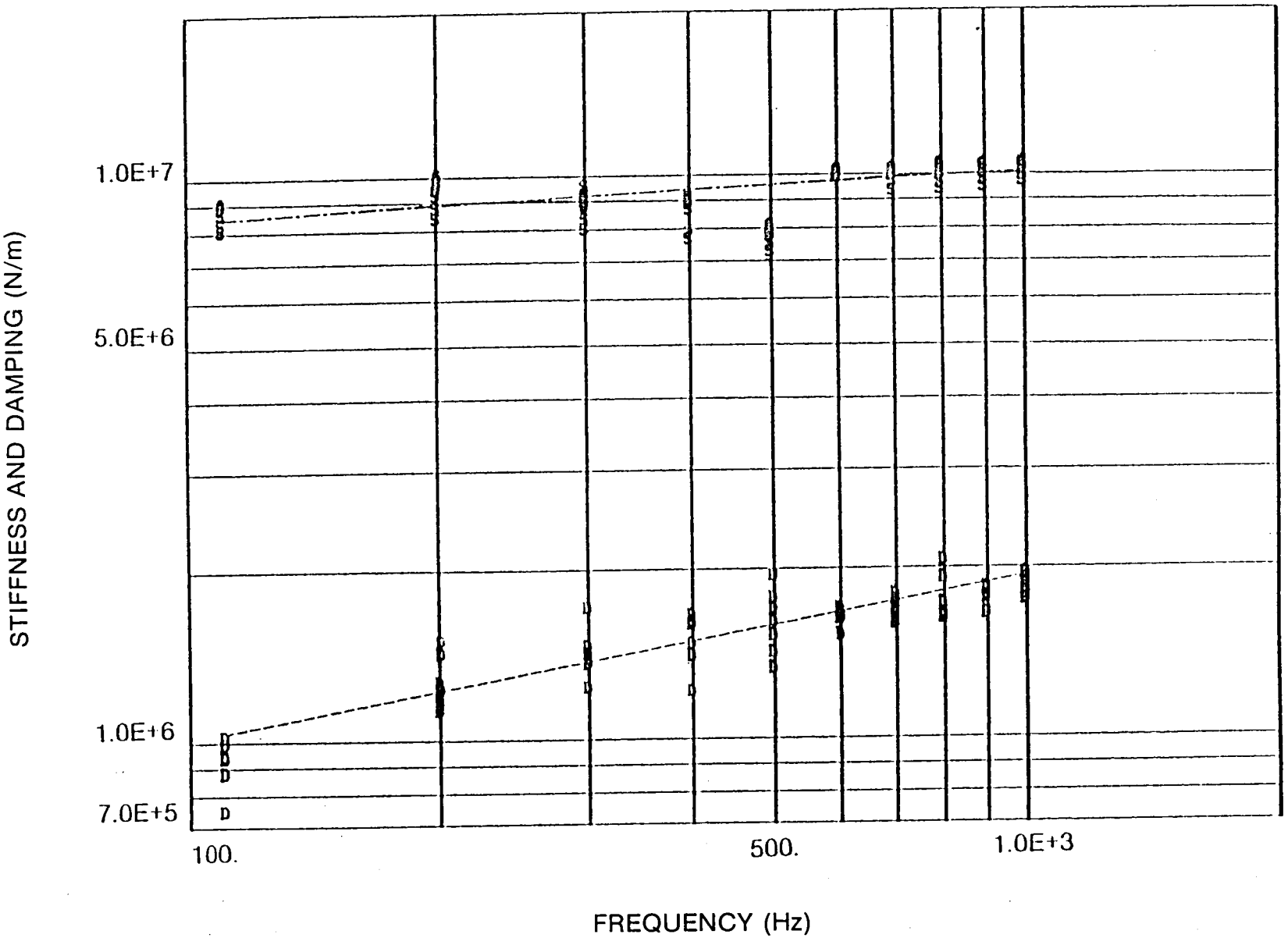

Figure 79 Shear Specimen Data Viton-70 at 80°C

80507

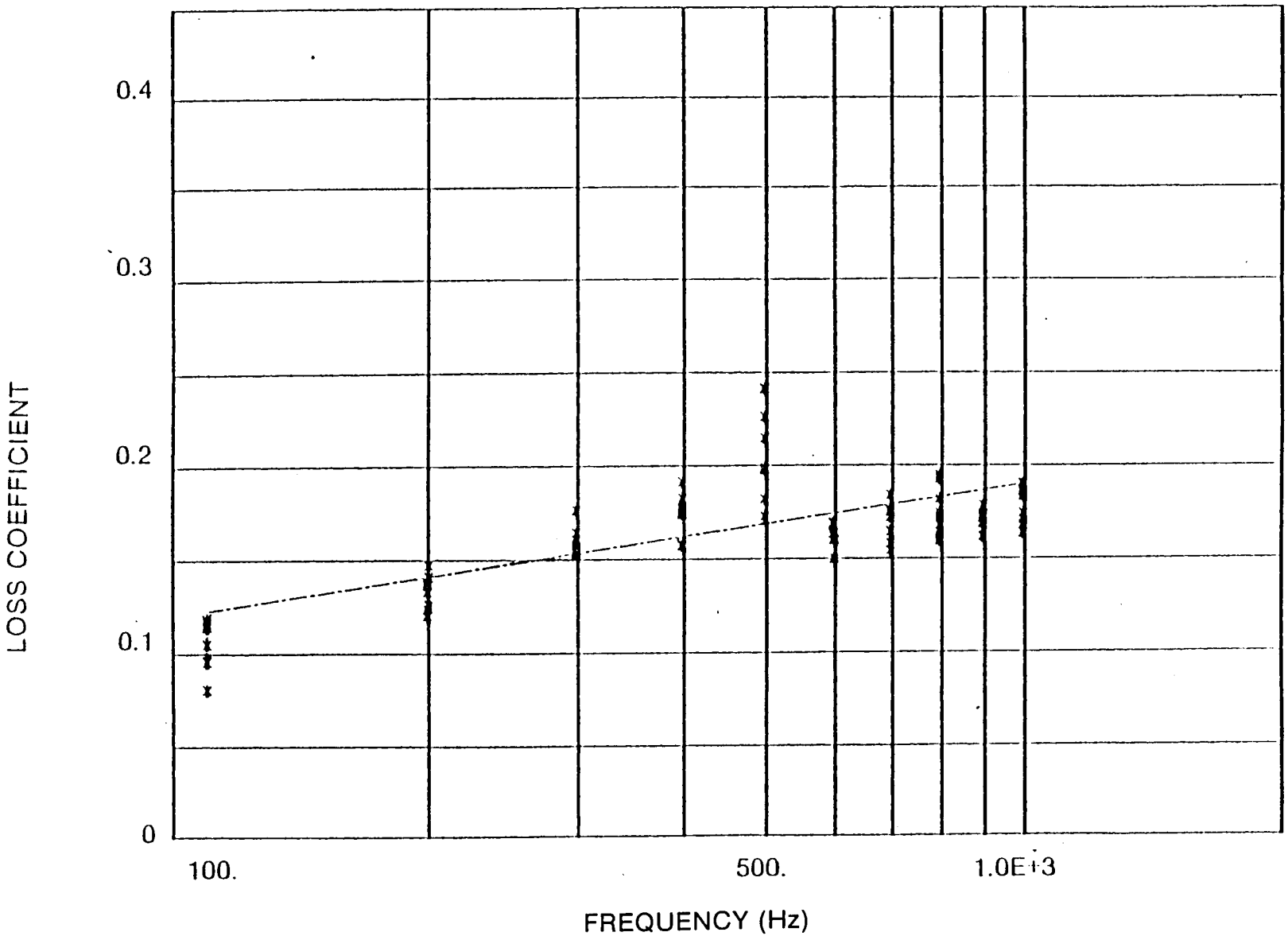

Figure 80 Shear Specimen Data Viton-70 at 80°C

80508

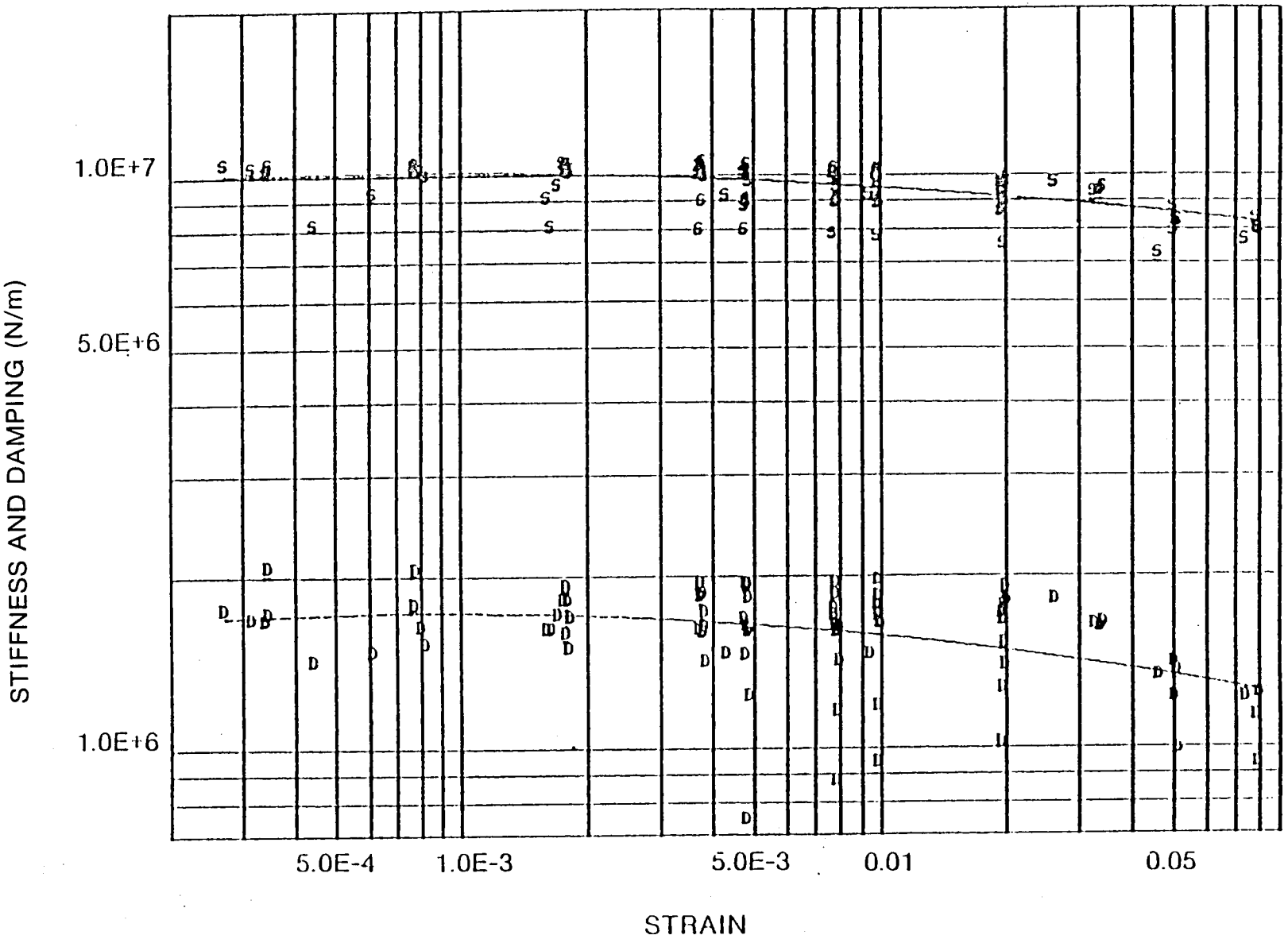

Figure 81 Shear Specimen Data Viton-70 at 80°C

80509

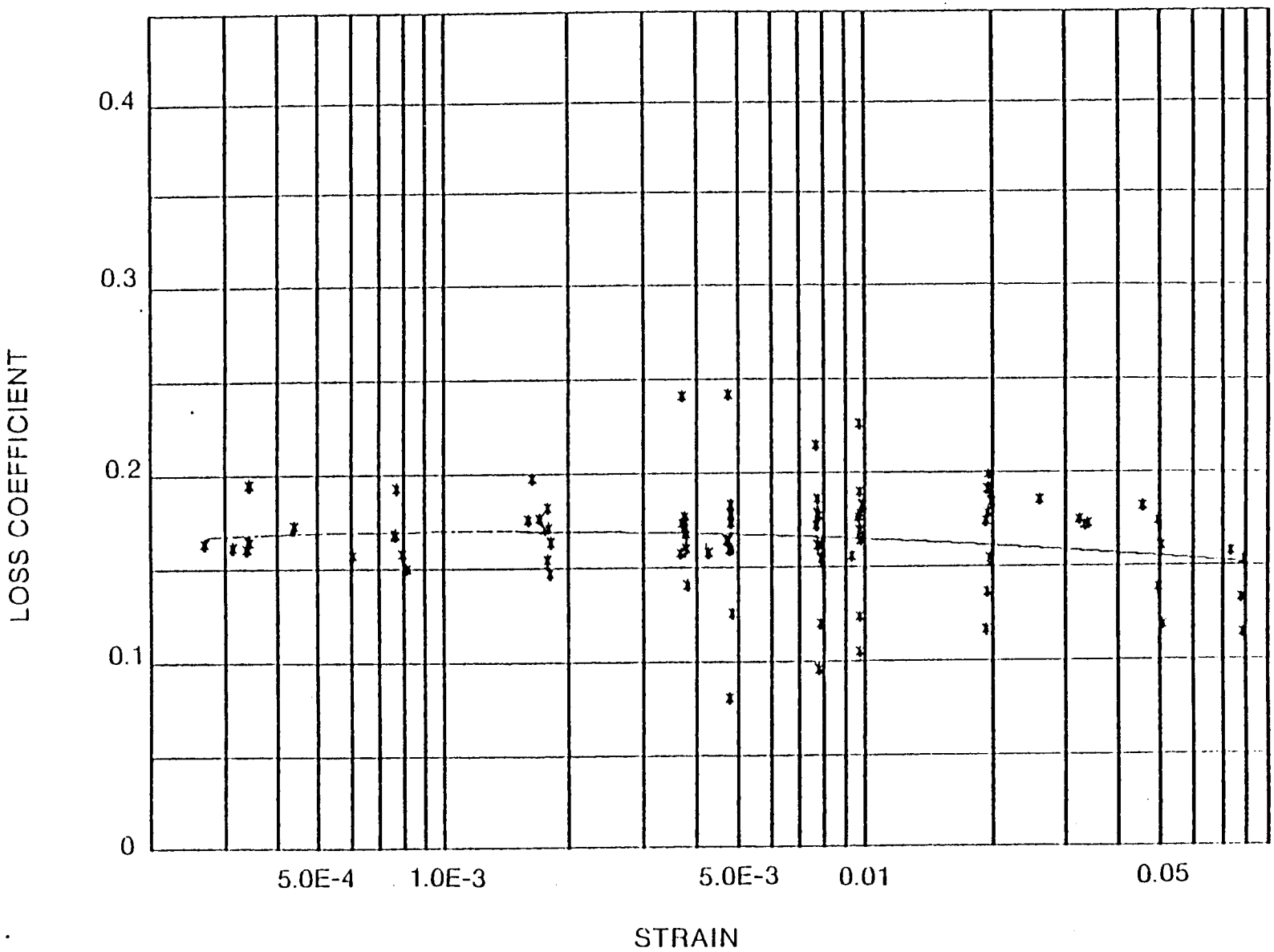

Figure 82 Shear Specimen Data Viton-70 at 80°C

80510

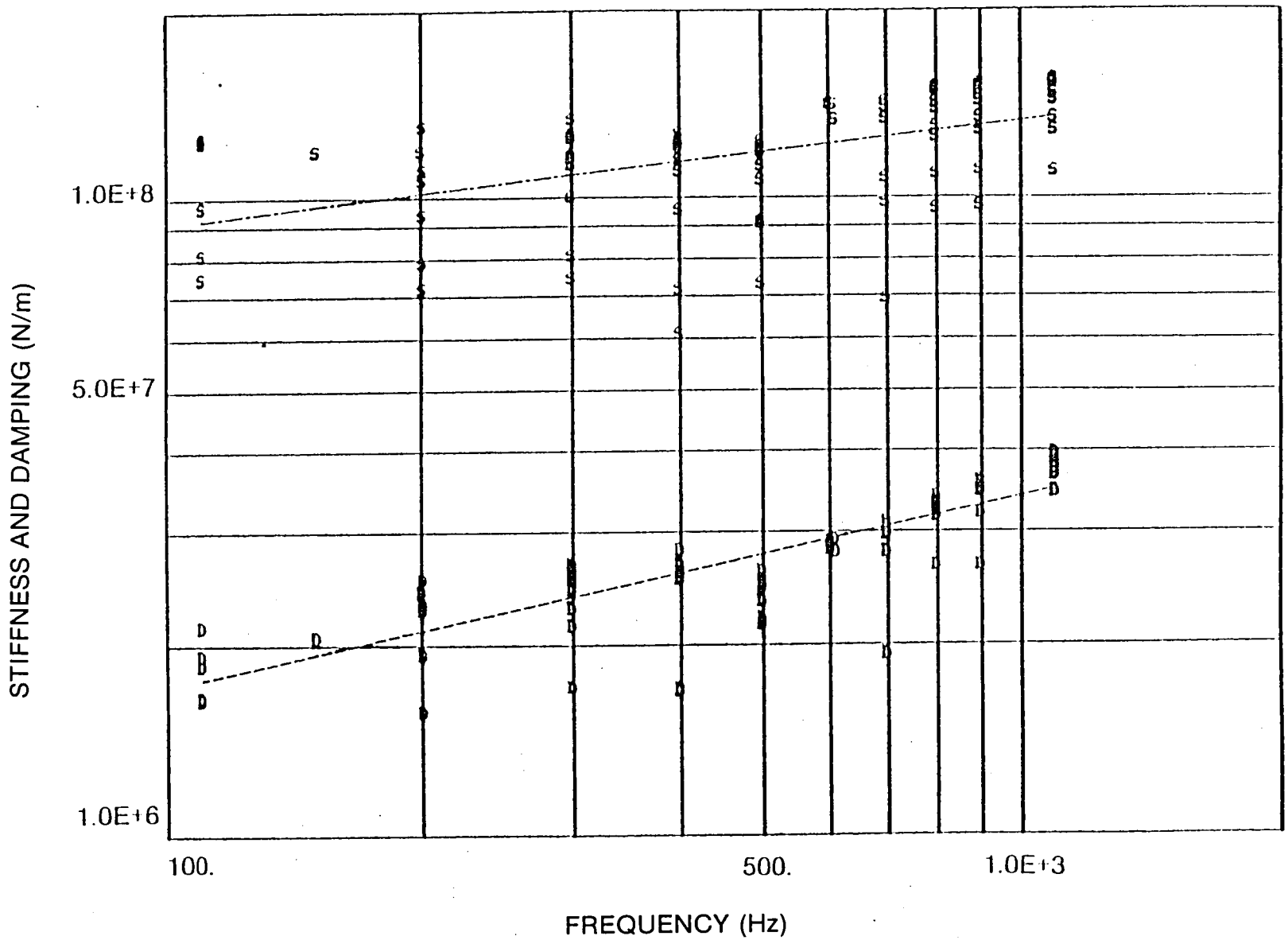

Figure 83 Shear Specimen Data Neoprene at 32°C

30511

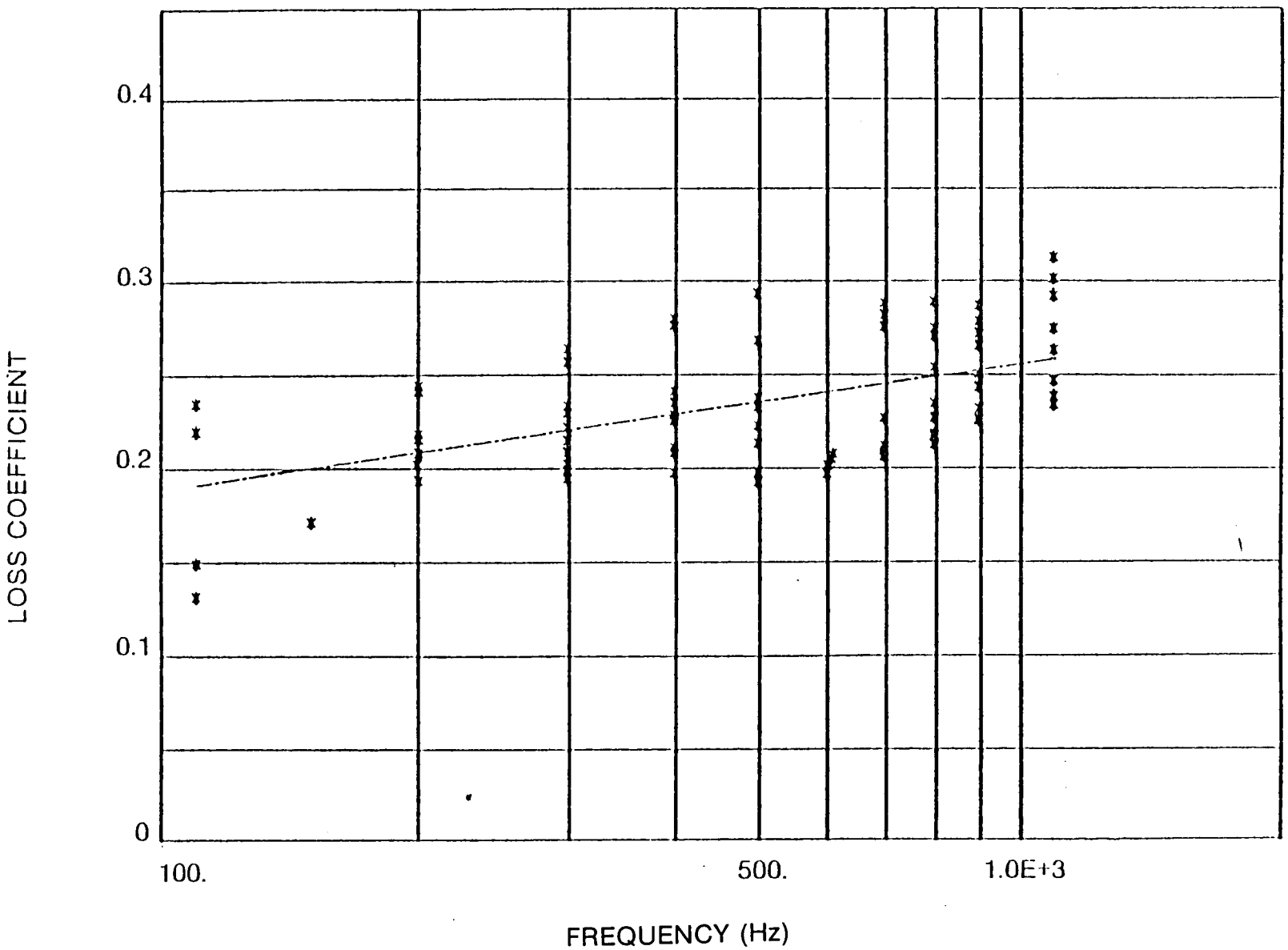

Figure 84 Shear Specimen Data Neoprene at 32°C

80512

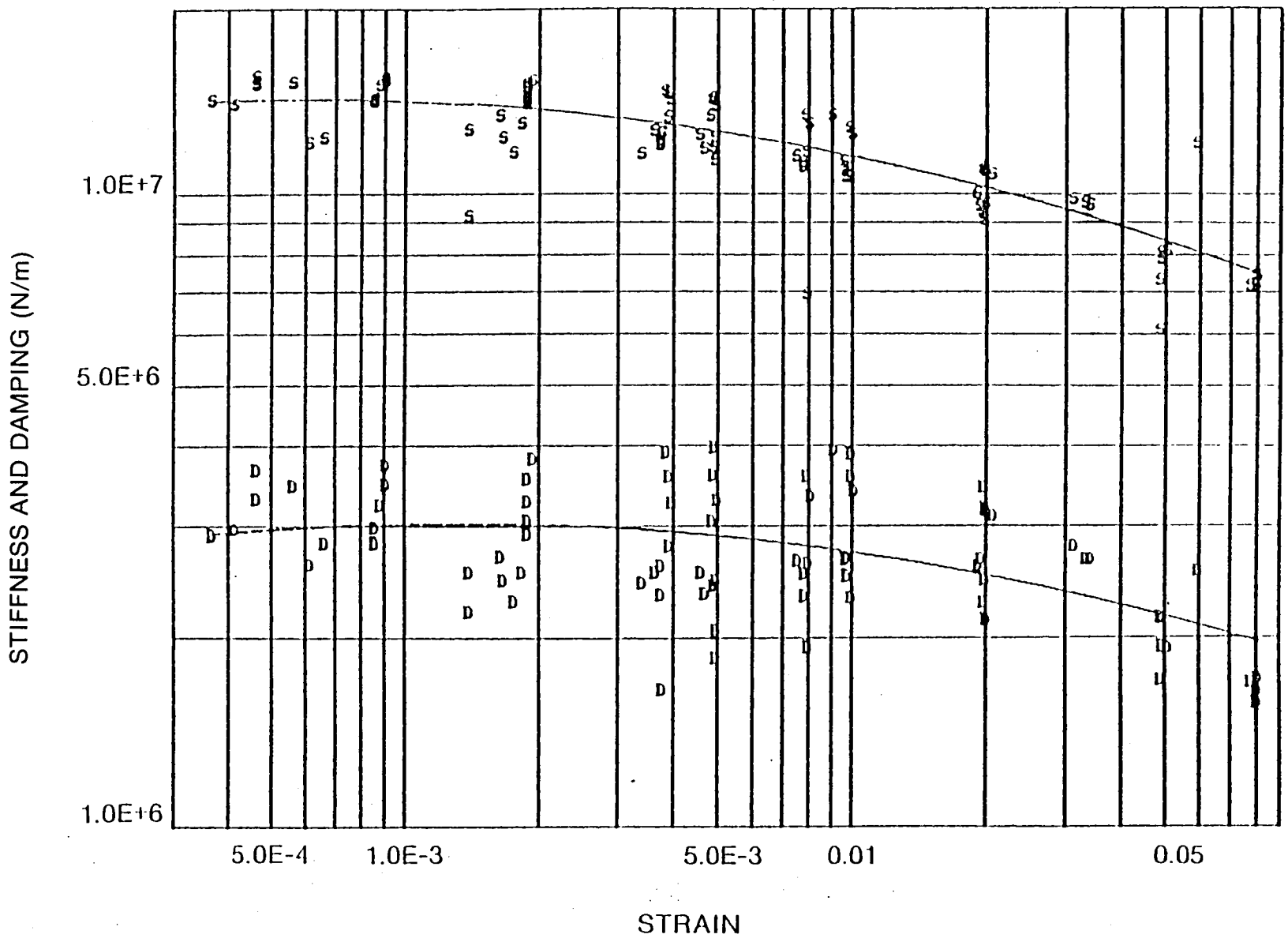

Figure 85 Shear Specimen Data Neoprene at 32°C

80513

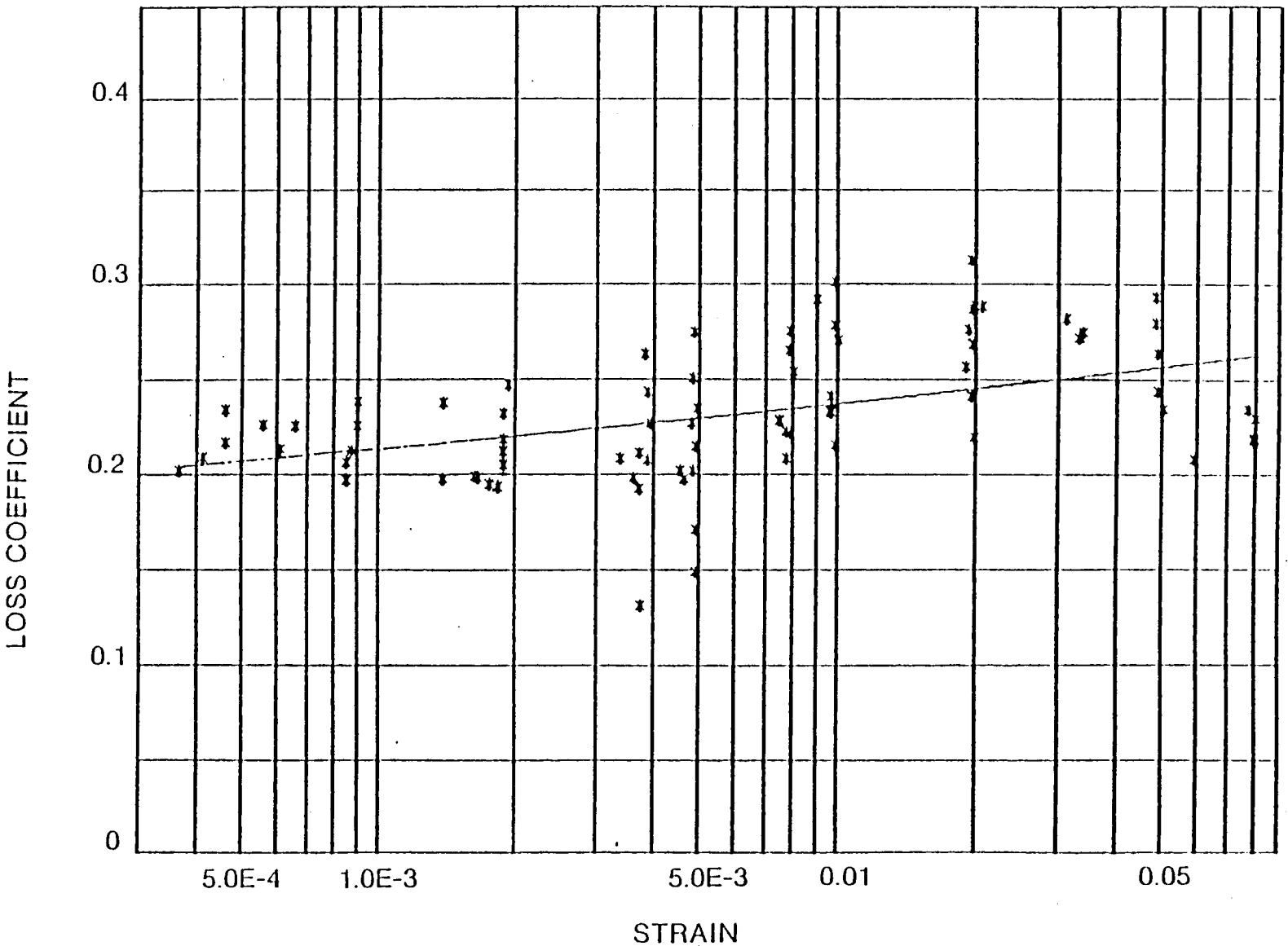

Figure 86 Shear Specimen Data Neoprene at 32°C

80521

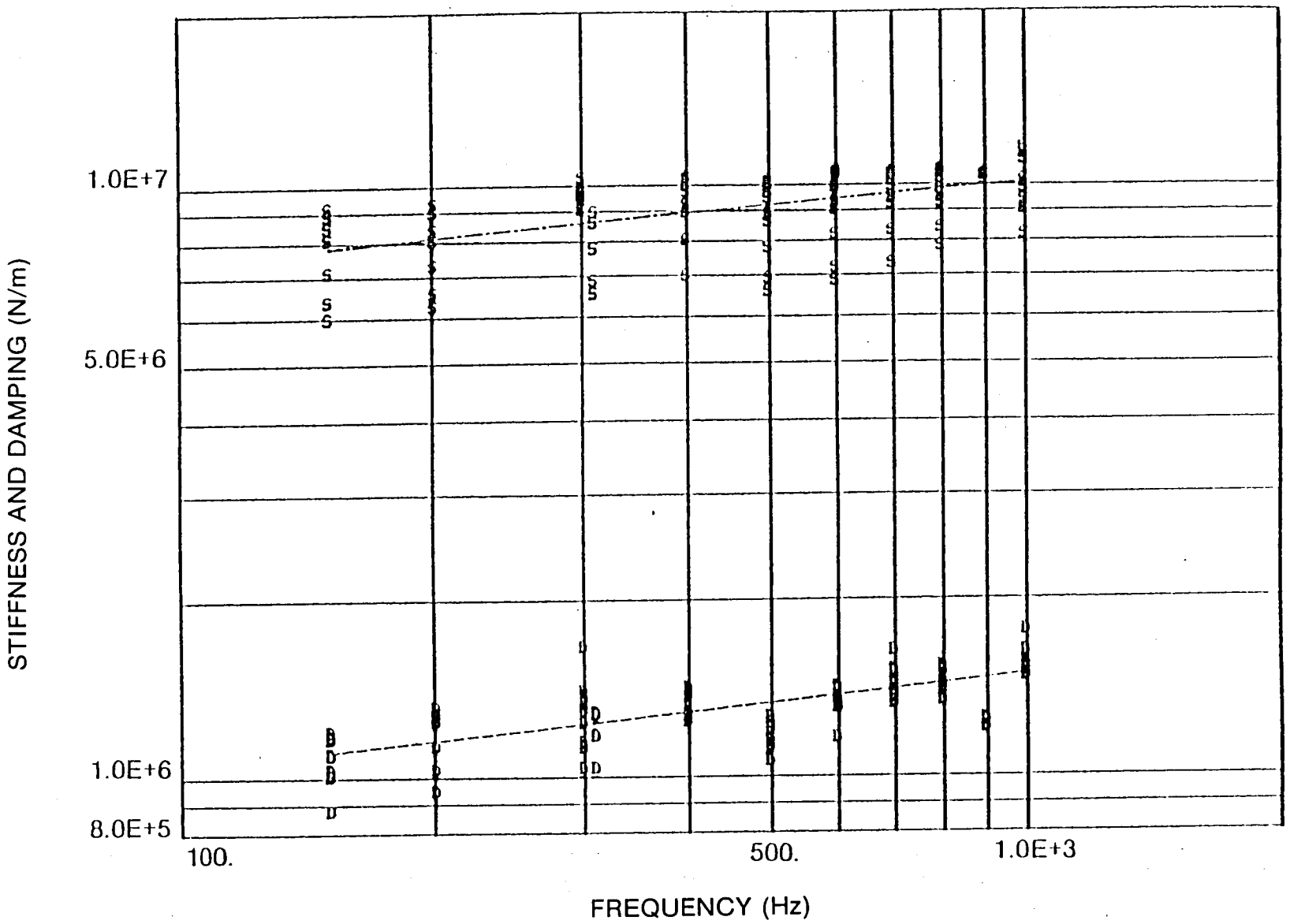

Figure 87 Shear Specimen Data Neoprene at 66°C

80522

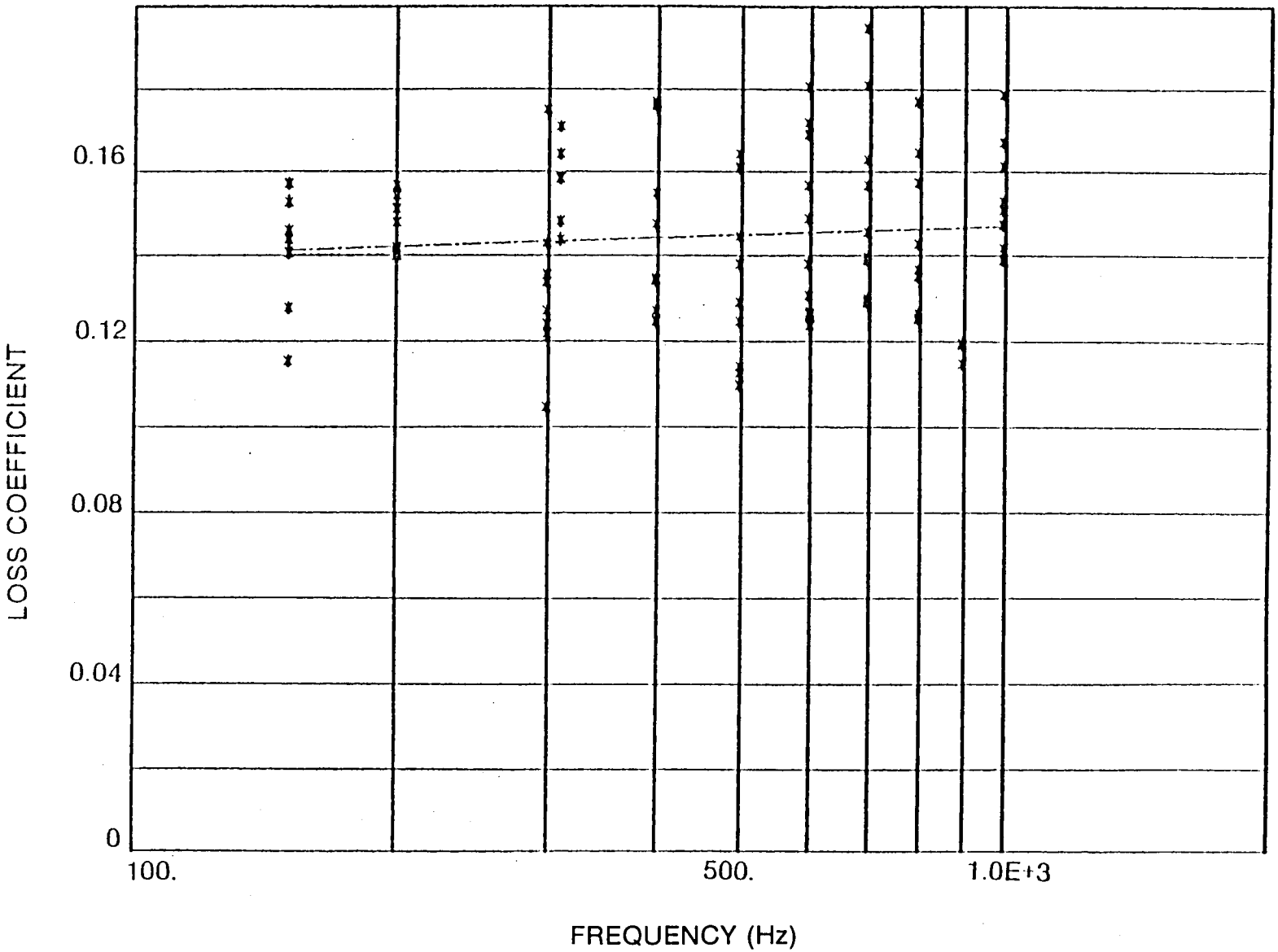

Figure 88 Shear Specimen Data Neoprene at 66°C

80514

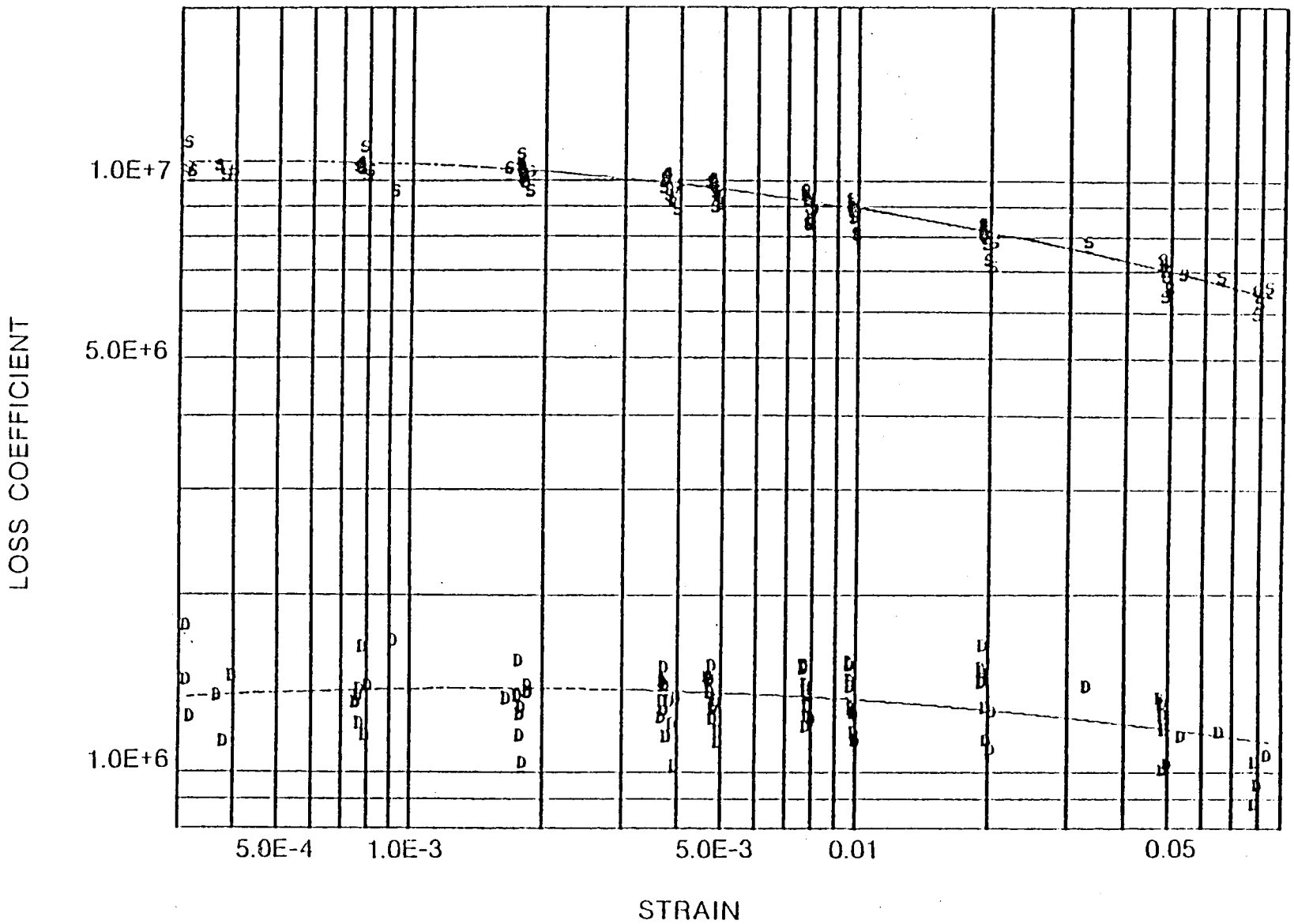

Figure 89 Shear Specimen Data Neoprene at 66°C

80515

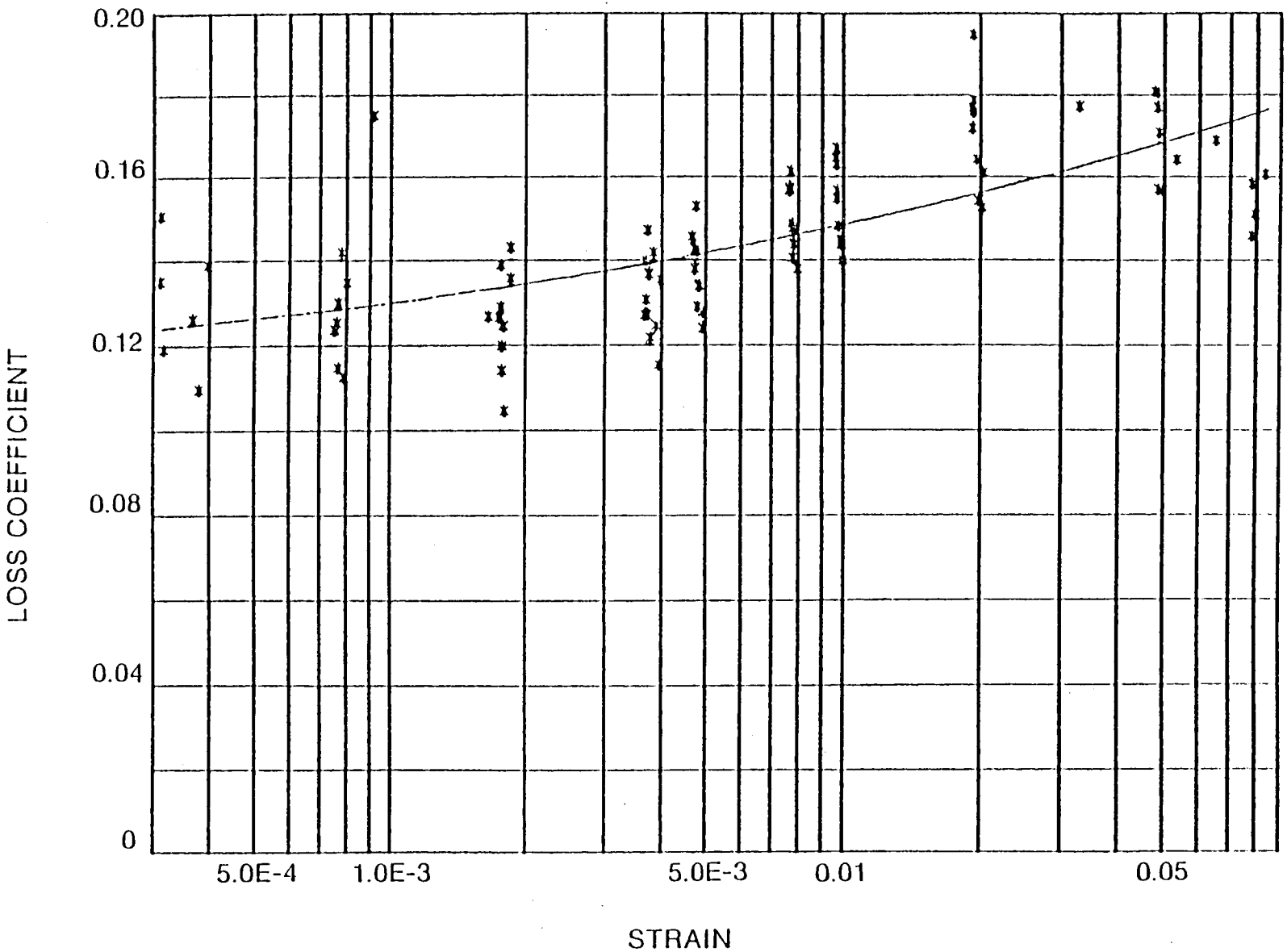

Figure 90 Shear Specimen Data Neoprene at 66°C

80516

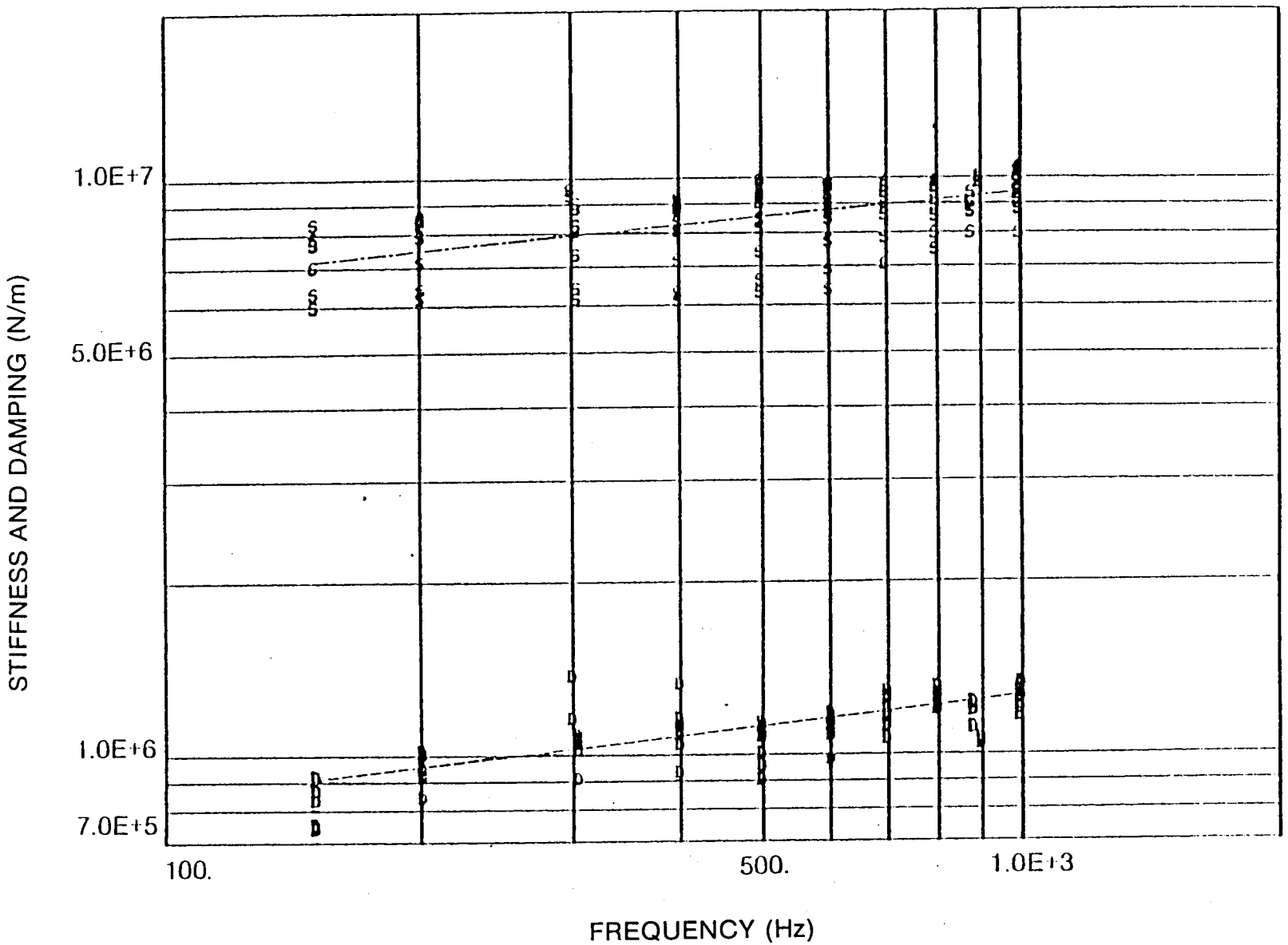

Figure 91 Shear Specimen Data Neoprene at 80°C

80517

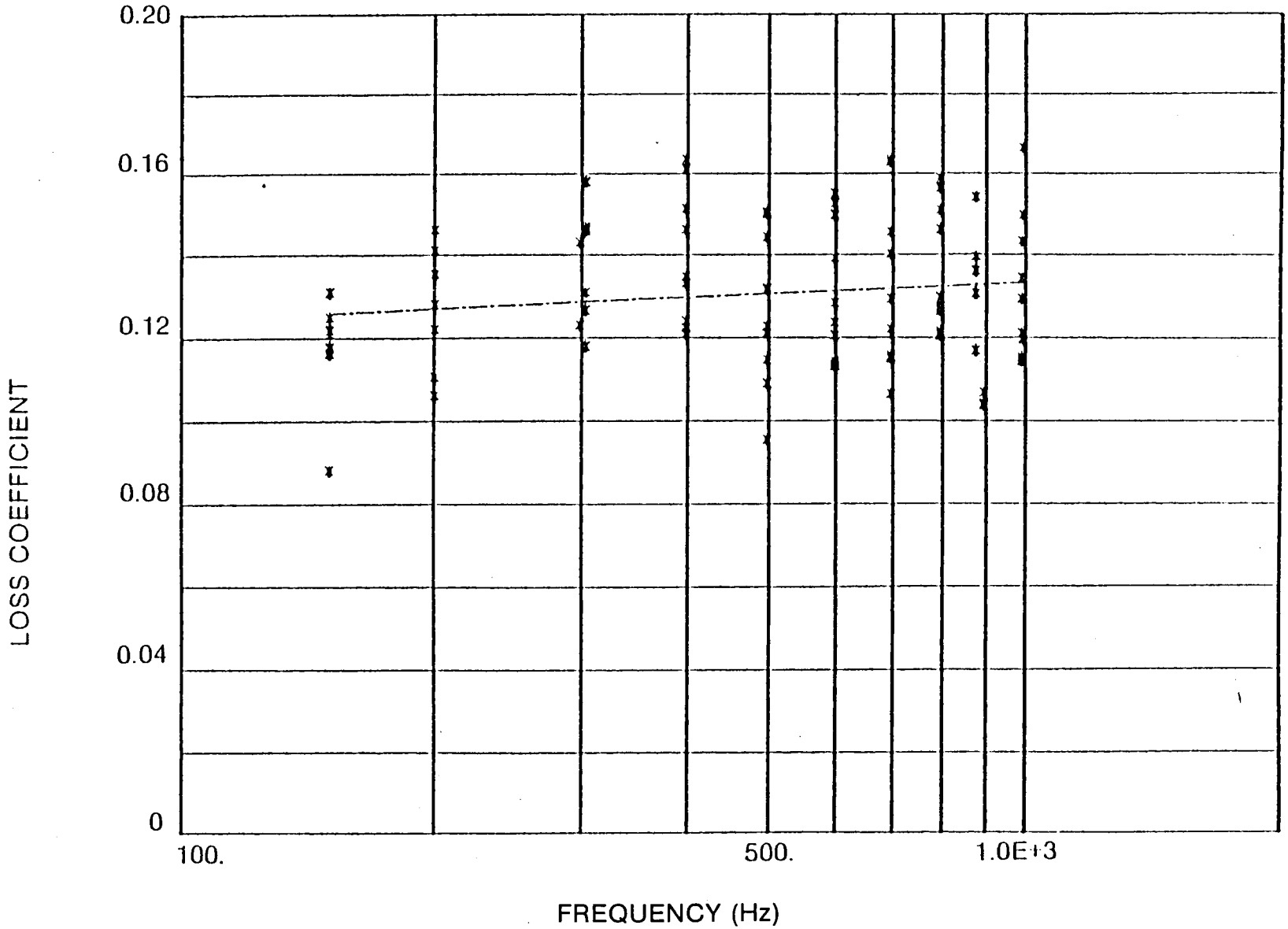

Figure 92 Shear Specimen Data Neoprene at 80°C

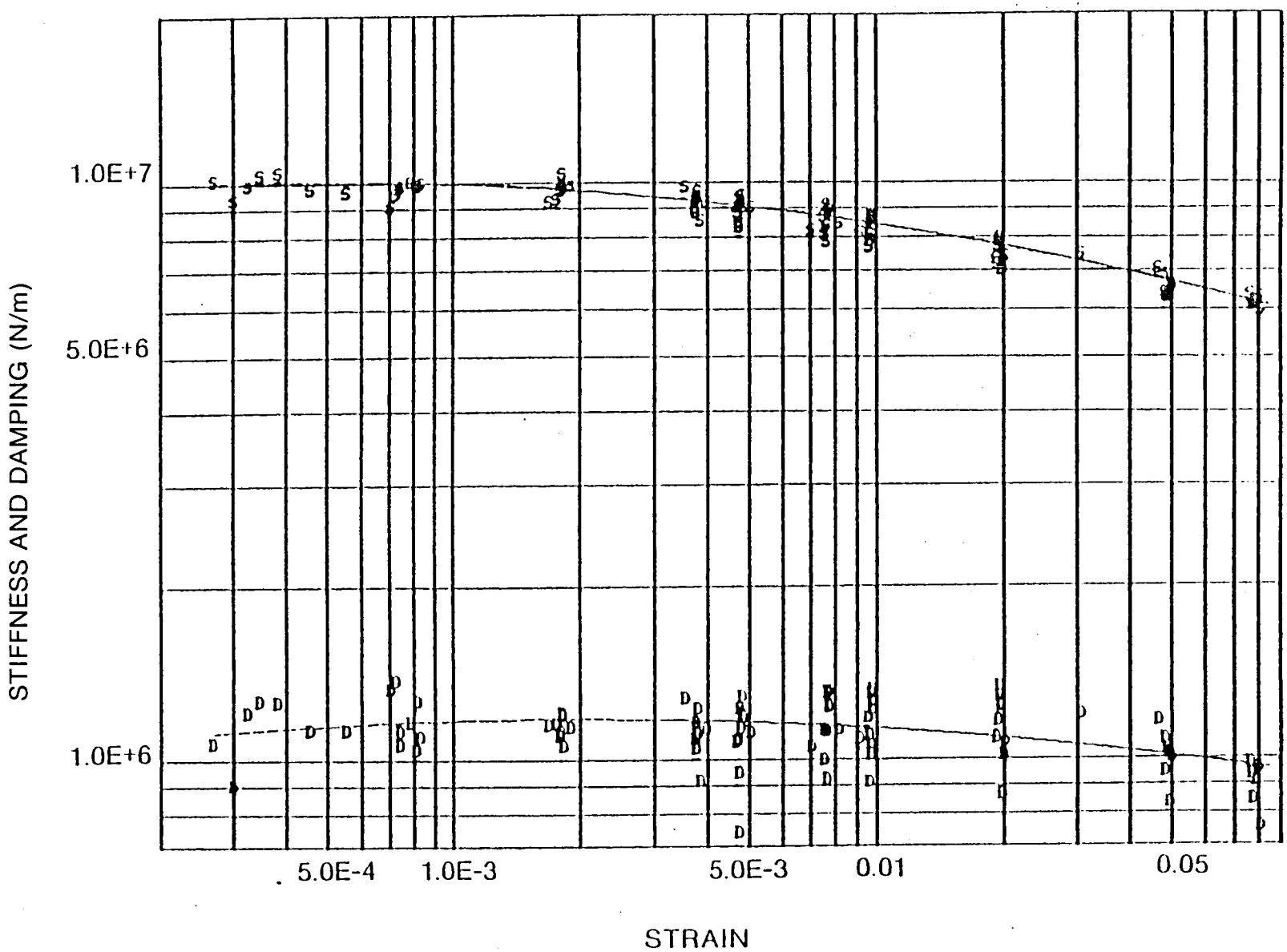

Figure 93 Shear Specimen Data Neoprene at 80°C

80519

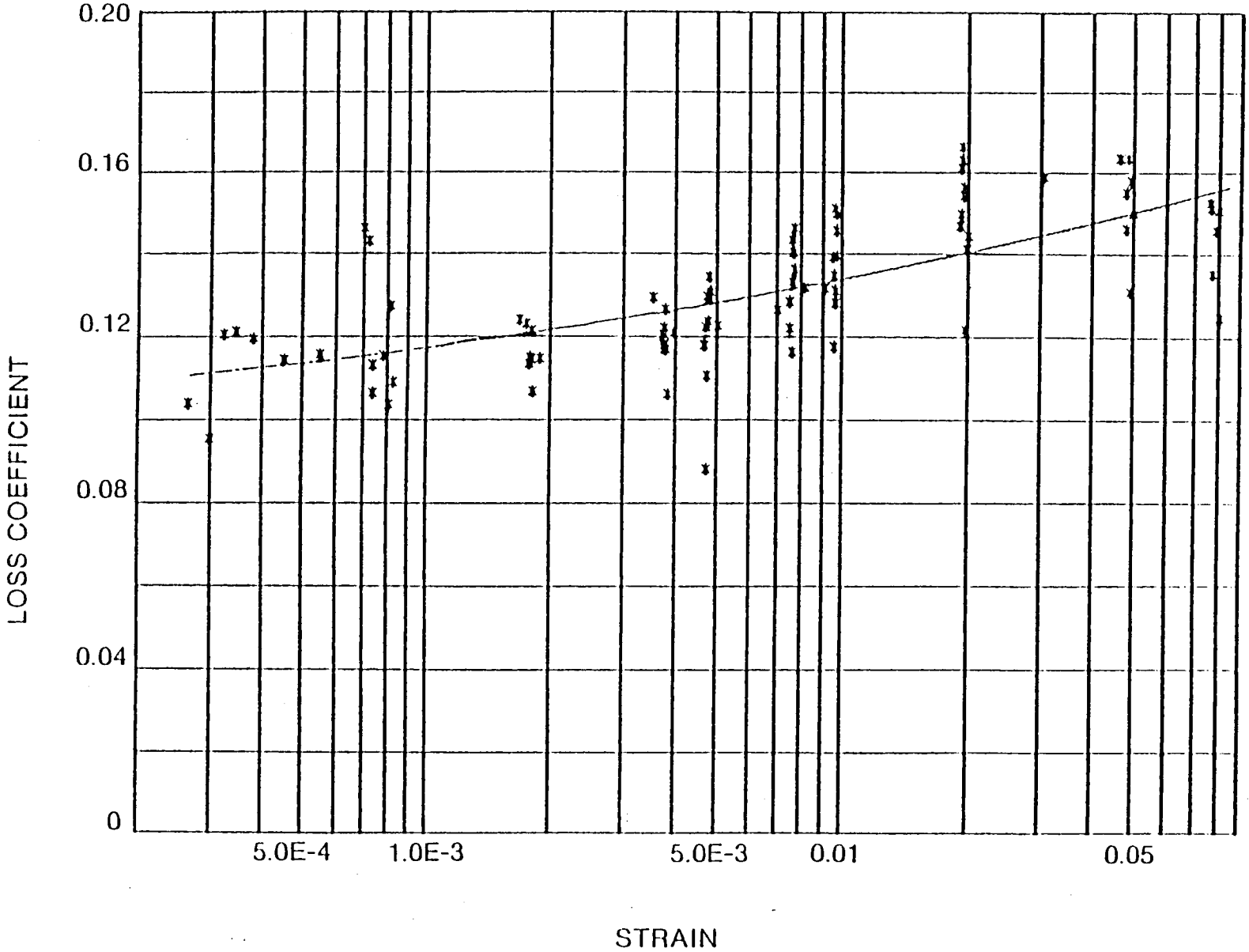

Figure 94 Shear Specimen Data Neoprene at 80°C

80520

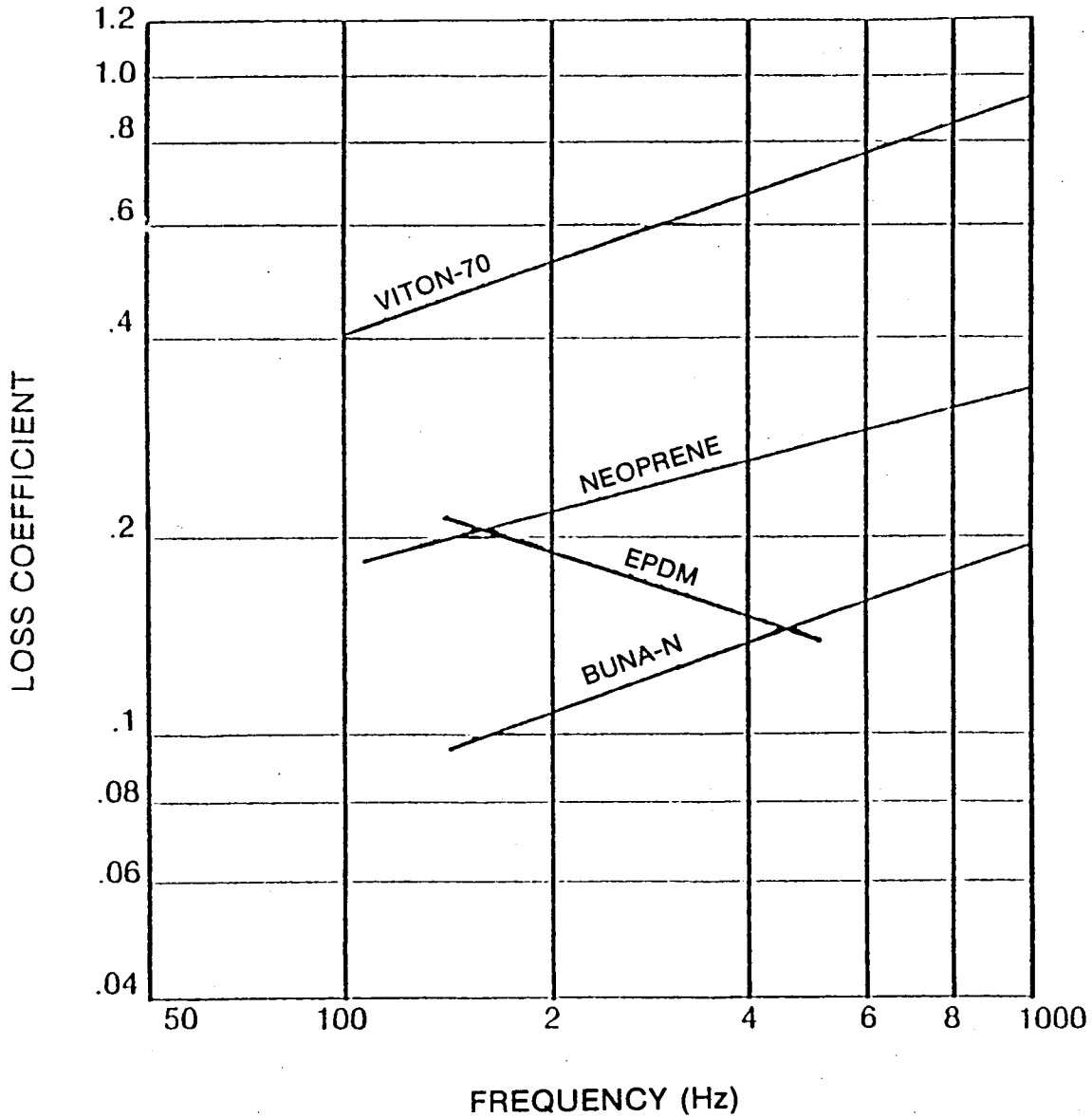

Figure 95 Shear Specimen Data at 32°C

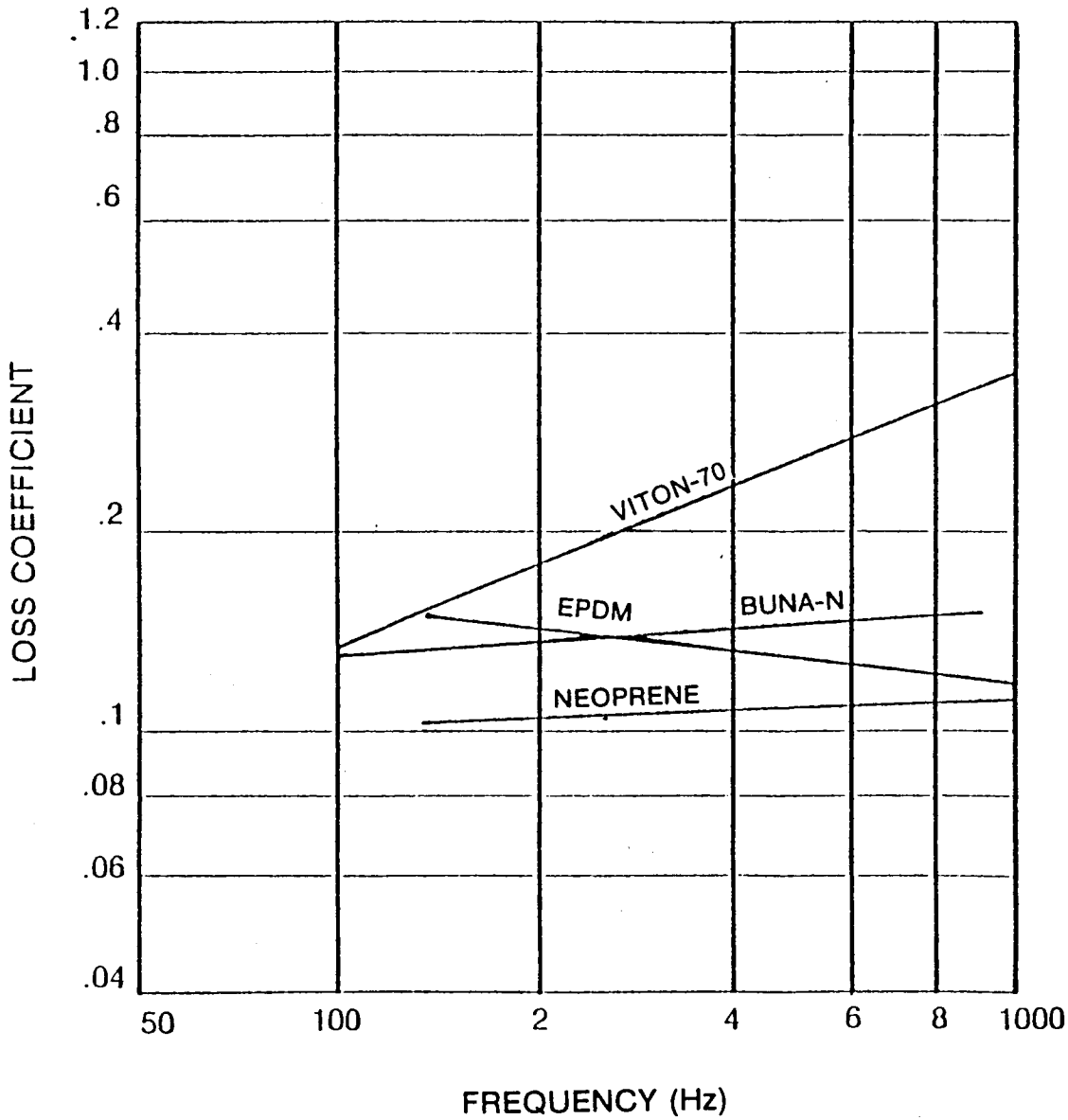

Figure 96 Shear Specimen Data at 66°C

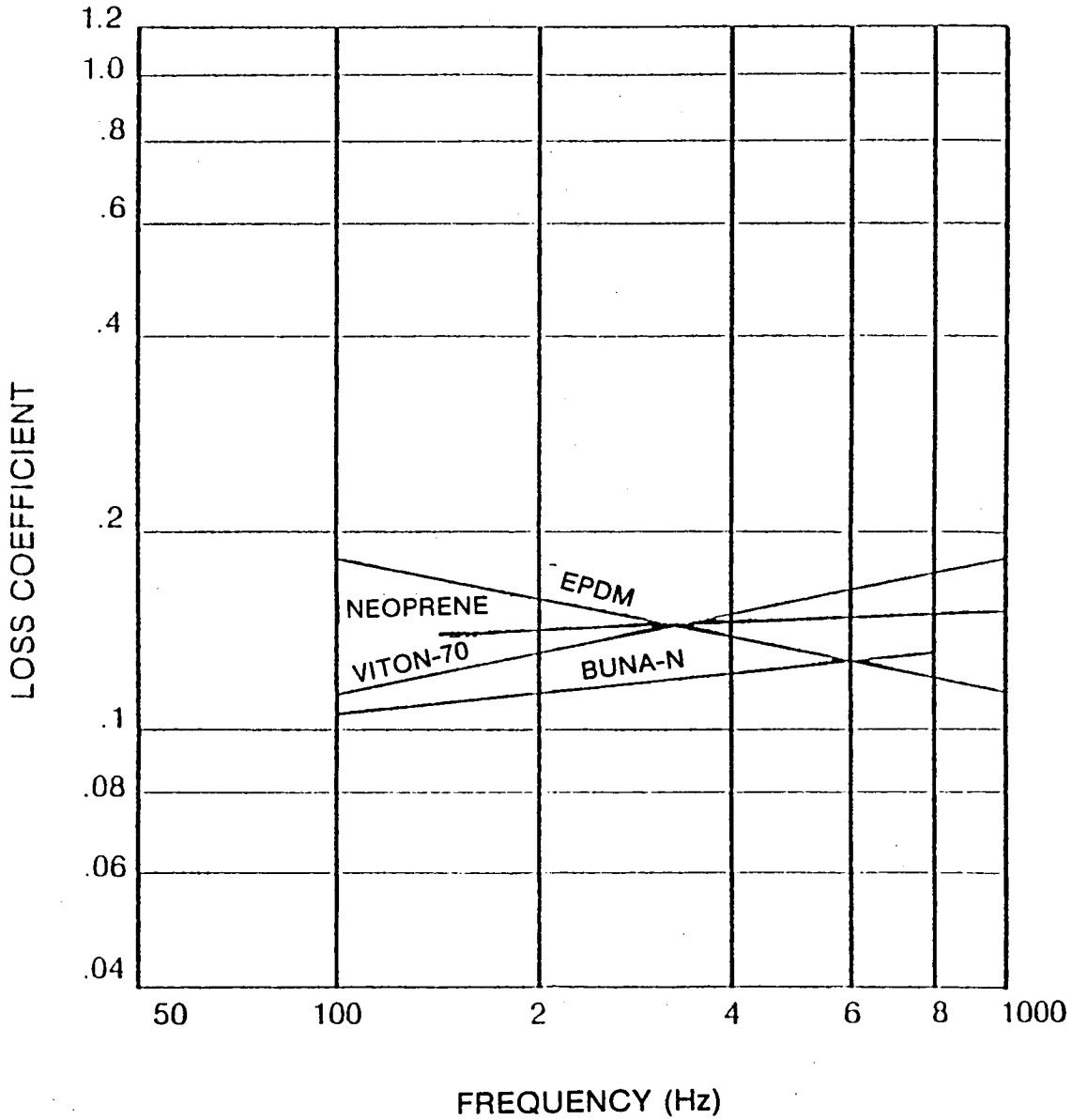

Figure 97 Shear Specimen Data at 80°C

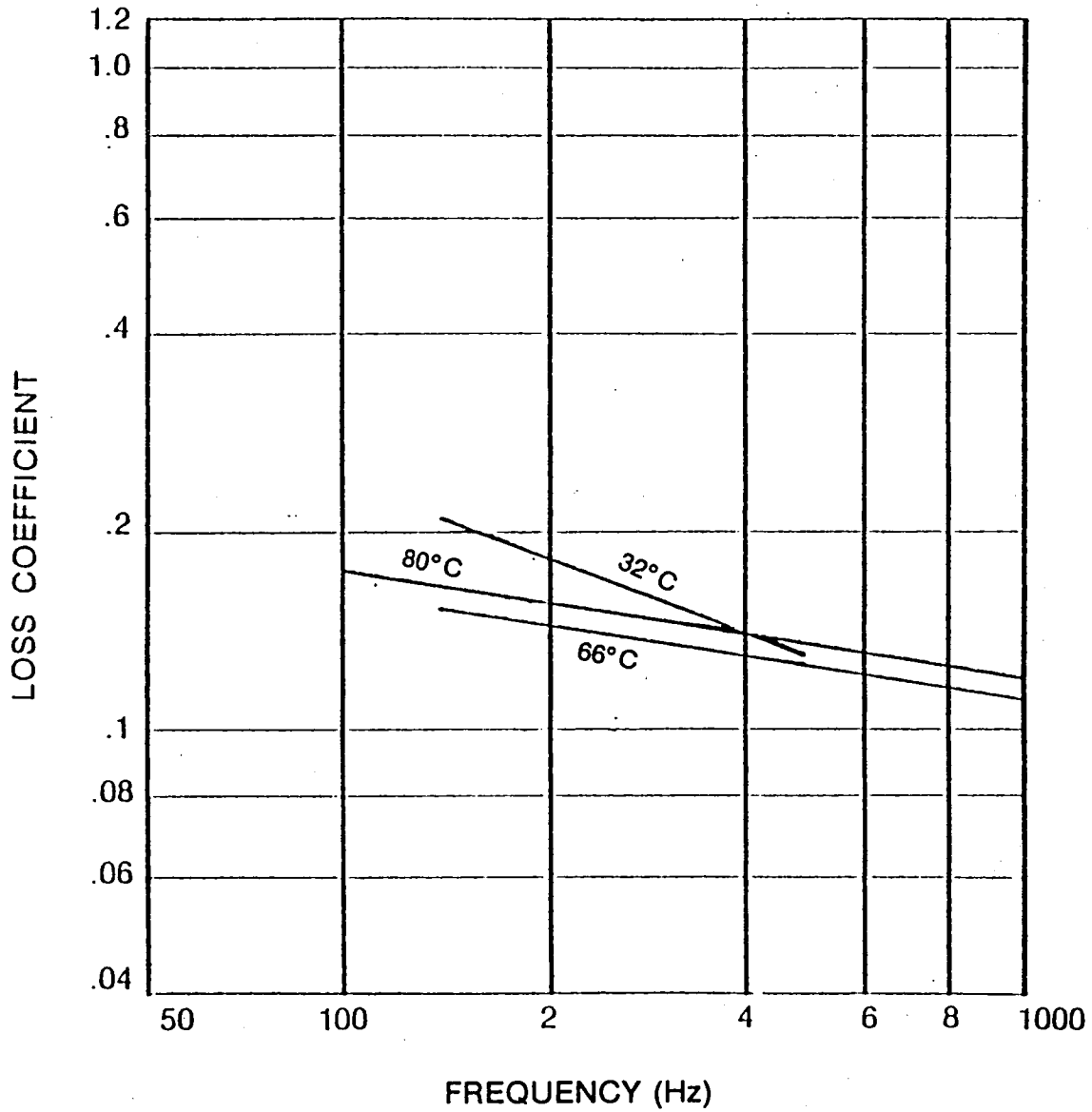

Figure 98 EPDM Shear Specimen Data

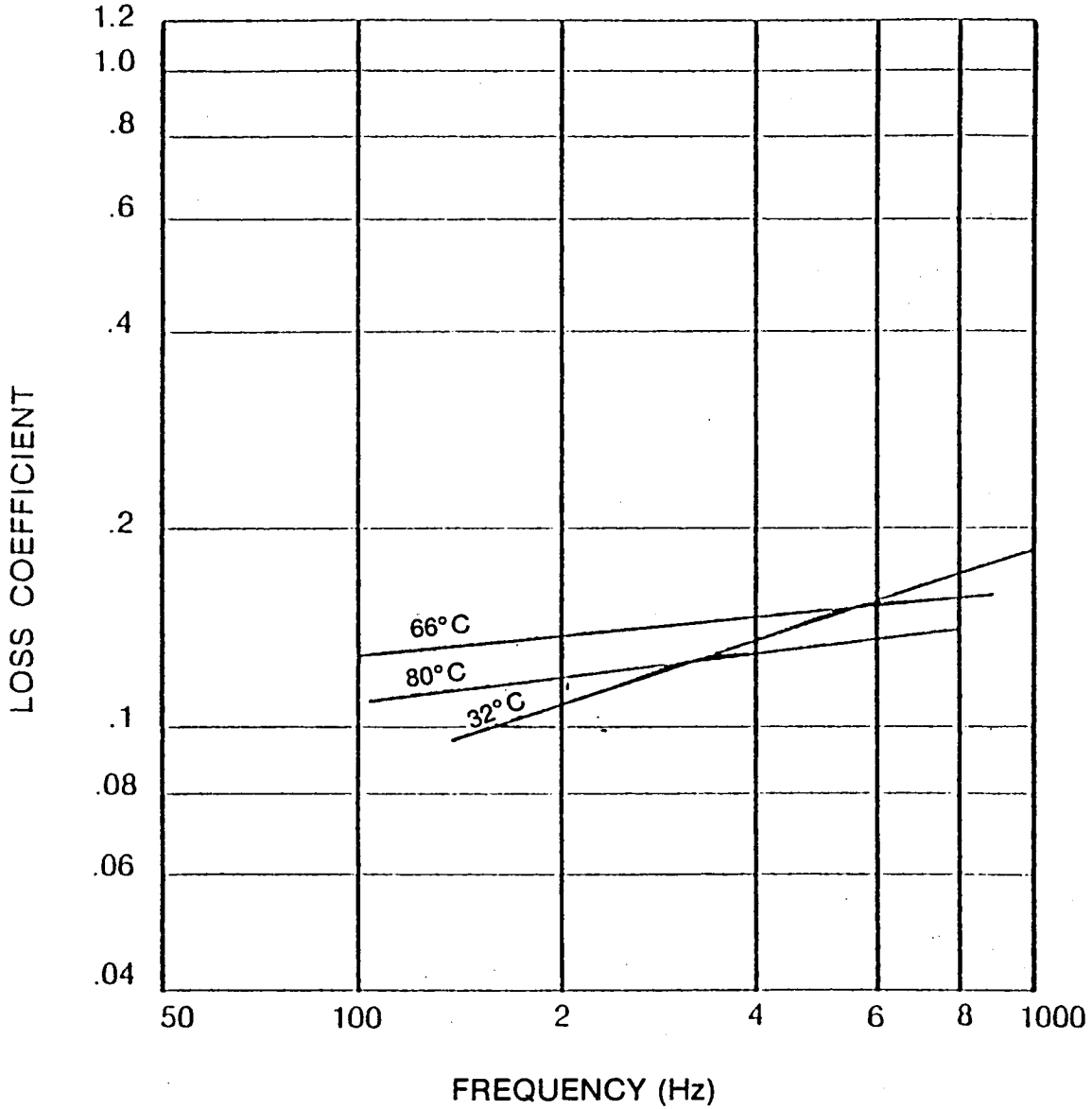

Figure 99 Buna-N Shear Specimen Data

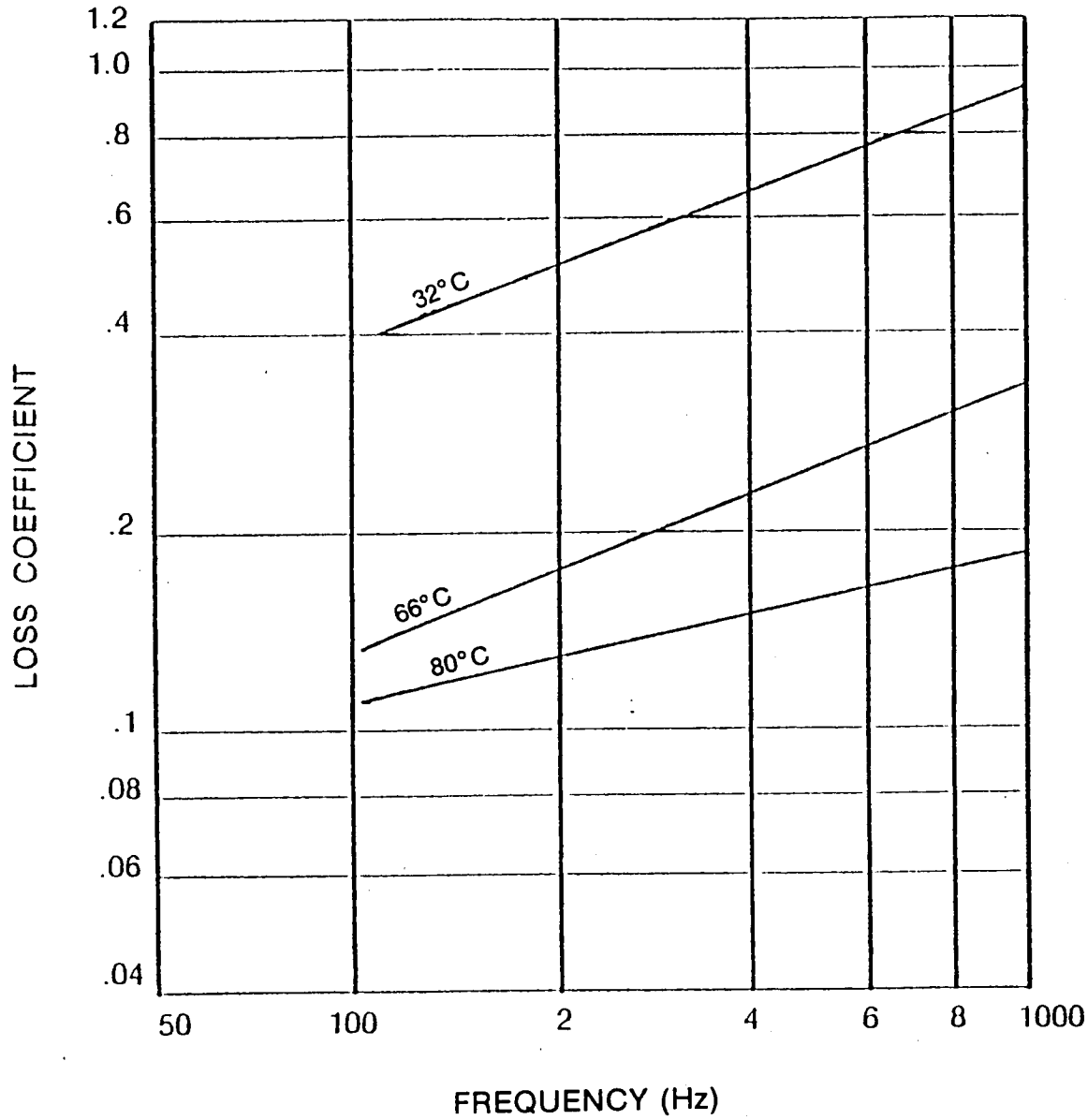

Figure 100 Viton-70 Shear Specimen Data

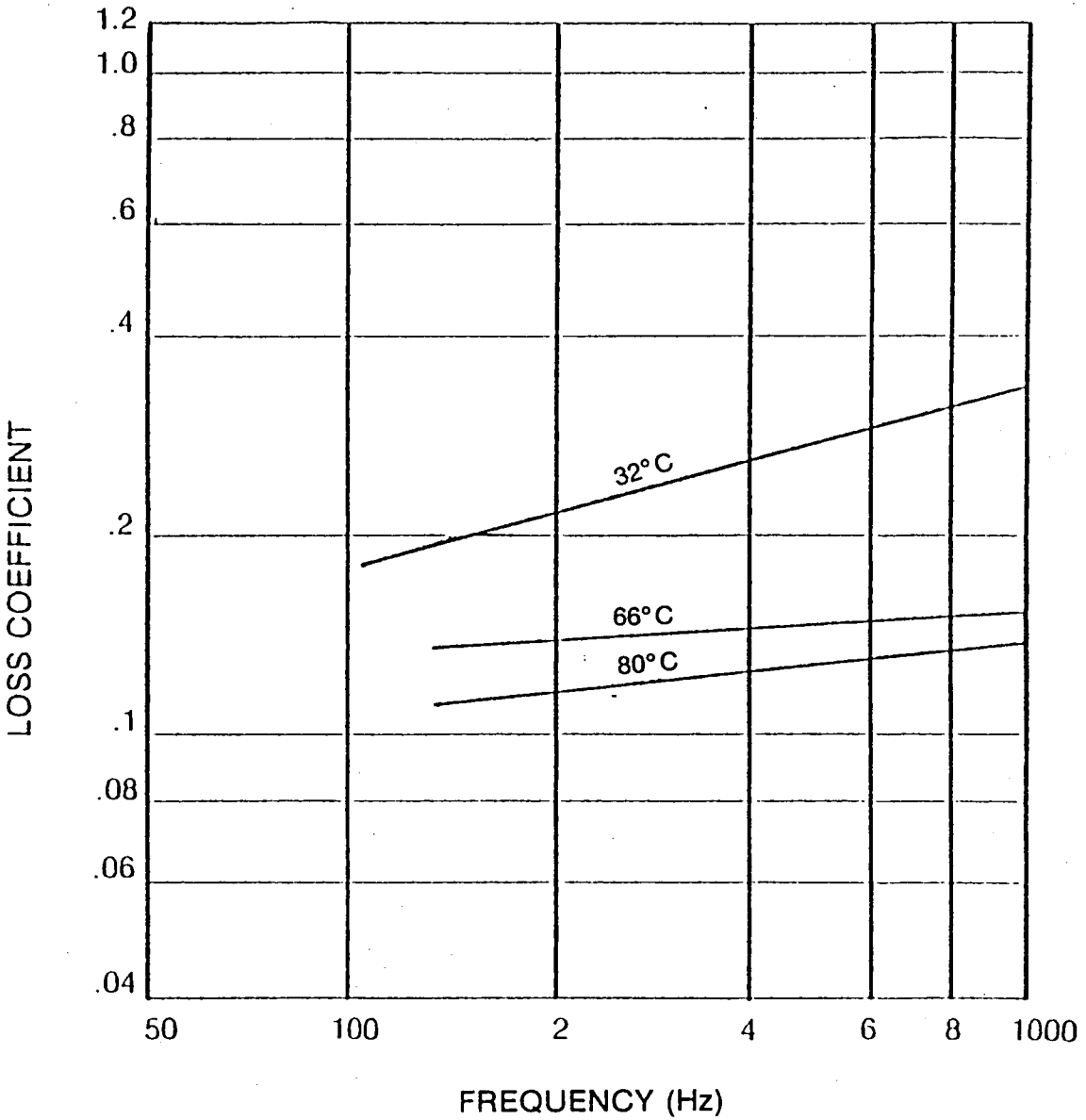

Figure 101 Neoprene Shear Specimen Data

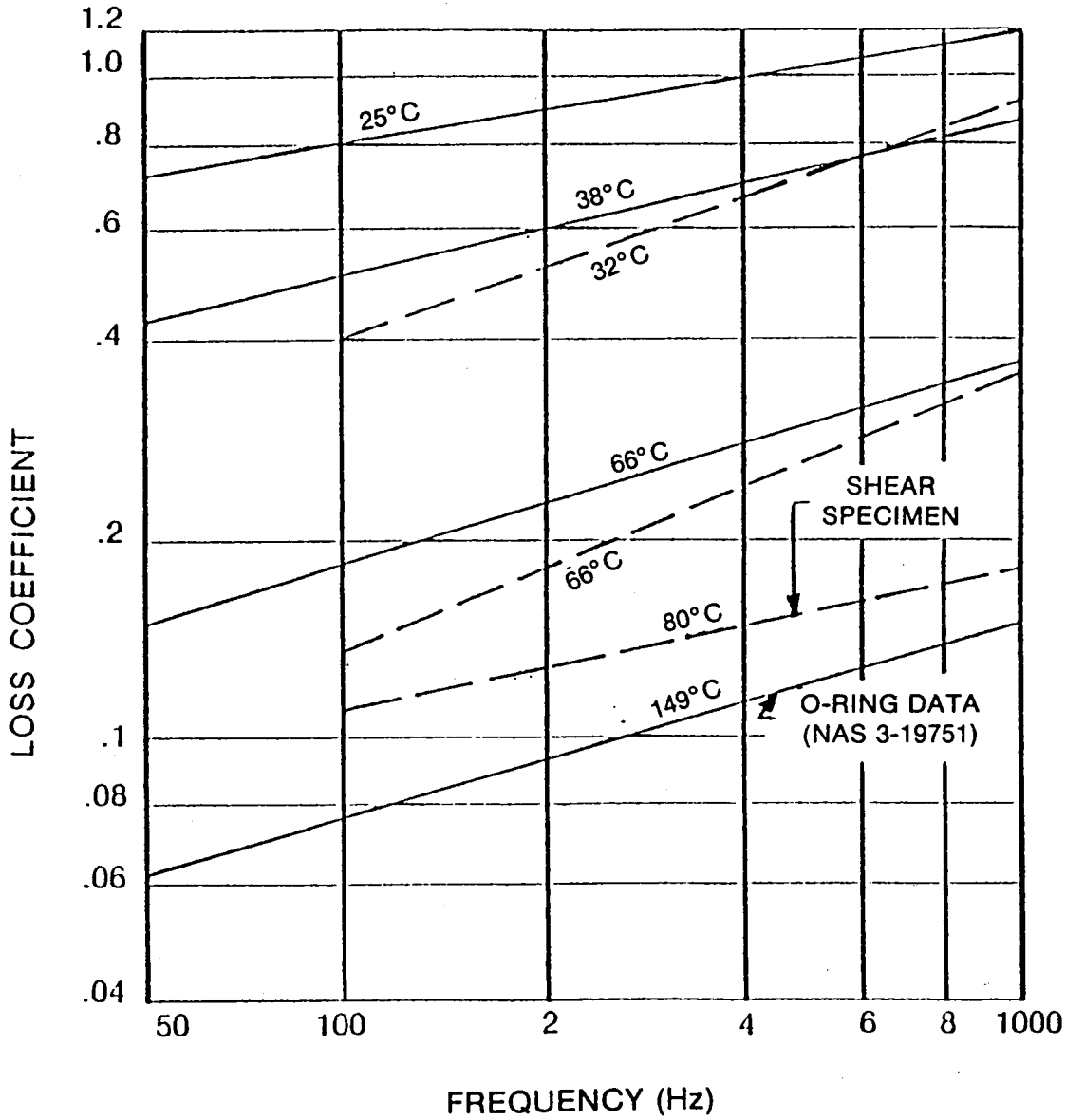

Figure 102 Comparison of Viton-70 Shear Specimen and O-Ring Test Data

80523

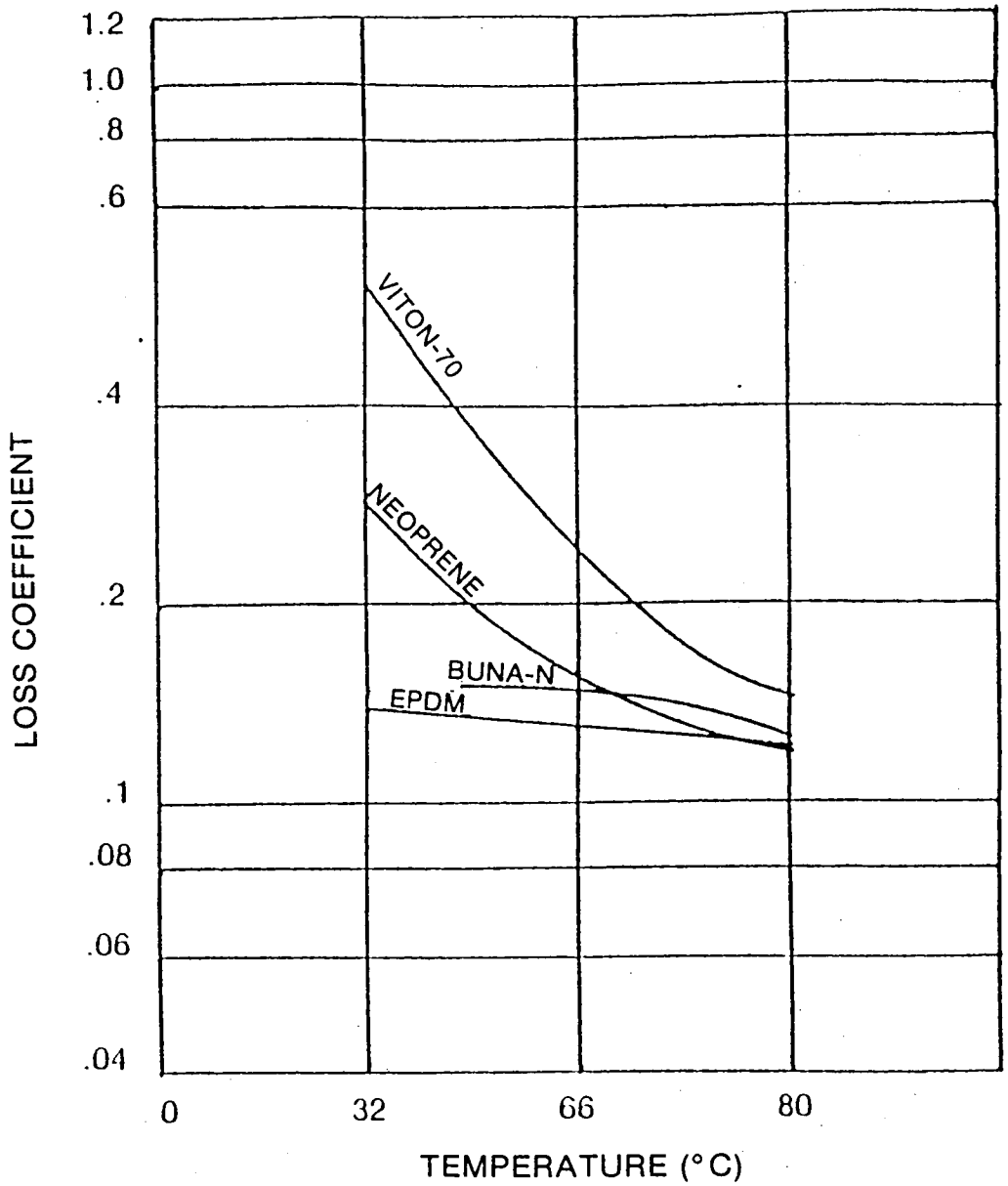

Figure 103 Temperature Variation of Elastomer Loss Coefficient at 500 Hz

80524

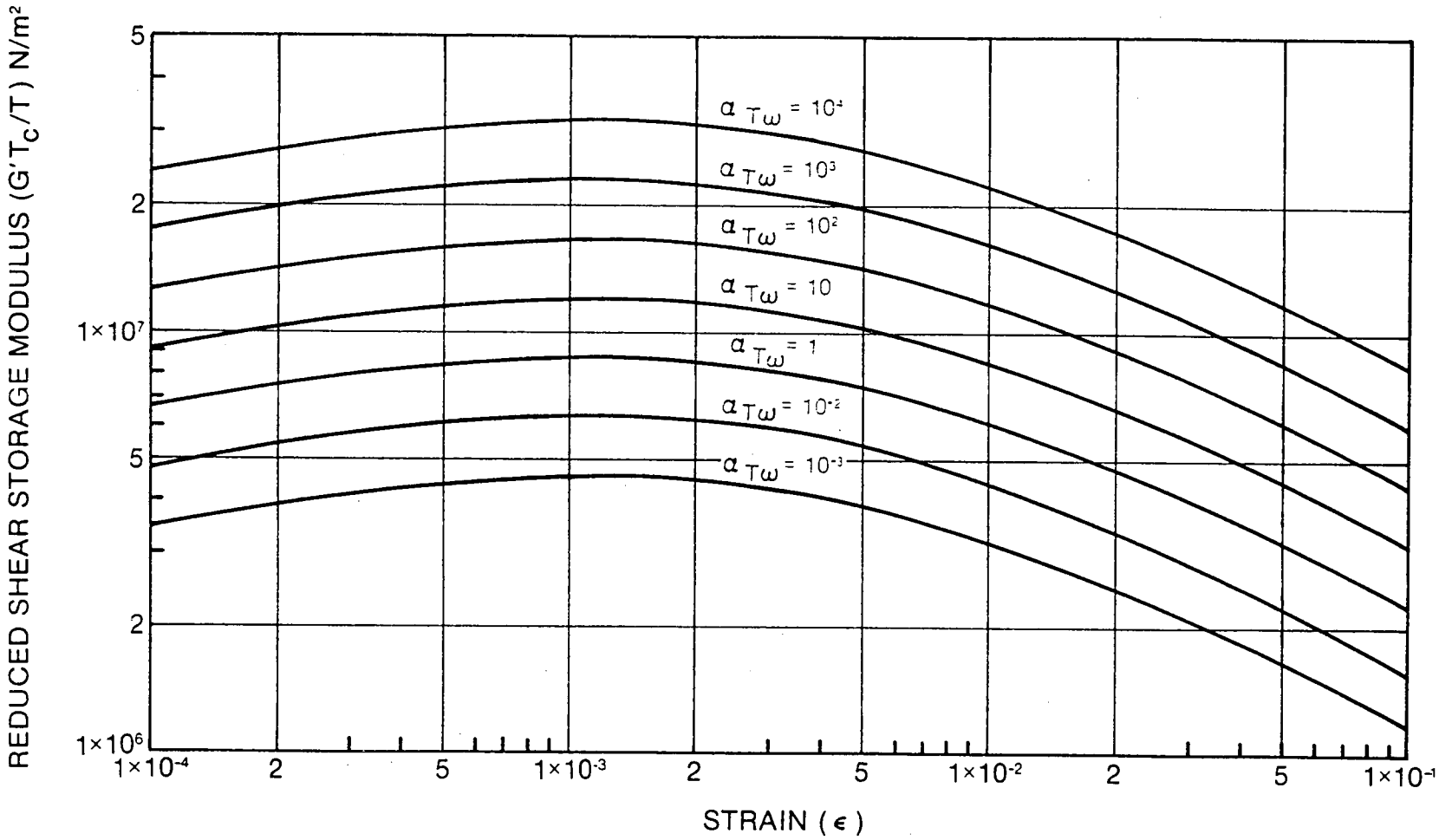

Figure 104 EPDM Design Curves

30889

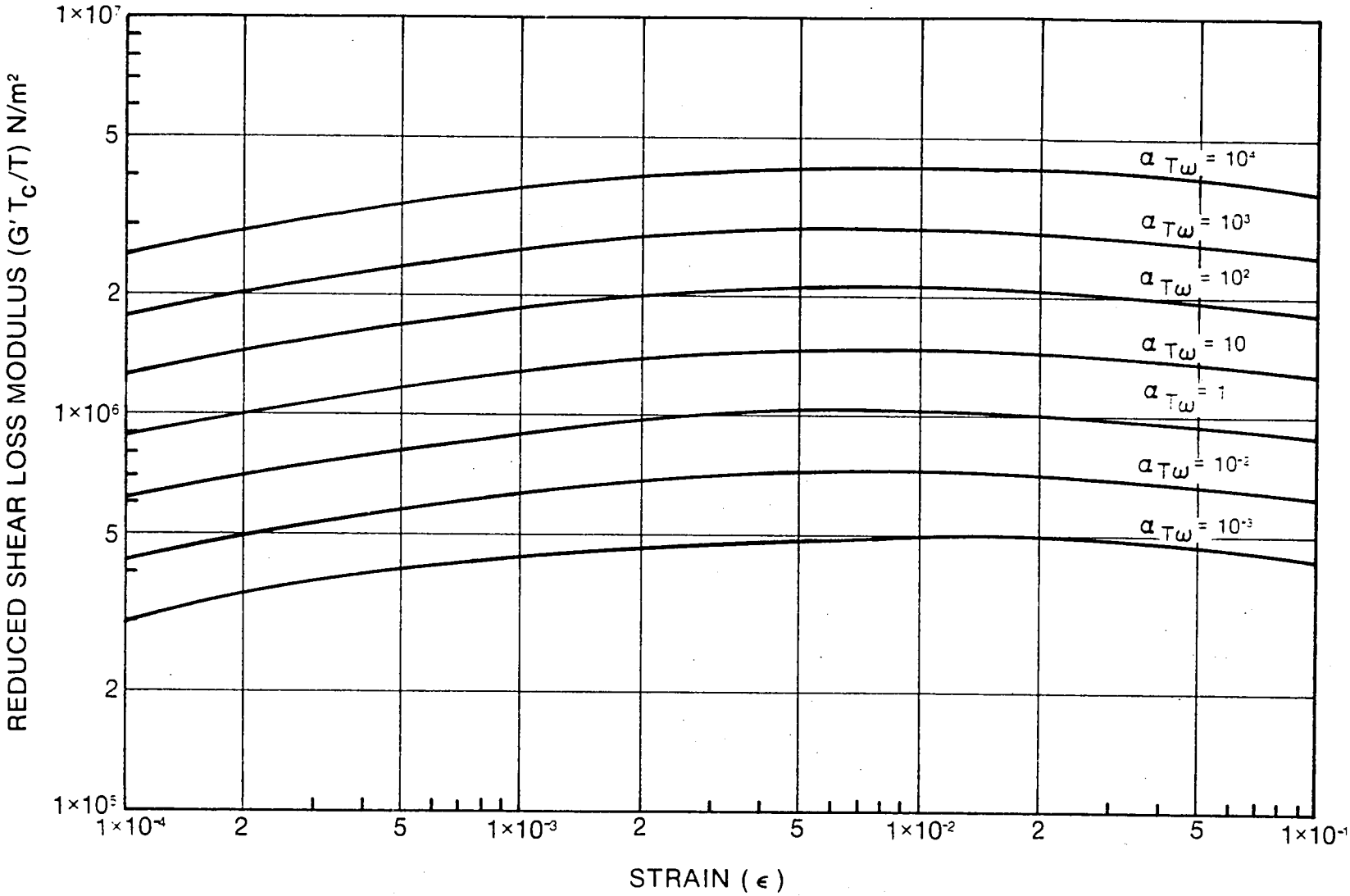

Figure 105 EPDM Design Curves

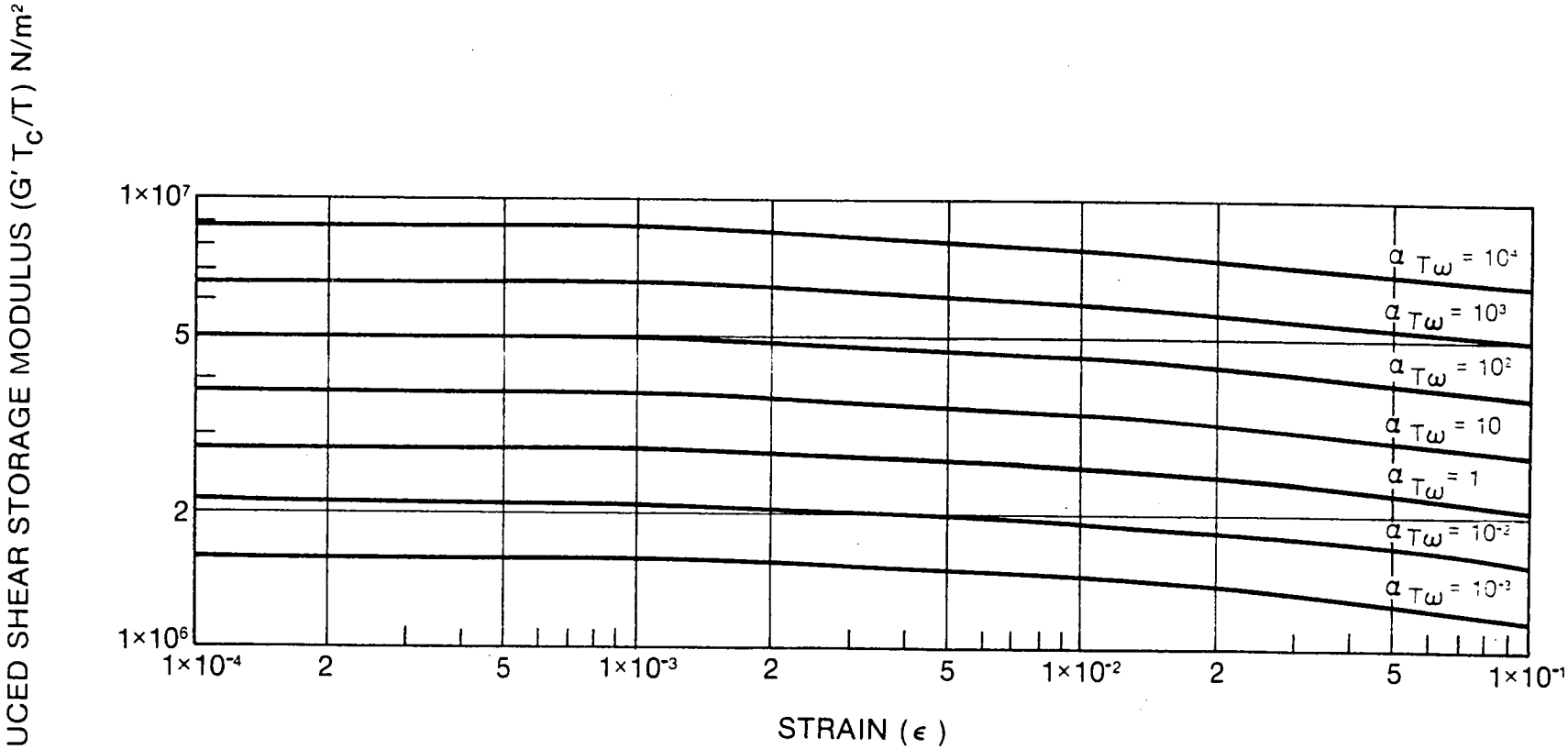

Figure 106 Buna-N Design Curves

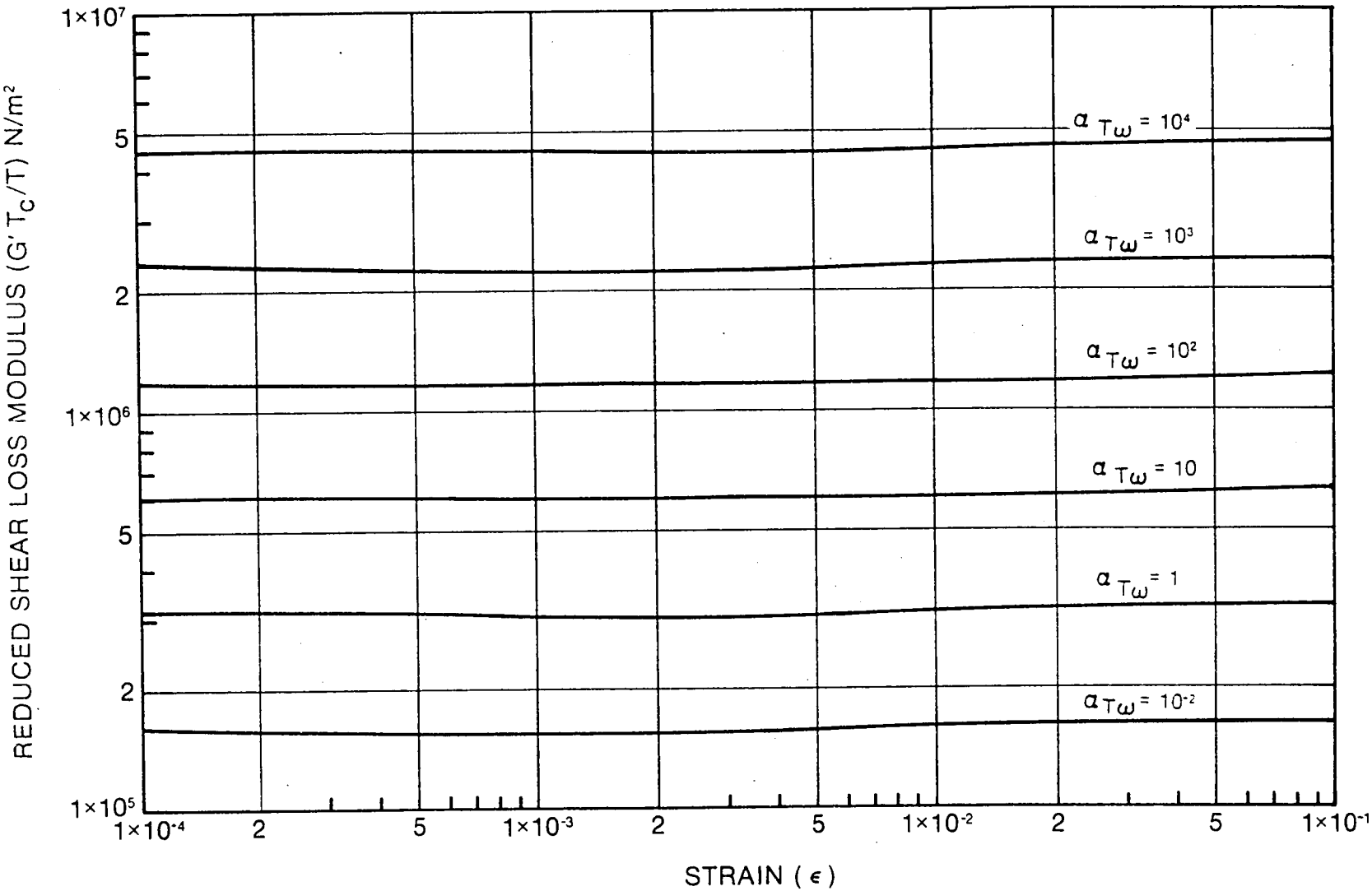

Figure 107 Buna-N Design Curves

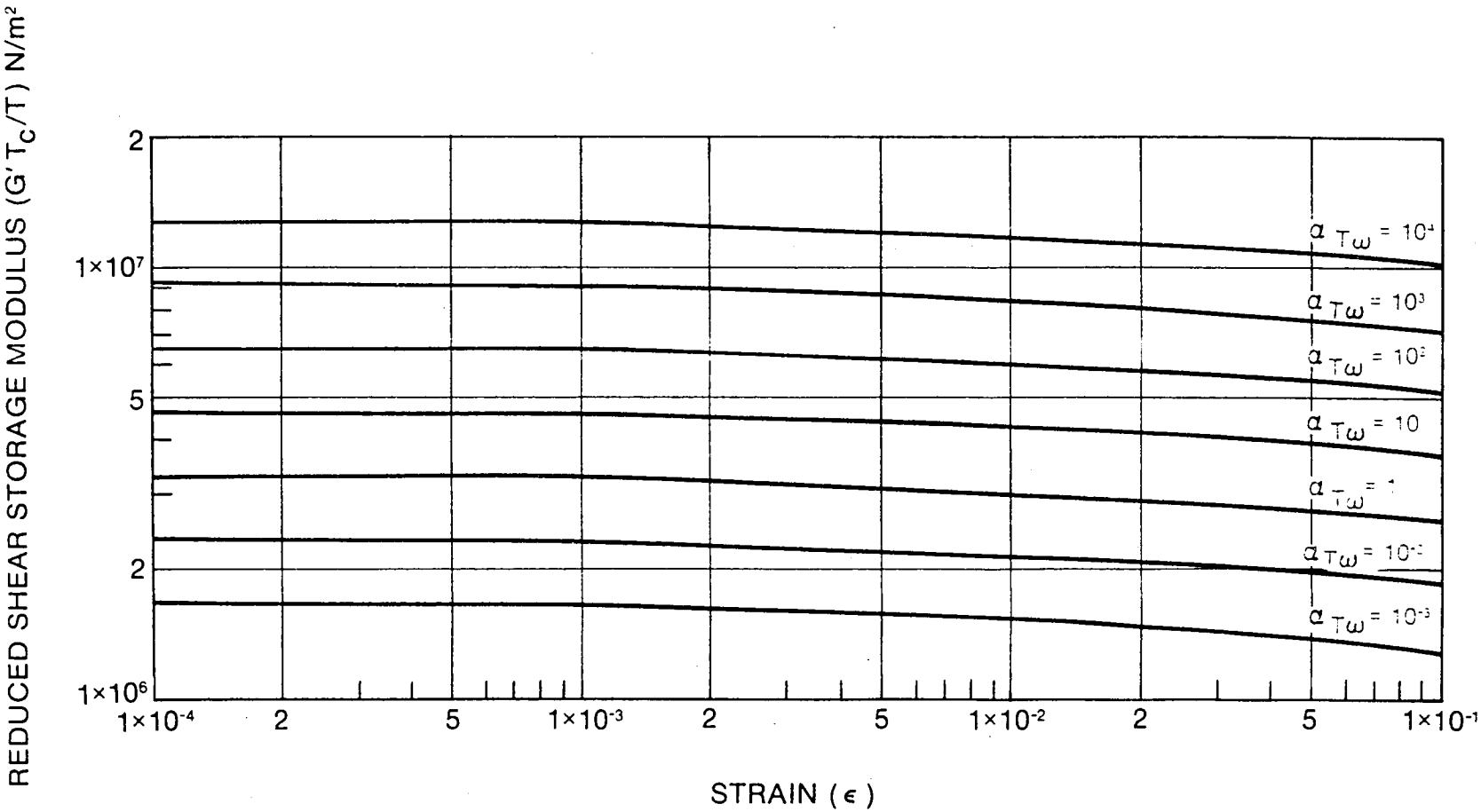

Figure 108 Viton-70 Design Curves

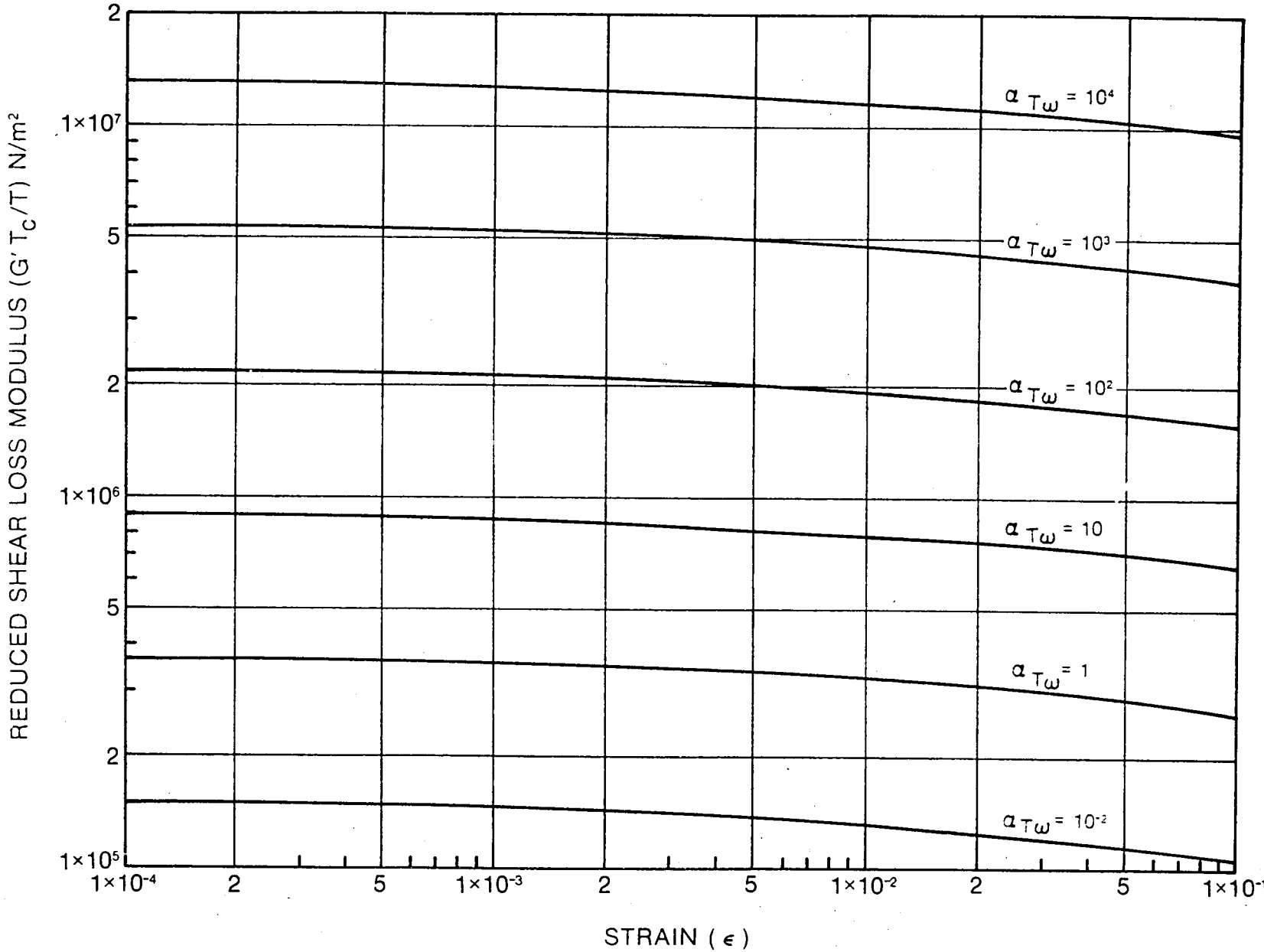

Figure 109 Viton-70 Design Curves

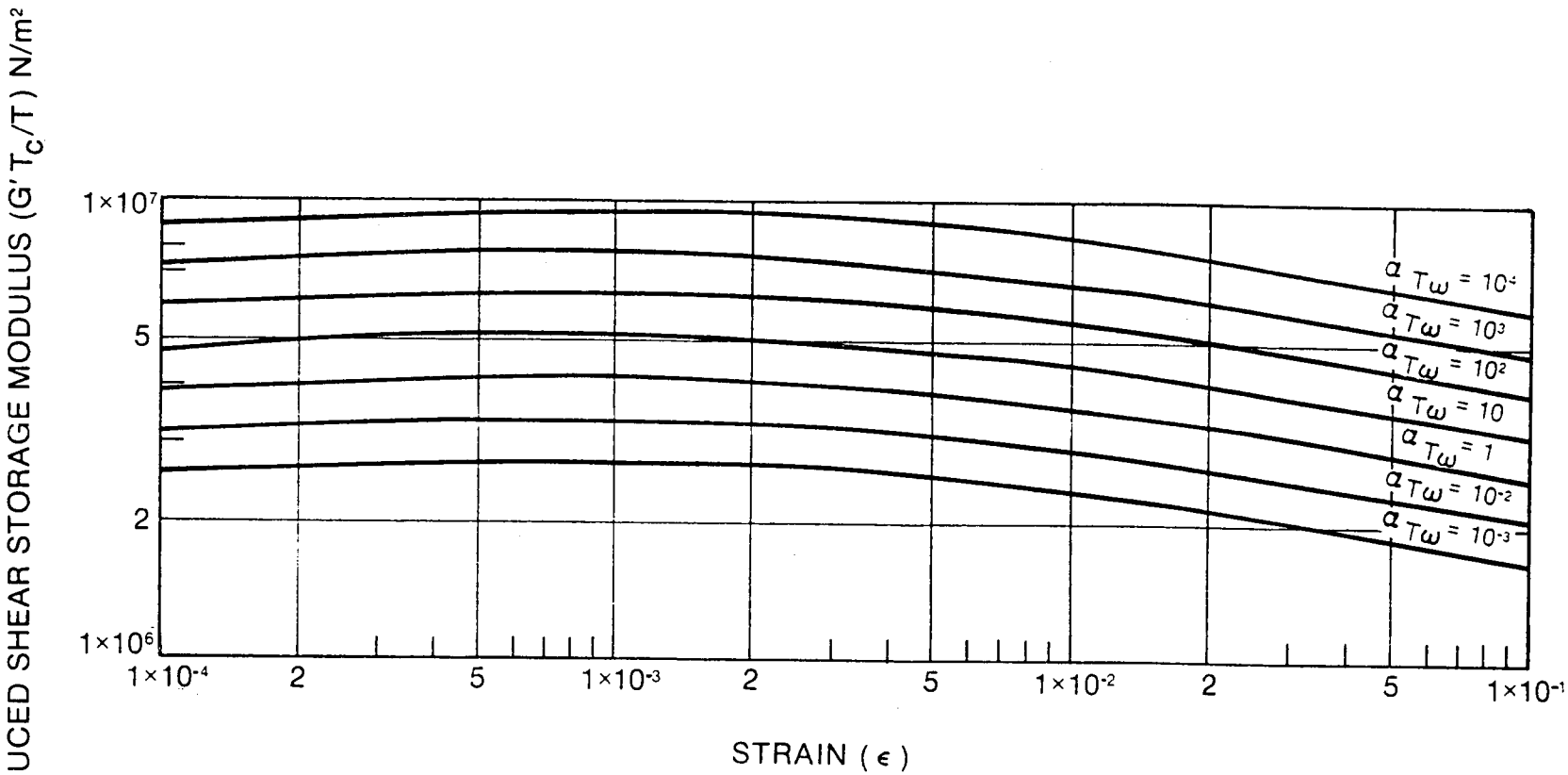

Figure 110 Neoprene Design Curves

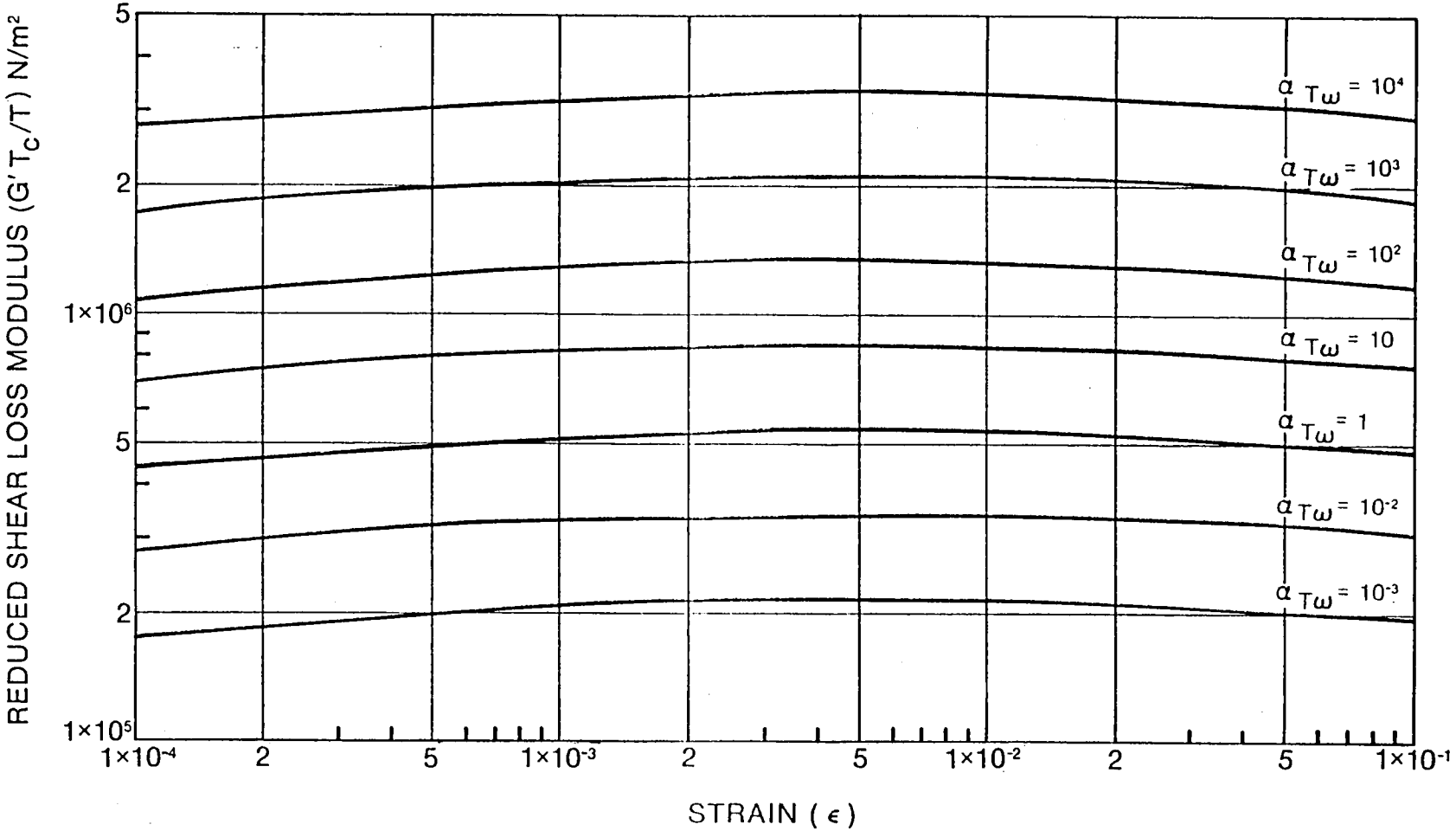

Figure 111 Neoprene Design Curves

80890.

REFERENCES

1. Tecza, J.A.; Darlow, M.S.; and Smalley, A.J., "Development of Procedures for Calculating Stiffness and Damping of Elastomers in Engineering Applications - Part V", NAS3-18546, February 1979.

2. Chiang, T.; Tessarzik, J.M.; and Badgley, R.H., "Development of Procedures for Calculating Stiffness and Damping Properties of Elastomers in Engineering Applications - Part I: Verification of Basic Methods", NASA Report CR-120905, March 1972.

3. Gupta, P.K.; Tessarzik, J.M.; and Cziglenyi, L., "Development of Procedures for Calculating Stiffness and Damping Properties of Elastomers in Engineering Application, Part II: Elastomer Characteristics at Constant Temperature", NASA Report CR-134704, April 1974.

4. Darlow, M.S., and Smalley, A.J., "Development of Procedures for Calculating Stiffness and Damping Properties of Elastomers in Engineering Application, Part IV: Testing of Elastomers Under a Rotating Load", NASA Report CR-135355, November 1977.

5. Darlow, M. and Smalley, A.J., "Design and Application of a Test Rig for Super-Critical Power Transmission Shafts", CR-3155, August 1979.

6. Smalley, A.J.; Darlow, M.S.; and Mehta, R.K., "Stiffness and Damping of Elastomeric O-Ring Bearing Mounts", MTI 78TR17, November 1977.

7. Darlow, M.S., and Zorzi, E.S., "Nonsynchronous Vibrations Observed in a Supercritical Power Transmission Shaft", ASME 79-9T-146.

DISTRIBUTION LIST
CR-159838 NAS 3-18546

Recipient	Number of Copies
NASA/Lewis Research Center 21000 Brookpark Road Cleveland, OH 44135	
Attn: R. E. Cunningham, MS 6-1	(15 + reproducible)
J. C. Freche, MS 49-1	1
W. J. Anderson, MS 23-2	1
H. W. Scibbe, MS 23-2	1
L. P. Ludwig, MS 23-2	1
D. Drier, MS 21-4	1
L. W. Schopen, MS 500-305	2
N. Musial, MS 500-311	1
Report Control Office, MS 5-5	1
Library, MS 60-3	2
Reliability & Quality Assurance Office, MS 500-211	1
Technology Utilization Office, MS 7-3	1
Resources Management Office, MS 3-10	1
NASA Scientific and Technical Information Facility P. O. Box 8757 Balt/Wash International Airport Maryland 21240 Attn: Accessioning Department	10
NASA Headquarters Attn: REC-1/J. E. Slomska Washington, DC 20546	1
NASA Headquarters Attn: RF-14/J. Anderson, Program Manager, OEP Washington, DC 20546	1
NASA/Ames Research Center Attn: Library Moffett Field, CA 94035	1
NASA/Hugh L. Dryden Research Center P. O. Box 273 Edwards, CA 93523 Attn: Library	1
NASA/Goddard Space Flight Center Greenbelt, MD 20771 Attn: Library	1
Jet Propulsion Laboratory 4800 Oak Grove Drive Pasadena, CA 91103 Attn: Library	1

Recipient	No. of Copies
NASA/Langley Research Center Langley Station Hampton, VA 23365 Attn: Library	1
NASA/Lyndon B. Johnson Space Center Houston, TX 77058 Attn: Library	1
NASA/Marshall Space Flight Center Marshall Space Flight Center, AL 35812 Attn: Library	1
NASA National Space Technology Laboratories NSTL Station, MS 39529	1
Aerospace Corporation P. O. Box 95085 Los Angeles, CA 91745 Attn: Library	1
AiResearch Manufacturing Co. Phoenix, AZ 85034 Attn: Library	1
AiResearch Manufacturing Co. 9851 Sepulveda Blvd. Los Angeles, CA 90009 Attn: Library	1
Air Force Aero Propulsion Laboratory Wright Patterson AFB, OH 45433 Attn: H. F. Jones R. Dayton	1
Battelle Columbus Labs 505 King Avenue Columbus, OH 43201 Attn: Library	1
Bendix Research Labs Division Detroit, MI 48232 Attn: Library	1
Boeing Co. Aerospace Division P. O. Box 3707 Seattle, WA 98124 Attn: Library	1

Recipient	No. of Copies
Boeing Company Vertol Division P. O. Box 16858 Philadelphia, PA 19142 Attn: Library	1
Continental Aviation and Engineering Corp. 12700 Kercheval Ave. Detroit, MI 48215 Attn: Library	1
Curtiss Wright Corporation Wright Aero Division Main & Passaic Streets Woodridge, NJ 07075 Attn: Library	1
Fafnir Bearing Co. 37 Booth St. New Britain, CT 06050 Attn: R. J. Matt	1
General Electric Company Aircraft Engine Technical Division Bearings, Fuels and Lubricants Evendale, OH 45215 Attn: E. N. Bamberger	1
General Electric Co. Gas Turbine Division Bldg. 53-330 Schenectady, NY 12345 Attn: C. C. Moore	1
General Electric Company Mechanical Technology Laboratory R&D Center Schenectady, NY 12301 Attn: Library	1
General Motors Corporation Allison Division Indianapolis, IN 46206 Attn: Library	1

Recipient	No. of Copies
Hughes Aircraft Corporation Centinda & Teale Avenue Culver City, CA 90230 Attn: Library	1
Industrial Tectonics, Inc. 18301 Santa Fe Avenue Compton, CA 90024 Attn: H. Signer	1
Institute for Defense Analyses 400 Army-Navy Drive Arlington, VA 22202 Attn: Library	1
Lockheed Missiles & Space Co. P. O. Box 504 Sunnyvale, CA 94088 Attn: Library	1
Massachusetts Institute of Technology Cambridge, MA 02139 Attn: Library	1
Mechanical Technology, Inc. 968 Albany-Shaker Rd. Latham, NY 12110 Attn: Library	1
National Science Foundation Engineering Division 1800 G Street, NW Washington, DC 20540 Attn: Library	1
Naval Air Systems Command Washington, DC 20360 Attn: Library	1
Naval Ship Engineering Center Washington, DC 20360 Attn: W. C. Lindstrom (NSC 613D4B)	1
David W. Taylor Naval Ship R&D Center Annapolis Division Annapolis, MD 21402 Attn: Library	1

Recipient	No of Copies
Naval Ship Systems Command Washington, DC 20360 Attn: J. E. Dray SNHIP 6148	1
Rockwell International 6633 Canoga Ave. Canoga Park, CA 91304 Attn: Library	1
Office of Naval Research Arlington, VA 22217 Sttn: S. W. Doroff (Code 438)	1
SKF Industries, Inc. Engineering & Research Ctr. 1100 First Ave. King of Prussia, PA 19406 Attn: T. Tallian L. Sibley	1 1
Sundstrand, Denver 2480 W. 70 Avenue Denver, CO 80221 Attn: Library	1
TRW, Inc. 23555 Euclid Avenue Cleveland, OH 44117 Attn: Library	1
TRW Marlin Rockwell Division 402 Chandler St. Jamestown, NY 14701 Attn: Library	1
U. S. Army Engineering R&D Labs Gas Turbine Test Facility Fort Belvoir, VA 22060 Attn: W. Crim	1
Pratt & Whitney Aircraft Division 400 Main St. East Hartford, CT 06108 Attn: R. Shevchenko P. Brown Dr. F. C.Hsing Library	1 1 1 1

Recipient	No. of Copies
United Aircraft Corporation Sikorsky Aircraft Division Stratford, CT 06497 Attn: L. Burroughs	1
U. S. Army Research & Technology Labs Applied Technology Laboratory Fort Eustis, VA 23604 Attn: Library	1
Rensselaer Polytechnic Institute Mechanics Division Troy, NY 12181 Attn: F. F. Ling	1
Southwest Research Institute P. O. Drawer 28510 San Antonio, TX 78284 Attn: Library	1
Tribon Bearing Co. Division of Pure Carbon Co. 5581 W. 164th St. Brookpark, OH 44132 Attn: D. W. Moyer	1
Materials Science Corp. Blue Bell Office Campus Merion Towel Bldg. Blue Bell, PA 19422 Attn: Library	1
Shaker Research Corp. Northway 10 Executive Park Ballston Lake, NY 12019 Attn: Dr. C. H. T. Pan	1
General Electric Co. P. O. Box 8, Malta Site Schenectady, NY 12301 Attn: Dr. A. J. Martenson	1
Northwestern University Department of Mechanical Engineering & Astronautical Science Evanston, IL 60201 Attn: Dr. R. Burton Dr. H. S. Cheng	1 1

Recipient	No. of Copies
Thiokol Corporation P. O. Box 524 Brigham City, UT 84302 Attn: Bliss Law, MS 308	1
Teledyne CAE, Turbine Engines 1330 Laskey Rd. Toledo, OH 43697 Attn: R. Beck	1
Ingersoll-Rand Corp. Phillipsburg, NJ 08865 Attn: R. G. Kirk	1
Deposits & Composites, Inc. 318 Victory Dr. Herndon Industrial Park Herndon, VA 22070 Attn: R. E. Engdohl	1
Williams Research Corporation 2280 W. Maple Rd. Walled Lake, MI 48088 Attn: G. Rourk	1
University of Virginia School of Engineering & Applied Science Charlottesville, VA 22901 Attn: Dr. E. J. Gunter	1
Chalk River Nuclear Labs Chalk, Ontario, Canada KOJIJO Attn: Dr. R. Metcalf	1